Characterization of the KdpFABC complex

from *Escherichia coli*, of soluble subdomains from KdpB,

and of a homologous protein of *Methanococcus jannaschii*

Dissertation

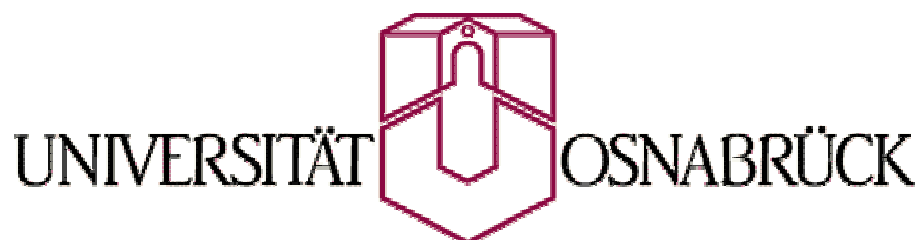zur Erlangung des Grades eines

Doctor rerum naturalium

(Dr. rer. nat.)

eingereicht am Fachbereich Biologie / Chemie der Universität Osnabrück

von

Marc Bramkamp

Osnabrück, Januar 2003

UNIVERSITÄT OSNABRÜCK

Die Hauptsache ist durchzuhalten und seine Arbeit zu Ende führen und zu sehen und zu hören und zu lernen und zu verstehen; und zu schreiben, wenn es etwas gibt, was man weiß; und nicht vorher; und nicht zu verdammt viel später. Last die, die es wollen, die Welt retten, wenn du nur dahin kommst, sie deutlich und als ganzes zu sehen. Dann wird jeder Teil, den du machst das Ganze repräsentieren, wenn es ehrlich gemacht ist. Was man tun muss ist arbeiten und lernen, wie es zu machen ist. Nein. Ich habe nicht genug aus diesem Buch gemacht. Dennoch waren da ein paar Dinge, die gesagt werden mussten. Es gab ein paar praktische Dinge, die gesagt werden mussten.

Ernest Hemingway, Tod am Nachmittag

to my parents

Acknowledgements

This work is, as it is with all things not only in science, the result of several collaborations and aids. Many persons contributed in one or the other way to this thesis either scientifically or private. Therefore, I want to express my sincere thanks to the people who supported my over the time.

First I want to thank my supervisor Prof. Dr. K. Altendorf, who supported my over the whole time with advice and the possibility to work as autonomously as possible. My great interest in traveling around the world to conferences confronting the "P-type ATPase community" with news about the strange, prokaryotic Kdp-ATPase found always his courtesy and founding. Furthermore, I want to thank for the critical correction of the manuscript.

I am grateful to Prof. Dr. W. Schoner for evaluation of the thesis.

I want to acknowledge Brigitte Herkenhoff-Hesselmann in a very warm and special way. She was a brilliant and uncomplaining help in the last quarter of this thesis.

I want to acknowledge Melina Haupt as well as Prof. Dr. H. Kessler for their patience in waiting for protein, their ongoing interest in our cooperation, and for introducing me in the complicated business of NMR spectroscopy.

I am deeply thankful to Dr. Gabriele Deckers-Hebestreit and PD. Dr. Heinrich Jung for the critical correction of the manuscript, as well as for uncountable advices supporting my work.

I want to acknowledge Drs. Michael Gaßel and Stefan Dröse, my "ancestors" and tutors in the Kdp business. I had patient, competent, and humorous teachers in both and hope they find their "style" of research within this work.

Furthermore, I am thankful to Dr. Jeffrey Froehlich who was always a great help in biochemical questions.

Special thanks go to all my lab colleagues in the 119 / 120 cosmos, Eva, Gerlinde, Ingo, Jörg, Kerstin, Roland, and Thomas. Everyone was always willing to help in either scientific or all day problems.

I want to acknowledge the new generation of 119ers Jessica, René, and Henrik for their friendship and interest in the Kdp research.

Beside all the "scientists" who supported me, I want to thank those persons who kept me aware that there is a life outside the "microbial" world of the lab. Those were in special my friends Jürgen, Thomas, Oliver, and Heiko with whom I had many excurses in the field of applied biotechnology of yeast and human ethology.

In special, I want to express my deepest thanks to the persons to whom this all is dedicated, my family, who supported my over all the years with comfort and help in times where science was rather frustrating than stimulating and encouraging.

Finally, I want to thank Anna Winnik. I will always be grateful for her love, undivided support and understanding.

I. Summary

The KdpFABC complex is a P-type ATPase. Several features make the inducible K^+-transporting ATPase a unique member of this enzyme family. Aspects of structure and function of KdpB, the catalytic subunit of the complex, were examined here.

Site-directed mutagenesis of the charged residues aspartate 583 and lysine 586 in the putative transmembrane helix 5 of KdpB revealed that these charges are involved in the coupling of ATP hydrolysis to ion translocation. Phenotypic characterization of KdpFABC derivatives carrying alterations at either D583 or K586 demonstrated that only restoration of charges at these positions allowed growth on low potassium concentrations. Substitutions, which eliminated the negative charge at position 583, did not allow growth below 15 mM potassium on solid media. In contrast, substitutions of the positive charge at position 586 allowed growth down to 0.3 mM potassium. The different phenotypes of D583 and K586 mutants, together with the fact that a double mutant, where both charges were eliminated, had the same phenotype as the D583 mutants, ruled out the formation of a salt bridge between D583 and K586. Purified KdpB mutant complexes exhibited ATPase activity, which was, however, found to be resistant to *ortho*-vanadate. Furthermore, elimination of the charges led to a complete loss of the ion-stimulated ATPase activity, while the total hydrolysis rate was comparable to wild-type activity, indicating an uncoupling between ATP hydrolysis and ion translocation. This fact was substantiated by reconstitution experiments, in which the D583A complex was unable to facilitate ion translocation, whereas the D583E mutant complex still exhibited ion translocating activity. Based on these results, a new transport model for the Kdp-ATPase is presented here, in which the amino acids D583 and K586 are supposed to form a strong dipole, which moves during the proposed reaction cycle and pushes the occluded potassium ion against the concentration gradient into the cytosol.

New biochemical aspects of the KdpFABC wild-type complex were examined. In analogy to other P-type ATPases, the Kdp-ATPase is inhibited in its catalytic activities by micromolar concentrations of FITC. The binding of FITC was shown to be specific and the binding site is within the nucleotide-binding domain of KdpB, most probably at lysine 395. Modification of KdpB with FITC was affected by adenosine nucleotides. A Mg^{2+}-dependent hydrolysis of *p*-nitrophenolphosphate was observed, which was inhibited by micromolar concentrations of *ortho*-vanadate and FITC. Low concentrations of ATP stimulated pNPP hydrolysis, while higher concentrations of ATP were inhibitory. ADP, AMP and P_i inhibited the pNPP hydrolysis.

Gene fragments of *kdpB* coding for the soluble subdomains of KdpB, the A-domain (H2H3), the P- and N-domain (H4H5) and the N-domain (KdpBN) were subcloned, expressed and the corresponding proteins were purified. The catalytic loop H4H5 and the KdpBN domain were able to bind FITC. The presence of adenosine nucleotides did not allow FTC modification of the H4H5 loop in analogy to the full-length KdpB, while for the KdpBN domain no such protection was found. H4H5

and KdpBN were able to bind TNP-nucleotides with high affinity. ATP, ADP and AMP were able to chase TNP-ATP competitively from its binding site in H4H5 and KdpBN, revealing binding constants in the millimolar range. Furthermore, H4H5 showed residual ATPase and pNPPase activity.

It was found that KdpBN was highly soluble and could be concentrated up to 1 mM and higher. The KdpBN domain was stable at these high concentrations in phosphate buffer at slightly acidic pH and temperatures up to 300 K for several days. Therefore, the KdpBN domain was used for further structural analysis using nuclear magnetic resonance spectroscopy. The KdpBN domain could be purified from cells grown in minimal medium with ^{15}N-ammonium sulfate and ^{13}C$_{1-6}$ glucose as sole nitrogen and carbon sources, respectively. The purified, labeled KdpBN protein was applied to NMR analysis. High quality multidimensional NMR spectra were obtained (M. Haupt and H. Kessler, TU Munich, personal communication) and structure calculations leading to backbone assignments were carried out.

An ortholog of the H4H5 domain of KdpB from the thermopilic archaeon *Methanococcus jannaschii*, Mj0968, was cloned, expressed, purified, and characterized. The existence of Mj0968 *in vivo* in the *M. jannaschii* cytosol was shown by using poylclonal antibodies raised against the heterologousely expressed Mj0968. Although Mj0968 was able to bind ATP with high affinity, as probed by TNP-ATP binding and chase experiments with ATP, only a low ATPase activity was observed. Surprisingly, the ATPase activity was untouched in the Mj0968-D7A mutant protein. The demonstration of high rates of pNPP hydrolysis, which increased with temperature up to 85°C, argues in favor of Mj0968 being a phosphatase rather than a P-type ATPase.

II. Abbreviations

ADP	adenosine-5'-diphosphate
AMP	adenosine-5'-monophosphate
AMP-PNP	adenosine 5'-(β, γ-imido)triphosphate
ATP	adenosine-5'-triphosphate
ATPase	adenosine triphosphatase activity
BCA	bicinchoninic acid
BCIP	5-bromo-4-chloro-3-indolyl-β-D-phosphat
CD	circular dichroism
DiSC$_3$(5)	3,3'-dipropylthiadicarbocyanin-jodide
dNTP's	desoxynucleotide-5-triphosphate
EDTA	ethylendiaminetetraacetic acid
FITC	fluorescein 5-isothiocynate isomer I
FPLC	„fast protein liquid chromatography"
GTP	guanosine-5'-triphosphate
H2H3	isolated, recombinant actuator domain of KdpB, including deca-histidinyl tag
H4H5	isolated, recombinant catalytic loop of KdpB, including deca-histidinyl tag
HEPES	N-(2-hydroxethyl)piperazin-N'-(2-ethansulfonic acid)
IPTG	isopropylthiogalactoside
ITP	inosine-5'-diphosphate
KdpBN	isolated, recombinant nucleotide-binding domain of KdpB, including deca-histidinyl tag
K$_i$	inhibition constant
K$_M$	Michaelis-Menten constant
NEM	N-ethylmaleimide
NMR	nuclear magnetic resonance
NTA	nitrilotriacetic acid
OD$_x$	optical density at a certain wavelength x
PAGE	polyacrylamid-gelelektrophorese
PCR	polymerase chain reaction
P$_i$	*ortho*-phosphat (inorganic phosphate)
PLB	phospholamban
pmf	proton motive force
pNP	*p*-nitrophenole
pNPP	*p*-nitrophenyl phosphate
pNPPase	*p*-nitrophenyl phosphatase activity

SDS	sodium dodecylsulfate
SERCA	Ca^{2+}-ATPase of sarcoplasmic reticulum
SLN	sarcolipin
TG	thapsigargin
TM	transmembrane helix
Tricin	N-tris-(hydroxymethyl)methylglycine
Tris	tris-(hydroxymethyl)-aminomethane
UV	ultraviolet light
v/v	volume per volume
V_{max}	maximal reaction velocity of enzyme catalyzed reactions
w/v	weight per volume
X-Gal	5-bromo-4-chloro-3-indolyl-β-D-galactopyranoside

1. Introduction

1.1. Influence of K^+-transporting proteins on the turgor pressure in bacteria

A vital prerequisite for the life of prokaryotic cells is the establishment of the turgor pressure. Every living cell, prokaryotic as well as eukaryotic, accumulates potassium ions (K^+) (Altendorf and Harold, 1974) within the cell plasma and exclude sodium ions (Na^+) (Bakker, 1993a). Establishment, maintenance, and regulation of these ion fluxes are mediated by a variety of membrane-bound proteins. It is remarkable that only potassium ions are used for the establishment of turgor pressure. A plausible explanation for this might be the fact that a Na^+ gradient in a sodium rich environment bears the possibility of an electrochemical gradient across the membrane. The Na^+ concentration gradient ($\Delta\mu_{Na^+}$) is used for several cellular functions, such as motion by Na^+ motive force driven flagella and ATP synthesis by Na^+ gradient-coupled ATP synthases (found in some bacteria). Thus, the Na^+ gradient plays a similar role as the proton gradient, which is in most cases used as a convertible energy source of living cells. Only H^+ and Na^+ are known to play such a central role in the energetics of the cell. Furthermore, prokaryotes and eukaryotes have established a variety of sodium co-transport systems, which use the energy of the Na^+-electrochemical gradient to drive substrate accumulation. While this sodium-coupled transport is a common rule in eukaryotes, prokaryotes living under moderate salinity conditions at neutral pH, mainly employ the proton gradient for symport of substrates, although these organisms have a variety of sodium/substrate symporters. However, halophilic prokaryotes use the Na^+ gradient coupled transport system for obvious reasons.

The net effect of protein-mediated exclusion of sodium ions and accumulation of potassium ions within the prokaryotic cell generates a negative turgor pressure, as a result of high internal K^+ concentrations. In addition, cytoplasmic K^+ plays a role in activation of enzymes (Suelter, 1970) and in regulation of the cell pH homeostasis (for a recent review see: Stumpe *et al.*, 1996). Regulation of the cytoplasmic pH is a sum effect of K^+, H^+-antiporter (Booth, 1995) and Na^+, H^+-antiporter action (Schuldiner and Padan, 1993).

Bacteria are extremely vulnerable to changes in the osmolality of the surrounding medium. In order to avoid extreme water efflux as a consequent response to an osmotic upshock, a massive K^+ accumulation in the cytoplasm can be observed. The increase in the cellular K^+ concentration is a first fast response towards increasing osmolality of the medium. The K^+ influx is mainly achieved by activation of the Trk potassium uptake systems (Rhoads and Epstein, 1978). The K^+ concentration, which is under normal conditions between 200-500 mM, can be increased up to molar concentrations. This increase is almost linear according to the increase of external osmolality; although, not all potassium ions are osmolytically active within the cytoplasm due to interference with macromolecule-bound negative charges (derived from proteins and nucleic acids). However, even at low external osmolality around 44 % of the K^+ remain as free ions within the cytosol (McLaggan et al., 1994).

Therefore, as a primary cation, K^+ plays a major role in the establishment of turgor pressure. Bacterial cells not only take up potassium but also start to synthesize organic anions, like glutamate (Measures, 1975; Christian and Waltho, 1962). These anions serve as a counterbalance for the positive charged potassium ions. When a critical K^+ concentration is reached, the cells start synthesis or uptake of neutral organic solutes, such as the zwitterions proline, glycine betaine or ectoine (Measures, 1975; Kushner and Kamekura, 1988; Imhoff, 1988; Galinski *et al.*, 1985). Beside this ionic compounds, uncharged carbohydrates, like trehalose, are synthesized (Larsen *et al.*, 1987; Dinnbier *et al.*, 1988). Taken together these cosmotrophic organic solutes are called compatible solutes (a recent review, see: Wood *et al.*, 2001), since they do not contribute in any means to the electrochemical gradient of the cell. The uptake or synthesis of the later is called the secondary response to an osmotic upshock. Bacteria counteract a fast decrease of medium osmolality (osmotic downshock) with a complete loss of potassium glutamate and trehalose (Schleyer *et al.*, 1993).

An overview about the K^+ transport systems described so far for *E. coli* is given in figure 1.
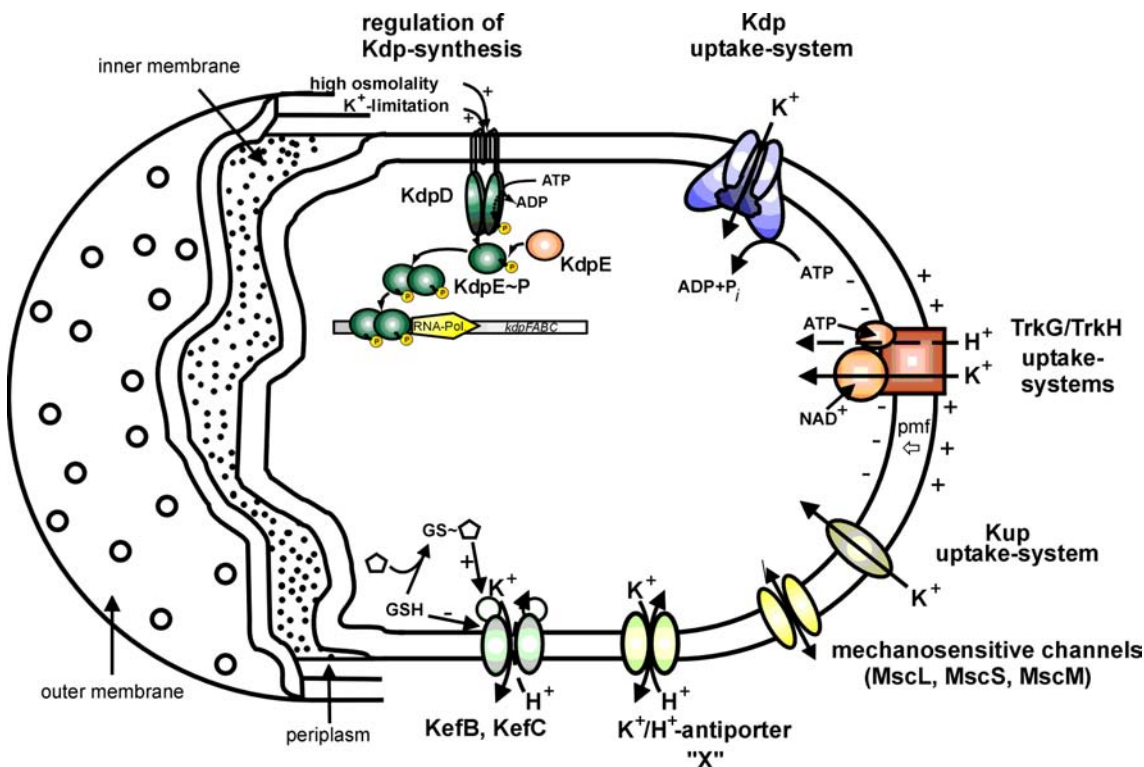
Figure 1: Schematic overview of K^+-transporting systems in *Escherichia coli*. Taken from Gaßel (1999). According to Helmer *et al.* (1982) with changes described by Stumpe *et al.* (1996), Ness and Booth (1999), Lucassen (1998) and Heermann *et al.* (1998).

The Kdp-system is an emergency potassium uptake system, employed at high osmoloaity in the medium or low internal K^+ concentration (discussed in detail below). The homologous systems KefB and KefC, which comprise K^+ channels (Booth *et al.*, 1996), are mainly involved in a fast K^+ efflux. Kef proteins play a key role for the detoxification of electrophilie reagents, such as NEM, methylglyoxal, and chlorodinitrobenzole (Ferguson *et al.*, 1997). The function of Kef proteins is

inhibited by glutathione. For a complete activation of the Kef K^+ channels, an additional binding of YheR to KefB or YabF to KefC is necessary (Ness and Booth, 1999). Opening of the Kef channels leads to a fast efflux of K^+ followed by an acidification of the cytoplasm and Na^+ influx (Ferguson *et al.*, 1995; 1997). In addition, an open reading frame (*kch*) was identified within the *E. coli* genome (Milkman, 1994). The gene product of *kch* shares similarities with eukaryotic K^+ channels of the "Shaker" family (Milkman, 1994). Overproduction and purification of Kch revealed that the protein probably forms a tetramer (Voges and Jap, 1998). However, a detailed biochemical characterization is still lacking as it is in the case of the Na^+ (K^+), H^+-antiporter (signed as "X" within figure 1) (Verkhovskaya *et al.*, 1995). In contrast to the Na^+ (K^+), H^+-antiporter, the NhaA Na^+, H^+-antiporter of *E. coli* is characterized in more detail and a low resolution structure is solved applying 3D and 2D crystallization (Williams, 2000).

A drastic decrease of external osmolality leads to K^+ efflux *via* mechanosensitive channels. Electrophysiological data suggest the existence of three different channel types within *E. coli*. The patch clamp technique revealed several types of mechanosensitive channels in the cell membranes of Gram-negative (Martinac *et al.*, 1987) as well as Gram–positive bacteria (Szabo and Zoratti, 1991). Patches from giant *E. coli* spheroplasts contain three types of mechanosensitive channels: MscL with 3 nS (Sukharev *et al.*, 1993), MscS with 1 nS (Martinac, *et al.*, 1987; Sukharev *et al.*, 1993) and MscM a channel occasionally smaller than 0.3 nS (Berrier *et al.*, 1996), with L, S, and M standing for large, small, and mini, respectively. An increase of the pressure gradient across the patch membrane first activates MscM, followed by MscS, whereas MscL only functions at high pressure rates (Berrier *et al.*, 1996). Recently, the structure of MscL from *Mycobacterium tuberculosis* was determined by X-ray crystallography (Chang *et al.*, 1998). The MscL channel was shown to be a homopentamer containing the typical channel elements of a membrane-helix flanked pore-helix (Chang *et al.*, 1998). Molecular modeling of the MscL from *E. coli* suggests a similar structure (Sukharev *et al.*, 2001).

The constitutively expressed K^+ uptake systems TrkG/TrkH and Kup (reviewed in Stumpe *et al.*, 1996) mediate the K^+ influx at external K^+ concentrations above 200 μM. The Trk systems transport potassium with high rates (240 μmol g^{-1} min^{-1} and 310-450 μmol g^{-1} min^{-1}, respectively) but moderate affinities (K_M: 0.3–1 and 2.2–3 mM, respectively) (Bakker, 1993b). The TrkH and TrkG polypeptides comprise 41 % identical amino acids within their sequence (Schlösser *et al.*, 1995). While the *trkH* gene is probably the *E. coli* intrinsic gene, the *trkG* gene is flanked by *rac* regions of a prophage containing an unusual GC content of 36 % leading to the suggestion that TrkG was inserted into the *E. coli* chromosome by a prophage (Bakker, 1993b; Schlösser *et al.*, 1995). The Trk transport complex is composed of the membrane integral TrkG/H proteins, the NAD(H)-binding protein TrkA (Schlösser *et al.*, 1993), and the membrane associated Sap proteins. K^+ uptake by Trk systems requires the proton motive force as well as ATP and is probably coupled to H^+ symport (Stumpe *et al.*, 1996). However, ATP is probably not hydrolyzed, but necessary for activating purposes (Steward *et al.*, 1985). The introduction of mutations within the Walker motif of SapD support the regulatory function of ATP

(Harms *et al.*, 2001). Furthermore, these studies provided evidence for an involvement of proteins other than SapD in Trk activation (Harms *et al.*, 2001). The other constitutively expressed K^+ uptake system Kup (former TrkD) is a low affinity K^+ uptake system with a K_M value around 0.3 mM and a V_{max} of 30 µmol g^{-1} min^{-1} (Bossemeyer *et al.*, 1989). As the Trk systems, Kup is probably acting as a K^+, H^+ symporter (Stumpe *et al.*, 1996). Kup cannot discriminate between K^+ and Rb^+ and also transports Cs^+. However, a contribution of Kup to osmoadaption was not observed (Dinnbier *et al.*, 1988; Schleyer *et al.*, 1993). Within the Bacteria another K^+ transport system, KtrAB, was recently described for *Vibrio alginolyticus* (Nakamura *et al.*, 1998). K^+ transport through the Ktr system is Na^+-dependent and the K_M value was determined to be 50 µM (Tholema *et al.*, 1999). Furthermore, in many prokaryotes the Kdp-ATPase is synthesized as high affinity K^+ uptake system (see below).

1.2. The prokaryotic K^+-transporting system Kdp

1.2.1. Regulation of Kdp expression

At low external K^+ concentrations (below 0.1 mM) the K^+ transport systems mentioned above (TrkG/H, Kup, KtrAB) are not able to provide bacterial cells with sufficient potassium ions, required for a proper ion homeostasis. Under these K^+-limiting conditions, many prokaryotes can initiate the synthesis of a high affinity K^+ transport system, Kdp (Laimins *et al.*, 1978; Epstein, 1985). The K^+ transport *via* Kdp is carried out by a membrane-bound complex with remarkably high affinity (K_M 2 µM), but moderate rates (V_{max} 150 µmol g^{-1} min^{-1}) for K^+ transport (Rhoads *et al.*, 1976). The Kdp system is genetically organized in a regulon consisting of two operons (compare figure 2).
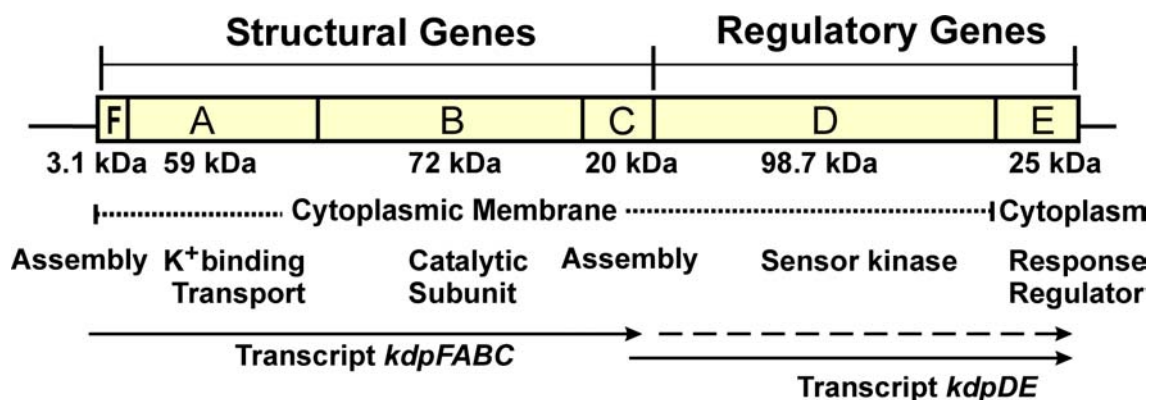
Figure 2: The *kdp*-regulon of *Escherichia coli*. According to Epstein (1985) and Altendorf *et al.* (1994).

One of the operons consists of four genes, *kdpFABC*, coding for the membrane-bound proteins of the KdpFABC transport complex (Laimins *et al.*, 1978; Hesse *et al.*, 1984; Siebers and Altendorf, 1993). The adjacent operon *kdpDE* codes for the polypeptides involved in regulation of *kdpFABC* (Walderhaug *et al.*, 1992; Polarek *et al.*, 1992).

The encoded proteins KdpD and KdpE are part of the two component sensor kinase / response regulator protein family (Altendorf *et al.*, 1994). The KdpD protein is the membrane-bound sensor kinase (Walderhaug *et al.*, 1992) and is composed of four transmembrane helices flanked by an N-terminal and a C-terminal stretch facing the cytoplasm (Zimmann *et al.*, 1995). Coelution studies revealed that KdpD is a homodimer and does not change this oligomerization state upon phosphorylation conditions (Heermann *et al.*, 1998). KdpD has autokinase activity and is subsequently phosphorylated by ATP at the conserved histidine residue 673 (Voelkner *et al.*, 1993). The phosphoryl group is transferred to the soluble response regulator KdpE (Nakashima *et al.*, 1992; 1993; Voelkner *et al.*, 1993) and after binding of the phosphorylated KdpE to the *kdp* promoter region transcription of the *kdpFABC* genes is induced (Nakashima *et al.*, 1993). KdpE and KdpE~P compete for the binding to the *kdp* promoter region, since the protein is able to bind sequence-specific DNA in the phosphorylated as well as in the unphosphorylated state (Sugiura *et al.*, 1992; Nakaschima *et al.*, 1993). However, KdpE~P has a 10-100-fold higher affinity towards the promoter region (Lucassen, 1998). Therefore, only the promoter-bound KdpE~P induces transcription. Subsequently, KdpE~P is dephosphorylated by KdpD (Jung *et al.*, 1997). KdpE~P is probably acting as a dimer, whereas KdpE is present in monomeric form (Lucassen, 1998).

KdpD has a stretch of positively charged arginine residues located directly C-terminal of the transmembrane helices. Replacements by glutamine altered the kinase / phosphatase ratio of KdpD suggesting an electrostatic switch mechanism (Jung and Altendorf, 1998b). This hypothesis was supported by the observation that the KdpD kinase activity is dependent on negatively charged phospholipids (Stallkamp *et al.*, 1999). The overall topology of the *E. coli* KdpD differs from similar sensor kinase proteins. The long N-terminal, cytoplasmic extension (reaching roughly from amino acid 1-395) is rather unique in the family of sensor kinase proteins (Puppe *et al.*, 1996; Jung and Altendorf, 1998a). However, the amino acid sequence of the N-terminal part of KdpD is even more conserved within the KdpD proteins of different origin compared to the rest of the polypeptide chain. Interestingly, DNA sequencing of cyanobacteria (two *Anabaena* species. and *Synechocystis* spec.) revealed the presence of *kdp* homologs in their genome (Kaneko *et al.*, 1996). In all three cases, the *kdpD* gene is truncated and is therefore equivalent to the N-terminal region of the *E. coli* KdpD (Alahari *et al.*, 2001). Yet, expression of the *kdpFABC* operon in cyanobacteria is regulated in a similar manner as in *E. coli* (Alahari *et al.*, 2001). A fusion protein between the *Anabaena* KdpD and a N-terminal truncated *E. coli* KdpD resulted in a functional hybrid polypeptide, being able to phosphorylate *E. coli* KdpE (Ballal *et al.*, 2002). This N-terminal stretch contains two sequence motifs, which are similar to well known ATP binding sites (Walker A and Walker B site). However, the motifs found within the N-terminal part of KdpD have each one additional amino acid, compared with the classical Walker sites (Jung and Altendorf, 1998a). ATP binding could be shown for the membrane associated separately expressed N-terminal domain of the *E. coli* KdpD (Heermann *et al.*, 2000). Furthermore, it was shown that the phosphatase activity of KdpD is significantly increased in

the presence of ATP or unhydrolyzable ATP analogs and that truncated KdpD lacking the amino acids 12-128 (which include the Walker sites) is not exhibiting an ATP-dependent phosphatase activity, supporting the idea that ATP binding to the N-terminal part of KdpD is of regulatory nature (Jung and Altendorf, 1998a). The four transmembrane helices of KdpD are important for the stimulus perception of KdpD. However, deletion of the four TM's leaving the positively charged stretch intact, led to a functional KdpD (Heermann *et al.*, 2003). A deletion of the transmembrane part together with the positively charged stretch led to a nonfunctional KdpD (Puppe *et al.*, 1996). Point mutations within this domain are characterized by an altered *kdpFABC* expression with increased basic expression level (Sugiura *et al.*, 1994; Jung *et al.*, 1998). However, the stimulus sensed by KdpD is still an object of debate. The K^+ transport complex KdpFABC is only expressed under limiting K^+ conditions. Nevertheless, the expression of KdpFABC can not be correlated with any particular internal or external K^+ concentration, but only with the K^+ concentration at which growth becomes limited (Laimins *et al.*, 1981). Therefore, it was proposed that changes in turgor pressure are sensed by KdpD (Laimins *et al.*, 1981; Malli and Epstein, 1998). Supportive evidence came from the observation that rapid turgor decrease without changes in external K^+ concentrations leads to *kdpFABC* expression. However, the turgor model is still being faced with contradicting results. An increase in medium osmolality with ionic, but not with unionic solutes, initiates *kdpFABC* expression (Sutherland *et al.*, 1986; Asha and Gowrishankar, 1993; Jung and Altendorf 1998b). Nevertheless, *kdp* expression is only observed under emergency conditions by either low external K^+ concentrations or / and high osmolality.

1.2.2. The K^+-transporting complex KdpFABC – a P-type ATPase

The *kdpFABC* operon contains the structural genes coding for the membrane-bound KdpFABC complex. In contrast to many other K^+-translocating proteins, KdpFABC has a high selectivity for K^+ (Siebers and Altendorf, 1993). ATP hydrolysis energizes the transport (Rhoads and Epstein, 1977), whereas micromolar concentrations of *ortho*–vanadate, FITC, and NEM inhibit the ATPase activity (Siebers and Altendorf, 1988; 1989). These biochemical features together with sequence alignments and the presence of a phosphorylated intermediate in the reaction cycle (Siebers and Altendorf, 1988) led to the notion that the Kdp-ATPase belongs to the family of P-type ATPases.

Pedersen and Carafoli (1987) established the group of P-type ATPases by their collective feature of forming an acid-stable and alkali-labile phosphointermediate. P-type transport ATPases comprise an important family of homologous enzymes, both of eukaryotic and prokaryotic origin, which are involved in the active pumping of charged substrates across cell membranes (for review see Møller *et al.*, 1996). Several attempts were made to determine subgroups within this still growing enzyme family. Two common accepted suggestions group the P-type ATPases according to their substrate specificity (Lutsenko and Kaplan, 1995;

Axelsen and Palmgren, 1998). Throughout this thesis the nomenclature of Axelsen and Palmgreen is used (P_{1A} ATPases (K^+); P_{1B} ATPases (Cu^+, Ag^+, Cu^{2+}, Cd^{2+}, Zn^{2+}, Pb^{2+}, Co^{2+}); P_{2A} ATPases (Ca^{2+}, Mn^{2+}, including SERCA pumps); P_{2B} ATPases (Ca^{2+}, including PMCA pumps); P_{2C} ATPases (Na^+/K^+, H^+/K^+); P_{2D} ATPases (Na^+ ?, Ca^{2+} ?); P_{3A} ATPases (H^+); P_{3B} ATPases (Mg^{2+}); P_4 ATPases (phospholipids ?); P_5 ATPases (no assigned specifity)). Prominent members of P-type ATPases in eukaryotes are the sarcoplasmic reticulum Ca^{2+}-ATPase, the renal Na^+, K^+-ATPase, the gastric H^+, K^+-ATPase, the plasma membrane H^+-ATPase and the heavy metal-transporting ATPases like Wilson's and Menkes disease protein. Whereas the heavy metal-transporting ATPases have so far not been characterized in detail, the other eukaryotic P-type ATPases are investigated for more than 40 years. P-type ATPase research was born when Hasselbach and Makinose (1961) and Ebashi and Lipmann (1962), respectively, first demonstrated that fragmented sarcoplasmatic reticulum from rabbit skeletal muscle could accumulate calcium. In accordance with the first observation of ion accumulation, which was later shown to be mediated by the Ca^{2+}-ATPase, it was again the same ATPase, which structure was finally solved at 2.6 Å resolution (Toyoshima *et al.*, 2000). The Ca^{2+}-ATPases are found not only in intracellular membrane systems (SERCA), but also in the plasma membrane (PMCA). The Na^+, K^+-ATPases, only present in animals, are involved in cellular volume regulation, development of membrane potential, and Na^+-dependent nutrient uptake as in Na^+ and iso-osmotic fluid transcellular transport in kidney, intestine, and other epithelial tissues. The H^+-ATPase from yeast and plants generates a H^+ gradient, which is essential for nutrient uptake. The H^+, K^+-ATPase, which is closely related to the Na^+, K^+-ATPase, is the central enzyme in the secretion of H^+ in the gastric ventricles. Copper-transporting ATPases are found in almost all organisms. The human P-type ATPases responsible for copper homeostasis, the Wilson's and Menkes disease proteins, respectively, build the link between the larger eukaryotic enzymes (average mass around 110 kDa) and the mainly smaller prokaryotic P-type ATPases (average mass around 70 kDa).

Examples for prokaryotic P-type ATPases are quite numerous these days mainly due to the increasing number of sequenced genomes. Examples that have been also characterized biochemically are the Mg^{2+}-ATPase from *Salmonella typhimurium*, involved in the outward transport of Mg^{2+}, the Cd^{2+}-ATPase and Cu^+-ATPase, involved in the heavy metal transport primarily in Gram-positive bacteria like *Enterococcus hirae* and *Staphylococcus aureus*. However, the first P-type ATPase discovered in a bacterium was the Kdp-ATPase of *E. coli*. The Kdp-ATPase is a P-type ATPase of unique structure and subunit composition. Many P-type ATPases contain more than one polypeptide chain in the final functional unit. Well studied examples are the α- and β-chains of the Na^+, K^+-ATPase. Nevertheless, despite Kdp, all other P-type ATPases known so far contain a central catalytic

subunit, which also facilitates the ion transport across the membrane. However in Kdp, ATP hydrolysis and hence phosphorylation are located on subunit KdpB, whereas K^+ binding and transport occurs within the KdpA subunit (for review, see: Altendorf and Epstein, 1996). Therefore, only the KdpB polypeptide is a homolog to the P-type ATPases and entitles the Kdp-ATPase to be a member of this enzyme family. Furthermore, it is discussed that the Kdp-ATPase may represent an ancient group of P-type ATPases and comprise a kind of ancestor for the P-type ATPases as such (Axelsen and Palmgren, 1998). Despite this hypothesis the KdpB chain may serve as a kind of core scheme for a P-type ATPase. Since all other enzymes of this family contain a similar architecture plus additional N- or C-terminal transmembrane spans. Figure 3 visualizes how KdpB shares the central part of P-type ATPases, while the heavy metal-transporting ATPases have only N-terminal additions (with the long cytoplasmic metal binding motifs) and other eukaryotic ion-transporting ATPases have only C-terminal additions.
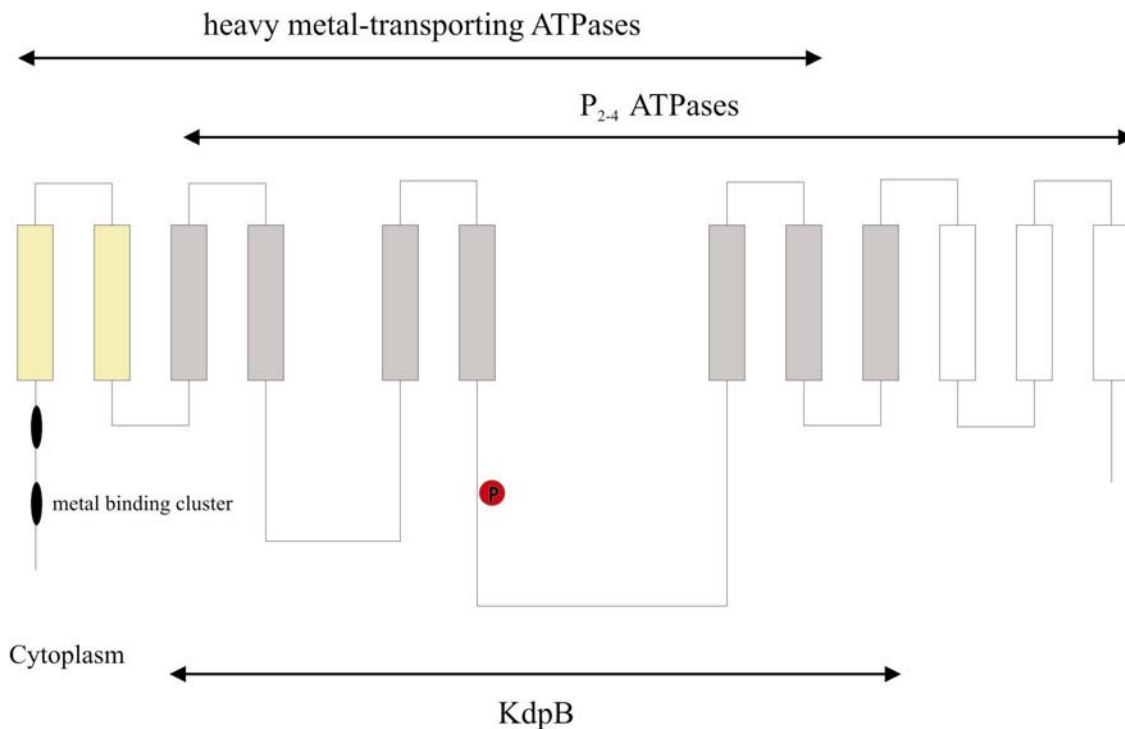
Figure 3: Schematic topology of P-type ATPases. The proposed topology of KdpB (type 1A class) is shown in gray. Heavy metal-transporting ATPases (type 1B class) have a N-terminal extension (shown in yellow). P-type ATPases of the type 2-4 class according to Axelsen and Palmgreen (1998) have 10 transmembrane helices (C-terminal additions are shown in white). The putative type 5 class of P-type ATPases (with unknown substrate specificy) might have 12 TM's (not shown). The phosphorylation site of P-type ATPases is a conserved aspartate residue in the large cytoplasmic loop (red circle).

1.2.3. The KdpB subunit

As already discussed the 72 kDa KdpB polypeptide shows homologies to other P-type ATPases (Epstein *et al.*, 1990). The homology is mainly due to highly conserved regions, which are found in all enzymes of the P-type ATPase class. These motifs were first described by Serrano (1988) and can be

used as a screening tool for this enzyme family within new sequence data. A common feature of the P-type ATPases is the ATP hydrolysis and the subsequent phosphorylation of an aspartate residue within the conserved DKTGT motif. It was shown for KdpB that mutation of aspartate 307, which is the correspondent residue within the DKTGT motif, to asparagine completely abolishes the enzymatic function (Puppe *et al.*, 1992). Formation of an acylphosphate was demonstrated (Epstein *et al.*, 1979; Siebers and Altendorf, 1988). The classical inhibitors of P-type ATPases were shown to inactivate ATP hydrolysis of Kdp (Siebers *et al.*, 1988; 1992). Topological models of KdpB were based on hydrophobicity plots and sequence comparison analysis. Therefore, a KdpB model containing six transmembrane spans was proposed (Siebers, 1988). After the determination of the structure of the sarcoplasmic reticulum Ca^{2+}-ATPase (Toyoshima *et al.*, 2000), computer-based modeling was possible and revealed that KdpB may contain seven instead of six transmembrane domains. These findings do not necessarily contradict the hydrophobicity analysis, since the C-terminal part of the enzyme (where the additional helix was introduced) is mainly hydrophobic, making it difficult to judge between two and three transmembrane helices. The recent KdpB model is widely accepted (compare P-type ATPase data base) and is shown in figure 4.

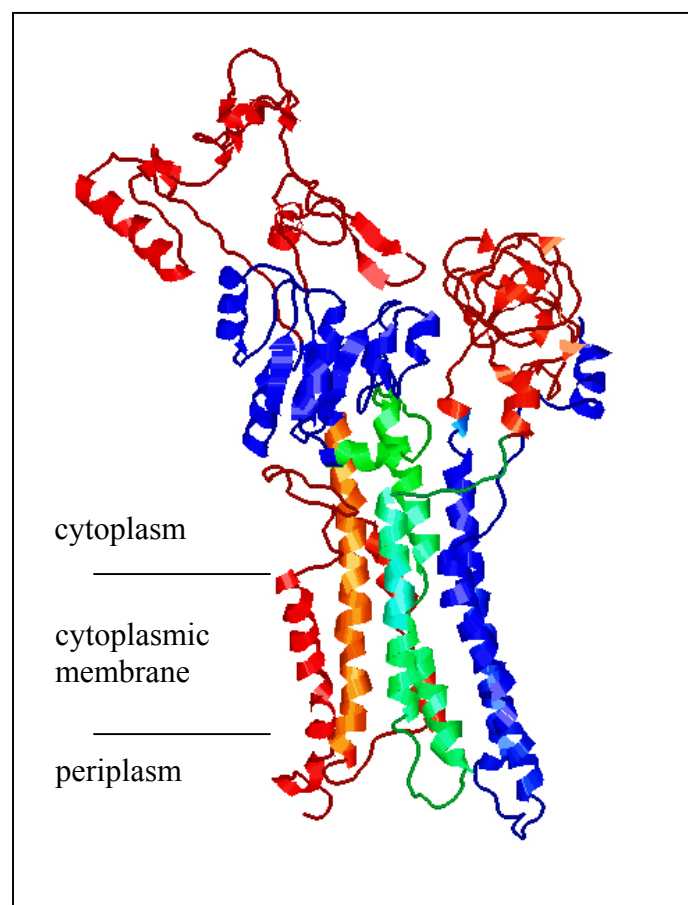**Figure 4: Structural model of KdpB.** The model of KdpB based on the structure of the Ca^{2+}-ATPase of sarcoplasmic reticulum (Toyoshima *et al.*, 2000; see section 3). The structural data of the SERCA pump structure are retrieved from the protein data bank (1EUL). Modeling of KdpB was performed using the computer programs "What If" and "O" (compare section 3.1. Drs. Engelbrecht and Gaßel, personal communication).

Although the KdpB polypeptide is much smaller compared to the SERCA pump, modeling of transmembrane domains and the phosphorylation domain as well as the actuator domain (nomenclature according the SERCA pump given by Toyoshima *et al.*, 2000) caused no major conflicts. A notable exception is the nucleotide binding domain being part of the large cytoplasmic loop between helices four and five. The KdpB nucleotide binding domain contains roughly 100 amino acids less compared with the SERCA pump, making a proper modeling impossible within this domain. In this context it is noteworthy that the closely related heavy metal-transporting ATPases and the plasma membrane H^+-ATPases have a nucleotide binding domain of similar size compared to KdpB.

1.2.4. The KdpA subunit

KdpA is a 52 kDa hydrophobic membrane-bound protein. Computer-based analysis of the KdpA topology first predicted 12 transmembrane helices (Siebers, 1988). Topological studies using the experimental approach of *lacZ* and *phoA* fusions, however, supported a model containing ten transmembrane helices (Buurman *et al.*, 1995). Genetic studies using *E. coli* mutants with reduced growth rates on media with low K^+ concentrations led to the hypothesis that KdpA might bind and transport the K^+ ions (Buurman *et al.*, 1995). The randomly introduced point mutations were found in the hydrophilic regions. Based on sequence alignment studies Jan and Jan (1994) concluded that KdpA contains, in analogy to K^+ channels, P-loop like structures. The KdpA model based on Buurman *et al.* (1995) contains two P-loop like structures between TM's 4 and 5 and TM's 8 and 9. Jan and Jan (1997) proposed a general scheme for K^+ channels containing four P-loop regions forming together a central pore. This hypothesis was confirmed by the resolution of the KcsA structure (Doyle *et al.*, 1998). The KcsA protein from *Streptomyces lividans* is a K^+-transporting protein sharing homologies to the eukaryotic K^+ channels of the "Shaker" family (Schrempf *et al.*, 1995). The KcsA structure shows that the functional channel is a tetramer with each monomer contributing one P-loop and the conserved residues forming the selectivity Filter (GYG in the case of KcsA, Shaker and ROMK1). If KdpA would have two P-loops (and hence selectivity filters) within one polypeptide chain a minimal stoichiometry of a dimer would be necessary for the functional transport complex. In fact early genetic data seem to support this idea, since intracistronic complementation suggested a dimer as functional unit (Epstein and Davies, 1970). More recently, Durell *et al.* (2000) proposed a new KdpA model, which differs in some parts from that of Buurman *et al.* (1995). Durell and colleagues pointed out the similarities between KcsA and other K^+ channels like Trk, HKT, Ktr, and KdpA (Durell *et al.*, 2000). In their model KdpA contains four P-loop structures and could function as a monomer. The Durell model is also taking into account that all these K^+-transporting channels may have evolved from a KcsA-like ancestor by gene fusion and duplication. Recently, Dorus *et al.* (2001) could identify four clusters of mutations affecting K^+-binding affinity. These four clusters are consistent with the four pore-forming regions proposed by Durell *et al.* (2000). Point mutations at amino acid residue 345

present in the proposed third selectivity filter according to Durell *et al.* (2000) (a stretch that is located in the cytoplasm by the model of Buurman *et al.,* 1995) showed that the substitution of the glycine residue to aspartate broadens the ion specificity (J. Bertrand, M. Bramkamp and K. Altendorf, unpublished results) in a similar way as it was found for the G232D mutation, which was analyzed in more detail (Buurman *et al.*, 1995; Schrader *et al.*, 1999; van der Laan *et al.*, 2002). Similar effects were observed for the "Shaker" K^+ channels after substitution of the conserved glycine residues (Heginbotham *et al.*, 1992; 1994; Nakamura *et al.*, 1997) and with the "inward rectifying" K^+ channel (Slesinger *et al.*, 1996). Furthermore, it should be noted that KdpA contains no significant homology to any transmembrane part of other P-type ATPases. Therefore, it cannot be concluded that KdpA may be an ancestor of the ion-binding domains being part of the core chain of other P-type ATPases.

1.2.5. KdpC and KdpF subunits

The small hydrophobic protein KdpF (3 kDa) was recently shown to be an integral part of the KdpFABC complex (Gaßel *et al.*, 1999). Sequence analysis between the *kdp* promoter and the *kdpA* start codon revealed that there is an additional small open reading frame with a GTG start codon. High resolution SDS-PAGE of KdpFABC complex preparations showed a corresponding protein band. A *kdpF* deletion mutant was still able to grow under limiting potassium concentrations, but the purified KdpABC complex lacked ATPase activity (Gaßel *et al.*, 1999). Addition of separately purified KdpF to KdpABC restored the full ATPase activity. Interestingly, the same effect was observed by addition of *E. coli* lipids (Gaßel *et al.*, 1999), suggesting that KdpF has a stabilizing, lipid-like function. Subunit KdpF is found in a variety of Kdp-ATPases from several organisms. Furthermore, some Gram-positive bacteria have similar putative ORF's, which code for hydrophobic peptides that have no sequence homology to KdpF. Examples are the *kdp* operons from *Corynebacterium acetobutylicum* and *Alicyclobacillus acidocaldarius*, which contain beside a *kdpF* / *kdpY* an additional *kdpZ* gene, whereas some cyanobacteria contain a larger gene, which might be a fusion between *kdpF* and a *kdpZ* gene, termed *kdpG* (Gaßel, 1999).

The KdpC subunit is an essential part of the transport complex. KdpC contains one transmembrane helix and a large extension facing the cytoplasm (Altendorf and Epstein, 1996; Gaßel and Altendorf, 2001), orienting the N-terminus towards the periplasm. Based on secondary structure prediction, hydropathy plot, and sequence alignment, KdpC seems to be composed of four parts (Gaßel and Altendorf, 2001). Two of these four segments are highly conserved among the KdpC polypeptides of different origin. The conserved segment 4 is located near the C-terminus while the other one, segment 2, is starting approximately 30 amino acids from the N-terminus (nomenclature according to Gaßel and Altendorf, 2001). While the membrane-bound part of KdpC is thought to be in close contact with KdpA, the function the cytoplamic extension is still unknown. Axelsen and Palmgren (1998) discussed the possibility that KdpC might be an ortholog of the β-subunit of Na^+, K^+-

ATPase and H$^+$, K$^+$-ATPase, which plays a stabilizing role in eukaryotic ATPases (Møller *et al.*, 1996). However, it should be noted that the soluble extension of the β-subunit is exposed to the extracellular space and not to the cytoplasmic site.

Within the P-type ATPase family several small proteins exist, which influence the activity of the pump. The Ca^{2+}-ATPases from sarcoplasmatic reticulum are regulated by a small membrane-integral protein with cytoplasmic extension, the phospholamban (for review, see: East, 2000). Phospholamban cannot only interact with the membrane part of the pump, but interacts also with defined amino acids located within the large cytoplasmic loop of the SERCA pump (MacLennan *et al.*, 1997; Kimura and Inui, 2002). Calmodulin takes the place of phospholamban in the case of the plasma membrane Ca^{2+}-ATPase (PMCA). Calmodulin acts as an endogeneous inhibitor of the pump activity, as phospholamban does for the SERCA pump (Carafoli, 1994). Phosphorylation seems to be a key towards the understanding of this regulatory mechanism in both cases (Carafoli, 1994; Kimura and Inui, 2002). The γ-subunit of the Na$^+$, K$^+$-ATPase is another example for a small membrane-integral subunit with a key regulatory role (Berrebi-Bertran *et al.*, 2001; Therien *et al.*, 1999; Arystarkhova *et al.*, 1999). It seems to be a common principle that P-type ATPase activity can be modulated by small proteins composed of a single membrane span and a cytoplasmic extension, which can get into contact with the catalytic core domain of the central subunit. Interestingly, when the KdpFABC complex is labeled with 2-azido-ATP, in addition to KdpB also KdpC is labeled (Dröse, 1997). Based on these observations, it is possible that also KdpC plays a regulatory role within the KdpFABC complex. On the other hand, Gaßel (1999) discussed the possibility that KdpF but not KdpC might be a functional homolog to the above mentioned γ-subunit of the Na$^+$, K$^+$-ATPase, or to phospholamban or calmodulin in the case of the SERCA or PMCA pump. However, the structure of the KdpFABC complex is very complex and yet insufficient characterized to allow by now an assignment for the *in vivo* function of KdpC and KdpF.

1.2.6. Distribution of Kdp

The *kdp* operon was found in a variety of prokaryotes. The expeditious genome sequencing delivers almost monthly a new putative *kdp* sequence. Today, more than 30 different organisms are known to contain a *kdp* operon. Noteworthy, not all organisms, containing the operon coding for the Kdp transport complex, hold the additional operon for the regulatory two component system. Recently, the *kdpFABC* operon was also found in Archaea, namely *Halobacterium* species NRC-1 and *Thermoplasma acidophilum* (http://biobase.dk/~axe/Patbase.html). Both lack the regulatory operon *kdpDE*, suggesting that the two component system-based regulation is a bacterial invention. The existence of the *kdp* operon is therefore proven for Bacteria and Archaea. Despite the evolutionary distance between Bacteria and Archaea, organisms from both kingdoms share the same fate: the direct influence of osmotic changes. Prokaryotes, both Bacteria and Archaea, have to respond immediately

towards changes in the environment. Therefore, osmotic stress is one of the most challenging problems prokaryotes are faced with and explains why Bacteria employ the Kdp-ATPase as a K^+-scavenging system. The role of Kdp in Archaea is still unknown. On the other hand, several organisms do not contain a *kdp* operon, some do indeed completely lack members of the P-type ATPase family, such as *Borrelia burgdorferi*, *Buchnera* spec. APS, *Rickettsia prowazekii*, *Xylella fastidiosa* and the archaeon *Pyrococcus horikoshii* (http://biobase.dk/~axe/Patbase.html).

1.3. Structure-function relationship of P-type ATPases

Research on P-type ATPases revealed that the two linked functions, the hydrolysis of ATP and the transport of charged substrates across membranes, are carried out by two distinct parts of the enzyme. The central role of the mechanism is therefore the coupling between these activities. Sequence analysis of members of P-type ATPases gave a first glimpse about their structural similarity, although the exact structure remained unclear. However, 2D-crystallography brought the first solutions towards this problem. Applying this technique Stokes and co-workers could determine the structure of the Ca^{2+}-ATPase at 8 Å (Zhang *et al.*, 1998). With the same method, Kühlbrandt and his colleagues solved the structure of the *Neurospora* H^+-ATPase at the same resolution (Auer *et al.*, 1998). Interestingly, the electron density maps of these related proteins differed in the cytoplasmic portions, while the proposed membrane spans matched closely. Since the Ca^{2+}-ATPase was crystallized in the presence of *ortho*-vanadate and the H^+-ATPase crystallization trials were performed without any additives, it was suggested that the Ca^{2+}-ATPase shape represents the enzyme in the E2 conformation, whereas the H^+-ATPase was probably in an open, E1-like, state. This first direct "look" onto members of the P-type ATPase family, where at least major domains and membrane-integral helices could be observed, provided strong evidence for a hypothesis that was commonly accepted for years: the existence of two separate enzymatic states. The first important demonstration of these conformational changes at the protein level involved the use of controlled proteolysis with trypsin. Peter Jørgensen (1975) demonstrated that the proteolytic pattern was altered depending on the presence of either Na^+ or K^+ ions in case of the Na^+, K^+-ATPase. Only few years later Steven Karlish and Uri Pick demonstrated that Na^+, K^+-ATPase and Ca^{2+}-ATPase are both labeled with FITC within their active site allowing the use of these labeled proteins for extensive investigation on the induced conformational changes (Karlish, 1979; Karlish, 1980; Pick and Karlish, 1980; Rephaeli *et al.*, 1986). Furthermore, the group around Steven Karlish succeeded in a conformational-dependent cleavage of the Na^+, K^+-ATPase catalyzed by Fe^{2+} using ascorbate and H_2O_2 as oxidative reagents (for review, see: Goldschleger *et al.*, 2001). It became obvious that the P-type ATPases undergo a reaction cycle with large domain movements. Therefore, this class of enzymes was also called E1 / E2 ATPases. The reaction cycle with two main conformational states, involving phosphorylation, substrate binding, and release, was put together in a reaction scheme, which became prominent under the name Albers-Post mechanism

(Post *et al.*, 1972; Albers, 1967). The reaction scheme proposed for the Kdp-ATPase is shown in figure 5. Biochemical analysis assigned several partial reactions to either the E1 or the E2 conformation.
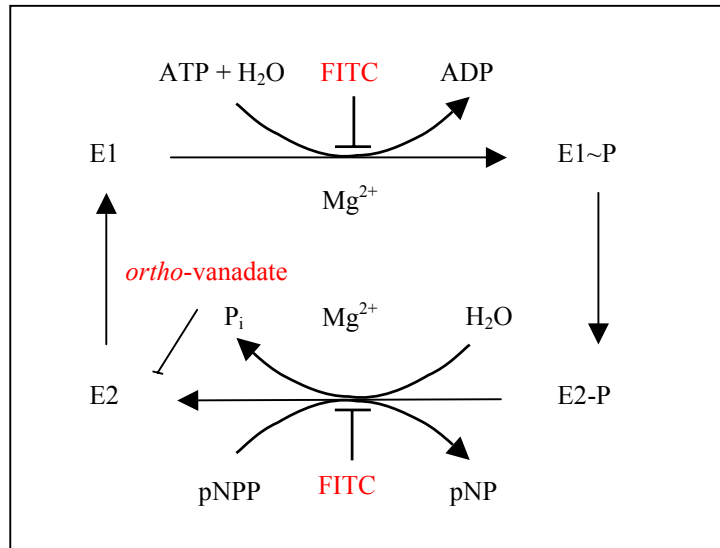
Figure 5: Schematic presentation of the reaction cycle of the Kdp-ATPase. Simplified reaction scheme of the Kdp-ATPase. Inhibitors are shown in red.

The high resolution structures of the Ca^{2+}-ATPase in the $E1Ca_2$ state (Toyoshima *et al.*, 2000) and in the E2TG state (Toyoshima and Nomura, 2002) finally supported the proposed domain movements of P-type ATPases. Consequently, structural details and the respective enzymatic functions will be discussed here on the information provided by the SERCA structure (figure 7).

The Ca^{2+}-ATPase has 10 membrane-integral helices (TM), with four stalk, or connecting helices, leading from membrane helices TM2, TM3, TM4 and TM5 to two cytoplasmic domains. The smaller cytoplasmic extension between TM2 and TM3 displays a mainly β-strand-composed structure (hence the domain was formerly known as β-strand domain). Toyoshima and co-workers (Toyoshima *et al.*, 2000) designated this 16 kDa domain as A-domain (actuator domain) because of its proposed role in the dephosphorylation step. The A-domain contains a highly conserved TGES motif, which has an important, but so far undefined role in energy transduction. Mutational analysis within the TGES motif of the SERCA pump led to loss of Ca^{2+} transport without a reduction of Ca^{2+} binding and phosphorylation capacity (Møller *et al.*, 1996; Clarke *et al.*, 1990). Therefore, it has been suggested that the A-domain is involved in the E1~P, E2-P conversion. The fact that mutations within the A-domain of the Ca^{2+}-ATPase and H^+-ATPase led to an altered *ortho*-vanadate sensitivity (Andersen and Vilsen, 1993; Morsomme *et al.*, 2000) support this idea. In addition, it has been proposed that the A-domain undergoes a large movement towards the large cytoplasmic loop. First evidence for this movement came from the two 8 Å resolution maps of the Ca^{2+}-ATPase and the H^+-ATPase (Zhang *et al.*, 1998; Auer *et al.*, 1998). The movement of the A-domain became obvious in the E2 structure of

the SERCA pump, were the A-domain rotated by about 110° horizontally. This dramatic movement allows close contact between the A-domain and the N- and P-domains (figure 8).

The large cytoplasmic domain is located between TM4 and TM5. Sequence analysis and the structure of the Ca^{2+}-ATPase revealed that this loop consists of two separate modules. This was confirmed by the Ca^{2+}-ATPase structure. The domains were, according to their function, named as P- (phosphorylation) domain and N- (nucleotide binding) domain. Among all P-type ATPase the DKTGT motif is conserved, since it contains the aspartate residue (Asp351 in case of the SERCA pump) that is subsequently phosphorylated by the γ-phosphoryl group of ATP. The topology of the P-domain was suggested to be an alternating structure between α-helices and β-strands (Green and Stokes, 1992). This seven-stranded parallel β-sheet together with eight short associated helices form a typical Rossman fold (Toyoshima *et al.*, 2000). A similar catalytic core domain was identified in a variety of enzymes. For that reason, Aravind and co-workers proposed a new superfamily of enzymes: the HAD superfamily (named after the L-2-haloacid dehalogenase) (Aravind *et al.*, 1998). This family of hydrolases includes several phosphatases (including phosphoserin phosphatase, phospho-mannomutase, phosphoglycolate phosphatase, and sucrose-phosphate synthase), dehalogenases, epioxide hydrolases, and response regulator proteins (Ridder and Dijkstra, 1999). Figure 6 displays the structure of the L-2-haloacid dehalogenase.
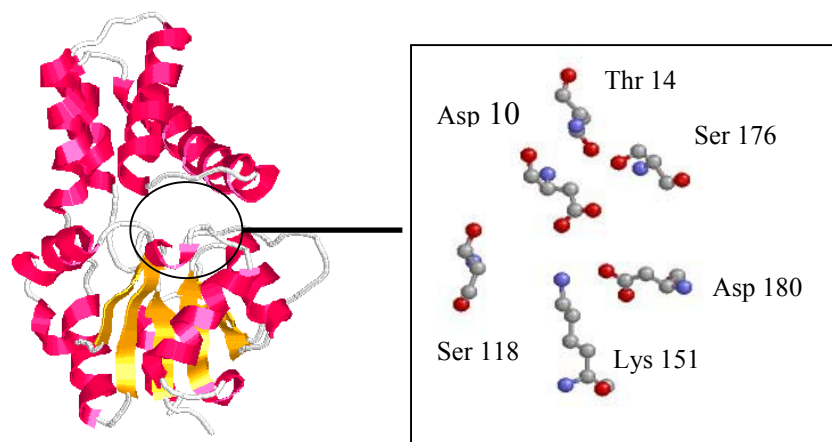
Figure 6. Structure of the L-2 haloacid dehalogenase of *Pseudomonas* spec. The structure of the L-2 haloacid dehalogenase was drawn according to the data set 1Jud.pdb (Hisano *et al.*, 1996). Highlighted are the amino acids contributing to the catalytic center as described by Aravind *et al.* (1998). Asp10 which is the homolog to the aspartate residue of the DKTGT motif found in P-type ATPases (Asp307 in *E. coli* KdpB) is the reactive residues responsible for the nucleophilic attack.

The core structure of the haloacid dehalogenase is a homolog to the P-domain of P-type ATPases. Multiple sequence alignments revealed that only a few amino acids are crucial for the hydrolytic activity of this class of enzymes (compare figure 6, where these amino acids are highlighted). These residues are located within the Rossman fold (therefore also named haloacid dehalogenase fold) (figure 7). The key role plays the aspartate residue homolog to the Asp in the

DKTGT motif of P-type ATPases. The side chain mediates the nucleophilic attack (figure 7) initiating the hydrolytic process (with the formation of the acylphosphate as a subsequent result).

The N-domain is the largest of the three cytoplasmic domains with a molecular mass around 27 kDa (it should be noted that the N-domain of the heavy metal-transporting ATPases and the Kdp-ATPase is roughly 10 kDa smaller in size). The N-domain is inserted within the P-domain and starts shortly after the DKTGT motif. A comparable domain insertion is found in the L-2-haloacid dehalogenase structure (see figure 6). The N-domain contains residues involved in nucleotide binding as revealed by TNP-AMP binding to Ca^{2+}-ATPase crystals (Toyoshima *et al.*, 2000). In a difference Fourier map, TNP-AMP is located near residues Phe487, Lys515 and Lys492. The well known inhibitor FITC was shown to bind to Lys515 and blocks ATP from binding to the ATPase (Pick, 1980). The residue Lys492 is labeled with 8-azido-TNP-AMP/ATP (McIntosh *et al.*, 1992). The positively charged binding pocket is in contrast to the negative charged active site within the P-domain. The N-domain is separated by two connecting loops from the P-domain and is believed to move around these flexible connections during the reaction cycle. While there is a general agreement that the N-domain binds nucleotides, there is, however, a long-standing discussion regarding the number of binding sites. Several biochemical data cannot be explained by a single ATP binding site, which binds one ATP molecule per reaction cycle. The discussion brings up all possibilities of different states from one binding site, two binding sites within one polypeptide chain, and the theory that the functional unit of a P-type ATPase is a dimer or an oligomer. The crystal structure of the SERCA pump cannot finally answer this question, although the data favor the one binding site model (with altered affinities towards adenosine nucleotides during the reaction cycle) (McIntosh, 2000). As a concluding remark, it should be noted that the archaeon *Methanococcus jannaschii* and *Methanothermobacter thermophilus* contain open reading frames, Mj0968 and Mt1493, respectively, which code for homologs to the large cytoplasmic loop. Therefore, the design of the P- and N-domain seems to be a common feature in nature.

The fact that P-type ATPases display two completely separated parts, the cytoplasmic domains and the membrane-integral parts, it is important to understand the coupling mechanism between both parts. Looking at the Ca^{2+}-ATPase structure, the long, central helix 5 is eye-catching. The helix TM5 starts almost directly at Asp351 (the phosphorylation site) spanning the stalk (within this area S5) and the membrane without any kink. This mast-like structure seems to be an ideal candidate to be directly involved in the coupling of conformational changes between hydrolytic parts and membrane domains. The other stalk helices (S) are located above helices TM2, TM3, and TM4. Mutational analysis of the helical stalk segments S4 and S5 confirmed their role in enzymatic function (Soteropoulos *et al.*, 2001). As a result of the A-domain rotation, the top part of the N-domain moves more than 50 Å towards the A-domain, the N-domain therefore inclines nearly 90° with respect to the membrane. The modules of the catalytic loop move as a whole in an TM10-TM1 direction (~23 Å for the P-domain) (Toyoshima and Nomura, 2002). However, despite the large movements of the N- and P-domain

relative to the membrane between the E1 and E2 state, the structures of these domains remain virtually the same, except the residues within the hinge region between N- and P-domain.
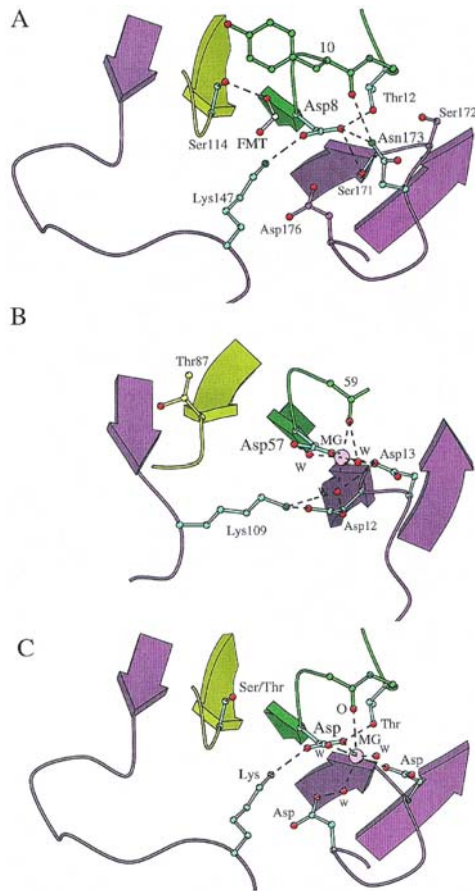

Figure 7: Active-site organization of the HAD-phosphatase model. Taken from Ridder and Dijkstra (1999). (**A**) Active site and central β-sheet of DhlB (L-2 halo acid dehalogenase homolog); colors according to sequence conservation in the HAD superfamily: motif I, dark green; motif II, yellow-green; motif III, purple; catalytic residues, light blue. Active site residues are shown in a ball and stick format; FMT, formate ion. (**B**) Active state of CheY with Mg^{2+} ion (Pdb code 1 CHN) in a view similar to that in (**A**); the ion (pink) is co-ordinated by Asp 57, Asn 59 (main chain), a pair of aspartate residues (Asp 12, Asp 13), one of which is co-ordinated *via* a water molecule, and two more water molecules (W). Upon phosphate binding a water molecule can be replaced by a phosphate oxygen atom. (**C**) Model for active site of P-type ATPases and phosphatase members of the HAD superfamily; Mg^{2+} is co-ordinated by motif I aspartate residues, a motif III aspartate residue, an oxygen atom of a main chain threonine / aspartate residue, and three water molecules (W), one of which is positioned by the second motif III aspartate residue. Upon phosphate binding a water molecule can be replaced by a phosphate oxygen atom.

The transmembrane region comprises ten α-helices (TM1-TM10). The Ca^{2+}-ATPase structure shows a clear segregation between the first six helices (TM1-TM6) and TM7-TM10. This finding lends support to the notion that helices TM7-TM10 are a more recent acquirement of the eukaryotic P-type ATPases (note the exception of the type I heavy metal-transporting P-ATPases). The membrane integral-helices TM4 and TM6 of the Ca^{2+}-ATPase are unwound within the membrane and helix TM10 is kinked. Especially, the unwounded areas of TM4 and TM6 contribute to the Ca^{2+} binding sites. In cooperation with TM8, the helices TM4-TM6 provide oxygen atoms of side chains and backbone to coordinate the calcium ions. Interestingly, the Ca^{2+} within the SERCA structure are arranged side-by-side, whereas sequential binding was predicted. The channel by which the ions gain access to the cavity (occluded state) is present between TM2, TM4, and TM6. The dissociation (or binding) of Ca^{2+} is mediated by large rearrangements of six (TM1-TM6) out of the ten transmembrane helices. The movements of the TM's are quite complicated and contain horizontal and vertical rearrangements. TM1 and TM2 move towards the cytoplasm, whereas TM3 and TM4 shift towards the luminal side. TM1 exhibits a lateral movement and TM3 and TM5 are strongly curved in the E2 state. This movements are coupled to the domain movements of the cytoplasmic parts discussed above. The coupling is achieved by hydrogen bonds between TM3-TM5 and the P-domain. Hence the top part of

TM5 moves as an entity with the P-domain. Consequently, the long TM5 helix is bend and seems to be tilted around a pivoting point (Gly770) within the membrane part. As a result, the luminal part of TM5 moves towards the cytoplasmic part, although this vertical movement is not as dramatic as seen for TM1 and TM2. The concerted action of the transmembrane domains induces changes around the Ca^{2+} binding sites. The two sites (I and II) have different coordination geometry and biochemical properties. Whereas site I entirely consists of side chain oxygen atoms of residues on TM5, TM6, and TM8, site II is composed of carbonyl oxygen atoms from residues on TM4. Upon conformational changes between E1 and E2, site I undergoes drastic changes by rotation of TM6. Essential residues (Asn796, Thr799, and Asp800) rotate clockwise accompanying the dissociation of Ca^{2+}. Inclination of TM5 decreases the number of oxygen atoms contributing to site I. In site II, Glu309 now points away from the binding site, TM4 is shifted downwards, and Asp800 moves away from the binding site. The decrease of Ca^{2+} affinity is clearly explained by these movements.
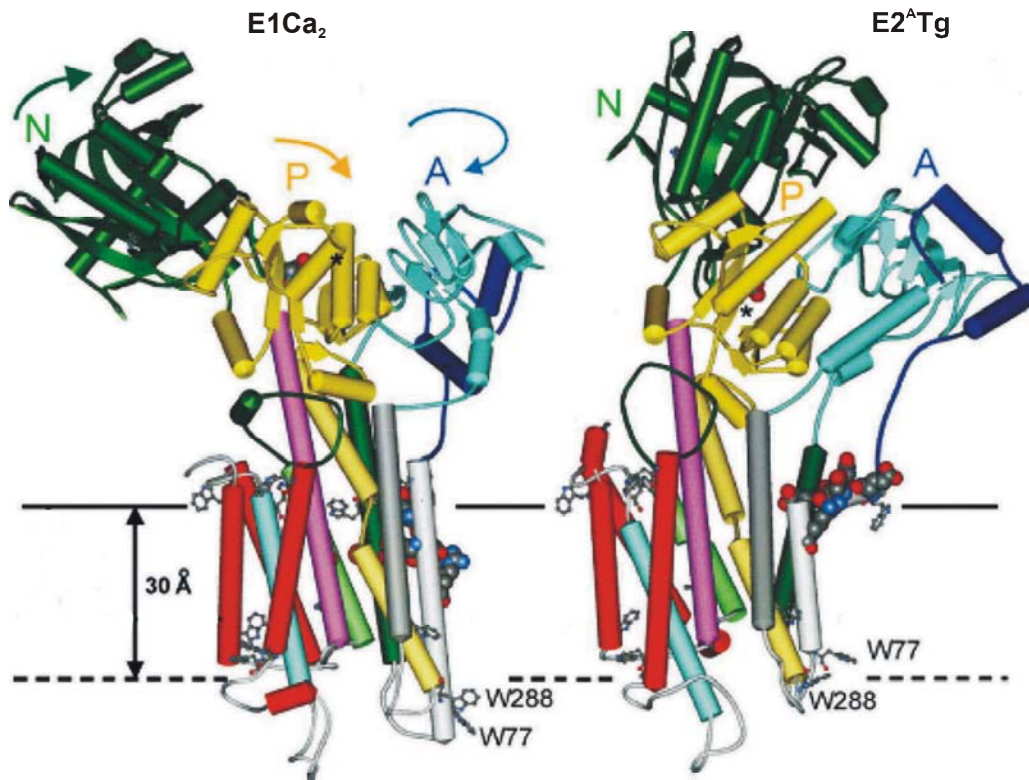
Figure 8. Comparison of the structures of the Ca^{2+}-ATPase in its Ca^{2+}-bound (E1Ca^{2+}) and Ca$_2$-free, thapsigargin-bound (E2ATg) forms. Taken from Lee (2002). The three cytoplasmic domains A, P and N are colored blue, yellow and green, respectively. The TM α-helices are colored as follows: TM1, light gray; TM2, dark green; TM3, dark gray; TM4, yellow; TM5, lilac; TM6, light green; TM7, red; TM8, light blue; TM9, red; TM10, red. Changes in helices TM7, TM9 and TM10 (red) are relatively minor between the E1Ca$_2$ and E2^{A}Tg conformations. Asp351, the residue phosphorylated by ATP, is shown in space-fill representation and marked with an asterisk. Charged residues in TM1 are also shown in space-fill representation. The two bound Ca^{2+}-ions in the E1Ca$_2$ structure are shown in orange. Trp residues are shown in ball-and-stick representation. One possible positions for the lumenal side of the membrane is marked, corresponding to hydrophobic thicknesses 30 Å (typical for a phospholipid bilayer) for the Ca^{2+}-ATPase. The arrows show the directions of rotation of the A, P and N domains required to convert from the E1Ca$_2$ to the E2^{A}Tg conformation. (PDB files 1EUL and 1IWO).

1.4. Objective of the thesis

The Kdp-ATPase was the first bacterial P-type ATPase, of which the sequence was known, the operon cloned, expressed, and the corresponding KdpFABC complex was purified (Epstein and Davies, 1970; Epstein and Kim, 1971; Laimins *et al.*, 1978; Siebers and Altendorf 1988; Siebers *et al.*, 1992).

Although, this encouraging start into the Kdp research gave rise to many initial characterizations, biochemical data and mutational analysis are mean compared to the better characterized eukaryotic P-type ATPases of the type I and type II class. At the start of this thesis no structural data of any P-type ATPase were available, beside low resolution maps, which could give valuable, but no detailed information about the architecture and hence the catalytic mechanism of P-type ATPases. Nevertheless, biochemical data and sequence alignments could determine the importance of distinct domains for either hydrolytic activity and ion transport. The KdpB subunit contains all these functional parts and the appropriate conserved motifs of P-type ATPases.

After the identification of the phosphorylation site in KdpB (Puppe *et al.*, 1992) and the biochemical characterization of the enzyme complex (Siebers et al, 1988; Siebers and Altendorf, 1989; Siebers *et al.*, 1992) the work focused on subunits KdpA, KdpC, and KdpF. These subunits comprise an ensemble, which is quite unusual in the P-type ATPase family. Especially KdpA, which shows some homologies to potassium channels (Jan and Jan 1997; Buurman *et al.*, 1995; Durell *et al.*, 2000), was investigated in detail (Schrader *et al.*, 2001; van der Laan *et al.*, 2002; Dorus *et al.*, 2001).

The aim of this thesis was to gain more knowledge about the catalytic subunit KdpB. Therefore, that parts of the *kdpB* gene coding for the soluble domains of KdpB should be subcloned, expressed, and the corresponding proteins should be purified. Biochemical and structural information about the catalytic parts of KdpB will be of general importance, since the N-domain of KdpB seems to represent a minimal scheme of this P-type ATPase module. The obtained proteins should be used for structural analysis by nuclear magnetic resonance spectroscopy (NMR) and examined with respect to their biochemical characteristics. However, for NMR analysis a number of prerequisites have to be fulfilled, such as the availability of pure protein at high concentrations and high stability of the protein at elevated temperatures for days or weeks. Furthermore, larger molecules have to be uniformly labeled with ^{15}N and ^{13}C (and eventually with ^{2}H) for multidimensional NMR. Therefore, a major effort of this thesis was the preparation of soluble domains of KdpB, which meet the demands of NMR. In order to determine proper folding of these soluble parts of KdpB, enzymatic activities or substrate binding were measured.

In addition, the ORF 0968 of the archaeon *M. jannaschii*, which codes for a putative ortholog of the large cytoplasmic loop of class I P-type ATPases, should be cloned and heterologously expressed since most archaeal proteins are often more stable at high temperature compared to their bacterial homologs. These features make them ideal candidates for structural analysis in cases where the bacterial proteins do not fulfill the prerequisites for structural determination by NMR.

Experiments with black-lipid membranes (BLM) indicated that possibly a protein-bound charge is moving during the proposed reaction cycle of the KdpFABC complex across the membrane (Fendler *et al.*, 1996; Fendler *et al.*, 1999). Therefore, a mutational analysis of charged amino acids within the long, mast-like transmembrane helix 5 was initiated to find out whether one of these amino acids is responsible for the observed movement of charge and whether these amino acids are involved in the energy transfer from the catalytic subunit KdpB to the ion-transporting subunit KdpA.

EXPERIMENTAL PROCEDURES

2. Experimental procedures

2.1. Materials

All chemicals used within this study were of analytical grade. Concentrations listed in percentage are given as weight/volume [w/v]. Polyclonal antibodies against KdpFABC, KdpB and KdpC were kindly provided by Dr. A. Siebers (Siebers *et al.*, 1988). Polyclonal antibodies against the *M. jannaschii* protein Mj0968 were raised in rabbits by Eurogentec (Seraing, Belgium) using dissolved SDS polyacrylamide gel slices, which contained the purified protein for immunization.

The list below contains all suppliers of chemical unless stated otherwise.

Amersham-Bioscience (Freiburg, Germany), [γ-^{32}P]ATP, [α-^{32}P]ATP, [α-^{32}P]-8-azido-ATP, Sure-clone ligation kit™, DEAE sepharose, Äcta-FPLC columns, proteinA sepharose

BDH Chemicals Ltd. (Pool, UK), Na-*ortho*-vanadate

Becton Dickinson Labware (Oxnard, USA), Falcon microtiter plates, 96 well

Bio-Rad (München, Germany), Low molecular weight molecular mass standard, Biobeads SM-2, Bradford protein estimation assay

Calbiochem (Bad Soden, Germany), *n*-octyl-β-D-glucopyranoside (octylglycoside, OG)

Frankenchemie (Wendelstein, Germany), Aminoxid WS 35 (mixture of C_7-C_{17} 1-alkylamino-3-dimethyl-amino-propan-3-*N*-oxide, AOX)

Glycon (Luckenwalde, Germany), *n*-decyl-β-D-maltopyranoside (decylmaltoside, DM), *n*-dodecyl-β-D-maltopyranoside (dodecylmaltoside, DDM)

ICN Biochmeicals (Aurora, USA), *p*-nitrophenyl phosphate, *p*-nitrophenol

Merck KaG (Darmstadt, Germany), Fractogel TSK-AF-Red

Molecular probes (Eugene, USA), TNP-ATP, TNP-ADP, TNP-AMP, EnzCheck® phosphate assay, DisC$_3$(5)

New England Biolabs (Schwalbach, Germany), restriction endonucleases, T4-ligase, DNA plymerase (Klenow-fragment), T4-polynucleotide phosphatase, calf intestine-phosphatase

Novagen (Groningen, Netherlands), protein molecular mass standard (pre-stained See Blue plus, MultiMark, Mark12), competent DH5α cells (subcloning efficiency)

Qiagen (Hilden, Germany), Qiaprep-spin-miniprep-kit, Qiaquick-gel-extraction kit, Ni-NTA agarose, monoclonal penta-His-antibody,

Roche Diagnostics (Penzberg, Germany), Complete™ protease inhibitor, BCIP / NBT stock solution

Roth (Karlsruhe, Germany), agarose

Sigma (Deisenhofen, Germany), ampicillin, carbenicillin, chloramphenicol, FITC isomer I, Red-*Taq*-polymerase, valinomycin,

All other chemicals were purchased from Sigma-Aldrich, Fluka, Riedel-De-Haen or Roth unless stated otherwise.

2.2. Strains, plasmids, and oligonucleotide primers

All bacterial and archaeal strains used within this study are listed in Table 1. All plasmids are listed in Table 2 and oligonucleotide primers used for cloning and sequencing are listed in Table 3.

Table 1. List of strains

Strain	Relevant genotype	Reference
TKW3205	*ΔkdpFABC Δatp thi rha lacZ nagA trkA405 trkD1*	Puppe (1991)
TKW1000	*kdp⁺ Δatp706 thi rha lacZ nagA trkA405 trkD1*	Siebers *et al.* (1988)
DH5α	*kdp⁺ recA1 endA1 gyrA96 thi1 relA1 hsdR17 supE44 Δ(lac-proAB)* F' [*traD36 laqI�q lacZ ΔM15 proA⁺ proB⁺*]	Hanahan (1983)
BL21(DE)/pLysS	*E. coli* B F⁻ *dcm ompT hsdS* (r_b⁻ m_b⁻) *gal* λ(DE3) [pLysS Cmr]	Weiner *et al.* (1994)
Epicurian Coli© BL21-Codon Plus™-RIL	*E. coli* B F⁻ *dcm⁺ ompT hsdS* (r_b⁻ m_b⁻) *gal* Tetʳ λ(DE3) *endA Hte* [*argU* (AGA, AGG) *ileY* (AUA) *leuW* (CUA) Camʳ]	Stratagene (La Jolla, USA)
SA1503(DE)	*E. coli* K12 F⁻ *dcm ompT hsdS* (r_b⁻ m_b⁻) *gal* λ(DE3)	Hoang *et al.* (1999)
Methanococcus jannaschii	wild-type strain	R. Hedderich (MPI Marburg)

Table 2. List of plasmids

Plasmid	Characteristic trait	Reference
pAMJEP60	pUC18 derivative with *M. jannaschii* chromosomal DNA cassette	ATCC*
pBad24	arabinose inducible vector	Guzman *et al.* (1995)
pBAD24ATP	KdpB:ATP loop expression vector	this study
pBAD24H2H3	KdpB:H2H3 loop expression vector	this study

pET16b	T7 polymerase based expression vector	Stratagene
pET16bH2H3	KdpB:H2H3 loop expression vector	this study
pET16bH4H5	KdpB:H4H5 loop expression vector	this study
pET16bKdpBN	KdpB:N-domain expression vector	this study
pET16bMj0968	Mj0968 expression vector	this study
pET16bMj0968D7A[#]	Mj0968-D7A expression vector	this study
pSM5	*kdpFABC*[+] (derivative of pSM1)	v. d. Laan *et al.* (2002)
pSMC10His[‡]	pSM5 derivative, 10-histidine codons downstream *kdpC*	this study
pSMC10HisD583A	*kdpFABC*[+]:KdpB-D583A	this study
pSMC10HisD583AK586A	*kdpFABC*[+]:KdpB-D853A:K586A	this study
pSMC10HisD583E	*kdpFABC*[+]:KdpB-D583E	this study
pSMC10HisD583K	*kdpFABC*[+]:KdpB-D583K	this study
pSMC10HisD583N	*kdpFABC*[+]:KdpB-D583N	this study
pSMC10HisD583S	*kdpFABC*[+]:KdpB-D583S	this study
pSMC10HisK586A	*kdpFABC*[+]:KdpB-K586A	this study
pSMC10HisK586D	*kdpFABC*[+]:KdpB-K586D	this study
pSMC10HisK586R	*kdpFABC*[+]:KdpB-K586R	this study
pSMC10HisK586T[§]	*kdpFABC*[+]:KdpB-K586T	this study
pSR4	*kdpFABC*[+]	Puppe (1991)
pSR5	*kdpFABC*:Q116R	Iwane *et al.* (1996)
pUC18	cloning vector	Amersham-Bioscience
pViet	pET16b derivative, single copy vector *oriV*	Hoang *et al.* (1999)
pVietH4H5	KdpB:H4H5 loop expression vector	this study

[‡] this plasmid was constructed by B. Herkenhoff-Hesselmann
[#] this plasmid was constructed by J. Bertrand during a lab course
[§] this plasmid was constructed by H. Strahl during a lab course
[*] ATCC (American Type Culture Collection), commercially available plasmid

All plasmids encode the *bla* gene, enabling transformants to grow on ampicillin or carbenicillin.

Table 3. List of oligonucleotides

Oligonucleotide	Sequence
ATP1	5'-<u>CCATGG</u>GCCATCACCATCACCATCACTTGTCAGCGAGTGCCGTCGCC-3' (2595-2615; *Nco*I)
ATP2	5'-<u>AAGCTT</u>TCACTAGGAGTCGGGCGAATGCAGGC-3' (3610-3629; *Hind*III)
H2H3BDfor	5'-AA<u>CCATGG</u>AGGCCCTGGCAGAAGG-3' (2024-2048; *Nco*I)
H2H3BDrev	5'-C<u>AAGCTT</u>CTATTAGTGATGGTGATGGTGATGCGCATGCTCGTTCGGCGTTTTGCGTCGCT-3' (2416-2438; *Hind*III)
H4H5for	5'-<u>CATATG</u>CTAGGCGCGAATGTGATT-3' (2629-2649; *Nde*I)
H4H5rev	5'-<u>GGATCC</u>TTACTATTACTGTTTGCCAATGTGCAC-3' (3469-3486; *Bam*HI)
H2H3for	5'-GGTAATT<u>CATATG</u>GAGGCCCTGGCAGAAGG-3' (2021-2048; *Nde*I)
H2H3rev	5'-CGC<u>GGATCC</u>TTACTATTCGTTCGGCGTTTTGCG-3' (2421-2438; *Bam*HI)
KdpBNfor	5'-ACA<u>CATATG</u>AACCGTCAGGCGTCGGAG-3' (2721-2747; *Nde*I)
KdpBNrev	5'-GCG<u>CTCGAG</u>CTATTAGCCTTTGACGATATCTTTCAG-3' (3118-3138; *Xho*I)
Mj0968for	5'-<u>CATATG</u>AAAGTGGCTATAGT-3' (*Nde*I)
Mj0968rev	5'-<u>CTCGAG</u>CTATTACGAACACTCCTTAATTTGC-3' (*Xho*I)
D7Afor	5'-C<u>ATATG</u>AAAGTGGCTATAGTGTTT**GCC**AGTGCTGGGACTCTTG-3' (*Nde*I)
WTKdpBrev	5'-GATAAAT<u>GTCGAC</u>AATGCCGG (3858-3879; *Sal*I)
KdpBD583A	5'-CGT<u>GGATCC</u>CTGACCACCTTCTCAATTGCCAAC**GCT**GTGGCGAAATAC-3' (3499-3546; *Bam*HI)
KdpBD583S	5'-CGT<u>GGATCC</u>CTGACCACCTTCTCAATTGCCAAC**AGT**GTGGCGAAATAC-3' (3499-3546; *Bam*HI)
KdpBD583N	5'-CGT<u>GGATCC</u>CTGACCACCTTCTCAATTGCCAAC**AAT**GTGGCGAAATAC-3' (3499-3546; *Bam*HI)
KdpBD583K	5'-CGT<u>GGATCC</u>CTGACCACCTTCTCAATTGCCAAC**AAA**GTGGCGAAATAC-3' (3499-3546; *Bam*HI)
KdpBD583E	5'-CGT<u>GGATCC</u>CTGACCACCTTCTCAATTGCCAAC**GAG**GTGGCGAAATAC-3' (3499-3546; *Bam*HI)
KdpBK586A	5'-CGT<u>GGATCC</u>CTGACCACCTTCTCAATTGCCAACGATGTGGCG**GCA**TACTTCGCC-3' (3499-3552; *Bam*HI)

24

KdpBK586R	5'-CGT<u>GGATCC</u>CTGACCACCTTCTCAATTG
	CCAACGATGTGGCG**CGA**TACTTCGCC-3' (3499-3552; *Bam*HI)
KdpBK586D	5'-CGT<u>GGATCC</u>CTGACCACCTTCTCAATTG
	CCAACGATGTGGCG**GAC**TACTTCGCC-3' (3499-3552; *Bam*HI)
KdpBK586T	5'-CGT<u>GGATCC</u>CTGACCACCTTCTCAATTG
	CCAACGATGTGGCG**ACG**TACTTCGCC-3' (3499-3552; *Bam*HI)
KdpBdouble	5'-CGT<u>GGATCC</u>CTGACCACCTTCTCAATTG
	CCAAC**GCA**GTGGCG**GCA**TACTTCGCC-3' (3499-3552; *Bam*HI)

Endonuclease restriction sites are underlined. Codons not homologous to the wild-type sequence are in bold letters. In brackets are positions of primer binding sites within the *kdpFABC* operon (position 1 is the start codon of KdpF as described by Sugiura *et al.* (1992)). The appropriate restriction enzymes are listed.

2.3. Growth conditions, media, and supplements

E. coli cells were routinely grown in Luria Bertani (LB) medium (Sambrock *et al.*, 1989) supplemented with the appropriate antibiotics. Expression experiments were done in either LB medium or K115 minimal medium. Strains carrying any mutation within the *kdp* operon were grown in KML, K115 minimal medium or K0 minimal medium (as described by Epstein and Kim, 1971) with different potassium concentrations, according to their ability to grow on low potassium concentrations.

In order to obtain ^{15}N- and ^{13}C / ^{15}N-labeled proteins for NMR analysis, strains were grown in minimal medium (K115) with ^{15}N-ammonium sulfate as nitrogen source and ^{13}C$_{1-6}$ labeled β-D-glucose as carbon source. The stable isotopes were purchased from Promochem (Wesel, Germany). Induction was achieved with 1 mM IPTG when the culture reached an optical density of 1.0. After three hours of induction, cells were harvested, shock-frozen in liquid nitrogen, and stored overnight at -80°C.

Supplements were added in the following final concentrations: ampicillin, 100 µg ml^{-1}; carbenicillin, 100 µg ml^{-1}; chloramphenicol, 60 µg ml^{-1}; rifampicin, 100 µg ml^{-1}; tetracycline, 12 µg ml^{-1}; thiamine, 1 mg ml^{-1}; IPTG, 1 mM, and X-Gal, 1 mM.

For transformation with plasmids *E. coli* cells were made competent with CaCl$_2$ as described by Sambrock *et al.* (1989).

2.4. Molecular biological methods

All molecular biological methods were performed according to the protocols described in Sambrock *et al.* (1989).

2.4.1. DNA amplification

DNA amplification was performed using the polymerase chain reaction (PCR). The PCR reaction was carried out in an Eppendorf thermocycler (Mastercycler Gradient©) using the Red-*Taq* polymerase (Sigma, Deisenhofen, Germany) according to the manufacturer's manual. The $MgCl_2$ concentrations was varied between 1 mM–5 mM, if necessary. The annealing temperature was 45°C unless stated otherwise. PCR products were separated using agarose gel electrophoresis (Sambrock *et al.*, 1989). The appropriate bands were cut out and eluted from the gel using the Qiaquick-gel-extraction kit following the manufacturer's protocol. Site-directed mutagenesis was carried out using single step PCR with oligonucleotide primer bearing the sequence variation. Purified PCR products were cloned into pUC18 using the Sure-Clone ligation kit (Amersham-Bioscience, Freiburg, Germany) and confirmed by DNA sequencing (MWG-Biotech or Department of Botany, University of Osnabrück).

2.5. Biochemical procedures

2.5.1. Purification of the KdpFABC complex and soluble domains of KdpB

The KdpFABC complex was prepared as described by Siebers *et al.* (1992). The final elution fraction from an TSK AF-Red affinity column contained 50 mM Tris-HCl pH 7.5, 20 mM $MgCl_2$, 10 % glycerol, 750 mM NH_4Cl, 0.2 % Aminoxid WS 35. The protein-containing fractions were pooled and dialyzed against 50 mM HEPES-Tris pH 7.5 and 0.035 % Aminoxid WS 35. The dialyzed fraction was concentrated as described and stored in liquid nitrogen until use.

Alternatively, a KdpFABC complex containing a deca-histidinyl fusion at the C-terminus of subunit KdpC was purified *via* metal affinity chromatography. For that purpose the enzyme was solubilized from membrane vesicles, with either 1 % Aminoxide WS 35 for 30 minutes or 1 % decyl-(or dodecyl-) maltoside for 60 minutes on ice. Solubilized proteins were collected by centrifugation at 4°C, 100.000 *g* for 90 minutes. The supernatant was applied to Ni-NTA agarose pre-equilibrated in 25 mM HEPES-Tris pH 7.8, 5 mM imidazole, 0.5 mM $MgCl_2$ and 0.2 % of the detergent used for solubilization. After binding at 4°C under constant shaking for 60 minutes the purification was performed in a batch procedure or using the Äcta-FPLC device (Amersham-Bioscience, Freiburg, Germany). In case of the batch procedure, the Ni-NTA resign was spun down at 2000 *g* and the supernatant was removed. The Ni-NTA agarose was washed with 20 volumes of equilibration buffer and 20 volumes of washing buffer, which contains in addition to the equilibration buffer 10 mM imidazole. Elution of KdpFABC complex from the Ni-NTA resign was performed in buffer containing 250 mM imidazole. Elution with one column volume was done at least three times, since the protein complex did not elute from the column completely at once. In case of the purification using the FPLC device, the Ni-NTA agarose was loaded with the protein in batch as described above. Subsequently,

Ni-NTA resign was transferred into a glass column (diameter 1.2 cm) and connected to the FPLC device.

For batch purification and FPLC purification of soluble domains of KdpB (H4H5, KdpBN, H2H3) and Mj0968, buffers described in the pET system manual, published by Novagen, were used with the following modifications: buffers containing 0.5 M or 0.25 M imidazole were used for elution.

2.5.2. Dialysis

Dialysis of protein solutions was performed in dialysis tubes (Serva, Heidelberg, Germany) with a pore size (M_w) of 10 kDa, which were boiled in the following solutions for 10 minutes each: 3 % Na_2CO_3, H_2O, 2 mM EDTA, H_2O. The tubes were sterilized by autoclaving and stored at 4°C until use. Protein solutions were dialyzed against a 1000-fold volume of the desired buffer with two buffer changes. Mj0968 protein was dialyzed at room temperature, while all other protein solutions were dialyzed at 4°C.

2.5.3. Concentration of protein solutions

In order to concentrate protein solutions, Centricon micro-concentrators were used as recommended by the supplier. Larger volumes (above 10 ml) were concentrated at 4°C under constant stirring using Amicon-cells (Millipore, Eschborn, Germany) equipped with either YM10 or YM30 membranes.

2.5.4. Immunoprecipitation

Immunoprecipitation of Mj0968 from *M. jannaschii* cytosolic extract was performed with polyclonal antibodies raised in rabbits against the heterologously expressed Mj0968 protein. Cytosolic extract of *M. jannaschii* cells were shock frozen in liquid nitrogen and cracked in a nitrogen bath using mortar and pestle. The cell powder was resuspended in 50 mM Tris-HCl, pH 8.0, 5 mM $MgCl_2$ and 1 mg ml^{-1} DNAse. Unbroken cells were removed by a low speed centrifugation step using an Eppendorf desk centrifuge at 3000 *g* for 10 minutes at room temperature. Cytosolic extract and membrane fractions were separated by a high speed centrifugation step at 140.000 *g* for 30 minutes at 20°C. 780 μl cytosolic extract were mixed with 20 μl anti-serum and stirred on ice for 2 hours. Equilibrated protein A- sepharose (250 μl) was added and further incubated for one hour. The sepharose matrix was pelleted and washed in two volumes of 50 mM Tris-HCl pH 7.5. Elution of precipitated proteins from protein A was performed in 50 μl 100 mM citric acid pH 2.5.

2.5.5. Reconstitution of the KdpFABC complex

Reconstitution of the KdpFABC complex into proteoliposomes was carried out as described by Gaßel (1999), based on established protocols (Fendler *et al.*, 1996; Dröse, 1997). KdpFABC complex purified using Ni-NTA metal affinity chromatography dissolved in 20 mM HEPES-Tris, pH 7.8, 0.5 mM MgCl$_2$, 0.2 % decylmaltoside and 250 mM imidazole was mixed with *E. coli* lipids (5 mg ml^{-1}) (Avanti Polar Lipids, Alabaster, USA) in a protein/lipid ratio of 1/20. The liposomes were partially solubilized by addition of Triton X100 (0.16 %). Detergents were removed by successive addition of pre-treated Biobeads SM-2 (Holloway, 1973). The proteoliposomes were spun down at 100.000 g in order to remove un-reconstituted protein. The proteoliposomes were washed twice 20 mM HEPES-Tris, pH 7.8, and 0.5 mM MgCl$_2$. The proteoliposomes were loaded with the appropriate ions by addition of salt (usually 50 mM) to the reconstitution buffer. Alternatively, three freezing, thawing, and sonication cycles were used to load the proteoliposomes with ions. Furthermore, the liposomes were shock-frozen in liquid nitrogen, thawed at room temperature for 20 minutes and sonicated in a sonifier bath for 1 minute.

2.6. Biochemical assays

2.6.1. Protein determination

Protein concentrations of membrane vesicles were determined using the method of Hartree (1972). Concentrations of purified Kdp complex and most other proteins were determined with Pierce BCA reagent (Perbio Science, Bonn, Germany) according to the manufacturer's protocol. Protein concentrations of proteoliposoms were determined using an amido-black assay (Schaffner and Weissmann, 1973). Bradford reagent (BioRad, München, Germany) was used for H4H5 and KdpBN, since both proteins lack most of the amino acids important for the BCA test.

2.6.2. SDS-Polyacrylamide gel electrophoresis (SDS-PAGE)

SDS polyacrylamide gelelectrophoresis was performed according to Laemmli (1970) using acrylamide concentrations between 10-14 %. Routinely, the Protean II system (BioRad, München, Germany) was used. The electrophoretically separated proteins were stained either with Coomassie blue G250 (Weber and Osborn, 1969) or with silver nitrate (Blum *et al.*, 1987).

2.6.3. CNBr cleavage and amino acid sequencing

N-terminal sequencing of protein fragments was carried out as described (Völker *et al.*, 1994) with modifications according to Antelmann *et al.* (1995). For cleavage with cyanogen bromide (CNBr), Coomassie blue stained protein bands were cut out from a SDS polyacrylamide gel and shaken overnight in 0.75 M CNBr dissolved in 80 % formic acid. After washing with 80 % formic acid, evaporation and neutralization of the formic acid, the peptides obtained were dissolved in SDS-PAGE sample buffer and separated by SDS-PAGE. The peptides were transferred onto a PVDF membrane, stained with Coomassie blue, the bands were cut out and sequenced using an Applied Biosystems A473a Protein Sequencer. Sequencing was carried out by Dr. Roland Schmid, Department of Microbiology, University of Osnabrück.

2.6.4. Immunoblotting

The proteins separated by SDS-PAGE were blotted onto nitrocellulose membranes at 20 V for 20 minutes (Schleicher and Schüll, Dassel, Germany) using a Trans-blot-SD apparatus (BioRad, München, Germany) with 25 mM Tris-HCl, 192 mM glycine pH 8.3 and 20 % [v/v] methanol as buffer system. The transfer was examined by staining the proteins blotted onto the membrane with a 0.2 % solution of Ponceau-S in 3 % TCA. Development of the blot was performed as described (Burkovski *et al.*, 1994).

2.6.5. ATPase assays

After incubation with different effectors the ATPase activity of the purified KdpFABC complex was determined using the microtiter plate assay of Henkel *et al.* (1988) following the modifications described previously (Altendorf *et al.*, 1998). Routinely, 0.5 µg purified protein was used for a single measurement. For ATPase measurements at elevated temperatures (37°C – 90°C) with Mj0968 protein the ATPase assay described by Henkel *et al.* (1988) was used, too. For a single measurement 50-100 µg protein were used.

For determination of low ATPase activities from Mj0968 and H4H5 proteins, the commercially available EnzCheck® test from Molecular Probes (Eugen, USA) was applied. The reactions were performed according to the manufacturer's protocol with 50 µg protein in 1 ml reaction volume.

2.6.6. Phosphatase assay

The phosphatase activity of the purified KdpFABC, H4H5, and Mj0968 was measured using a microtiter assay. The total reaction volume was 100 µl containing 20 mM HEPES-Tris pH 7.8, 15 mM

MgCl$_2$, and 5 µg protein. The mixture was pre-incubated at 37°C for 5 minutes and the reaction was started by adding 15 mM *p*-nitrophenyl phosphate. The reaction was stopped after 15 minutes at 37°C with 0.1 M NaOH. The absorbence of the reaction product *p*-nitrophenolate was immediately measured in an ELISA reader at 410 nm after calibration with a water blank to give the results as true extinction values. The total amount of released *p*-nitrophenol was calculated with an ε = 18.5 M^{-1} cm^{-1}. For determining Michaelis–Menten kinetics equimolar concentrations of Mg^{2+}, and *p*-nitrophenyl phosphate were used. Each data point was an average out of duplets. As control, duplets of the non-enzyme control were subtracted from each data point. The effects of nucleotides, ions or inhibitors were measured after preincubation for 1 or 5 minutes at 37°C.

2.6.7. Fluorimetric measurements

The fluorimetric measurements with reconstituted KdpFABC protein were carried out as described (Fendler *et al.*, 1996; Dröse, 1997; Altendorf *et al.*, 1998; Gassel, 1999). Based on the potential-sensitive dye DiSC$_3$(5), a fluorescent quench after KdpFABC mediated potassium transport was observed. The measurements were performed in 20 mM HEPES-Tris, pH 7.8, 2 mM MgCl$_2$ and 50 mM cations in a 1 ml reaction volume using a SLM-Aminco-8100-spectro-fluorimeter (SLM-Aminco, Rochester) with the following parameters: Excitation 650 nm, emission 675 nm, bandwidth of mono-chromators was 4 nm, integration time was one second. The reaction mix contained 1 µM DiSC$_3$(5) and the reaction was started by adding 1 mM Na$_2$ATP. Inhibitors (*ortho*-vanadate) and ionophores (valinomycin) were added in 100 µM and 1 µM concentrations, respectively.

2.6. 8. Circular-dichroism spectroscopy

CD-spectroscopical data of purified H4H5, KdpBN, and Mj0968 were collected on a Jasco J-600 spectropolarimeter equipped with a 0.1 mm path length cell at room temperature, which was calibrated using (+)-10-camphorsulfonic acid as described by Johnson (1988) and Greie *et al.* (2000). For each data set, 50 spectra were acquired at a scan of 50 nm min^{-1} with a step resolution of 1 nm together with a response time of one second and a bandwidth of one nanometer. Protein spectra were corrected by subtraction of the buffer control spectra. Data sets were converted to mean residue ellipticities using a mean residue mass of 115 and deconvoluted by the self-consistent method (Sreerama and Woody, 1993; Sreerama and Woody, 1994), which is derived from the variable selection analysis (Manavalan and Johnson, 1987).

2.7. Substrate binding studies

2.7.1. Azido-ATP labeling studies

Photoaffinity-labeling studies with purified Mj0968 and H4H5 proteins were performed using $[\alpha\text{-}^{32}\text{P}]$-8-Azido-ATP. The purified proteins were incubated with 5 µCi of 8-Azido-$[\alpha\text{-}^{32}\text{P}]$-ATP (stock solution 20 mCi mmol^{-1}) in a buffer containing 50 mM Tris-HCl pH7.8 and 2 mM MgCl$_2$ using 5 µg of protein in a reaction volume of 25 µl. Prior to the addition of 8-Azido-$[\alpha\text{-}^{32}\text{P}]$-ATP the samples were incubated for 5 minutes with either 2-20 mM ATP, 2-20 mM AMP or 15 µM FITC. Cross-linking was achieved by irradiation with UV light at 302 nm for 1 minute. Subsequently, the samples were mixed immediately with 5 µl of a 4-fold concentrated SDS-PAGE sample buffer (in case of Mj0968 plus additional 5 mM β-mercaptoethanol) and subjected to SDS-PAGE. The gels were stained with Coomassie blue and dried on filter paper. The dried gels were exposed on a Phosphorscreen (Molecular Dynamics) and the radio-labeled proteins were visualized using a Phosphorimager system from Molecular Dynamics (Amersham-Bioscience, Freiburg, Germany).

2.7.2. ATP binding / phosphorylation studies

ATP binding / phosphorylation studies with Mj0968 were carried out as described (Ogawa *et al.*, 2000). Purified Mj0968 was incubated in 30 µl of 50 mM HEPES-Tris pH 7.8 and 4 mM MgCl$_2$. After 5 minutes preincubation with 10 mM ATP at 56°C, $[\gamma\text{-}^{32}\text{P}]$ATP or $[\alpha\text{-}^{32}\text{P}]$ATP was added to a final concentration of 0.33 mM. The reaction was stopped after different time points by addition of 2 volumes of chilled 20 % trichloroacetic acid. The denatured proteins were sedimented by centrifugation at 14000 *g* at room temperature. The pellets were neutralized using 4 µl 1 M Tris base and resuspended in SDS-PAGE sample buffer containing 50 mM β-mercaptoethanol. The samples were applied to SDS-PAGE according to Laemmli (1970), dried, and exposed to a phosphorscreen.

2.7.3. TNP-nucleotide binding studies

Fluorescent changes upon TNP-nucleotide binding to H4H5, KdpBN, and Mj0968 were measured at room temperature using a SLM-Aminco-8100-spectro-fluorimeter (SLM-Aminco, Rochester, England). The excitation wavelength was 408 nm and the emission was recorded at 545 nm. The reaction was carried out in 1 ml of 20 mM HEPES-Tris pH 7.8 and 0.5 mM MgCl$_2$, unless stated otherwise with 5 µg of enzyme. The TNP-nucleotides (TNP-ATP, TNP-ADP, TNP-AMP) were titrated from a 1 mM stock solution to obtain concentrations between 0 and 40 µM with a volume increase less than 10 %. The measurements were recorded as time trace experiments. After addition of the TNP-nucleotide the total fluorescence was recorded for at least 10 s, in order to determine an

average fluorescence. This procedure was more accurate, compared with a single point determination, since the fluorescence oscillated sometimes within a small range. The data were plotted after subtraction of the non-enzyme control and standardization. The data were fitted using the following equation: a [TNP-nucleotide]/b + [TNP-nucleotide], with 'a', representing the maximum fluorescence change and 'b', the apparent K_d.

The data plots are usually shown in a range up to 25 µM, since the total fluorescence is decreasing at a certain TNP-nucleotide concentration. This phenomenon is due to quenching-effects, which are probably due to unspecific binding of TNP-nucleotides to the proteins, which interfere in their fluorescence with the "proper" bound molecules.

In order to determine the apparent affinity constants (K_d) for ATP, ADP and AMP, competition experiments with TNP-nucleotides were performed. Therefore, the proteins were preincubated with different concentrations of the desired nucleotide for 5 minutes at room temperature in 20 mM HEPES-Tris pH 7.8. Subsequently, the titration experiments were performed as described above. The fluorescence background of unbound TNP-nucleotides was subtracted and data were standardized. For every different nucleotide concentration the titration curve was plotted and fitted to determine the apparent affinity constants, which were than plotted against the nucleotide concentrations to obtain the K_d value for the given nucleotide.

2.7.4. FITC binding studies

FITC modification of either the KdpFABC complex (purified after the method of Siebers *et al.*, 1988), the H4H5 loop or the KdpBN domain was performed using 10 µg protein dissolved in 25 mM Tris-HCl pH 9.2, 150 mM choline chloride, 12.5 mM histidine, and 1 mM $MgCl_2$. Labeling was carried out with 15 µM FITC in the dark using black reaction tubes at 37°C for 30 minutes. The influence of nucleotides was tested by adding 5 mM of the desired nucleotide 5 minutes prior to FITC addition. To test FITC binding to unfolded proteins, the KdpFABC complex, the H4H5 loop or KdpBN were denatured with 1 % SDS at 80°C for 10 minutes. The labeled proteins were separated by SDS-PAGE and FITC fluorescence was visualized under UV light (366 nm). Subsequently, the gels were stained with Coomassie blue.

3. Results

The major aim of this work was to gain structural information about the soluble parts of the KdpB subunit of the KdpFABC complex. Therefore, a basic prerequisite for this study was to develop strategies, which might be useful to test the structural properties of subdomains of KdpB with biochemical methods. Thus, the first part of this section will deal with the properties of the native, full-length KdpB polypeptide and the native transport complex. These studies include the results of a mutagenesis study within KdpB and biochemical features, which can be addressed to the KdpB subunit, namely ATP hydrolysis and inhibitor binding studies. Site-directed mutagenesis was performed, in order to test a hypothetical transport model, which is based on the differences in ion transport of the Kdp-ATPase in comparison to other P-type ATPases.

Cloning, expression, purification, and characterization of soluble subdomains of KdpB is described in an adjacent chapter, followed by the structural investigation of the N-domain of KdpB applying multi-dimensional NMR. Finally, a biochemical analysis of an archaeal ortholog of the large cytoplasmic loop of KdpB, the putative Mj0968 protein, is described.

3.1. Modeling of the KdpB subunit

In order to have a suitable working model for the possible 3D structure of KdpB, advantage was taken from the structural similarity of the enzymes of the P-type ATPase family. Since the structure of the Ca^{2+}-ATPase was resolved in the E1 state (2.6 Å) (Toyoshima *et al.*, 2000) and in the E2 state (3.1 Å) (Toyoshima and Nomura, 2002) it was possible to use computer based modeling for a putative KdpB structure. A crucial step in homology modeling is the alignment quality. Amino acid sequence alignments revealed similarity between the P-type ATPases KdpB and SERCA, although the sequence homology is only around 26 %. Therefore, some essential motifs were used as landmarks for the alignment. Overhanging ends of the SERCA sequence were cut and gaps in the Ca^{2+}-ATPase and KdpB sequences were eliminated, in order to obtain sequences of identical length. The homology modeling with shortened sequences was performed using the programs "What If" (Vriend, 1990) and "O" (Jones and Kjildgaard, 1998). KdpB was modeled in the E1 state according to the 1EUL data (Toyoshima *et al.*, 2002) and according to the 1KJU data (Xu *et al.*, 2002) in the proposed E2 state. Alignment of the shortened KdpB and SERCA sequences revealed that the transmembrane regions align reasonably well (figures 9 and 63). The modeling in analogy to the Ca^{2+}-ATPase made clear that KdpB might contain seven instead of six transmembrane helices. Hydrophobicity analysis of KdpB revealed that a large hydrophobe region at the C-terminus might contain three instead of two transmembrane helices, supporting the findings of the homology modeling. However, there are no detailed experimental data on the topological arrangement of KdpB available, yet. The distinct separation of different domains in the cytoplasmic part of P-type ATPases can be deduced from the

Ca^{2+}-ATPase structure, namely the nucleotide binding domain (N-domain), the phosphorylation domain (P-domain) and the actuator domain (A-domain). This clear separation made it possible to identify the corresponding domains within KdpB. N- and P-domain together form the large cytoplasmic loop between TM4 and TM5. The smaller actuator domain is formed by the loop between TM2 and TM3 together with an alpha-helical portion of the N-terminal region of the enzyme. Sequence alignments and modeling showed clearly that the nucleotide-binding domain of KdpB is much smaller in size compared to the Ca^{2+}-ATPase. The N-domain of KdpB is roughly 100 amino acids smaller as the corresponding domain in the SERCA pump. It is unclear, whether the N-domain of KdpB, which has a similar size as the Menkes and Wilson's disease proteins and the plasma membrane H$^+$-ATPase, is forming a more compact structure or if it is less densely packed. This study is focusing on the clarification of structure / function relationships of the catalytic parts of KdpB.
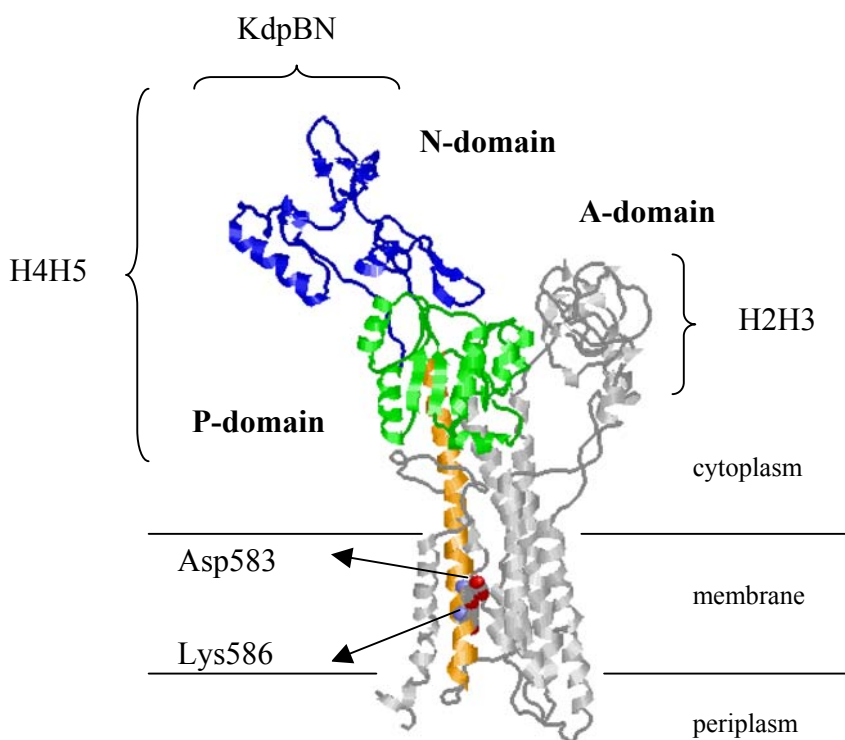

Figure 9: KdpB model according to the Ca^{2+}-ATPase structure. The Ca^{2+}-ATPase structure (1EUL.pdb; according to Toyoshima *et al.*, 2000) was used to model the KdpB subunit (Drs. S. Engelbrecht and M. Gaßel, personal communication). The nucleotide-binding domain (N; called "KdpBN" within this study) is colored in blue and the phosphorylation domain (P) in green. The P- and N-domain together form a large cytoplasmic loop between the transmembrane helices 4 and 5 (hence the loop is called H4H5 loop within this study). TM5, colored in orange, is spanning the membrane, extending into the stalk segments, and starts directly under the phosphorylation motif. Two charged residues (Asp583 and Lys586) are located in the membrane. These residues are highly conserved among the KdpB polypeptides of different origin.

Finally, it should be mentioned again that homology modeling using a template, which has only minor sequence identity to the protein which structure should be modeled is strongly dependent on the quality of the alignment. The alignment of KdpB and SERCA reveals that there are areas that do align quite well (transmembrane domains, P-domain, and A-domain) and areas, which have large gaps (N-domain) (figure 63). The models of KdpB in E1 and E2 should therefore be treated with extreme

caution. They serve as model for the planning of mutagenesis studies, but they do not have the intention to provide true structural data by themselves.

3.2. Mutagenesis of charged residues within the putative transmembrane helix 5

It was pointed out in the introduction that the Ca^{2+}-ATPase contains essential residues for binding, occlusion, and translocation of the ions in transmembrane helices TM4, TM5, TM6, and TM8. The side chain oxygen atoms of Asn768, Glu771 (TM5), Thr799, Asp800 (TM6), and Glu908 (TM8) contribute to the calcium binding site within the SERCA pump (Toyoshima *et al.*, 2000). The modeling of KdpB, described in the previous section, revealed that the putative transmembrane domain TM5 of KdpB contains two charged residues, Asp583 and Lys586. Both residues have no homologue in other P-type ATPases, but they are highly conserved throughout the KdpB polypeptides. Since KdpB is not directly involved in ion binding or transport, the question arose, whether Asp583 and Lys586 are involved indirectly in ion transport *via* KdpA. In order to elucidate this hypothesis both residues were subjected to site-directed mutagenesis.

The *kdpFABC* genes expressed from the pSMC10His vector resulted in a KdpFABC complex, which carried a C-terminal deca-histidinyl tag at subunit KdpC. The restriction sites *Bam*HI and *Sal*I were used to introduce the mutated *kdpB* cassette, generated by PCR. The used oligonucleotid primer (see section 2.2, table 3.) changed the Asp583 to alanine (D583A), serine (D583S), asparagine (D583N), lysine (D583K), and glutamate (D583E). The Lys586 was substituted by alanine (K586A), arginine (K586R), aspartate (K586D), and threonine (K586T). The *kdpB* cassettes containing the mutated codons were first cloned into a pUC18 vector and sequenced. Constructs with the right sequence were cut, using the restriction endonucleases *Bam*HI and *Sal*I and the resulting fragments were cloned into pSMC10His digested with the same restriction enzymes. Constructed pSMC10His(D583) and pSMC10His(K586) derivatives were finally transformed into TKW3205. This strain was routinely used for expression of *kdp* constructs, since it lacks the chromosomally encoded *kdp, atp, trkA,* and *trkD* genes, respectively. Expression of the pSMC10His vector is under control of the *kdpD* and *kdpE* gene products. First, the growth of the resulting strains was tested on minimal media containing different concentrations of potassium. *E. coli* wild-type cells containing the native *kdpFABC* operon were able to grow on minimal medium without added potassium (K0 medium), since due to the chemical impurities traces of K^+ are present, which are sufficient for growth. Complementation tests with strain TKW3205 carrying the pSMC10His derivatives are listed in Table 4 (wild-type: KdpFABC-His$_{10}$ complex encoded by pSMC10His).

Table 4. Complementation tests with TKW3205 carrying pSMC10His plasmids. Plasmids code for KdpFABC-His$_{10}$ with mutations in KdpB as indicated. Cell growth was tested on minimal medium agar plates supplemented with different potassium concentrations (mM). Plates were incubated at 37°C for 24 h. (-) no growth; (0) poor growth; (+) moderate growth; (++) optimal growth

	WT	D583A	D583S	D583N	D583K	D583E	K586A	K586T	K586D	K586R	D583A/ K586A
K115	++	++	++	++	++	++	++	++	++	++	++
K15	++	0	0	0	0	++	++	++	++	++	-
K10	++	-	-	0	-	++	++	++	++	++	-
K5	++	-	-	-	-	++	++	++	++	++	-
K2.5	++	-	-	-	-	++	++	++	++	++	-
K1	++	-	-	-	-	++	++	++	++	++	-
K0.5	++	-	-	-	-	++	+	+	+	++	-
K0.3	++	-	-	-	-	++	0	0	0	++	-
K0.1	++	-	-	-	-	++	-	-	-	++	-

The most obvious result was that the conservative mutants, restoring the charges at positions 583 and 586, namely D583E and K586R, exhibited a growth phenotype comparable to that of the wild-type. The D583 substitutions, which do not restore the negative charge, led to an altered phenotype. The TKW3205 strains carrying the D583A, D583S, D53N and D583K mutations were all unable to grow on medium containing less than 15 mM KCl. Even on K15 medium only poor growth was observed. In order to test, whether the two charges at position D583 and K586 form a salt bridge, a double mutant was constructed (D583A:K586A). The phenotype of this double mutant was identical to that in which the charge at position 583 was eliminated. These results, together with the observation that the substitution of residue D583 caused a different phenotype than exchange of K586 made it unlikely that the amino acid pair D583 and K586 form a salt bridge.

Since mutations within transmembrane helices may result in not correctly folded proteins it was tested, whether the mutated KdpFABC complexes were inserted into the cytoplasmic membrane. Figure 10 shows an immunoblot of membrane vesicles containing the different mutant KdpFABC complexes. On each lane of 50 µg of protein were loaded and the blot was developed using the KdpFABC antibody.
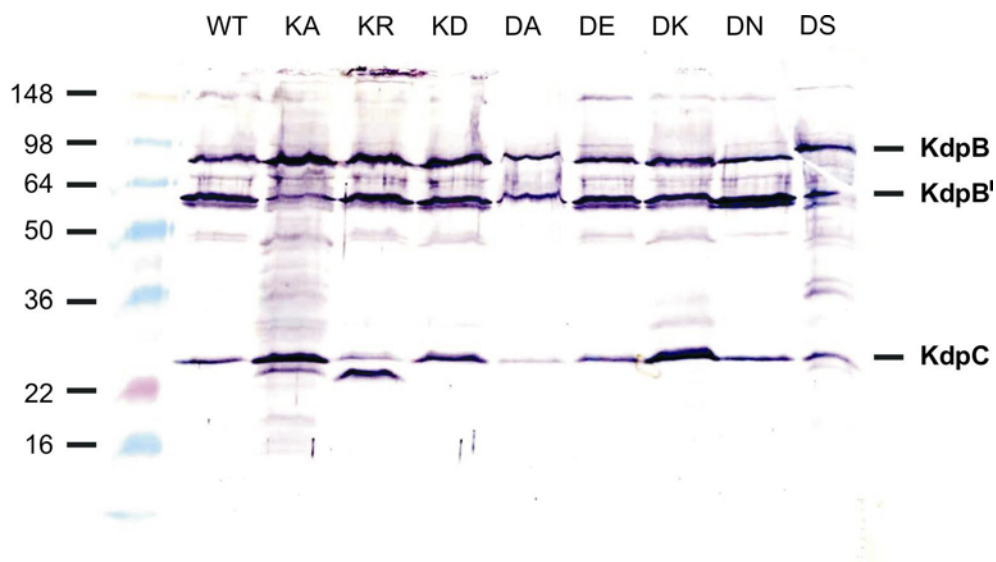
Figure 10: Immunoblot of membrane vesicles containing the mutated KdpFABC complexes. Membrane fractions of TKW3205/pSMC10His cells (carrying the different mutations) were applied to SDS-PAGE. The gel was blotted onto a nitrocellulose membrane. Kdp proteins were detected with KdpFABC antibodies. A secondary antibody conjugated with alkaline phosphatase was used for visualization. On each lane 50 μg of protein were loaded. KdpB' represents a degradation product of KdpB, while KdpA was not detected by the antibodies. WT, wild-type; KA, K586A mutation; KR, K586R mutation; KD, K586D mutation; DA, D583A mutation; DE, D583A mutation; DK, D583K mutation; DN, D583N mutation; DS, D583S mutation.

Immunoblot analysis revealed that all mutated Kdp complexes were synthesized in similar amounts compared to the wild-type KdpFABC complex. Furthermore, it was concluded that the KdpFABC-His$_{10}$ derivatives were membrane-integrated and that any dysfunction was not due to misrouting of the altered complexes. Cells for immunoblot analysis were harvested in the stationary phase; as a result, KdpB is degraded to some extent. Consequently, the blot revealed the degradation product (KdpB'), which was observed in the wild-type protein as well as in all mutant complexes.

3.2.1. Biochemical analysis of KdpB mutants

TKW3205 cells carrying the pSMC10His derivatives with the mutated KdpB were grown in K0 medium supplemented with different potassium concentrations. D583 mutants were grown overnight in K5 and transferred to K0 medium. After 1–3 hours cells were induced by adding 2.5 mM KCl. When the cell culture reached an optical density around 1.0, cells were harvested, in order to prevent degradation of the KdpFABC complex within the stationary phase. The K586 mutants were grown in K1 medium over night and transferred into K0 medium and induced twice with 0.5 mM KCl. The Kdp complexes were purified, after cell lyses using a Ribi cell fractionator, by solubilizing the membrane vesicles with decylmaltoside or aminoxide as described in experimental procedures. The solubilized Kdp complexes were purified applying metal affinity chromatography (see 2.5.1.). Elution was carried out with 250 mM imidazole. Figure 11 shows a typical purification scheme of the D583A mutant complex. However, it should be noted that purification of the mutants D583K and K586D resulted

always in a loss of KdpB in the final elution. It is most likely that the mutated KdpB polypeptide is degraded in the cells prior purification.
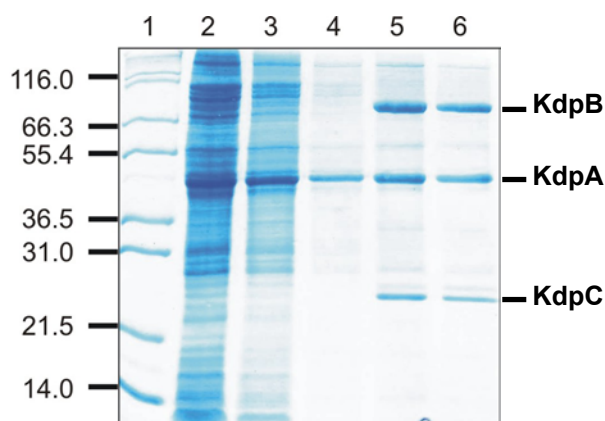

Figure 11: Purification scheme of a D583A mutant KdpFABC complex. A Coomassie stained 12 % Laemmli-gel showing the different purification steps. 10 µg protein were loaded to each lane. (1) molecular mass standard (in kDa); (2) solubilized membrane extract; (3) flow through fraction; (4) third washing fraction; (5) first elution fraction; (6) second elution fraction.

Biochemical characteristics of the D583A, D583E, and K586R mutants were examined in more detail, using ATPase activity assays. The D583A, D583E, and K586R mutant enzyme complexes exhibited similar ATPase activities compared to the wild-type enzyme complex. The ATPase activities of D583A are shown in figure 12. Although, the maximal activity is comparable between D583A and wild-type enzyme, the ATPase activity of the D583A mutant was not further stimulated by potassium; furthermore, the mutant was more resistant towards *ortho*-vanadate. Interestingly, the D583E mutant exhibited potassium stimulated ATPase activity and *ortho*-vanadate inhibition comparable to the wild-type enzyme (figure 13).

Purification of the K586A complex was not successful, because the KdpB subunit was found to be degraded. This degradation must have occurred already in the growing cells, since no protease inhibitor cocktail, added during purification, could prevent KdpB degradation. However, it was possible to purify and characterize the K586R complex. Interestingly, this derivative displayed a potassium stimulated ATPase activity, although the effect of K^+ was reduced compared to the wild-type enzyme (figure 14). Moreover, the K586R complex was more resistant towards *ortho*-vanadate, similar to the results of the D583A complex.
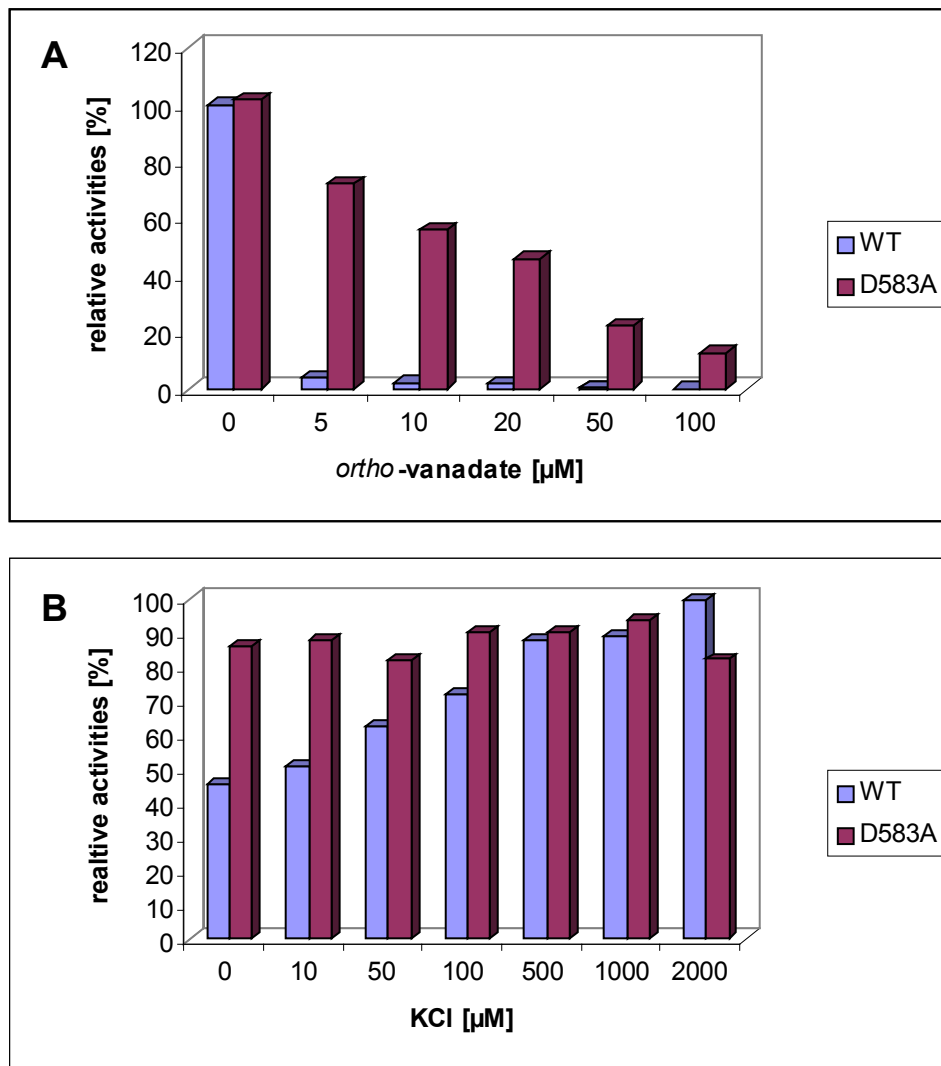
Figure 12: ATPase activities of the KdpFABC and D583A complex. Enzymes were solubilized with decylmaltoside (0.2 %). The upper plot (**A**) shows the *ortho*-vanadate inhibition of the ATPase activity. The lower plot (**B**) shows the effect of potassium towards the ATPase activity. The maximal wild-type activity (3164 nmol mg^{-1} min^{-1} for the KCl stimulation and 2736 nmol mg^{-1} min^{-1} for the vanadate inhibition experiment) was set to 100 %. The activities are mean values out of three independent measurements.
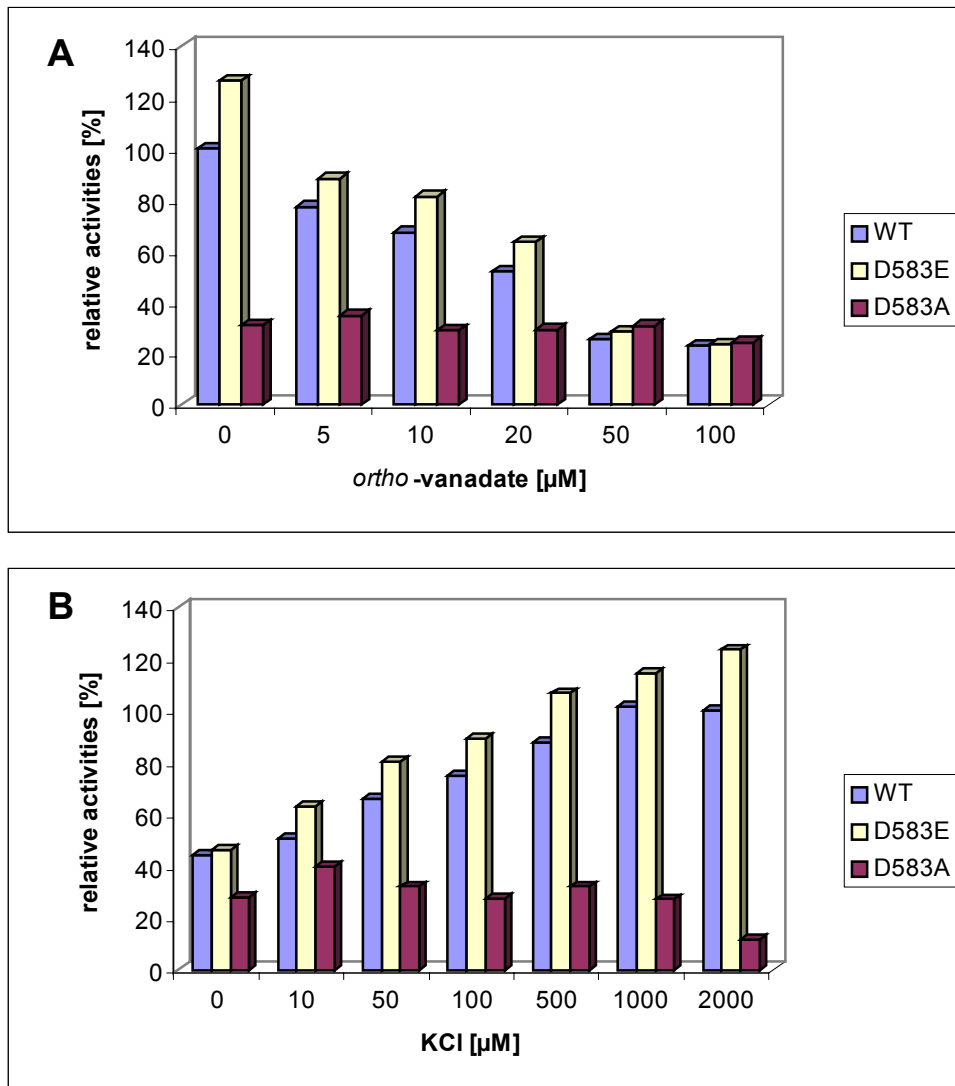
Figure 13: Comparison of ATPase activities between the D583A, D583E and wild-type KdpFABC complexes. Enzymes were solubilized with aminoxide (0.2 %). The upper plot (**A**) shows the *ortho*-vanadate inhibition of the ATPase activities. The lower plot (**B**) shows the effect of potassium towards the ATPase activities. The activities are the mean out of three independent measurements. The maximal wild-type activity (4950 nmol mg^{-1} min^{-1} for the KCl stimulation and 4370 nmol mg^{-1} min^{-1} for the vanadate inhibition experiment) was set to 100 %.
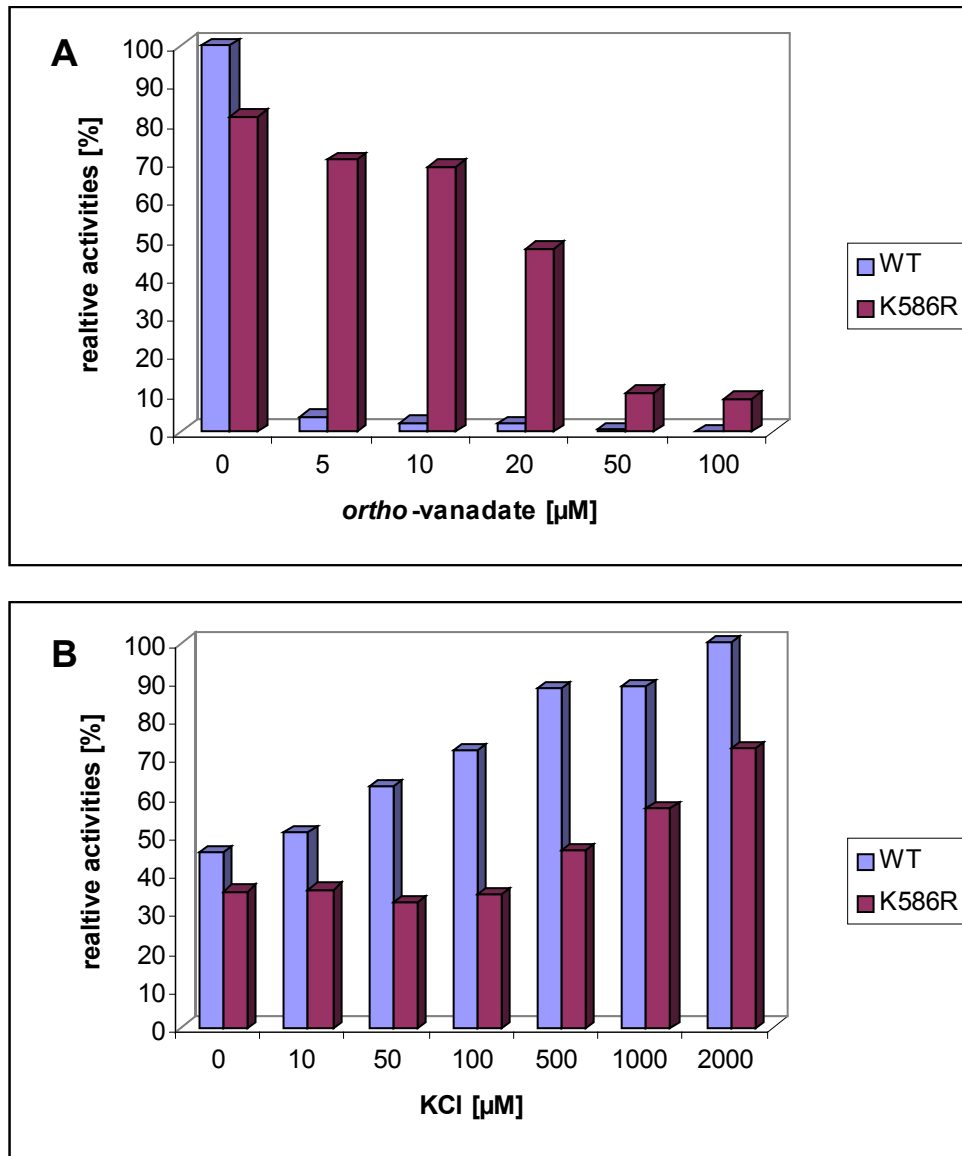
Figure 14: ATPase activities of the KdpFABC wild-type and K586R complex. The K586R enzyme complex was solubilized with aminoxide (0.2 %). The wild-type (WT) was solubilized with decylmaltoside (0.2 %). The upper plot (**A**) shows the *ortho*-vanadate inhibition of the ATPase activity. The lower plot (**B**) displays the effect of potassium towards the ATPase activity. The maximal wild-type activity (3164 nmol mg^{-1} min^{-1} for the KCl stimulation and 2736 nmol mg^{-1} min^{-1} for the vanadate inhibition experiment) was set to 100 %. The activities are mean values out of three independent measurements.

3.2.2. Transport activities of the reconstituted D583A and D583E complexes

Reconstitution of the altered complexes into proteoliposomes was performed, to test whether the D583A and D583E derivatives are able to transport K$^+$ ions. KdpFABC reconstitution into liposomes as described by Fendler *et al.* (1996) and Dröse (1997), is a well-established method to demonstrate indirectly the electrogenic K$^+$ transport, mediated by the Kdp-ATPase. Gaßel (1999) described a modified reconstitution protocol using protein complexes solubilized with dodecylmaltoside. Since decylmaltoside was comparably well suited for the reconstitution of the Kdp complex and was found

to preserve a higher specific activity of the solubilized Kdp-ATPase, decylmaltoside solubilized protein was used for reconstitution. The proteoliposomes were loaded with 50 mM KCl and 20 µl of proteoliposomes were used in a total reaction volume of 1 ml. Addition of the potential sensitive dye $DiSC_3(5)$ increased the fluorescence, which was calibrated to 100 %. The transport of K^+ from the lumen of the proteoliposome into the medium was mediated by inside-out reconstituted Kdp-ATPase molecules started by addition of 1 mM Na_2ATP. The loss of positive charges in the lumen of the proteoliposome led to a fluorescence decrease. Addition of 100 µM *ortho*-vanadate completely inhibited the Kdp-ATPase and resulted in a slow backflow of K^+, since the proteoliposomes were not tightly sealed (figure 16 part A). The K^+ ionophore valinomycin completely abolished the potential by transporting the K^+ along the gradient into the proteoliposomes, thus showing that the potential was generated by K^+ transport. In contrast, the D583A complex did not show any transport activity at all (figure 16 part B), whereas the D583E enzyme did show transport activity, although to a much smaller extent as the wild-type KdpFABC complex. In order to test, whether the reconstituted D583A complex were still exhibiting ATPase activity, the same proteoliposomes, used for the transport assay, were used for an ATPase assay. The D583A complex showed specific activity of 6300 nmol mg^{-1} min^{-1}. The activity of the mutant enzyme was only inhibited to 47 % (3362 nmol mg^{-1} min^{-1}) by 100 µM *ortho*-vanadate, reflecting the same relative resistance as observed in the solubilized state (figure 15). In summary, it can be stated that mutations at the charged residue Asp583 led to an uncoupling of K^+-transport and ATP hydrolysis, while the conservative exchange D583E still allows K^+-translocation, although to a much lower extent.
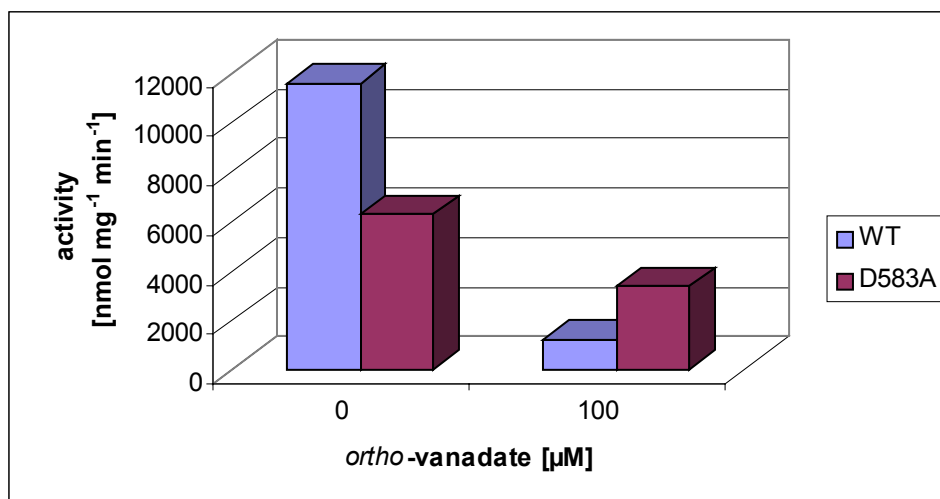
Figure 15: ATPase activity of KdpFABC-His$_{10}$ and KdpFABC-His$_{10}$-D583A reconstituted in proteoliposomes. Proteoliposomes were prepared as described in experimental procedures (2.5.5.). The test was carried out in 20 mM HEPES-Tris pH 7.8, 2 mM $MgCl_2$, and 1 mM KCl. In a total reaction volume of 50 µl, 1 µl proteoliposomes were used.
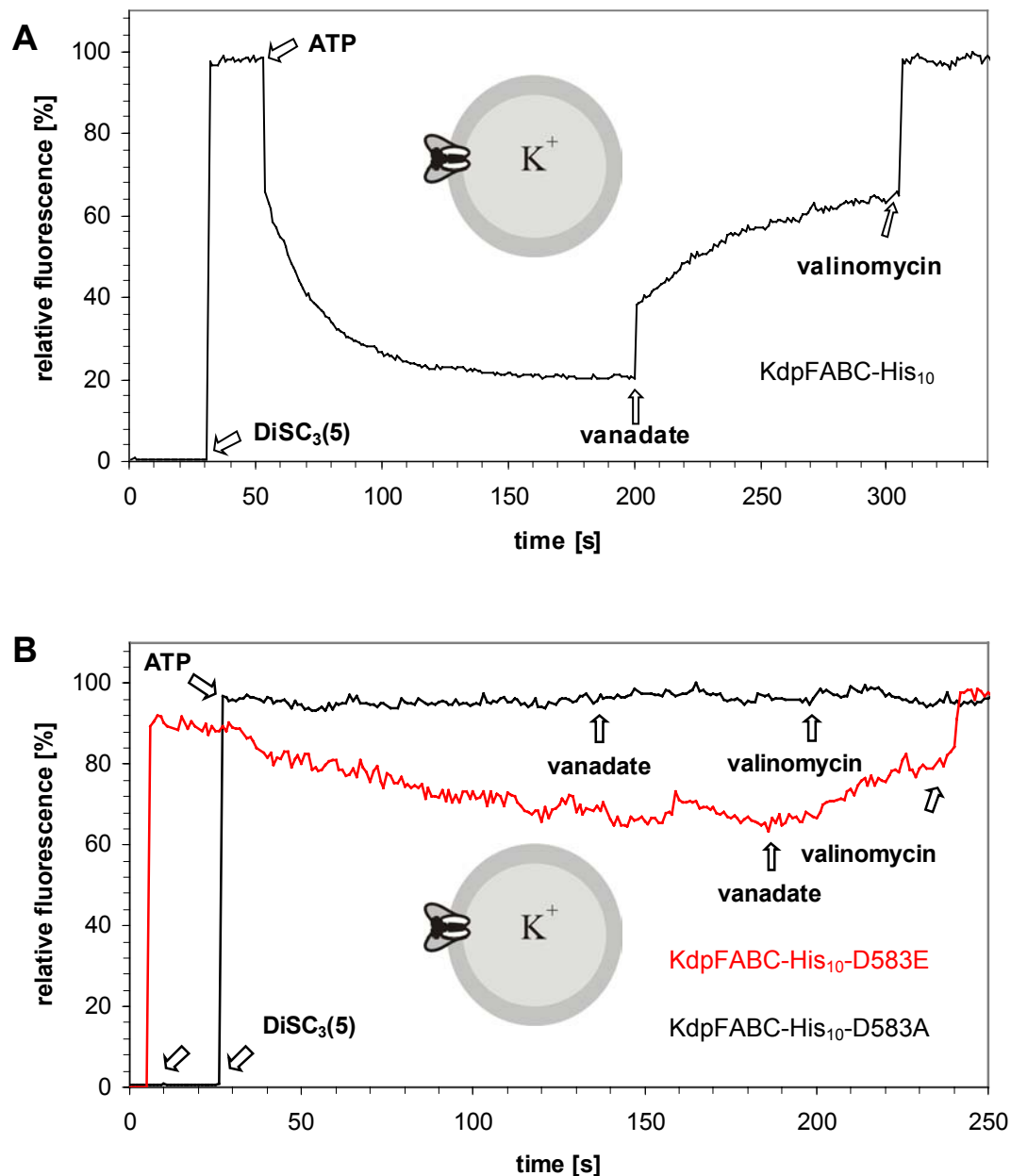
Figure 16: Electrogenic K$^+$-transport of reconstituted KdpFABC-His$_{10}$ wild-type, -D583E, and -D583A complexes. Reconstitution of the KdpFABC complexes was performed as described (2.5.5.). DiSC$_3$(5) fluorescence measurements were performed as described (2.6.7.) using 20 µl proteoliposomes in a 1 ml reaction volume. KdpFABC-His$_{10}$ (WT) complex (plot **A**), the D583A, and D583E complexes (plot **B**) complexes were solubilized with decylmaltoside. The buffer contained 50 mM KCl, both inside the proteoliposomes and outside. Substances were added in following concentrations: 1 mM ATP, 100 µM *ortho*-vanadate, and 1 µM valinomycin. The maximal fluorescence was set to 100 %.

3.3. Biochemical properties of the KdpFABC complex

3.3.1. Modification of the KdpFABC complex with FITC

For P-type ATPases, like the Na^+, K^+-ATPase (Karlish, 1980) and the Ca^{2+}-ATPase (Pick, 1980), it was shown that incubation with stoichiometric concentrations of FITC leads to complete inactivation of ATP hydrolysis. The conserved lysine residues K501 and K515 in the sodium pump and the Ca^{2+}-ATPase, respectively, were found to be modified by FITC (Farley *et al.*, 1984; Pick and Bassilian, 1981). These lysine residues belong to a conserved KGAPE motif that is found in many P-type ATPases (for review, see: Møller *et al.*, 1996). The KdpB subunit of *E. coli* shares this motif with other P-type ATPases, but only the first two amino acids 395-KG are identical to the KGAPE motif of the eukaryotic P-type ATPases (KGSV motif in KdpB.). Therefore, it was unclear, whether the FITC molecule exclusively binds to lysine residue 395 in KdpB. Previous labeling studies showed that FITC binds to all three large Kdp subunits (figure 17), KdpABC, respectively (Siebers, 1988).

Figure 17: FITC labeling of the KdpFABC complex. 20 μg protein were incubated with 15 µM FITC in either 50 mM Tris-HCl pH 9.2, 12.5 mM histidine, and 1 mM $MgCl_2$ (lane 1) and 50 mM Tris-HCl pH 9.2, 150 mM choline chloride, 12.5 mM histidine, and 1 mM $MgCl_2$ (lane 2). Incubation was done for 30 minutes at 37°C in the dark. The reaction was stopped by adding SDS sample mix. The whole samples were applied to SDS-PAGE and the gel was visualized under UV-light (366 nm).
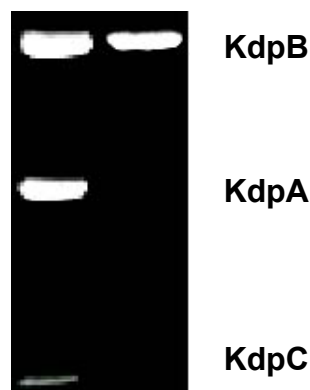
Addition of salts like NaCl or choline chloride (thus maintaining high ionic strength) reduced the unspecific labeling of Kdp subunits by FITC. Addition of 150 mM choline chloride in the labeling buffer led to a specific modification of KdpB (figure 17). The modified KdpFABC complex was separated using SDS-PAGE. Subsequently, the band corresponding to KdpB was cut out and treated with CNBr. This cleavage results in a distinct band pattern (Altendorf and Dröse, unpublished results) showing six major digestion products. After blotting still two of these bands were exhibiting the characteristic FITC fluorescence (figure 18). Amino acid sequencing showed that both peptides contained the lysine residue 395. The bigger fragment was cleaved after methionine 383 (sequence, see figure 18). Sequencing of the smaller peptide showed that the cleavage site was behind methinonine 392. This partially incomplete digestion was typical for KdpB. Both peptides were part of the putative N-domain of KdpB (the N-domain contains the amino acid residues 310-445). In analogy to other P-type ATPases, the FITC binding site was located within the putative N-domain of KdpB and hence most probably Lys395 was covalently labeled by FITC.

Figure 18: CNBr cleavage of a FITC-modified KdpB subunit. The Kdp-ATPase (250 µg) was labeled with 15 µM FITC for 30 minutes. The complex was separated by gel electrophoresis. The KdpB band was cut from the gel and cleaved with CNBr. The peptides were transferred onto a nitrocellulose membrane. Examination of the blot membrane under UV light revealed that two of these bands still showed the typical FITC fluorescence. The sequences of the labeled peptides were determined by amino acid sequencing (Roland Schmid, personal communication). The sequences of the peptides 1. and 2. are shown on the right panel. In bold is the conserved sequence of the FITC binding site in P-type ATPases. In red are lysine residues within the peptide fragments 1. and 2.

3.3.2. Influence of nucleotides on the FITC modification

The fluorescent dye FITC was shown to bind specifically in or nearby the high affinity nucleotide binding site of P-type ATPases (Karlish, 1980; Pick and Karlish 1980; Pick, 1981; Tran and Farley, 1986). For KdpB it was demonstrated in the previous section that FITC binds within the putative nucleotide binding domain, probably to Lys395. The FITC modification of the KdpB subunit was prevented by preincubation with adenine nucleotides (figure 19). Interestingly, AMP protected the solubilized enzyme even better than ATP or ADP, whereas in the case of the Na$^+$, K$^+$-ATPase, AMP had no effect on FITC modification (Karlish, 1980; Gatto *et al.*, 1998). In analogy to the Na$^+$, K$^+$-ATPase, it was found that ATP and ADP protect the Kdp-ATPase from modification by FITC. Other nucleotides like GTP or ITP had no effect on the FITC modification of the Kdp-ATPase. SDS denatured enzyme was not modified by FITC, indicating the necessity of a proper folded nucleotide binding domain for FITC binding (figure 19).
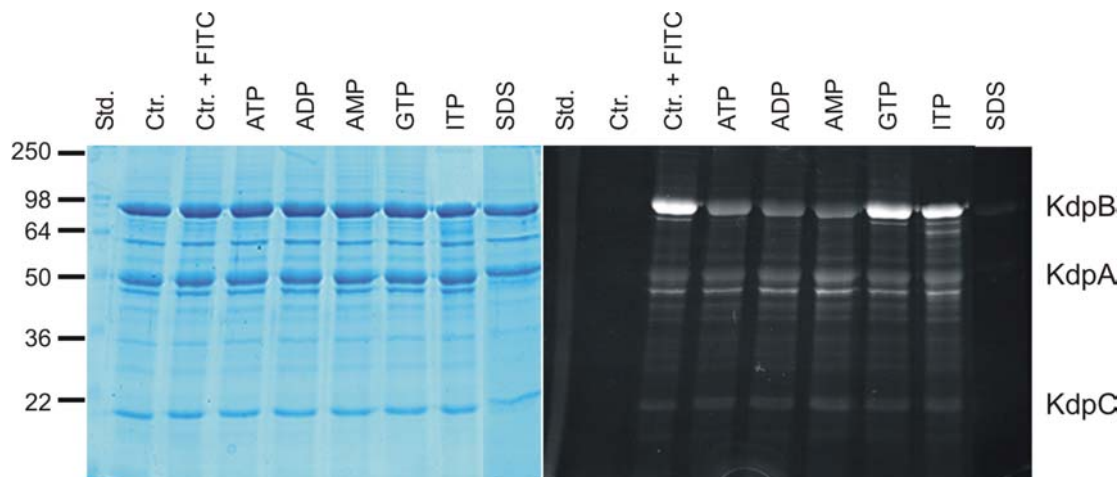
Figure 19: Influence of nucleotides on the FITC modification of KdpB. The Kdp-ATPase (10 µg) was labeled with 15 µM FITC. In order to examine the effect of nucleotides towards the FITC modification the Kdp-ATPase was incubated for 5 minutes with 5 mM of the indicated nucleotides. The abbreviations used are: Std., molecular weight marker (kDa); Ctr., protein without FITC added; Ctr. + FITC, protein incubated with FITC without added nucleotides; ATP, Kdp-ATPase incubated with 5 mM ATP prior FITC addition; ADP, AMP, GTP, ITP, enzyme incubated with the indicated nucleotides prior FITC labelling, respectively; SDS, denatured Kdp-ATPase using 1 % sodium dodecylsulfate prior FITC addition. The left panel shows a Coomassie blue stain of the acryl amide gel, while the right panel shows the same gel under UV light before staining.

3.3.3. *p*-Nitrophenyl phosphatase activity of the Kdp-ATPase

Eukaryotic P-type ATPases lack a stringent substrate specificy for both substrate hydrolysis and phosphorylation. Compounds such as acyl phosphate, carbamyl phosphate, *p*-nitrophenyl phosphate and purine nucleotides were shown to be suitable phosphate donors for the Ca^{2+}-ATPase (Inesi, 1971; Pucell and Martonosi, 1971; Nakamura and Tonomura, 1978; Rossi *et al.*, 1979; Bodley and Jencks, 1987). Compared to these enzymes the Kdp-ATPase has a more narrow substrate specificy (Siebers, 1988). In contrast to earlier observations, a Mg^{2+} dependent pNPP hydrolysis of the purified enzyme could be measured. Mg^{2+} was essential for pNPP hydrolysis, as it is in case of all P-type ATPases (figure 21). The kinetics followed a classical Michaelis-Menten scheme (figure 20) with an apparent K_M of 2,9 mM for the purified wild-type enzyme and a maximal reaction velocity of 11 µmol mg^{-1} min^{-1}. It should be noted that the rate of hydrolysis of pNPP by the Kdp-ATPase was constant for more than 30 minutes, thus allowing to use an endpoint determination for kinetic analysis.
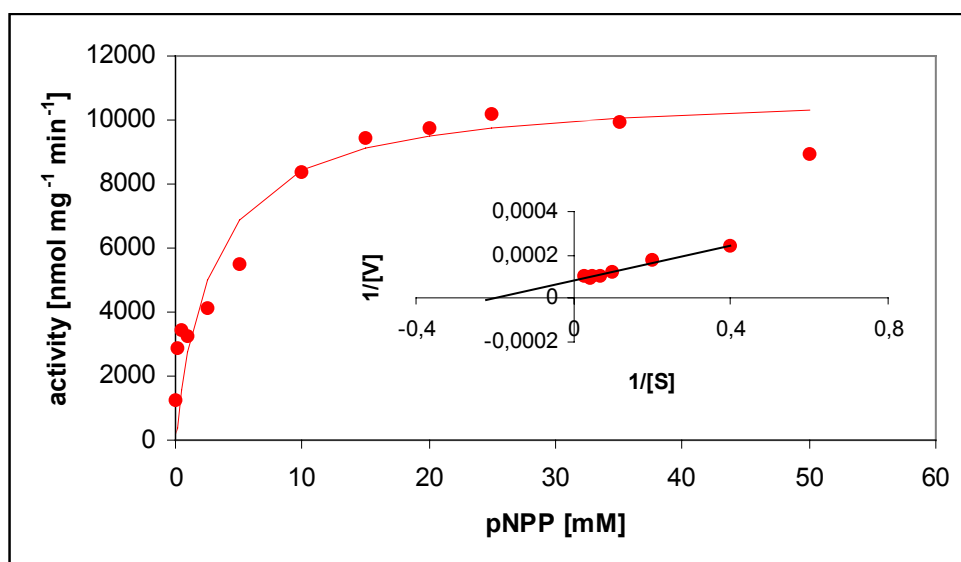
Figure 20: Hydrolysis of pNPP by the Kdp-ATPase. Shown is a Michaelis-Menten diagram of the pNPP hydrolysis mediated by the Kdp-ATPase. The enzyme concentration was 50 mg ml^{-1}. The pNPP hydrolysis was measured for 30 minutes and stopped with 100 µl 0.1 M NaOH. The specific activity was calculated with a *p*-nitrophenol standard curve. All data points are mean values out of three independent experiments, the mean of three non-enzyme controls were subtracted. Equimolar concentration of MgCl$_2$ and pNPP were used in all cases (indicated on the X-axis). A double reciprocal plot is shown in the inset.
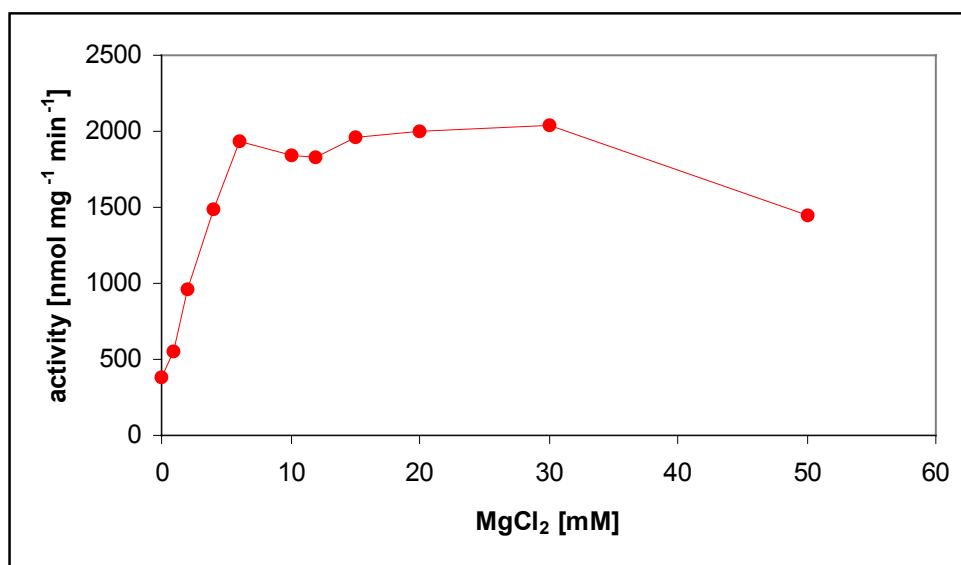
Figure 21: Mg^{2+} dependency of the pNPP hydrolysis. 50 µg ml^{-1} KdpFABC complex were incubated with different MgCl$_2$ concentrations for 5 minutes. The pNPP hydrolysis was measured by adding 15 mM pNPP. The pNPP hydrolysis was measured for 30 minutes and stopped with 100 µl 0.1 M NaOH. The specific activity was calculated with a *p*-nitrophenol standard curve.

Figure 22: pH dependency of pNPP hydrolysis. The pH dependency of the pNPP hydrolysis mediated by the KdpFABC complex was measured in buffer systems with different pH values. For pH 5.5 MES was used, between pH 6.0 and pH 7.5 HEPES-Tris was used and tests between pH 7.8 and pH 9.5 were carried out in Tris-HCl. All buffer solutions contained 15 mM $MgCl_2$ and the reaction was started by adding 15 mM pNPP.

The pH optimum of this reaction was found to be in the same range (pH 8.0 – pH 8.5) as determined for the ATPase activity (pH 7.8) (Siebers, 1988). Since pNPPase is stimulated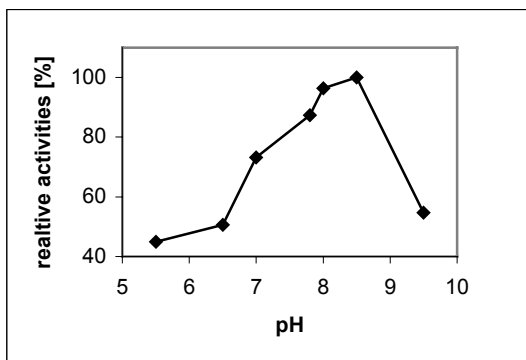 by potassium ions in the case of the sodium pump (Robinson *et al.*, 1983) and since it was proposed that the Kdp-ATPase has a similar reaction cycle (Fendler *et al.*, 1999), the influence of ions towards the pNPP hydrolysis was tested. K^+, Rb^+, Na^+, and NH_4^+ had no stimulating effect on the pNPP hydrolysis. However, it was found that potassium, ammonium and rubidium ions slightly inhibit the pNPP hydrolysis (data not shown). In contrast to the sodium pump the Kdp-ATPase shows no ion stimulated pNPPase activity. Addition of sucrose had no effect on the pNPP hydrolysis (data not shown).

3.3.4. Influence of *ortho*-vanadate on the ATPase and pNPPase

The phosphate analogue *ortho*-vanadate was previously shown to inhibit the ATPase activity of the Kdp-ATPase (Siebers *et al.*, 1988). Here, the inhibitory effect of *ortho*-vanadate towards the ATPase and pNPPase activity is compared. It can be seen in figure 23 that the inhibition kinetic of *ortho*-vanadate towards the ATP hydrolysis is more complex compared to the inhibition of the pNPPase activity. Like other P-type ATPases the Kdp-ATPase exhibits a non-linear kinetics in a double reciprocal plot of the ATP hydrolysis, indicating the non-Michaelean kinetic. The Michaelis-Menten plot of the ATP hydrolysis of the Kdp-ATPase is sigmoid (figure 23) with a corresponding Hill coefficient of 1.4, indicating allosteric or cooperating effects of the ATP binding sites.

The K_i values for the ATPase activity were determined to be 19.9 µM in the presence of potassium and 21.62 µM in the absence of potassium. At low ATP concentrations, less than 200 µM ATP, the double reciprocal plot showed a true uncompetitive inhibition kinetics, indicating that the inhibitor could bind both, enzyme and enzyme-substrate complex, with almost the same affinity. The feature of uncompetitive inhibition is an increasing K_M and increasing V_{max} with increasing inhibitor concentrations. However, at higher ATP concentrations (above 500 µM ATP) the ATPase activity was inhibited strictly non-competitive by *ortho*-vanadate (figure 24).

The *ortho*-vanadate inhibition of the pNPPase activity mediated by the Kdp enzyme was not as complex. Figure 25 shows that the inhibition kinetics of the pNPP hydrolysis was competitive with an

apparent K_i of 1.35 µM. The K_i value could also be calculated using the following equation: $K_{M(app)} = K_M(1+[I]/K_i)$.
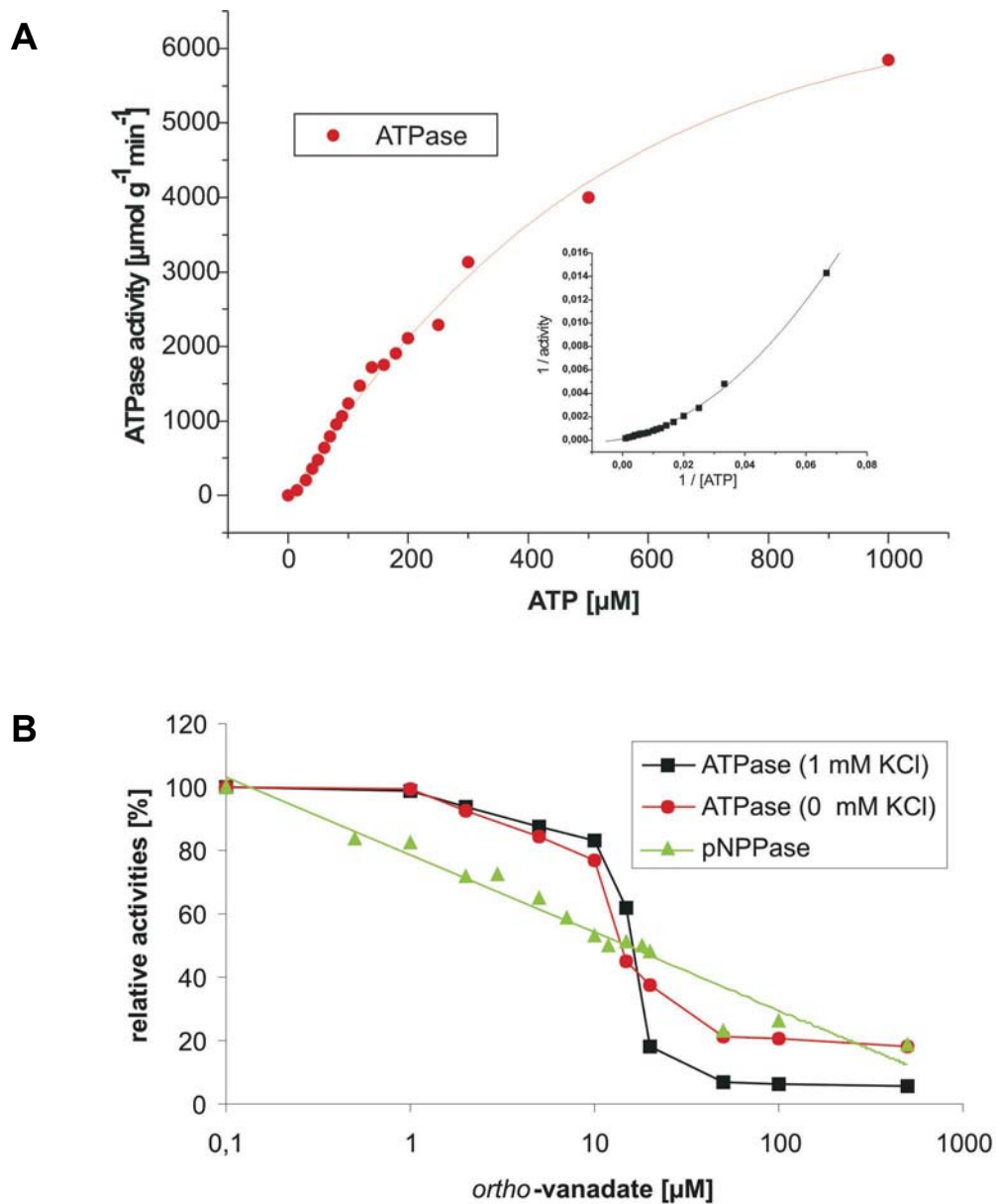
Figure 23: ATPase activity of KdpFABC and *ortho*-vanadate inhibition of ATPase and pNPPase activity.
(**A**) ATPase activity of the Kdp-ATPase in the solubilized state. 0.5 µg purified KdpFABC complex were used in the microtiter ATPase assay as described in experimental procedures (2.6.5.). The inset in **A** displays a double-reciprocal plot fitted by a 2. order polynom. (**B**) Relative activities of pNPP hydrolysis and ATPase activity with and without potassium were plotted against the *ortho*-vanadate concentration. 0.5 µg purified KdpFABC complex were used in the microtiter ATPase assay as described in experimental procedures (2.6.5.). The KdpFABC ATPase was incubated with *ortho*-vanadate for 5 minutes at 37°C prior ATP (1 mM) addition.

A

B
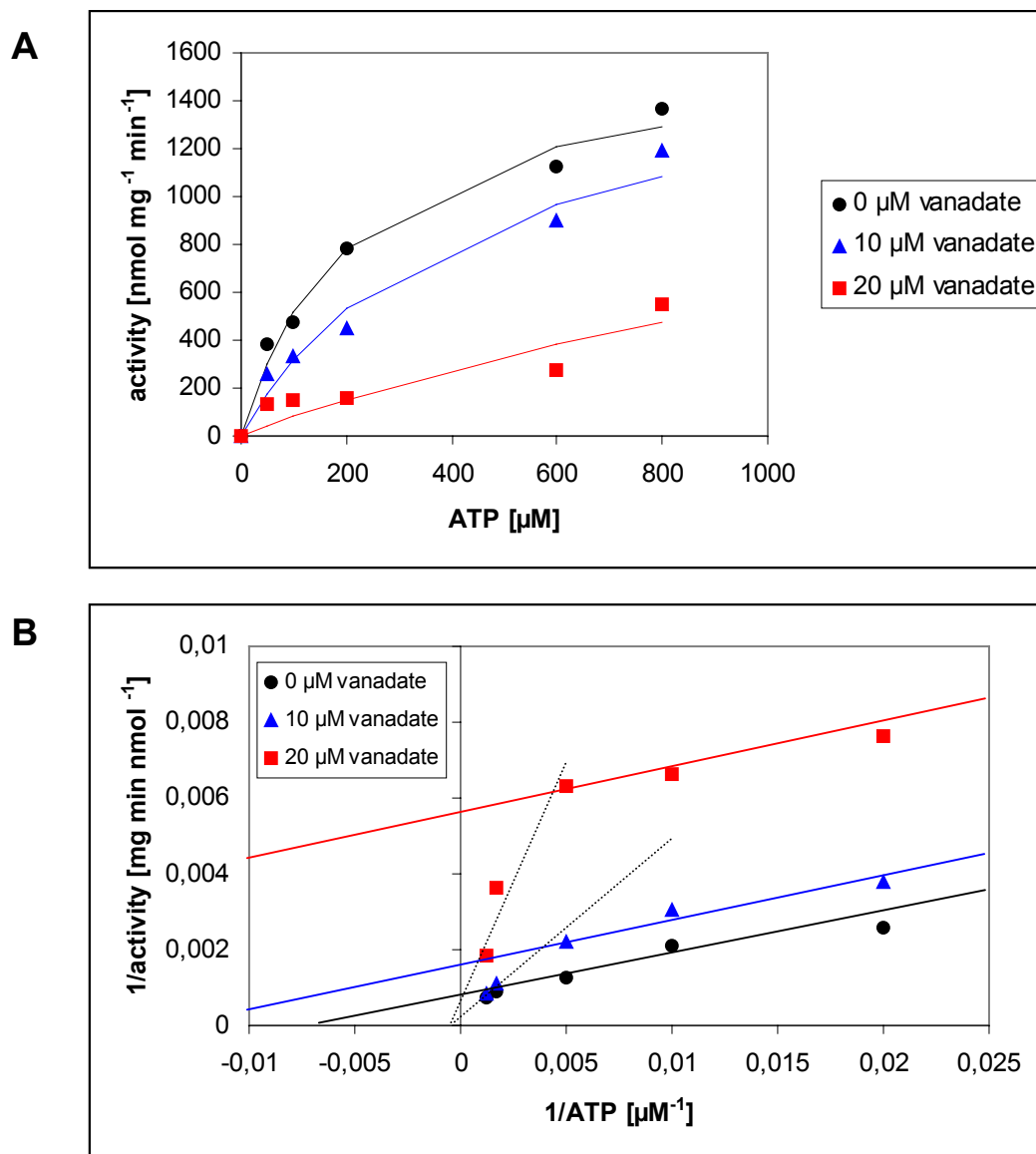
Figure 23: Inhibition kinetics of *ortho*-vanadate on ATP hydrolysis. The ATP hydrolysis was measured at varying ATP concentrations with and without prior adding of *ortho*-vanadate. The enzyme (0.5 µg) was pre-incubated with the inhibitor for 5 minutes at 37°C. The reaction was started by adding ATP solution as described in experimental procedures (2.6.5.). (**A**) A Michaelis–Menten plot of the Kdp-ATPase activity with 0 µM, 10 µM, and 20 µM *ortho*-vanadate. (**B**) A double reciprocal plot of the kinetics showing a typical uncompetitive inhibition at low ATP concentrations and a non-competitive inhibition of *ortho*-vanadate at high ATP concentrations. Lines in **B** were drawn by eye.
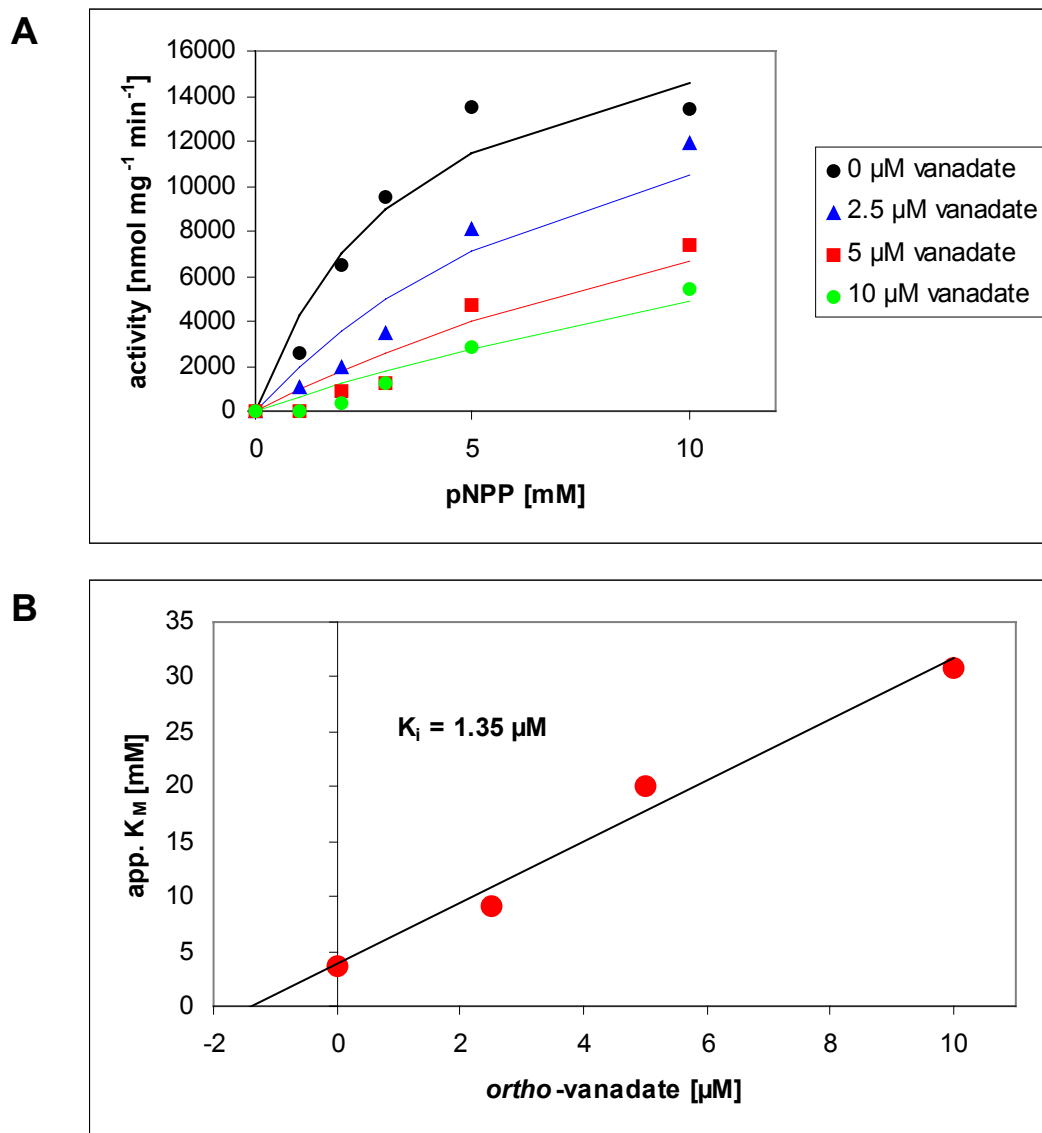
Figure 25: Inhibition kinetics of *ortho*-vanadate towards pNPP hydrolysis. (A) A classical Michaelis-Menten plot of *ortho*-vanadate inhibition of the pNPP hydrolysis is shown. The enzyme (5 µg) was pre-incubated with the inhibitor for 5 minutes at 37°C. The reaction was started by adding pNPP solution as described in experimental procedures (2.6.6.). The reaction product *p*-nitrophenolate was measured in an ELISA reader at 410 nm. **(B)** The inhibition kinetic is competitive, as indicated by the linear correlation between the apparent K_M values observed for pNPP hydrolysis in the presence of different inhibitor concentrations. The calculated K_i was 1.35 µM *ortho*-vanadate.

3.3.5. Influence of adenine nucleotides on the pNPPase activity

It was reported for the Na^+, K^+-ATPase (Scheiner-Bobis *et al.*, 1993) that low concentrations of ATP stimulate the hydrolysis of pNPP while concentrations above 100 µM inhibit this reaction. For the sarcoplasmatic reticulum Ca^{2+}-ATPase it was reported that the fluorescein derivatives eosin and erythrosin were able to stimulate pNPP hydrolysis in the presence of Ca^{2+}. In the absence of the transported ion this effect was abolished (Mignaco *et al.*, 1996). This turnover was not due to a change on the apparent affinity for substrate, but is indeed due to the acceleration of the turnover

51

A

B
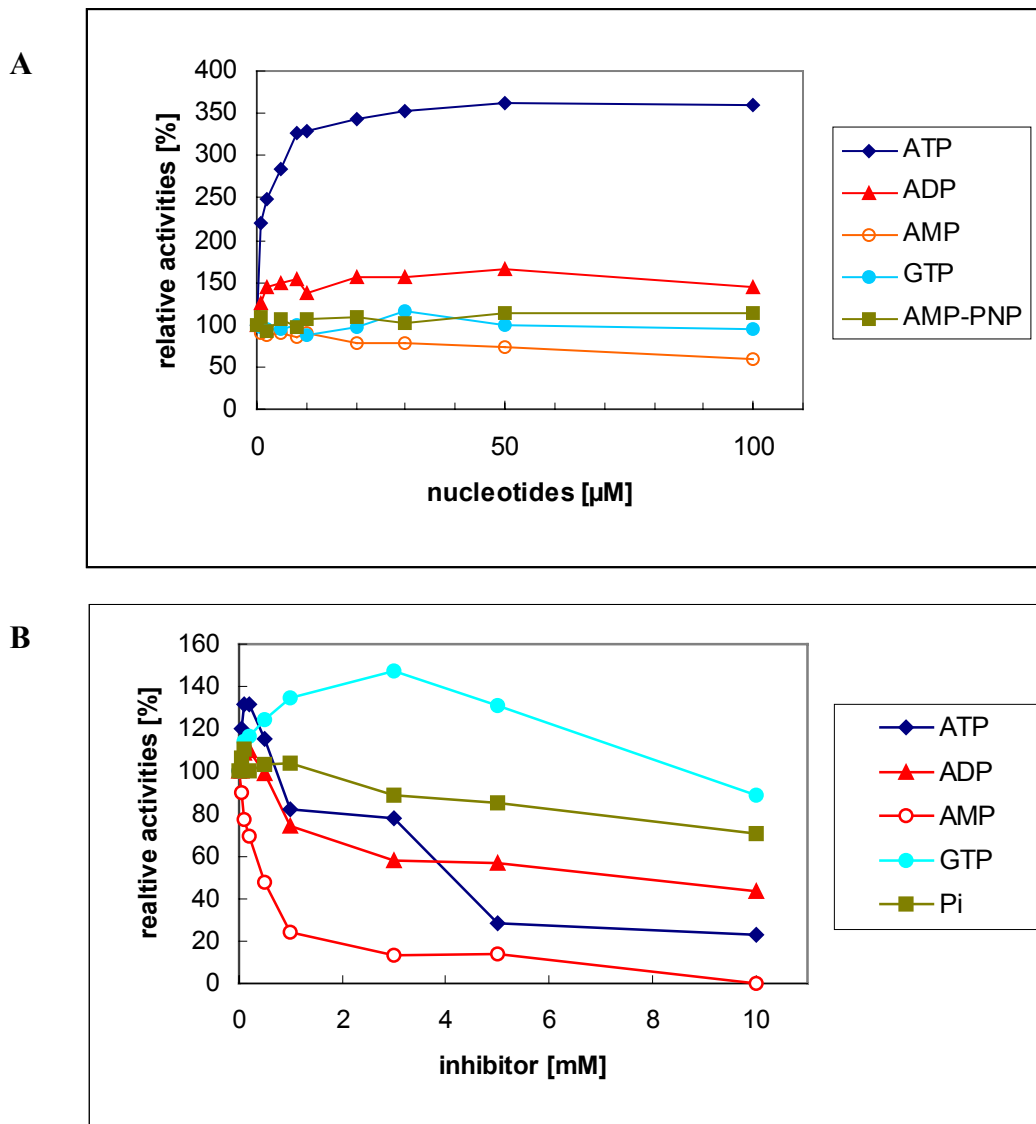
Figure 26: Effect of nucleotides towards the pNPP hydrolysis of the KdpFABC complex. Prior pNPP addition, the KdpFABC complex (5 µg) was incubated for 5 minutes with the different nucleotides (or P_i) in HEPES-Tris, pH 7.8, 15 mM $MgCl_2$. The pNPPase reaction was started with 15 mM pNPP and stopped by addition of 0.1 M NaOH after 15 minutes. (**A**) Shown is the effect of nucleotides in a range below 100 µM. (**B**) Shown is the inhibitory effect of nucleotides and P_i in a mM range. The activities are indicated as percent values with an activity of 2066 µmol g^{-1} min^{-1} as 100 % value.

rate of the enzyme. The pNPP hydrolysis of the Kdp-ATPase was shown to be stimulated up to three-fold at ATP concentrations below 100 µM (figure 26, part A). The stimulation reached a maximum at 30 µM ATP and at ATP concentrations higher than 500 µM an inhibition of the pNPPase activity was observed. ADP showed only a very slight stimulatory effect while other nucleotides like AMP had no effect. Even the unhydrolysable ATP analogue AMP-PNP had no stimulatory effect, indicating that ATP hydrolysis was necessary for this stimulation. GTP was found to have a slight stimulatory effect at higher concentrations (3 mM) (figure 26.). ATP, ADP, and inorganic phosphate showed an inhibitory effect at milli-molar concentrations with K_i values of 2.7 mM for ATP, 4.5 mM for ADP

and 25.6 mM for P_i. In contrast, a potent inhibition of the pNPPase activity with AMP with an apparent K_i around 500 µM was observed (Table 6).

Table 6.: K_i values of inhibitors of the hydrolytic activities of the Kdp-ATPase. The K_i values for different inhibitors are listed. All inhibitors were pre-incubated with the enzyme solution before starting the reaction with ATP or pNPP, respectively. n.d., not determined

Inhibitor	pNPPase	ATPase
FITC	at pH 7.5: 30.1 µM	at pH 7.5: 32.1 µM
		at pH 9.2: 3.08 µM
ortho-vanadate	1.35 µM	+ K^+: 19.9 µM
		- K^+: 21.6 µM
ATP	2.69 mM	n. d.
ADP	4.5 mM	n. d.
AMP	0.51 mM	n. d.
P_i	25.6 mM	n. d.
GTP	73 mM	n. d.

3.3.6. Comparison of the FITC effect on the pNPPase and ATPase activities

Labeling with FITC has extensively been used as a tool to study effects related to the nucleotide binding sites of various P-type ATPases (Pick and Karlish 1980; Pick, 1981; Rephaeli *et al.*, 1986; Ward and Cavieres, 1998). It was reported that the covalently bound FITC inhibited ATP hydrolysis in a submilimolar range. However, it is well known that FITC labeled Ca^{2+}-ATPase and Na^+, K^+-ATPase were still able to hydrolyze *p*-nitrophenyl phosphate (Scheiner-Bobis *et al.*, 1995; Ward and Cavieres, 1998; Donnet *et al.*, 1998). Here, the effect of the FITC modification of KdpB towards the ATPase and pNPPase activity is described. In contrast to the larger eukaryotic ATPases mentioned above the inhibitory kinetics of FITC for ATPase and pNPPase activity were identical in case of KdpB (figure 27).
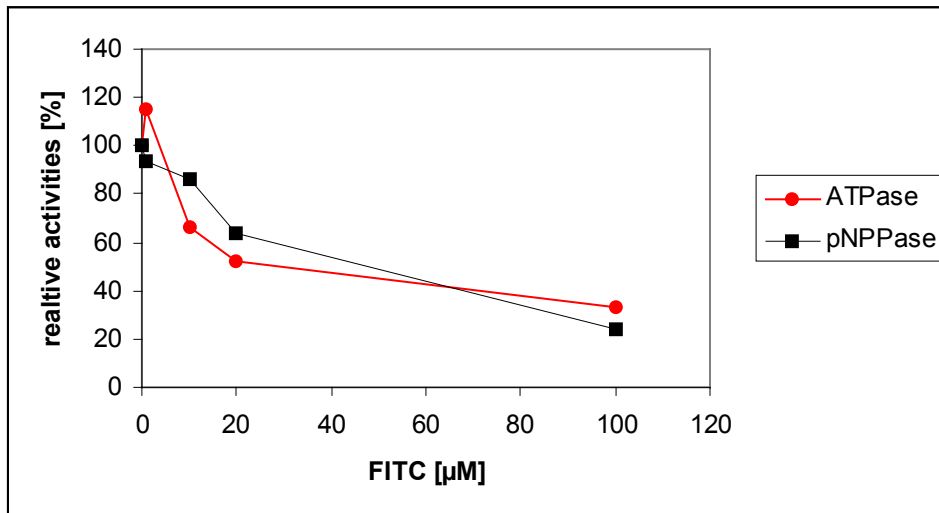
Figure 27: Comparison of FITC inhibition on ATPase and phosphatase activity. The inhibitory effect of FITC towards ATPase activity and pNPP hydrolysis was tested using the microtiter assay described in experimental procedures (2.6.5. and 2.6.6.). In order to compare the inhibitory effect both activities are given as percent values with 10.2 µmol mg^{-1} min^{-1} as 100 % value for the pNPP hydrolysis (at 37°C) and 3.5 µmol mg^{-1} min^{-1} as 100 % value for the ATPase activity (at 37°C).
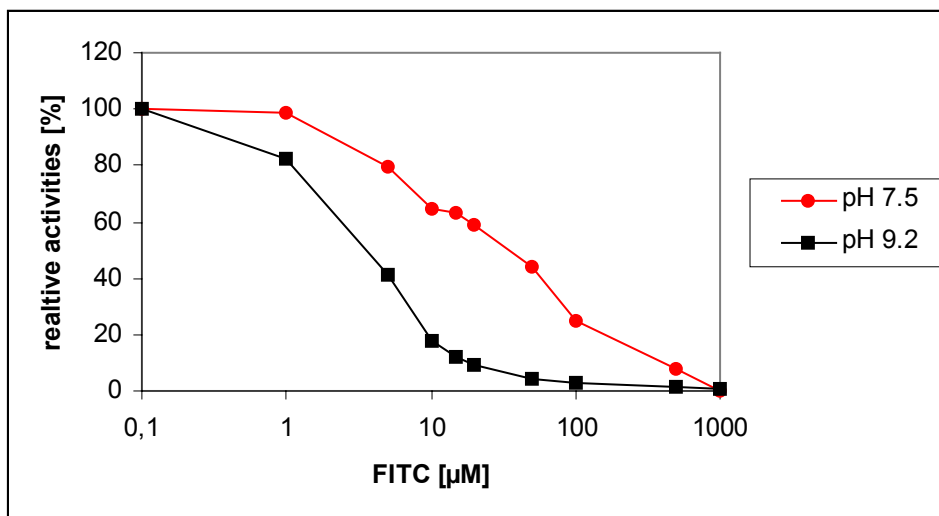
Figure 28: Influence of the pH value on FITC inhibition. Tested was the inhibition of the ATPase activity of KdpFABC by FITC at pH 7.5 and 9.2. Both measurements were done in 25 mM Tris-HCl buffer with the indicated pH values. 15 µM FITC were pre-incubated for 30 min at 37°C.

Since the pH optima for ATP and pNPP hydrolysis were in the same range (pH 8.0), measurements were performed at pH 7.8, although the K_i for FITC is shifted to 32 µM compared to a K_i around 3 µM at pH 9.2 (see figure 28). The FITC concentrations, used for half maximal or complete inhibition, were therefore adapted to these pH values, since protein activity was optimal around pH 7.8. The pNPP hydrolysis was inhibited by FITC with a K_i of 30 µM. Obviously, FITC has the same inhibitory effect on ATPase and pNPPase activity in case of the Kdp-ATPase.

3.4. Production and characterization of soluble subdomains of KdpB

The KdpB subunit is the catalytic subunit of the KdpFABC complex. Sequence similarities and biochemical features revealed that the Kdp-ATPase is a member of the P-type ATPase family (see introduction). As other members of this enzyme family, KdpB undergoes a reaction cycle with the subsequent formation of a phosphointermediate (Siebers and Altendorf., 1989). The hydrolysis of ATP is completely inhibited by micro-molar concentrations of *ortho*-vanadate, a well-known inhibitor of all P-type ATPases, as described above. The overall architecture of KdpB seems to resemble those of other P-type ATPases as indicated by sequence analysis and computer modeling based on the structural data of the Ca^{2+}-ATPase (section 3.1.). The large cytoplasmic loop of KdpB (H4H5) between helix four and helix five comprises the putative ATP binding loop of KdpB. The loop contains two separate modules, the phosphorylation domain - a classical Rossman fold - and the inserted nucleotide binding domain (compare figure 9). In order to assign different biochemical features to either the H4H5 loop, the nucleotide binding domain (KdpBN) of KdpB, and the H2H3 loop, all three *kdpB* parts were subcloned, separately expressed in *E. coli* and the corresponding proteins were purified and biochemically characterized.

3.4.1. Subcloning and expression of H2H3, H4H5, and KdpBN

Although, the Ca^{2+}-ATPase structure was not published at the intention of this thesis and consequently the KdpB model, presented here, was not invented, a construct containing all residues belonging to the large cytoplasmic loop of KdpB was developed using the conserved region of P-type ATPases (Serrano, 1988) as landmarks. The construct, named H4H5, ranged from methinonine 282 to glutamine 567 (figure 31, part B). The computed M_w of H4H5 was 32563.89 Da including the deca-histidinyl tag and linker.

Figure 29: pET16b expression vector. Characteristic traits: Multiple cloning sites (319-335), *lac*I coding sequence (869-1948), pBR322 origin (3885) and *bla* coding sequence (4646-5503).
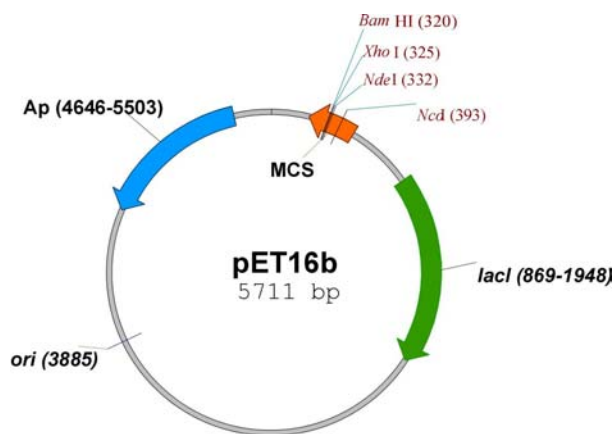
Primers were designed with *Nde*I and *Bam*HI restriction sites for a convenient cloning into the pET16b vector from Stratagene (La Jolla) (figure 29). Cloning of the corresponding PCR fragment of

KdpB into the pET16b vector resulted in the synthesis of the H4H5 protein carrying a N-terminal deca-histidinyl tag (sequence: MGHHHHHHHH HHSSGHGGRH). The resulting pET16bH4H5 vector was transformed in Bl21(DE) cells from Stratagene (La Jolla, USA). In order to lower the basal expression level Bl21(DE) /pLysS cells were used. The pLysS plasmid codes for a T7 lysozyme, which is an inhibitor of the T7 polymerase. After IPTG induction BL21(DE) / pLysS cells start to synthesize the T7 polymerase and hence the transcription of the H4H5 gene encoded by the pET16bH4H5 plasmid. Bl21(DE) /pLysS /pET16bH4H5 cells were grown in LB medium as described in experimental procedures. Figure 30 shows the expression of H4H5 achieved in Bl21(DE) cells grown in LB medium.
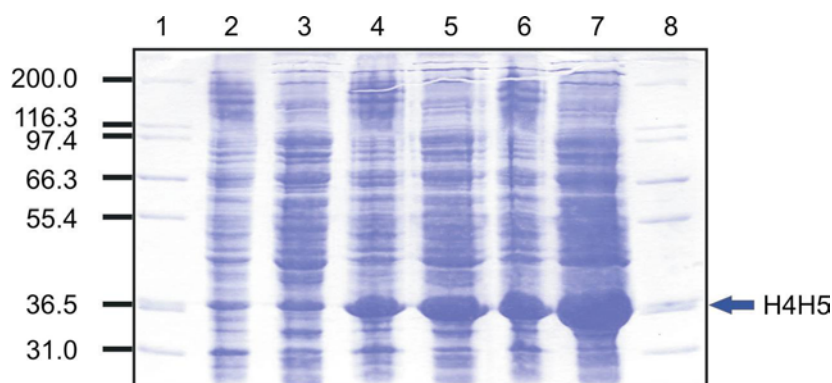
Figure 30: Synthesis of the H4H5 loop in Bl21(DE) /pLysS /pET16bH4H5 cells grown in LB medium. Cells were grown in LB medium and lysed using a Ribi cell fractionator. Insoluble material was removed by ultra centrifugation. The pellet containing the insoluble fraction was solved in Laemmli SDS sample buffer. The supernatant, containing the soluble proteins was mixed with SDS sample buffer. 5 μl of the resuspended pellets and the soluble extract were subjected to SDS-PAGE. (1) molecular mass standard (kDa); (2) 0 minutes induction, insoluble material; (3) 0 minutes induction, soluble proteins; (4) 1 h induction, insoluble material; (5) 1 h induction, soluble proteins; (6) 2 h induction, insoluble material; (7) 2 h induction, soluble proteins; (8) molecular mass standard (kDa).

It should be noted that the expression was also successful in K115 minimal medium (Epstein and Kim, 1971), which is a prerequisite for obtaining labeled proteins for NMR analysis (see section 3.5.). Induced cells were passed through a Ribi cell fractionator and insoluble material was removed by ultra centrifugation. The supernatant was applied to metal affinity chromatography. Protein purification was monitored by SDS-PAGE as demonstrated in figure 31.

A

B

Figure 31: Purification of the H4H5 loop. A: The H4H5 loop was purified using metal affinity chromatography. Aliquots from different purification steps were subjected to SDS-PAGE. Each lane was loaded with 5 µl of the following samples: (1) molecular mass standard (kDa); (2) whole cell extract of uninduced cells; (3) whole cell extract of induced cells; (4) soluble fraction after cell lyses; (5) flow through fraction; (6) washing step I; (7) washing step II; (8) elution fraction; (9) molecular mass standard. The purification procedure was done as described in experimental procedures. The binding buffer contained 10 mM imidazole, the washing buffer 60 mM imidazole, and the elution buffer was supplemented with 0.25 M imidazole.
B: H4H5 loop according to the KdpB model. Amino acids contributing to the H4H5 loop according to the KdpB model are colored in red (see section 3.1.). The structural model is based on the Ca^{2+}-ATPase structure (Toyoshima *et al.*, 2000) as described in section 3.1.

The experiments revealed that the H4H5 loop was soluble and synthesized in large amounts but the protein was degraded very fast. Even addition of different protease inhibitor cocktails during purification could not stop the degradation. Therefore, it is most likely that the H4H5 loop was degraded already within the cells. Furthermore, the formation of inclusion bodies was observed. However, this problem could partially be solved by shifting the growing cells from 37°C to 30°C prior induction.

As the next step only the N-domain (named KdpBN) was subcloned, expressed and purified. That part of the *kdpB* gene corresponding to the N-domain was cloned into the pET16b vector thus giving a deca-histinyl fusion protein. The computed M_w for the KdpBN protein including the deca-histidinyl tag was 17134.23 Da. Expression experiments in Bl21(DE) /pLysS /pET16bKdpBN were performed in analogy to the H4H5 domain. However, the temperature was not shifted to 30°C before induction, since KdpBN was much more stable compared to the H4H5 loop. Induction was also achieved by adding 1 mM IPTG to the cell culture, when an optical density between 0.7 and 1.0 was reached. Figure 32 shows the purification of KdpBN.

Figure 32: Purification of the KdpBN domain. A: The KdpBN domain was purified using metal affinity chromatography. Aliquots from different purification steps were subjected to SDS-PAGE. Each lane was loaded with 5 µl of the following samples: (1) molecular mass standard (kDa); (2) flow through fraction; (3) washing step I; (4) washing step II; (5) washing step III; (6) elution fraction I; (7) elution fraction II. The purification procedure was essentially performed as described in section 2.5.1. Washing step I was done in the presence of 10 mM imidazole and washing steps II and III were carried out in the presence of 60 mM imidazole. The elution buffer contained 0.25 M imidazole. The protein bands below the 17 kDa band of KdpBN are degradation products.

B: KdpBN domain according to the KdpB model. Amino acids contributing to the KdpBN domain are colored in red. Note that modeling of this domain was not possible according to the Ca^{2+}-ATPase structure, since KdpBN is roughly 100 amino acids smaller in size.

Both proteins, the H4H5 loop and the KdpBN domain, were used for biochemical studies. It was observed that imidazole increased the protein stability, therefore, dialyzed protein in HEPES-Tris was only used in experiments were imidazole did interfere with the test system. The H4H5 loop at concentrations above 2 mg ml^{-1} could only be maintained in solution at high ionic strength (e.g. 100 mM imidazole or above). In contrast, the KdpBN domain could be concentrated up to 20 mg ml^{-1} in a 50 mM phosphate buffer without further additives.

The gene fragment of *kdpB* corresponding to the small cytoplasmic loop H2H3 was also subcloned into a pET16b vector and expressed in Bl21(DE) /pLysS cells. The computed M_w of H2H3 was 16257.18 Da including the deca-histidinyl tag. The procedure was identical to that of KdpBN and H4H5. The purification procedure is shown in figure 33.
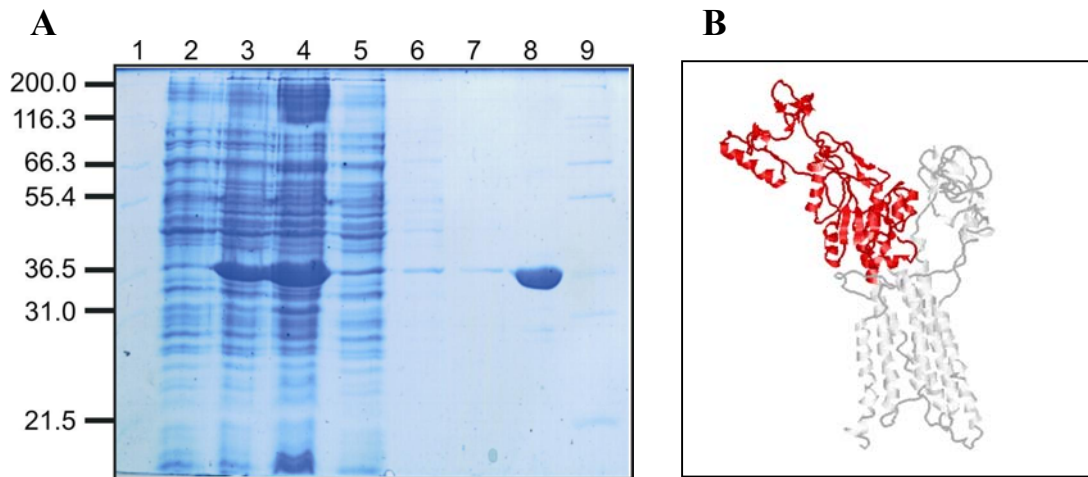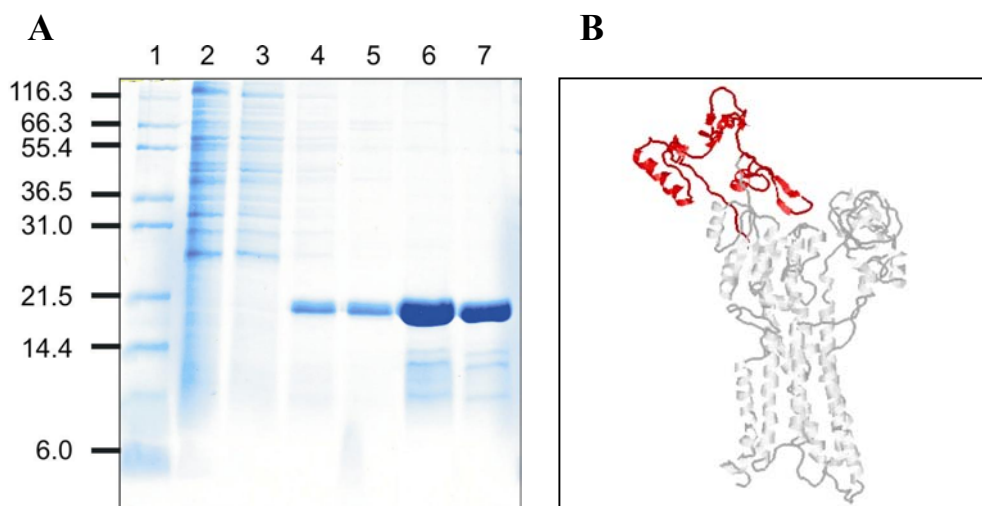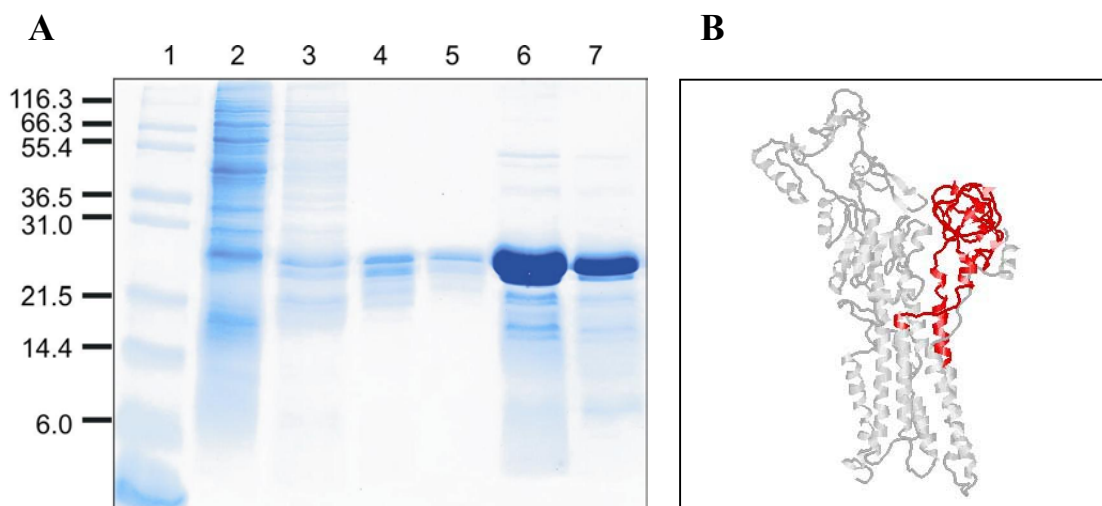
Figure 33: Purification of the H2H3 loop. A: The H2H3 loop was purified using metal affinity chromatography. Aliquots from different purification steps were subjected to SDS-PAGE. On each lane 5 μl of the following samples were loaded: (1) molecular mass standard (kDa); (2) flow through fraction; (3) washing step I; (4) washing step II; (5) washing step III; (6) elution fraction I; (7) elution fraction II. The purification procedure was essentially done as described in section 2.5.1. Washing step I was done in the presence of 10 mM imidazole and washing steps II and III were done in the presence of 60 mM imidazole. Elution was carried out using 0.25 M imidazole.
B: H2H3 loop according to the KdpB model. Amino acids contributing to the H2H3 loop are colored in red.

The H2H3 loop could be dialyzed against phosphate or HEPES-Tris buffer. However, in accord with the H4H5 loop, high ionic strength was necessary to maintain H2H3 at higher concentrations in solution. Since the H2H3 loop is lacking any substrate binding properties or hydrolytic activity, it was not possible to apply a biochemical assay, in order to test the native folding. Therefore, biochemical analysis was focused on the H4H5 loop and the KdpBN domain.

3.4.2. CD spectroscopical analysis of H4H5 and KdpBN

The secondary structure of the recombinant proteins was analyzed using CD spectroscopy. The obtained data sets were converted to mean residue ellipticities using a mean residue mass of 115 Dalton and deconvoluted by the self-consistent method (Sreerama and Woody, 1994). The spectra of H4H5 and KdpBN are shown in the figures 34 and 35, respectively. Both proteins showed minima, which are indicative of an α-helical structure. The minima for the H4H5 loop were at 207 nm and 221 nm, respectively (figure 34). The minima of the KdpBN domain were found at 208 nm and 219 nm (figure 35). The minimum at 207 nm in case of the H4H5 loop is more negative compared to the minimum at 221 nm. The minimum at 208 nm measured for the KdpBN domain is more negative than the minimum at 219 nm, which is not really forming a distinct minimum, rather decreasing slowly towards the absolute minimum at 208 nm. The calculated values were 38 % alpha helix and 13 % beta-sheet for the H4H5 loop and 40 % alpha helix and 10 % beta sheet for the KdpBN domain. Although this method does not allow a detailed structural analysis, the data revealed that the H4H5

loop and the KdpBN domain were properly folded. It was also tried to observe structural changes upon ligand and substrate binding. The H4H5 loop was incubated with ATP (1 mM) and the KdpBN domain with 15 µM FITC (data not shown). Binding of ATP to H4H5 shifted the CD spectrum. Minima were detected at 208 nm and 218 nm, but the overall secondary structure was not altered. The minimum at 208 nm was less negative upon ATP binding compared to the non-treated loop. The FITC labeled KdpBN displayed no changes in the CD spectrum at all.
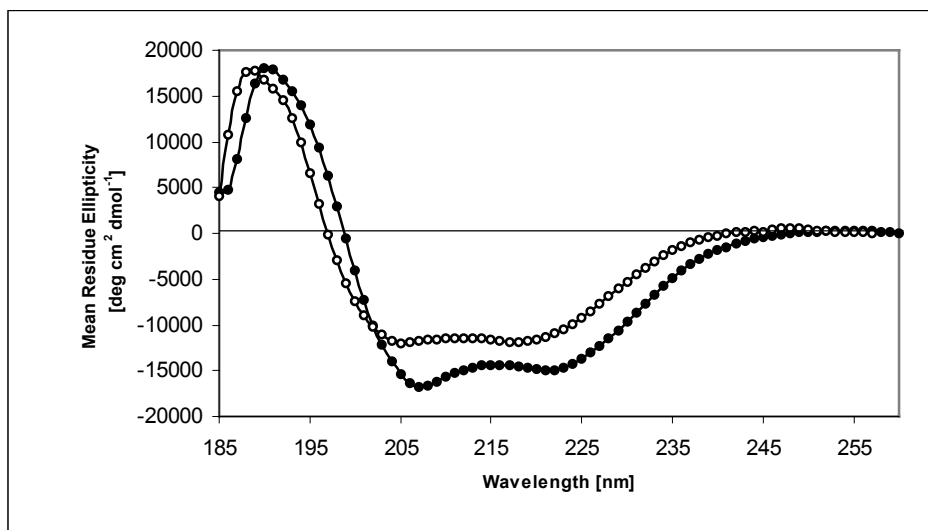
Figure 34: CD spectra of the purified H4H5 loop. H4H5 was purified and dialyzed against 50 mM potassium phosphate buffer, pH 7.8. The protein concentration was 0.5 mg ml^{-1}. H4H5 was analyzed without any additives (filled circles) and in the presence of 1 mM ATP (open circles). 50 spectra were acquired, co-added and corrected by the corresponding buffer spectra. The data were converted to mean residue ellipticity, using an average amino acid mass of 115 Dalton.
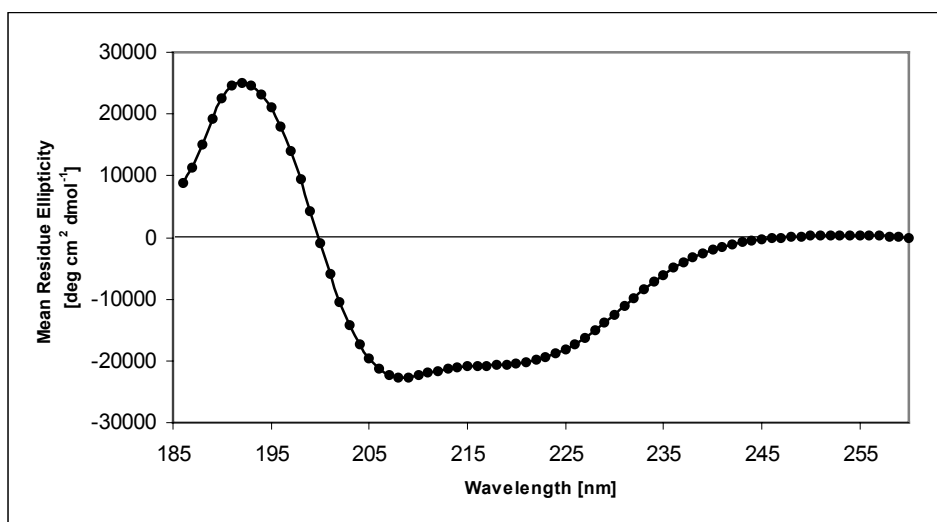
Figure 35: CD spectra of the purified KdpBN. KdpBN was purified and dialyzed against 50 mM potassium phosphate buffer, pH 7.8. The protein concentration was 1.8 mg ml^{-1}. KdpBN was analyzed without any additives (filled circles) and in the presence of 15 µM FITC (data not shown, since the curve is indistinguishable from that of the unmodified protein). 50 spectra were acquired, co-added and corrected by the corresponding buffer spectra. The data were converted to mean residue ellipticity, using an average amino acid mass of 115 Dalton.

3.4.3. FITC modification of H4H5 and KdpBN

Within this thesis (section 3.3.1.), it was demonstrated that the KGSV motif of KdpB is the homologue to the KGAGE motif of other P-type ATPases and resembles probably the exclusive FITC binding site within the Kdp-ATPase (see section 3.3.1.). For the native Kdp complex it was shown that FITC labeling was prevented by adenosine nucleotides prior FITC adding (as described in 3.3.). This fact indicated that the FITC binding-site of KdpB is within or near the nucleotide binding site, as this is the case in all other P-type ATPases sharing the FITC binding motif. Denatured KdpFABC complex failed to bind FITC indicating that a properly folded protein is necessary for FITC modification. Therefore, FITC labeling of the soluble H4H5 loop and the KdpBN domain was used to test folding of these recombinant KdpB modules. Figure 36 summarizes the results obtained with both soluble domains in comparison with the KdpFABC complex.
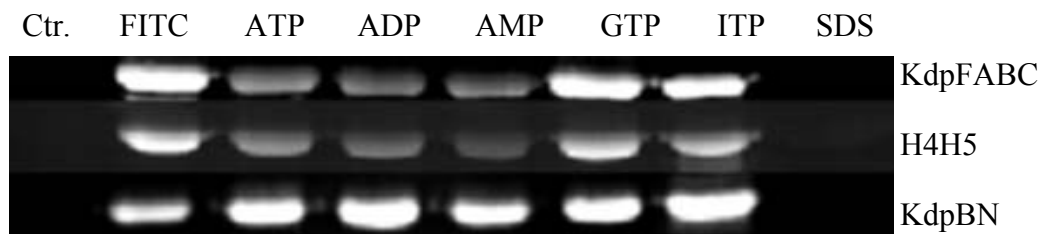
Figure 36: FITC binding to KdpFABC, H4H5 and KdpBN. Purified KdpFABC complex, H4H5 loop and KdpBN domain were incubated with 15 µM FITC for 30 min at 37°C. To test the protective effect of nucleotides the proteins were pre-incubated with 5 mM of the different nucleotides (as indicated). The FITC modification was stopped by addition of Laemmli SDS sample buffer and the mixture was applied to SDS-PAGE. The gels were visualized under UV-light (366 nm). The upper lane shows only the KdpB subunit from the native KdpFABC complex. SDS denatured protein was used as control for specific binding (protein was incubated with 1 % SDS at 80°C for 5 min prior FITC addition. A fluorescent control with untreated protein (Ctr.) was added to show that the protein does not exhibit autofluorescence. FITC modified protein (FITC) shows the modification without any additives, except FITC.

Adenosine nucleotides prevented FITC modification of H4H5 in the same manner as observed for the native KdpB. GTP and ITP mediated no protective effect. Interestingly, the KdpBN domain, which is referred to be the nucleotide binding domain, was labeled with FITC as expected. However, all nucleotides failed to protect against FITC modification. Since ATP binding is reversible and FITC binding is a covalent modification, it was checked, whether a short incubation (a time course from 0.5 -30 minutes was performed) with adenosine nucleotides revealed a protective effect. However, even after 0.5 minutes incubation no protective effect of ATP, ADP, and AMP was found. Unspecific labeling with FITC was ruled out, since SDS denaturation prior FITC addition abolished the modification in all cases.

3.4.4. TNP-nucleotide binding studies with H4H5 and KdpBN

TNP-nucleotides are a useful tool to the examination of ATP binding sites, since these nucleotide derivatives increase their fluorescence at 545 nm drastically upon binding to an appropriate binding site. It was shown that TNP-ATP binds to members of the P-type ATPase family (Moczydlowski and Fortes, 1981; Dupont *et al.*, 1982), as well as to isolated loops of P-type ATPases (Gatto *et al.*, 1998; Tsivkovskii *et al.*, 2001; Capieaux *et al.*, 1993; Moutin *et al.*, 1993). TNP-ATP, TNP-ADP, and TNP-AMP were used to examine nucleotide binding to the H4H5 loop and the KdpBN domain of KdpB. Figure 37 shows the interaction of H4H5 with the three TNP-nucleotides. TNP-ATP had the highest affinity with an apparent K_d of 18.5 µM. The calculated K_d values for TNP-ADP and TNP-AMP were 24.2 µM and 52 µM, respectively. Binding constants for the recombinant KdpBN domain were 12.23 µM for TNP-ATP, 12.53 µM for TNP-ADP, and 22.2 µM for TNP-AMP. It should be noted that it was impossible to determine the affinity constants for the native KdpFABC complex, since the KdpFABC complex displays in the solubilized as well as in the reconstituted state larger areas of hydrophobicity as compared to other P-type ATPases. As a result unspecific binding of TNP-nucleotides was drastically increased leading to a high fluorescent background.

A total of 1.23 mol of nucleotide sites per mol of H4H5 polypeptide chain was calculated. Figure 38 displays a calculation for the binding of TNP-ATP to H4H5. The values for TNP-ATP, TNP-ADP, and TNP-AMP were 1.23, 1.05 and 1.5 mol of binding sites per mol H4H5 for the mentioned TNP-nucleotides, respectively. The average value determined for the KdpBN domain was 1.096 mol of nucleotide binding sites per mol KdpBN. Plot and calculations were performed according to Gutfreund (1972), as applied by Carvalho-Alves *et al.* (2000).
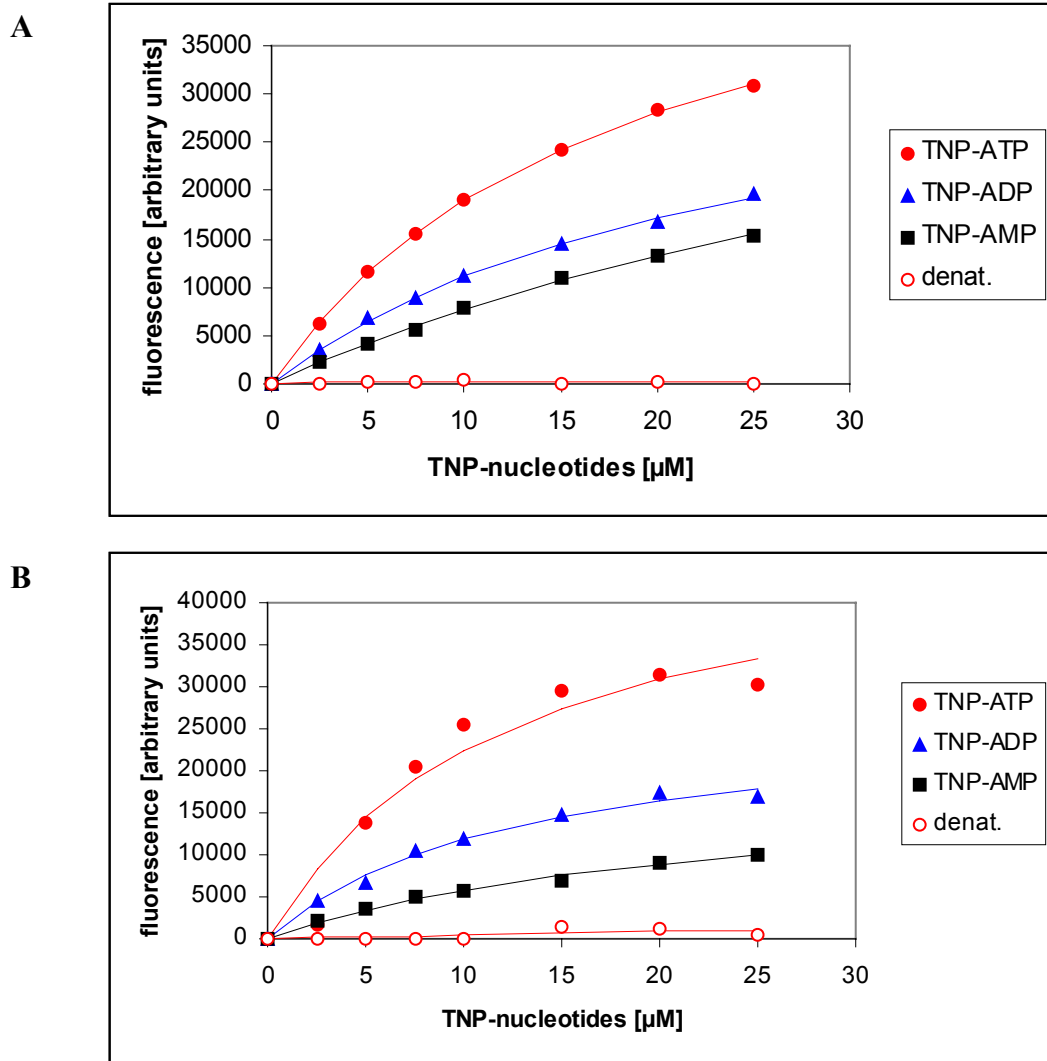
Figure 37: Nucleotide binding to H4H5 (A) and KdpBN (B). The fluorescence change of TNP-adenosine nucleotides upon binding to H4H5 and KdpBN was measured at 545 nm after excitation at 408 nm. To demonstrate the specific binding, SDS denatured proteins (denat.) were used as a control. Data were fitted to the equation: a [TNP-nucleotide] / b + [TNP-nucleotide], with 'a' representing the maximum fluorescence change and 'b' the apparent K_d.
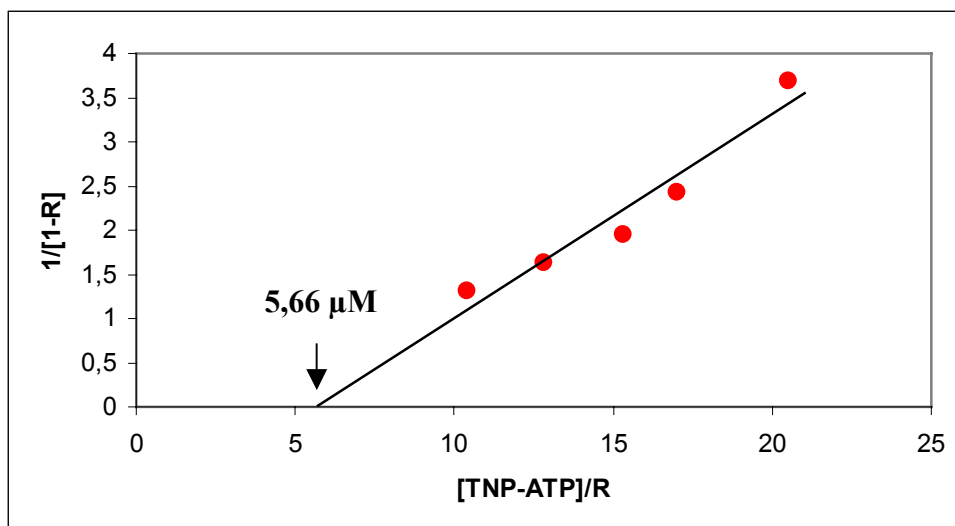
Figure 38: Determination of the number of nucleotide binding sites for H4H5. The fraction of fluorescence saturation at each TNP-ATP concentration (R-F/F_{max}) was calculated and plotted as $1/(1$-$R)$ versus [TNP-ATP]/R. The concentration of TNP-ATP binding sites of H4H5 (arrow) can be obtained from the relation $1/(1$-$R)$=K_d^{-1}[TNP-ATP]/R-(n/K_d), according to Gutfreund (1972). Since 5 µM H4H5 loop were used in the binding experiment, 1.23 mol TNP-ATP binding sites per mol H4H5 loop were calculated. The data are derived from the TNP-ATP binding curve displayed in figure 37 A.

3.4.5. TNP-nucleotide displacement studies with H4H5 and KdpBN

Since TNP-nucleotides are only nucleotide analogs, it was necessary to perform displacement studies with nucleotides, in order to determine the affinity constants for ATP, ADP, and AMP, respectively. For the displacement studies the H4H5 loop and the KdpBN domain were pre-incubated with nucleotides for 5 minutes at room temperature (see experimental procedures 2.7.3.) and subsequently titrated with TNP-ATP. The data obtained were fitted as previously described (experimental procedures 2.7.3.) and the apparent K_d values were determined. These apparent K_d values were plotted against the nucleotide concentration, in order to obtain the affinity constants for ATP, ADP, and AMP, respectively (figure 39).

A

B
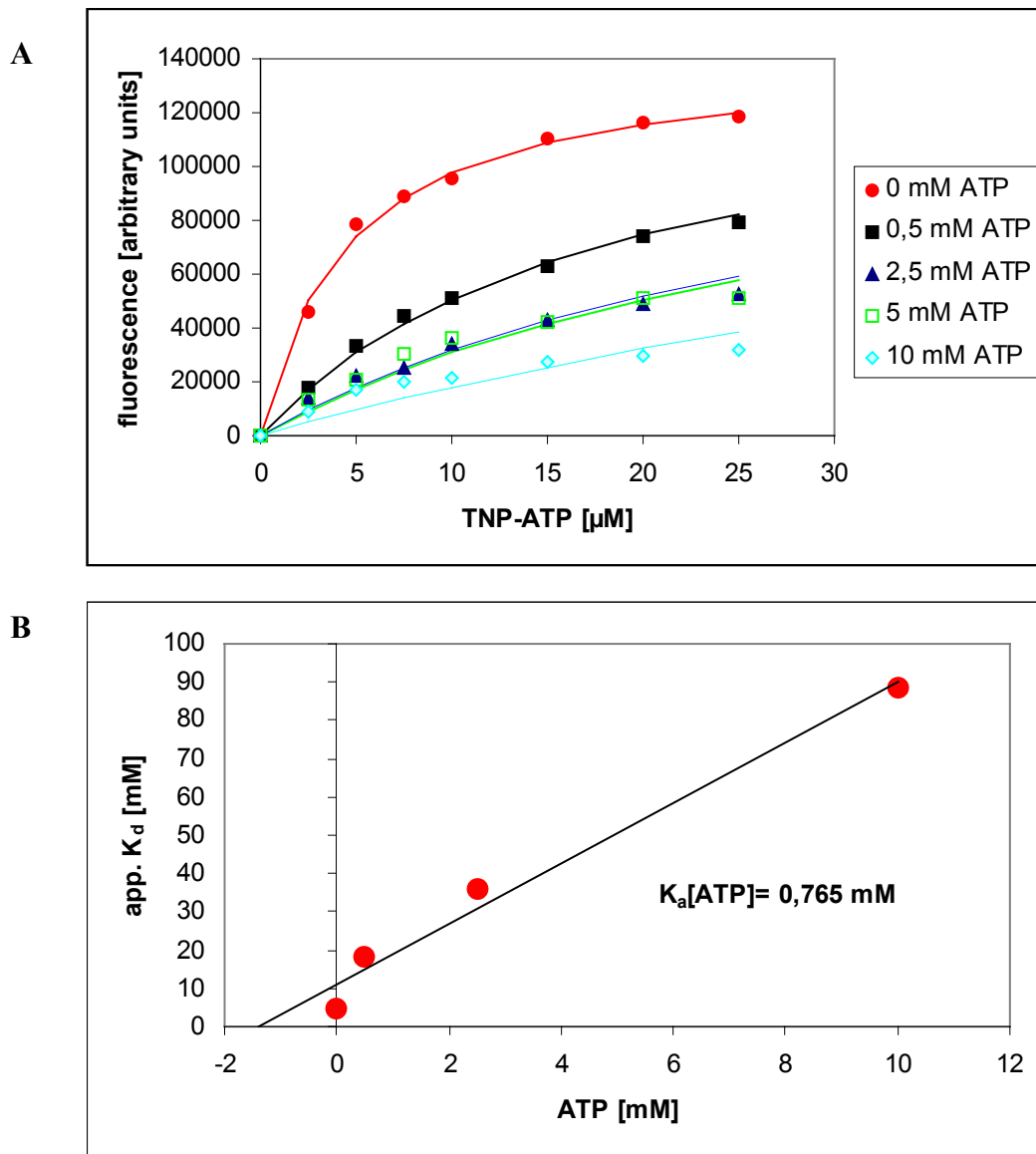
Figure 39: TNP-ATP displacement by ATP. Purified KdpBN (5 µM) was incubated with different concentrations of ATP for 5 minutes at room temperature. The buffer solution contained 20 mM HEPES-Tris pH 7.8. The pre-incubated enzyme solution was titrated with TNP-ATP and the fluorescence was measured. A non-enzyme control was subtracted from each data point. The fluorescence was plotted against the TNP-ATP concentration (upper plot) and the apparent K_d values for the different ATP concentrations were determined. A plot of these app. K_d values against the corresponding ATP concentrations resulted in a line (lower plot) indicating a competitive effect between TNP-ATP and ATP. The K_d for ATP can directly be taken from this plot. All other K_d values (ADP, AMP, and the series for the H4H5 domain) were determined the same way.

The apparent K_d value for ATP binding to the H4H5 loop was 0.68 mM. ADP and AMP were not able to displace ATP properly in case of the H4H5 loop. The apparent K_d for ATP binding to KdpBN was 0.765 mM, for ADP 1.43 mM, and for AMP 5.09 mM. All displacements were competitive, indicating that ATP, ADP, and AMP bind to the same binding site as TNP-ATP.

3.4.6. 8-azido-[α-^{32}P]ATP labeling studies with H4H5

Previously, it was reported that the KdpFABC complex can be labeled with 2-azido-[α-^{32}P]ATP and 8-azido-[α-^{32}P]ATP (Dröse, 1992; 1997). Beside KdpB, KdpC was also found to be labeled. However, binding of 8-azido-[α-^{32}P]ATP could not be prevented by addition of ATP. Furthermore, 8-azido-[α-^{32}P]ATP was shown to be a weak substrate for the Kdp-ATPase (Dröse, 1992). Nevertheless, 8-azido-[α-^{32}P]ATP-binding can be taken as a hint for nucleotide binding. Binding of adenosine nucleotides to the H4H5 loop was tested by using 8-azido-[α-^{32}P]ATP. As shown in figure 40 the H4H5 loop was labeled by 8-azido-[α-^{32}P]ATP. Competition with a ten-thousand-fold excess of ATP (20 mM) could prevent the modification to some extent. The same protection was observed by addition of FITC. However, a specific displacement should be observed using much lower ATP concentrations. Therefore, it is difficult to judge the specificity of 8-azido-[α-^{32}P]ATP binding. Since, binding of 8-azido-[α-^{32}P]ATP is only possible to properly folded enzymes, the labeling studies at least show that the H4H5 loop retained much of its native structure.
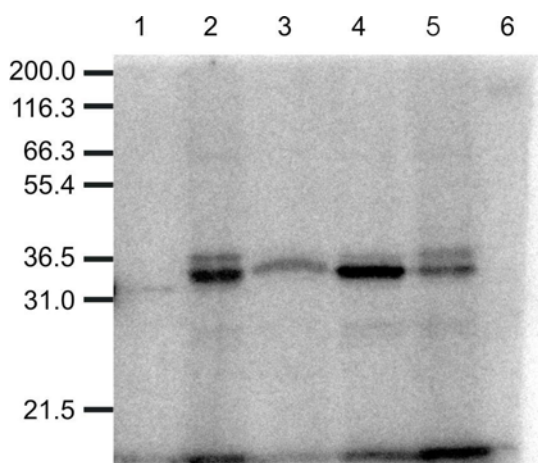
Figure 40: 8-azido-[α-^{32}P]ATP labeling of H4H5. Purified H4H5 (5 µg) was labeled with 5 µCi 8-azido-[α-^{32}P]ATP that corresponds to 8 µM 8-azido-[α-^{32}P]ATP. The labeling reaction was carried out as described in experimental procedures (2.7.1.). (1) dark control without light activation, (2) label without additives, (3) 20 mM ATP added prior to light activation, (4) 20 mM AMP added prior to light activation, (5) 15 µM FITC added prior to light activation, (6) molecular mass standard (kDa)

3.4.7. Hydrolytic activity of the H4H5 loop

An even more convincing argument for the binding of ATP to the H4H5 loop was obtained by measuring ATP hydrolysis. Using the very sensitive phosphate determination assay EnzCheck® purchased from Molecular Probes, H4H5 loop catalyzed ATP hydrolysis (figure 41) was measured. Control experiments without enzyme revealed autohydrolysis of ATP. The specific activity was around 20 nmol mg^{-1} min^{-1}. This activity is 250-500 fold lower compared to the native complex (5000-10000 nmol mg^{-1} min^{-1}). However, the specific activity was in the same range as determined for the soluble cytoplasmic loop of the Wilson's disease protein (ATP7B) (Tsivkovskii *et al.*, 2001), which had a similar size. P-type ATPases hydrolyze the small pseudosubstrate pNPP. For the native KdpFABC complex the hydrolysis of pNPP was demonstrated in this study (compare section 3.3.).
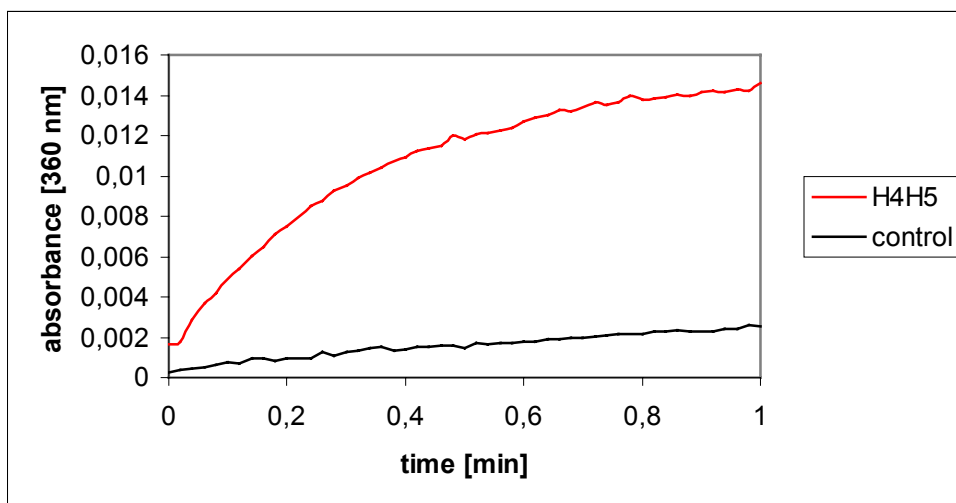
Figure 41: ATPase activity of H4H5 domain measured with the EnzCheck® phosphate assay. The EnzCheck® test was from Molecular Probes (Eugene, Oregon, USA). In a total reaction volume of 1 ml, 100 µg protein were present and the test was carried out according to the manufacturer's protocol. A "non enzyme" control showed the auto-hydrolysis of ATP at 37°C. The total activity was 7.2 nmol mg^{-1} min^{-1}.
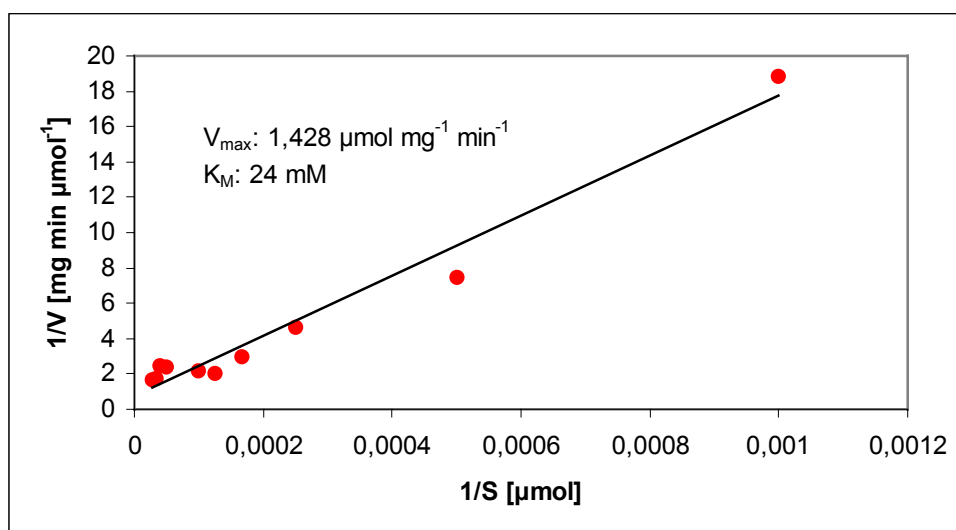
Figure 42: Lineweaver-Burk plot of the pNPPase activity of the H4H5 loop. In a total reaction volume of 100 µl 5 µg protein were incubated in 20 mM HEPES-Tris buffer containing 15 mM MgCl$_2$. The reaction was started by addition of 15 mM pNPP and stopped after 30 minutes by addition of 0.1 M NaOH. The production of p-nitrophenolate was determined using a p-nitrophenolate standard curve. K_M and V_{max} values were calculated from the double reciprocal plot.

In case of the isolated cytoplasmic loop of the Na$^+$, K$^+$-ATPase it was shown that these domains were still able to hydrolyze pNPP (Tran and Farley, 1999; Obsil *et al.*, 1998). Consequently, the ability of the KdpB H4H5 loop to hydrolyze pNPP was tested. Results are shown in figure 42 were substrate dependency of the H4H5 loop is displayed in a double reciprocal plot. The specific activity was 1.4 µmol mg^{-1} min^{-1} and the apparent K_M value was 24 mM. The reaction was not inhibited by *ortho*-vanadate and not stimulated by potassium ions (data not shown). The hydrolytic activity of the H4H5

loop of KdpB is the most convincing evidence for a properly folded protein, which retained much, if not all, of its native structure.

3.5. NMR analysis of KdpBN

As already pointed out, the N-domain of KdpB is much smaller in size compared to the N-domain of the Ca^{2+}-ATPase and resembles those of the heavy metal-transporting ATPases. Therefore, the N-domain of KdpB displays a kind of minimal scheme of a nucleotide-binding domain, making it an interesting candidate for structural analysis. An important prerequisite for NMR is the stability of the protein at temperatures between 25 and 30°C for several days. Therefore, stability tests were undertaken in order to figure out, whether the H4H5 loop or KdpBN could fulfill the stability criteria necessary for NMR analysis.
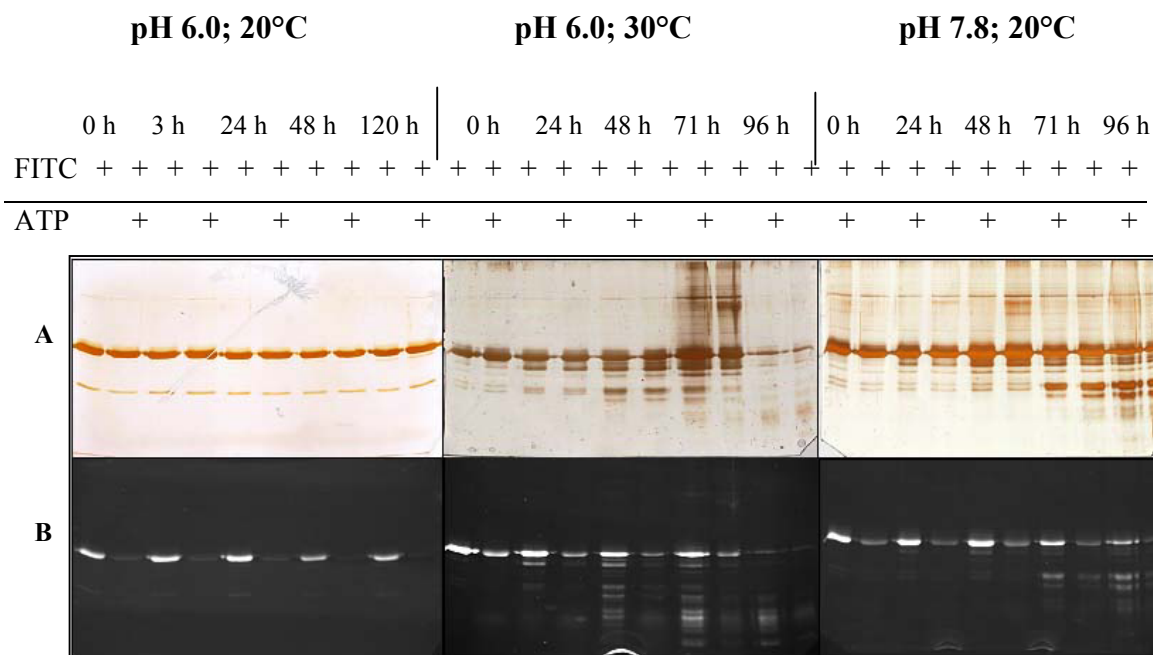
Figure 43: Stability tests with H4H5 at different temperatures and pH values. The H4H5 protein was dialyzed against 50 mM potassium phosphate buffer with the indicated pH values. The protein concentration was 2 mg ml^{-1}. Azide (0.05%) was added to prevent microbial growth. 1 ml aliquots were incubated at each temperature and 20 µl samples were taken at the indicated time points. The samples were divided and 10 µl of each sample were incubated with 5 mM ATP prior FITC binding for 5 minutes. 15 µM FITC were added to each sample. The labeling reaction was stopped after 30 minutes at 37°C by addition of SDS sample buffer. The whole mixtures were subjected to SDS-PAGE. The gels were examined under UV-light at 366 nm (**B**) prior to silver staining (**A**).

Figure 43 demonstrates the stability of H4H5 at various pH values and temperatures. The test was performed in 50 mM potassium phosphate buffer with 0.05 % azide present. Interestingly, at higher temperatures or pH values the degradation of the polypeptide was increased. The H4H5 sample in phosphate buffer with pH 6.0 at 20°C was stable for at least 5 days. However, it should be noted that

the protein concentration was only 2 mg ml^{-1}, which was at least 10 times less than needed for NMR analysis. The native folding of the H4H5 loop was tested by the ATP protection of FITC binding. Interestingly, the degradation products still exhibited a protective effect of ATP towards modification with FITC, suggesting a proper folded ATP binding site present in the H4H5 degradation products. These findings supported the idea that the H4H5 loop was not degraded randomly, but rather cleaved at specific sites, leaving the cleavage products folded in a native manner. Since the H4H5 loop precipitated at concentrations above 2 mg ml^{-1} in buffer of low ionic strength this protein was not used for structural analysis.

The KdpBN polypeptide was much more stable in 50 mM phosphate buffer, and hence, it could be concentrated up to 1 mM and above. A stability test, shown in figure 44, illustrates that KdpBN is stable at 30°C in 50 mM potassium phosphate buffer (0.05 % azide) for at least 9 days. The sample was concentrated up to 20 mg ml^{-1}. Furthermore, the silver stained SDS-PAGE demonstrated the high purification grade of the protein and the resistance against proteolytic cleavage.

pH 6.0; 30°C
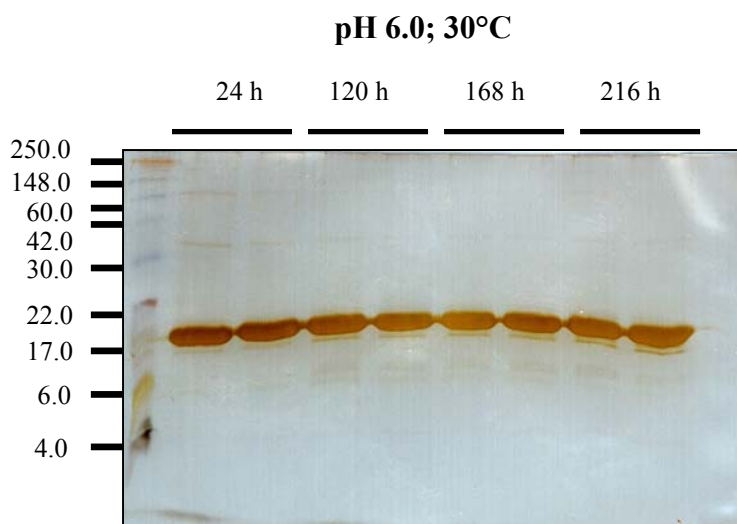
Figure 44: Stability test of KdpBN. The KdpBN protein was dialyzed against 50 mM potassium phosphate buffer pH 6.0. The protein concentration was 20 mg ml^{-1}. Azide (0.05%) was added to prevent microbial growth. A 100 μl sample was incubated at 30°C. 10 μl samples were taken at the indicated time points and 1 μl out of each was subjected to SDS-PAGE. The gel was stained with silver according to Blum *et al.* (1987). A degradation product can be seen as faint band below the KpBN band.

The stability, the high solubility, and the biochemical characteristics made the KdpBN domain an interesting candidate for structural analysis using the NMR technique. KdpBN is roughly 17 kDa in size (including the deca-histidinyl tag). Therefore, the protein had to be labeled with ^{15}N and ^{13}C for multidimensional NMR analysis, which is necessary for structural determination. In order to test, whether the protein fulfills the prerequisites for NMR, a ^{15}N labeled KdpBN was prepared. The Bl21(DE) /pLysS /pET16bKdpBN cells were therefore grown in K115 medium with ^{15}N-ammonium sulfate (purchased from Promochem, Wesel) as sole nitrogen source. Induction was achieved by adding 1 mM IPTG when the optical density was between 0.7-1.0. The culture was incubated for three

more hours and harvested. The protein purification was performed according the standard metal affinity chromatography protocol. Since purity of the protein is a very important prerequisite for NMR analysis, the Ni-NTA matrix was overloaded (figure 45) in order to avoid unspecific binding of proteins.
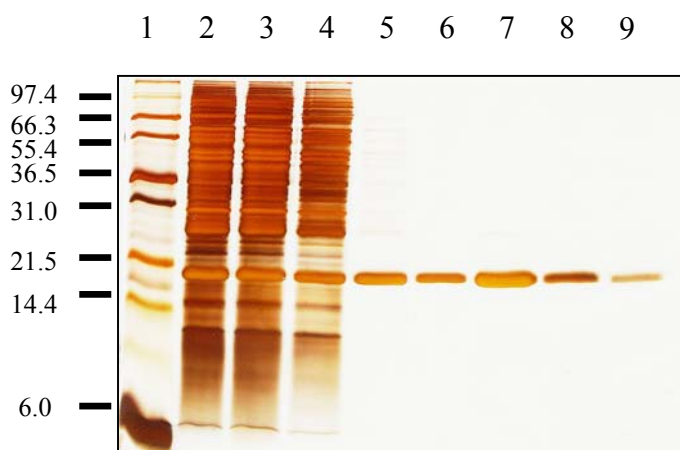
Figure 45: Purification of ^{15}N-labeled KdpB. In order to obtain highly purified protein for NMR analysis the Ni-NTA matrix (binding capacity 10 mg ml^{-1}) was overloaded with protein. The purification was done as described in experimental procedures. (1) molecular mass standard; (2) soluble extract of induced cells; (3) flow through; (4) first washing step with 10 mM imidazole; (5) last washing step with 60 mM imidazole; (6) first elution with 0.25 M imidazole; (7) second elution with 0.25 M imidazole; (8) third elution with 1 M imidazole; (9) fourth elution with 1 M imidazole.

The purified KdpBN was dialyzed extensively against 50 mM potassium phosphate buffer. The dialyzed KdpBN was concentrated using an Amicon cell (equipped with a YM10 membrane) and finally using microconcentration tubes (Millipore Centricon 5) up to 20 mg ml^{-1}. The ^{15}N-HSQC (<u>H</u>eteronuclear <u>S</u>ingle <u>Q</u>uantum <u>C</u>oherence) spectrum detects all nitrogen-atoms and hence all peptide bonds and all side chains containing a nitrogen atom. The spectra were collected at 300 K on a 600 MHz Bruker DMX600 spectrometer (M. Haupt and H. Kessler, personal communication). The spectra obtained contained all signals expected for the 17 kDa KdpBN and revealed that the protein was in a highly ordered structure. Figure 46 shows the ^{15}N-HSQC of a 1-day-old sample. The cross signals were well separated.
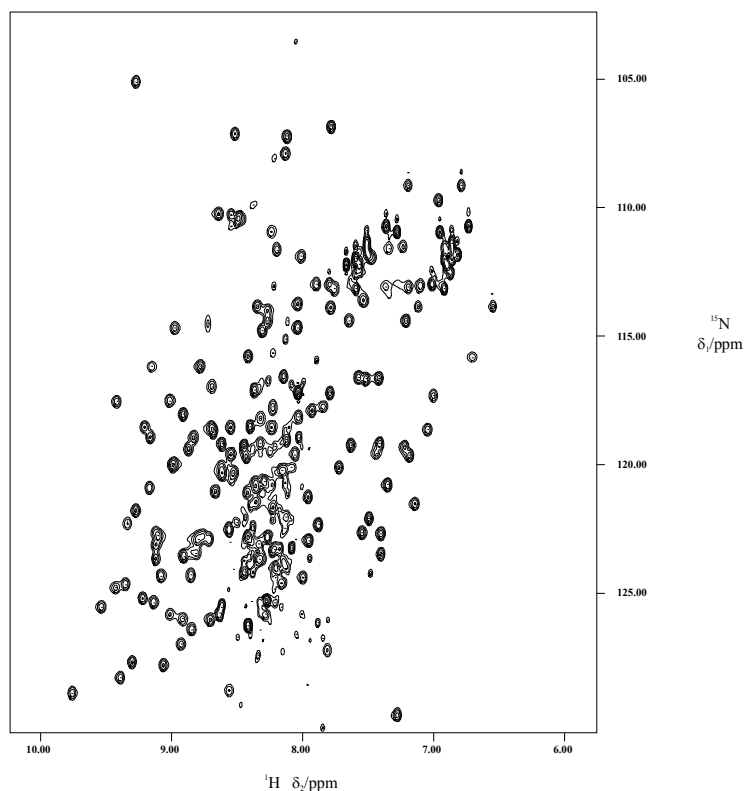
Figure 46: ^{15}N, ^{1}H-HSQC spectrum of KdpBN. KdpBN protein purified from cells grown in minimal medium supplemented with ^{15}N-ammonium sulfate as sole nitrogen source was concentrated up to 1.3 mM in 50 mM potassium phosphate buffer (pH 6.0). The spectra were acquired at 300 K on a Bruker DMX600 spectrometer and processed using the X-WINNMR software. The spectra were recorded with 1024 * 128 complex points in t2 and t1, respectively and 8 scans per increment. The observed number of signals is in agreement with the molecular mass and amino acid composition of the 17 kDa protein. (Melina Haupt, personal communication)

Degradation of the KdpBN protein started after a few days. The time course of degradation could be visualized by NMR analysis. The signals were getting broader and started to accumulate around δ_1/ppm 122 and δ_2/ppm 8.5.

Since KdpBN is 17 kDa in size, ^{13}C and ^{15}N labeling is required for complete structure determination using multidimensional NMR. In order to obtain uniformly ^{13}C and ^{15}N-labeled protein, two strategies were applied. Beside growth of the cells in minimal medium containing ^{15}N-ammonium as sole nitrogen source and ^{13}C$_{1-6}$ glucose as sole carbon source, a commercially available rich medium (Silantes, München, Germany), which contains only ^{13}C and ^{15}N labeled substances could be used for ^{13}C and ^{15}N labeling. In order to check, which medium gave best overproduction of the protein, pre-experiments were carried out. Cells of Bl21(DE) /pLysS /pET16b were grown in K115 minimal medium with 1 %, 0.5 %, and 0.25 % glucose and in a commercially available rich medium obtained from Silantes (Silantes, München). For the pre-experiments the Silantes OD ~2.0 concentrate was used. The strain was grown in the different media and induced with 1 mM IPTG when an optical density of 1.0 was reached (figure 47). Figure 48 shows that KdpBN production in cells grown in 1.0 % glucose and 0.5 % glucose did not differ, significantly. The cells grown in 0.25 % glucose, however, produced less KdpBN. Immunoblot analysis of the Silantes OD2 medium showed a good

expression even after one hour. Since degradation of the protein in growing cells with prolonged induction time was always a problem, the Silantes medium was chosen for the first ^{13}C and ^{15}N labeling experiments.
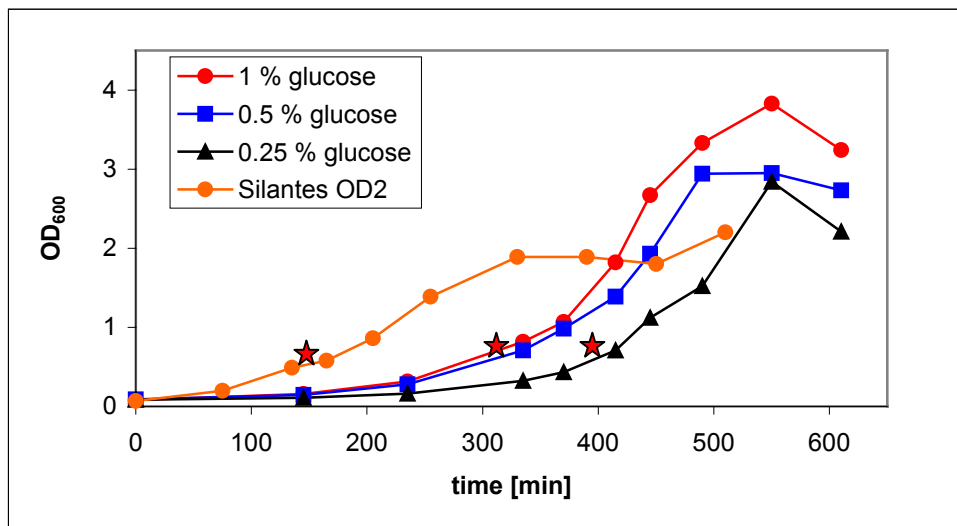
Figure 47: Growth curves of strain Bl21(DE) /pLysS /pET16bKdpBN. The expression strain Bl21(DE) /pLysS /pET16bKdpBN was grown in 50 ml culture flasks. The minimal media were supplemented with the indicated glucose concentrations (1 %, 0.5 %, and 0.25 %). The Silantes OD2 medium is a commercially available rich medium, which can be obtained as an unlabeled sample (as used here). The red stars indicate the time point of induction with 1 mM IPTG. 1 ml samples were taken before induction and every hour after induction.
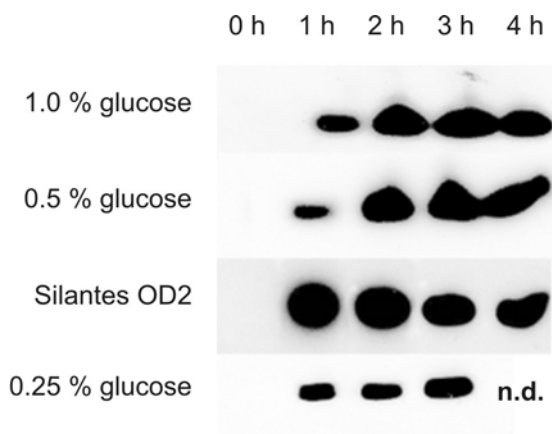
Figure 48: Synthesis of KdpBN in different media. Whole cell extracts from the induction experiment shown above were subjected to SDS-PAGE and blotted. A 1 ml sample of the cell culture was collected and each cell pellet was dissolved in 150 µl Laemmli SDS sample buffer. 5 µl of this cell lysates were applied to each lane. The synthesis of KdpBN was visualized using anti-penta-His antibodies obtained from Qiagen.

To obtain ^{13}C and ^{15}N labeled KdpBN, the strain Bl21 (DE) /pLysS /pET16bKdpBN was fermented in Silantes OD4 CN (Silantes media are available in concentrations allowing growth to different optical densities and the indication CN is referring to ^{13}C and ^{15}N.) medium using a Biostad fermenter at 37°C. The KdpBN protein was purified as described before and the concentrated sample was used for NMR analysis. To our great surprise, the NMR spectra revealed that the double-labeled KdpBN protein was unfolded, although it was soluble. CD spectra of the sample supported these findings (data not shown). After three days the protein precipitated. For renaturation of the protein the sample was diluted in 50 mM potassium phosphate buffer containing 1 % (27 mM) octylglycoside, 5 mM EDTA, and 5 mM β-

mercaptoethanol to a protein concentration of 1 mg ml^{-1}. Interestingly, the precipitated protein could be redissolved completely after stirring for 3 hours at room temperature. CD spectroscopic measurements illustrated that KdpBN regained some of its native folding. However, NMR analysis of the dialyzed and re-concentrated sample revealed that the protein remained mainly unfolded.
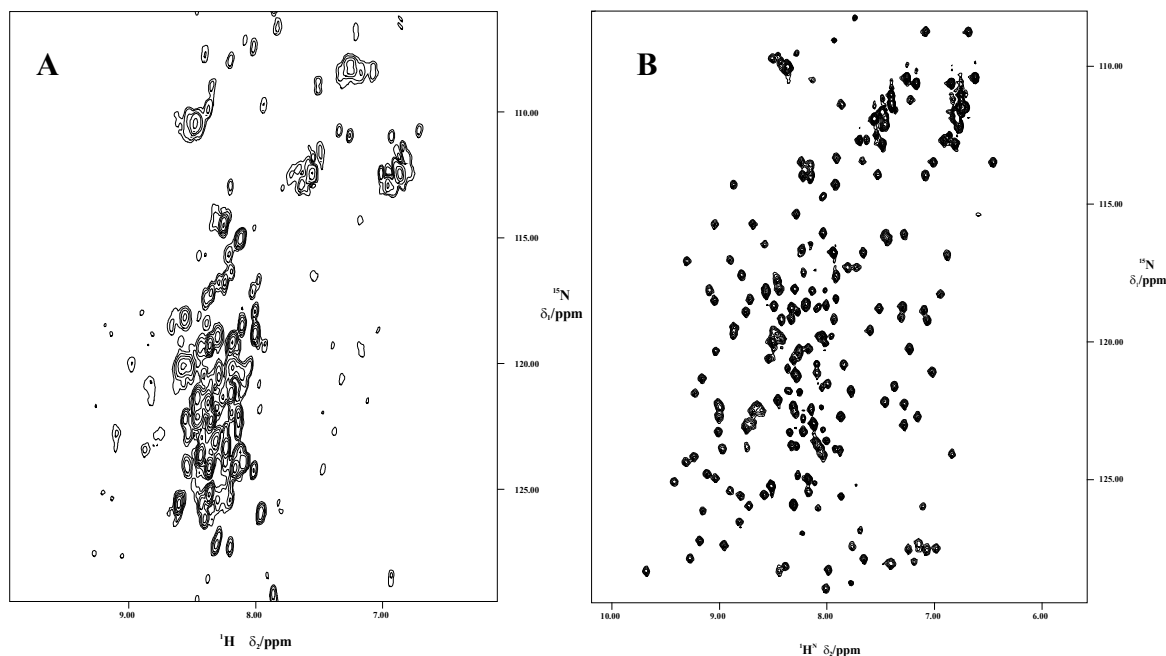
Figure 49: ^{15}N, ^{1}H-HSQC spectrum of ^{13}C, ^{15}N-labeled KdpBN synthesized in SILANTES medium (A); ^{15}N, ^{1}H-HSQC spectrum of ^{13}C, ^{15}N-labeled KdpBN synthesized in minimal medium (0.2 % ^{13}C$_{1-6}$-glucose) (B). ^{15}N-HSQC spectra of KdpBN purified from Silantes OD4 medium (A) and minimal medium (B). Recombinant KdpBN was concentrated up to 0.7 mM in 50 mM potassium phosphate buffer (pH 6.0). The spectra were acquired at 300 K on a Bruker DMX600 spectrometer and processed using the X-WINNMR software. The spectra were recorded with 1024*128 complex points in t2 and t1, respectively and 8 scans per increment. (Melina Haupt, personal communication)

In order to test, whether the incorrect folding of KdpBN synthesized in the Silantes medium, is due to the presence of a rich medium, KdpBN samples derived from Silantes medium, LB medium, and minimal medium with 0.25 % glucose were prepared. These unlabeled samples were applied to ^{1}H-NMR. These proton NMR spectra revealed that KdpBN derived from minimal medium and LB medium were properly folded. In contrast, the KdpBN purified from the Silantes medium was unfolded (figure 50).
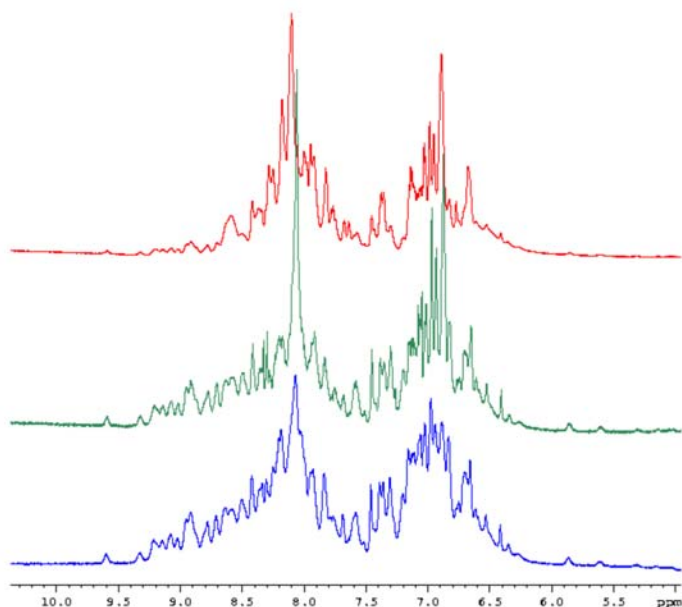
Figure 50: ^{1}H-NMR spectra of KdpBN. ^{1}H-NMR spectra of KdpBN purified from cells grown in (red) Silantes medium, (green) LB medium, (blue) minmal medium. The X-axis is in δ_1 / ppm.
(Melina Haupt, personal communication)

The signals between 8.5 ppm and 10 ppm are much lower in case of the KdpBN from Silantes medium (figure 50). Above 9 ppm no signals are detected at all. Further, the $C_\alpha H$ signals around 7.5 ppm are much lower compared to the KdpBN proteins synthesized in minimal and LB medium. Therefore, it is quite clear that expression of KdpBN in Silantes medium leads to unfolded protein, a phenomenon, which was unexpected and which cannot be explained so far.

Since KdpBN synthesized in cells grown in minimal medium supplemented with glucose was shown to be properly folded, ^{13}C / ^{15}N labeled protein was synthesized in minimal medium supplemented with 0.25 % glucose. The low glucose concentration was chosen for financial reasons. A total of 4-litres K115 medium supplemented with 4.53 g ^{15}N ammonium sulfate and 8 g ^{13}C$_{1-6}$ glucose were used for the production of labeled KdpBN. The pre-cultures were grown in the same medium, in order to adapt the cells. The main culture was inoculated to an optical density of 0.1 and induction was carried out with 1 mM IPTG at OD 0.7. The cells were harvested after 2.5 hours, when the culture had reached the early stationary phase. The ^{15}N / ^{13}C KdpBN was purified as described in experimental procedures. The purified protein was not dialyzed, but applied to size exclusion chromatography using a Pharmacia SPX75 column (Amersham-Bioscience, Freiburg, Germany). The column was run with 50 mM potassium phosphate buffer pH 6.0 and 100 mM NaCl. Stability assays with KdpBN revealed that addition of salt increased the solubility of the protein. NaCl did not alter the chemical shifts at concentrations around 100 mM, this amount of salt was used here. The protein was concentrated up to 1.5 mM (26 mg ml^{-1}). Multi-dimensional NMR spectra were obtained. An example of a 3D NMR spectrum is shown in figure 51. The well-separated peaks allowed a complete backbone assignment (figure 52).
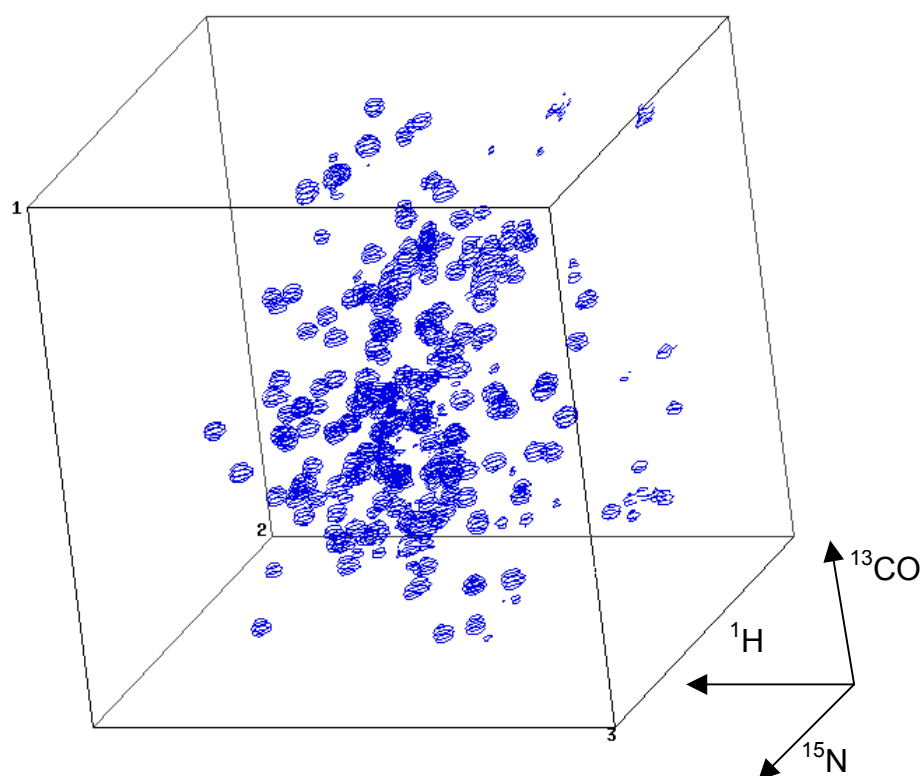
Figure 51: 3D NMR (HNCO) experiment with KdpBN. KdpBN was synthesized by cells grown in minimal medium supplemented with $^{13}C_{1-6}$ glucose and ^{15}N-ammonium sulfate as sole carbon and nitrogen source, respectively. The protein was concentrated up to 1.5 mM in 50 mM potassium phosphate buffer (pH 6.0) and 100 mM NaCl. A HNCO reveals the correlation of nitrogen to the carbonyl carbon atoms in i-1 position. The coordinates are: F1 = 15N, F2 = 13C und F3 = 1H (Melina Haupt, personal communication)

Figure 52: Secondary structure of KdpBN (chemical shift index plot). Applying multi-dimensional NMR a backbone assignment of KdpBN was possible. The quality of the assignment was verified by two independent methods, the chemical shift index (CSI) (light blue) and the structure prediction *via* the homonuclear $3J(H^NH^\alpha)$ coupling constants (red). The X-axis reflects the sequence positions within the KdpB sequence.
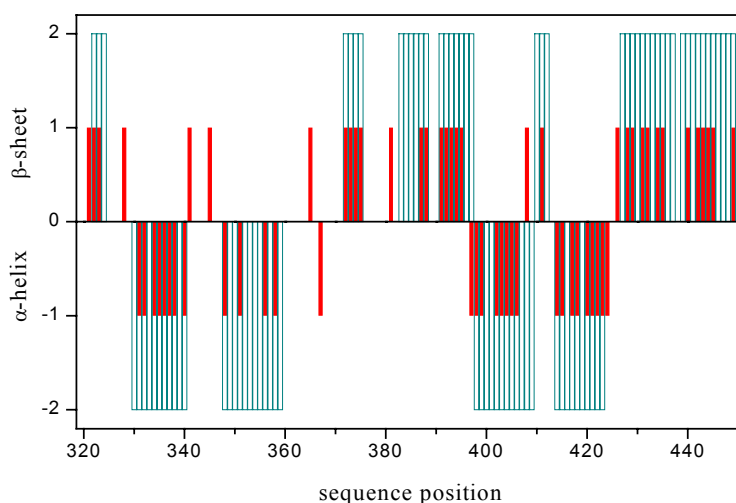
3.6. Cloning, expression, purification and characterization of Mj0968 – a thermophilic ortholog of H4H5

Aravind and co-workers (1998) hypothesized that the catalytic core domain of P-type ATPases (the large cytoplasmic loop and hence the H4H5 domain of KdpB) is related to the haloacid dehalogenase fold and that fusion of the catalytic core domain with a membrane-integral protein formed the known P-type ATPases. Aravind *et al.* (1998) also pointed out that the genomes of two archaea, *Methanococcus jannaschii* and *Methanobacterium thermoautothrophicum* (now *Methanothermobacter thermoautothrophicum*), contain two open reading frames, which encode orthologous proteins (Mj0968 and Mth1483, respectively) that are highly similar to the core catalytic center of P-type ATPases. Since a major goal of this study was to provide suitable samples for structural analysis, leading to a detailed understanding of the catalytic domain of KdpB and hence of other P-type ATPases as well, the Mj0968 protein was chosen as an ortholog for the H4H5 loop, with the hope that the Mj0968 protein would fulfill the prerequisites for structural analysis either by NMR or X-ray crystallography.

3.6.1. Cloning, expression and purification of deca-histidine-tagged Mj0968 and Mj0968-D7A

Heterologous expression of archaeal proteins in a bacterial host like *E. coli* is often limited by the different codon usage of these organisms. To circumvent this problem for Mj0968 in the *E. coli* host, the Bl21(DE)-Codon Plus®-RIL expression strain from Stratagene (La Jolla, USA) was used. The AMJEP60 plasmid, containing the genomic DNA fragment of *M. jannaschii* including ORF 0968, was obtained from the American Type Culture Collection (ATCC) and served as template DNA. The Mj0968 gene was amplified using PCR and subcloned using *Nde*I and *Xho*I restriction sites of the pET16b vector. The resulting gene product contained a N-terminal deca-histidinyl fusion for convenient metal affinity chromatography. Competent Bl21(DE)-Codon Plus®-RIL cells were transformed with the plasmid pET16bMj0968. Cells were grown in a fermenter at 37°C to minimize the formation of inclusion bodies. Induced cells were lysed as described in experimental procedures and the soluble extract was purified using Ni-NTA chromatography. The final protein yield was around 8 mg of Mj0968 out of 1-liter culture medium. In order to reduce the amount of contaminating proteins, the Ni-NTA matrix was overloaded, resulting in losses of Mj0968 in the flow through and washing fractions. Those fractions were applied to the affinity matrix again. A good enrichment of the archaeal protein was achieved by heating the host cyotosolic extract twice up to 80°C (figure 53). The precipitated proteins were removed by centrifugation at 14.000 g at 25°C. SDS-PAGE analysis of the purification procedure showed a dominant protein band around 36 kDa, which corresponds to the monomeric Mj0968 (M_w 32667,23 Da including tag). At least two higher molecular weight bands

were observed (figure 53), which represent oligomers of Mj0968, and which could be reduced with β-mercaptoethanol to the monomeric form.
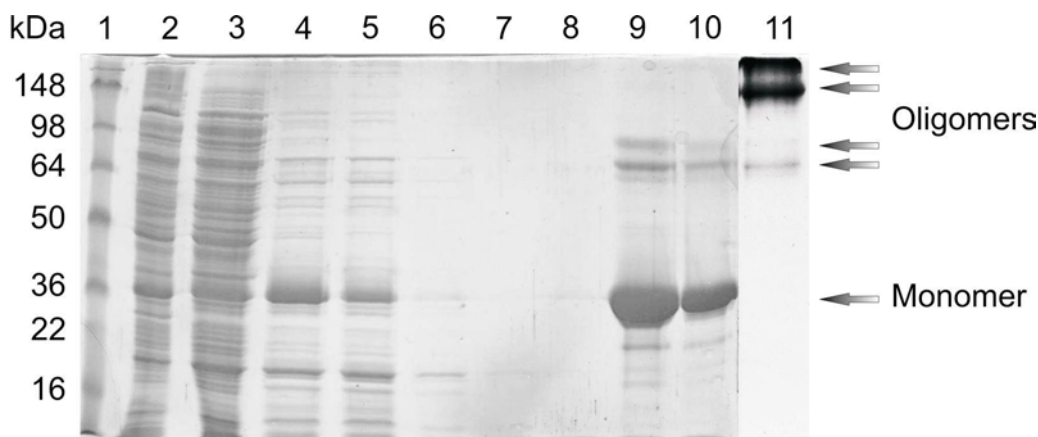
Figure 53: Purification of the Mj0968-His$_{10}$ fusion protein. Coomassie Blue stained SDS-PAGE of different purification steps. Lane 1, molecular standard in kDa, lane 2, whole cell extract, lane 3, cytosolic extract, lane 4 and 5, supernatant after 80°C precipitation of host cell proteins, lane 6-8, washing fractions from metal affinity chromatography, lane 9, fraction of the first elution, lane 10, fraction of the second elution, lane 11, Mj0986 in the absence of β-mercaptoethanol. Arrows point to oligomeric and monomeric forms of Mj0968-His$_{10}$.

For further analysis, the protein was dialyzed against 50 mM HEPES-Tris pH 7.8 containing 150 mM NaCl at 25°C. Dialysis at lower temperature caused precipitation of the protein, which could be resolved by gentle heating. The dialyzed protein was concentrated up to 9 mg ml^{-1}. The protein could be stored at 4°C for over six month without loosing activity.

With the intention to test the importance of Asp7, which is the corresponding residue to the phosphorylated aspartate residues of P-type ATPases, a substitution to alanine was carried out. Construction of the D7A mutant was achieved using a forward primer with the altered codon at position 7. The PCR procedure, cloning and expression were carried out in analogy to the wild-type enzyme.

3.6.2. Specific antibodies against Mj0968 and detection of the protein in *M. jannaschii*

Specific antibodies against Mj0968 were raised to find out, whether the protein was expressed *in vivo* in *M. jannaschii* cells. The antibodies were raised by Eurogentec using immunized rabbits as described in experimental procedures. The pre-sera showed no cross reactivity with either *M. jannaschii* or *E. coli* Bl21(DE) cell extracts. Since the antibody titer in the obtained sera was quite high, immunoblotting could be carried out with 1:10.000 dilutions (figure 54). Beside the monomeric bands, the oligomers were detected by the antibody (figure 54).
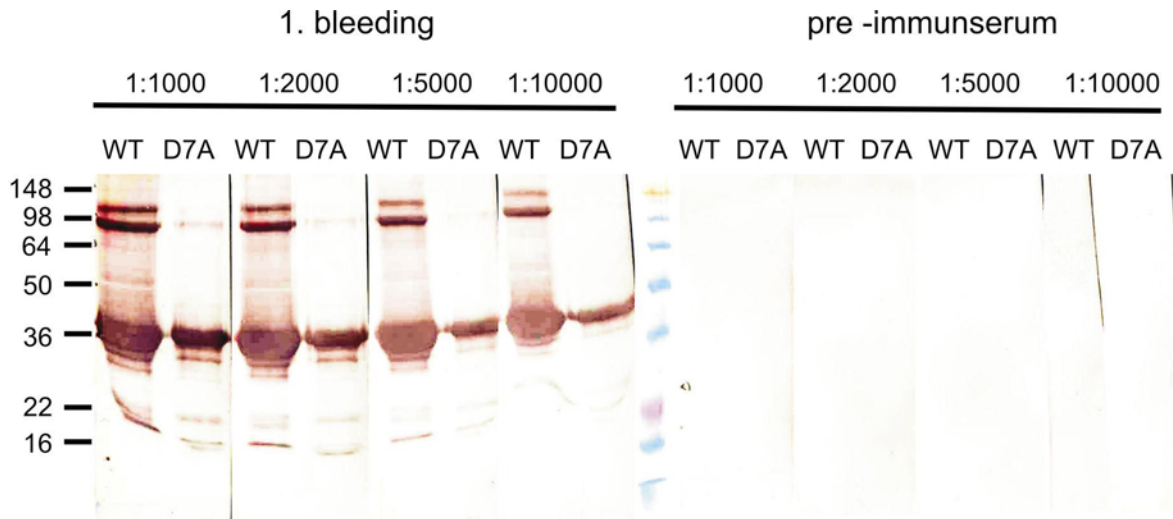
Figure 54: of Heterologously expressed Mj0968-His$_{10}$ detected by immunoblotting. Purified Mj0968-His$_{10}$ wild-type and Mj0968-D7A-His$_{10}$ mutant proteins were purified from the *E. coli* host and blotted onto a nitrocellulose membrane. The left part of the figure shows the reaction of serum obtained from the first bleeding. The right part of the figure shows the equivalent blot incubated with the pre-immunserum. The dilutions of sera in buffer are indicated and arranged from 1:1000 to 1:10.000. Both blots were stained with anti-rabbit IgG-AP antibody in a 1:10.000 fold dilution.

The *M. jannaschii* cells used in this study were a kind gift of Dr. R. Hedderich (MPI, Marburg). After cell disruption, the cell material was separated into insoluble and soluble parts by centrifugation (200.000 *g*, 25°C). The insoluble parts were dissolved in Laemmli SDS sample mix while the soluble extract was mixed with concentrated SDS sample mix. Aliquots of both parts were subjected to SDS-PAGE and finally blotted. Mj0968 proteins were detected using the polycolnal antibodies in a 1:1000 dilution. The resulting blot suggested that Mj0968 is a soluble, cytoplasmic protein, present *in vivo* in *M. jannaschii* cells. Applying immunoprecipitation using polyclonal antibodies against the recombinant Mj0968 protein, the existence of Mj0968 in the cytosol of *M. jannaschii* was confirmed (figure 55). The Mj0968 protein precipitated from *M. jannaschii* extract is found in a high oligomeric form (148 kDa). The same oligomerization state was observed for the heterologously expressed Mj0968 (compare figure 53).
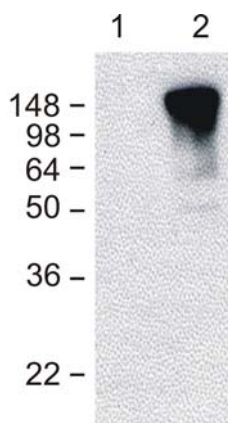
Figure 55: Immunoprecipitation of Mj0968 from *M. jannaschii* cytosolic extract. *M. jannaschii* cytosol was incubated with polyclonal antibodies against the heterologously expressed Mj0968. 10 µl of the elution fraction (lane 2) were separated by SDS-PAGE and examined by immunoblot analysis. Lane 1 shows the protein A spharose fraction after elution.

3.6.3. Kinetic characterization of Mj0968 and Mj0968-D7A

Ogawa *et al.* (2000) reported that the purified Mj0968 protein exhibited ATPase activity, which was at least in part inhibited by the phosphate analog *ortho*-vanadate. Interestingly, the ATPase activity decreased rapidly at temperatures above 55°C.
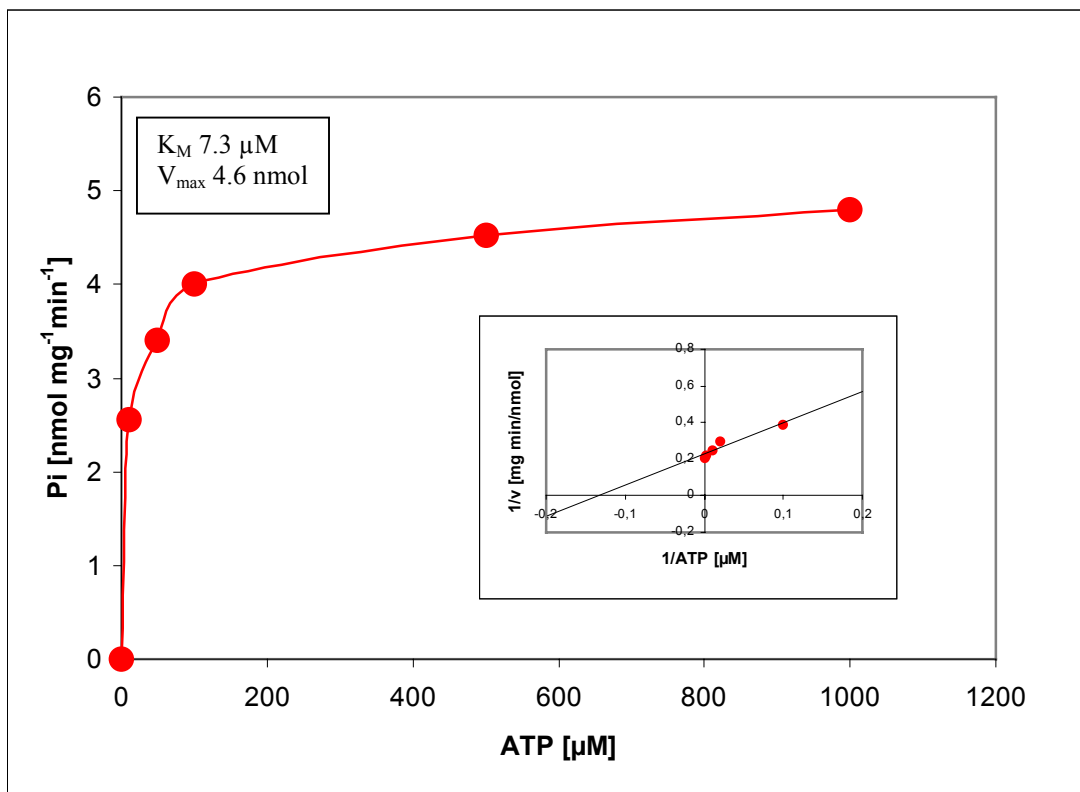
Figure 56: ATPase activity of Mj0968 wild-type. The ATPase activity was measured using the EnzCheck[®] test obtained from Molecular Probes with 50 µg of protein in a 1 ml reaction volume. A non-enzyme control was subtracted from each data point. In the inset a Lineweaver-Burk plot is shown.

Since the growth optimum of *M. jannaschii* is around 85°C, it was postulated that the protein needs a membrane bound counterpart for full activity (Ogawa *et al.*, 2000). In contrast to these findings a very low ATPase activity of maximal 4.6 nmol mg^{-1} min^{-1} detectable only using the EnzCheck[®] test from Molecular Probes (Eugene, Oregon, USA) (figure 56) was found here. Further, the ATPase activity was tested at various temperatures (37°C-85°C) using the microtiter assay as described in experimental procedures (2.6.5.) (Henkel *et al.*, 1988). Using this microtiter ATPase assay no ATP hydrolyzing activity was observed.
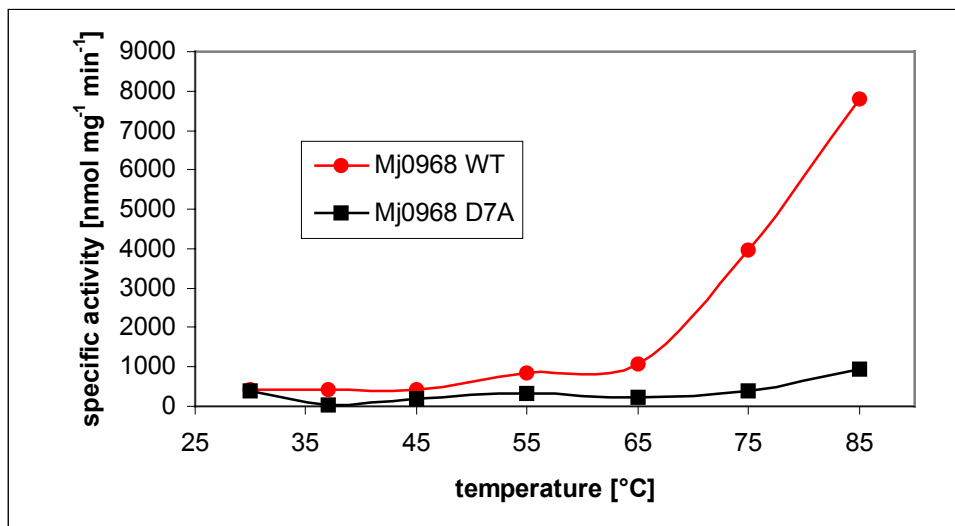
Figure 57: Dependence of Mj0968-His$_{10}$ pNPP hydrolysis on temperature. The pNPP hydrolysis rates of Mj0968-His$_{10}$ wild-type and Mj0968-D7A-His$_{10}$ mutant were determined at different temperatures. The pNPP hydrolysis was measured at 85°C using 5 µg of purified protein in a reaction volume of 100 µl. 15 mM pNPP and equimolar amounts of Mg^{2+} were used. A non-enzyme control was subtracted from each data point. All data are mean values out of three measurements.
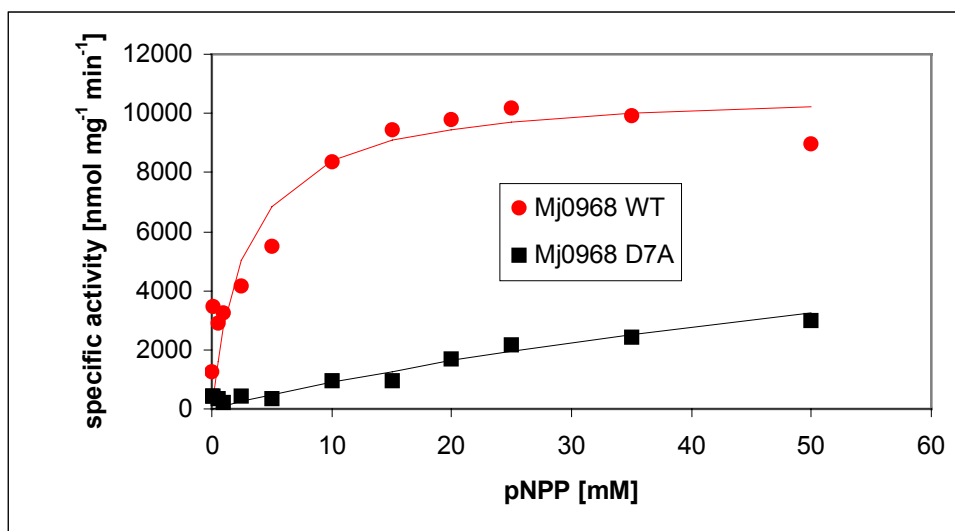
Figure 58: Phosphatase activity of Mj0968-His$_{10}$ wild-type and Mj0968-D7A-His$_{10}$ mutant. A Michaelis-Menten plot for the pNPP hydrolysis by Mj0968-His$_{10}$ and Mj0968-D7A-His$_{10}$ (5 µg) mutant protein measured at 85°C is shown. The data were fitted using the Michaelis-Menten equation.

Despite the low ATPase activity a high Mg^{2+}-dependent phosphatase activity, measured as hydrolysis of pNPP, was observed. The pNPPase activity was carried out as described in experimental procedures (2.6.6.). The pNPP hydrolysis increased drastically at temperatures above 55°C. A temperature maximum could not be determined, since the experimental setup reached a limit at 85°C (figure 57). The hydrolytic activity follows classical Michaelis-Menten kinetics (figure 58). In contrast to P-type ATPases (Ferreira-Pereira *et al.*, 1994), the pNPP hydrolysis was almost unaffected by *ortho-*

vanadate. It was found that the phosphatase activity of Mj0968 was inhibited by ATP, ADP, and to some extent by inorganic phosphate. It should be mentioned that pNPPase and ATPase activity were tested using Mj0968 protein, which was purified without heating the cell extract up to 80°C in pre-experiments. The activities measured for protein, which was not heated during the purification step were identical to those protein samples, which were purified using the 80°C step in order to achieve an enrichment of Mj0968. Therefore, it can be excluded that the heating of Mj0968 has decreased its ATPase activity.

If Mj0968 would be a P-type ATPase, the conserved residue Asp7 in the DSAGT motif should play an essential role in the hydrolytic activity. Substitutions of the corresponding amino acid in P-type ATPases resulted always in a complete loss of activity, since the aspartate residue in the DKTGT motif becomes phosphorylated during the reaction cycle of P-type ATPases. Here, it was demonstrated that Asp7 does indeed play a central role in hydrolytic activity of Mj0968 but the D7A mutant was still able to hydrolyze pNPP with an apparent K_M of 96.5 mM and a maximal activity of 9.5 µmol mg^{-1} min^{-1} (calculated according to the Michaelis–Menten equation upon data displayed in figure 58). This residual activity speaks against the formation of a stable phosphointermediate. Furthermore, the ATPase activity remained untouched by the substitution of aspartate 7 to alanine.

3.6.4. TNP-nucleotide binding to Mj0968

The interaction of wild-type Mj0968 with nucleotides was studied using fluorescent nucleotide analogues (TNP-ATP, TNP-ADP, and TNP-AMP). TNP-adenosine nucleotides were shown to bind with high affinity to the Na$^+$, K$^+$-ATPase, as well as to other members of the P-type ATPase family (Moczydlowski and Fortes, 1981a; Moczydlowski and Fortes, 1981b; Chapron and Pougeois, 1982). Binding of TNP-ATP to the soluble ATP binding loop of the Na$^+$, K$^+$-ATPase, which reflects a protein similar in structure and size to Mj0968, was also reported (Gatto *et al.*, 1998). The apparent binding affinities for TNP-ATP, TNP-ADP, and TNP-AMP, respectively, were determined by adding nucleotides to a Mj0968 solution and the resulting fluorescence change was recorded using a spectro-fluorimeter. Binding constants of the nucleotides were estimated by plotting the relative fluorescence changes against the TNP-nucleotide concentration (figure 59). The apparent affinities for TNP-ATP and TNP-ADP were determined to be 0.4 µM. For TNP-AMP the apparent affinity was around 1.0 µM. In order to test the specificity of the TNP-nucleotide binding, SDS denatured Mj0968 was titrated with TNP-ATP. Only a slight fluorescent change was detected (figure 59), probably caused by partly denatured protein.
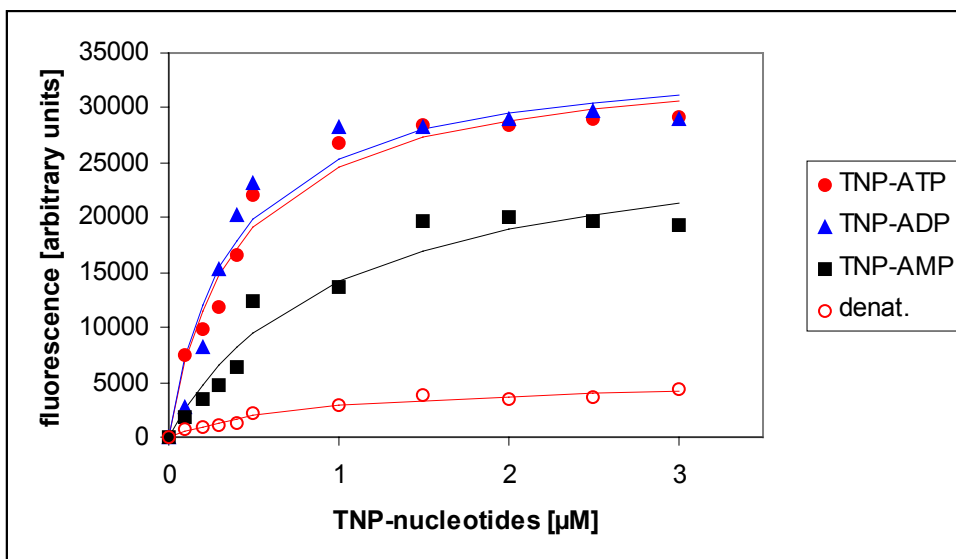
Figure 59: Nucleotide binding to Mj0968-His$_{10}$. The fluorescence change of TNP-adenosine nucleotides upon binding to Mj0968-His$_{10}$ was measured at 545 nm after excitation at 408 nm. The nucleotides were titrated to the protein solution. To demonstrate specific binding, SDS denatured proteins (denat.) were used as a control. Data were fitted to the equation: a [TNP-nucleotide] / b + [TNP-nucleotide], with 'a' representing the maximum fluorescence change and 'b' the apparent K$_d$.

3.6.5. TNP-nucleotide displacement studies with Mj0968

To determine the correct affinity constants of ATP, ADP, and AMP to Mj0968, displacement studies with TNP-ATP were carried out. These experiments were essentially performed as described for the H4H5 loop and the KdpBN domain (compare section 3.4.5.). Mj0968 (2.5 µM) was pre-incubated with different concentrations of the adenosine nucleotides at room temperature for 5 minutes. Then, TNP-ATP was titrated to the pre-incubated enzyme solution. The apparent K$_d$ values were determined and plotted against the nucleotide concentration in order to determine the K$_d$ value for the nucleotide (figure 60). Since these apparent affinity constants fit a straight line, the displacement was competitive (figure 60). The affinity constant (K$_d$) for ATP was 0.27 mM, for ADP 0.76 mM and for AMP 17.1 mM. The results are only shown for the ATP binding.
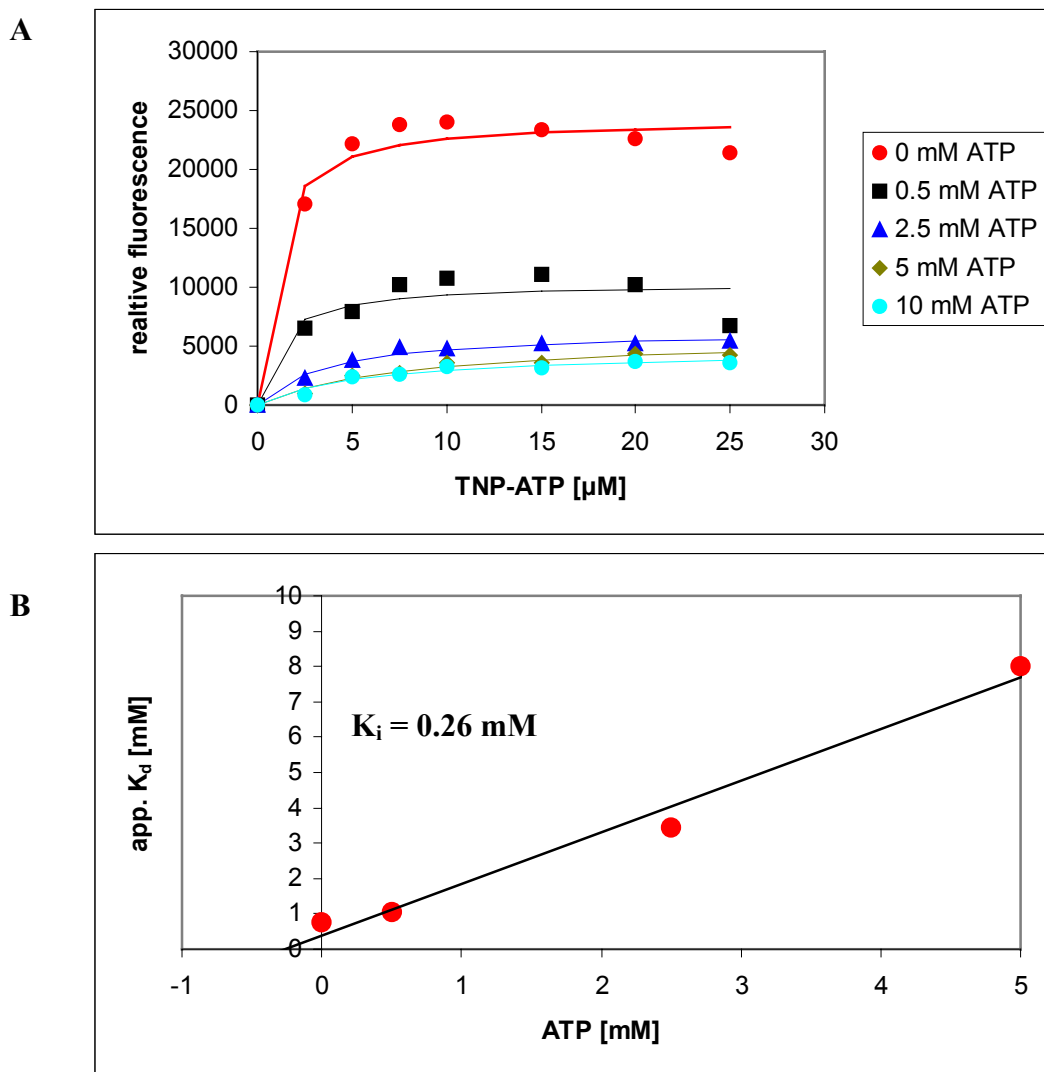
Figure 60: TNP-ATP displacement studies with Mj0968-His$_{10}$. In order to determine the affinity constants of adenosine nucleotides binding to the Mj0968-His$_{10}$ protein, displacement of TNP-ATP was measured. The Mj0968 protein was pre-incubated for 5 min at room temperature with ATP, ADP, and AMP, respectively. (**A**) The protein was than titrated with TNP-ATP and changes in fluorescence were determined. (**B**) The calculated apparent K$_d$ values were plotted against the nucleotide concentration.

3.6.6. Substrate binding studies of Mj0968 and Mj0968-D7A

All P-type ATPases are sharing the well-known DKTGT motive located within the phosphorylation domain. The aspartate residue within this motif becomes phosphorylated during the reaction cycle (Møller *et al.*, 1996). Based on these results it was of interest to find out, whether the aspartate residue Asp7 in the DSAGT motive of Mj0968 was forming a stable phophointermediate. As already reported by Ogawa *et al*. (2000) phosphorylation of Mj0968 with [γ-^{32}P]ATP could be demonstrated (figure 61). However, the same level of phosphorylation was also observed for the Mj0968-D7A mutant protein. Furthermore, labeling of wild-type and mutant protein was also observed using [α-^{32}P]ATP (figure 61, right panel) as a control. Preincubation reduced the amount of labeling to some extent.

Unspecific binding to Mj0968 and Mj0968-D7A was excluded by using TCA denatured proteins. Taken together, these results are not in accord with the formation of a phosphointermediate, but rather point to ATP being trapped within the proteins after TCA denaturation. Of course, adenylation of the proteins would be another alternative.
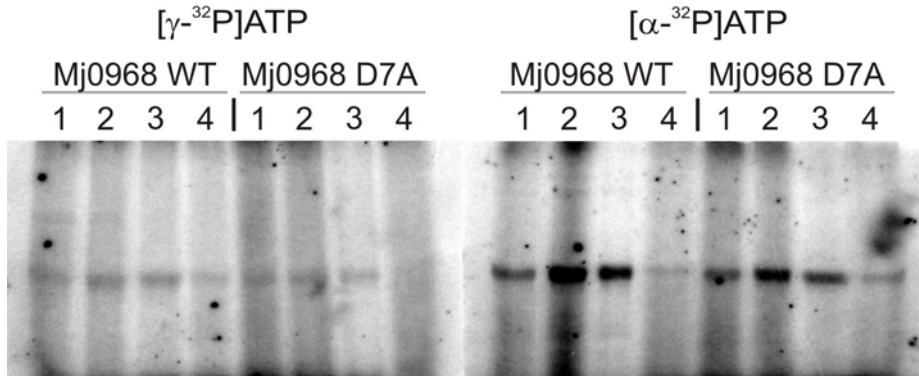
Figure 61: Autoradiography of Mj0968-His$_{10}$ wild-type and Mj0968-D7A-His$_{10}$ mutant. Purified proteins (5 µg) were incubated either with 0.33 mM [γ-^{32}P]ATP or [α-^{32}P]ATP at 56°C. Lane 1, 5 minutes incubation; lane 2, 20 minutes incubation; lane 3, pre-incubation with 10 mM ATP and incubation for 20 minutes with radioactive ATP derivatives; lane 4, TCA denatured protein was used as control.

3.6.7. 8-azido-[α-^{32}P]ATP labeling studies with Mj0968

ATP-binding to Mj0968 was demonstrated by labeling with 8-azido-[α-^{32}P]ATP (2 µM) (figure 62). However, labeling was not prevented by addition of ATP (2 mM – 20 mM) even in a thousand or ten-thousand-fold excess, indicating that 8-azido-[α-^{32}P]ATP and ATP might not bind exactly to the same site. The effects observed with the Mj0968 protein were found to be quite similar to the H4H5 loop.
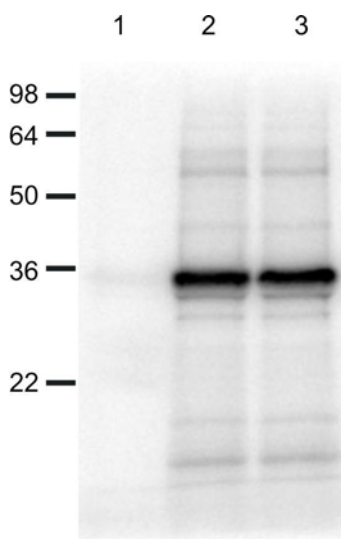
Figure 62: 8-azido-[α-^{32}P]ATP labeling of Mj0968-His$_{10}$. Purified Mj0968-His$_{10}$ (5 µg) was labeled with 5 µCi 8-azido-[α-^{32}P]ATP that results in an 8 µM 8-azido-[α-^{32}P]ATP concentration. The labeling reaction was carried out as described in section 2.7.1. (1) dark control without light activation, (2) positive control, (3) 2 mM ATP added prior light activation.

4. Discussion

Because of the different aspects processed within this study, the discussion cuts into several parts, according to the result part. First of all, the topology of KdpB is discussed in comparison to the high-resolution structure of the SERCA pump. The results of the mutagenesis study within KdpB are discussed below ending up with a new transport model for the Kdp-ATPase. The new biochemical properties of the wild-type KdpFABC complex are discussed next, followed by a section, which deals with the cloning, production and biochemistry of soluble subdomains of KdpB. The structural analysis of the nucleotide-binding domain (KdpBN) of KdpB will be discussed in an adjoining section. Last, cloning, production, and biochemistry of an archaeal protein (Mj0968), described as soluble P-type ATPase (Ogawa *et al.*, 2000), will be discussed.

4.1. A new structural model of KdpB

For more than a decade, the topology model of KdpB was only based on hydrophobicity plot analysis (Siebers *et al.*, 1988; Altendorf *et al.*, 1998). This old model predicted six transmembrane helices (TM) for KdpB. Support for this model came from the topology of heavy metal-transporting ATPases, which have, in addition to the two N-terminal transmembrane helices, a six TM core domain (compare figure 3, introduction). Therefore, Axelsen and Palmgren (1998) hypothesized that the Kdp-ATPase might represent an ancestral P-type ATPase and that in later-evolved P-type ATPases the ATP hydrolyzing subunit (KdpB) and the ion transporting subunit (KdpA) might have fused. Against this hypothesis speaks the fact that none of the transmembrane helices of KdpA shares any homology with the TM's of P-type ATPases involved in ion transport (Buurman *et al.* (1995) discussed that parts of TM9 of KdpA around residue 501 have similarities with the Ca^{2+}-ATPase, but the corresponding parts in the SERCA pump are around residue 720, which is part of the P-domain and therefore facing the cytoplasm). However, weak homologies between KdpA and potassium transporting channels of the 2TM-type superfamily were found (Durell *et al.*, 2000). The idea of a gene fusion between KdpA and a KdpB ancestor is therefore unlikely. The KdpB topology came into focus when experiments were initiated to isolate the cytoplasmic portion of KdpB with the final aim of structural analysis. The first construct was cloned according to the old, six TM topology model. The region between TM4 and TM5 (ranging from leucine 271 to serine 615) was synthesized in *E. coli* cells and found to be still membrane integral (data not shown).

α1   α2   α3   α4

SERCA1

```
1        10        20        30        40        50        60
SERCA1  MEAAHSKSTEECLAYFGVSETTGLTPDQVKRHLEKYGHNELPAEEGKSLWELVIEQFEDLLVRILLL
KdpB    ..............MSRKQLALFEPTLVVQALKEAVKKLNPQAQWRNPVMFIVWIGS.......LL
```

α5   η1   β1

SERCA1

```
70        80        90        100       110       120       130
SERCA1  AACISFVLAWFEE.GEETITAFVEPFVILLILIANAIVGVWQERNAENAIEALKEYEPEMGKVYRAD
KdpB    TTCISIAMASGAMPGNALFSAAISGWLWITVLFANFAEALAEGRSKAQANSLKGVKKTAFARKLREP
```

β2   TT   TT   β3   TT   β4   β5   β6

SERCA1

```
140       150       160       170       180       190
SERCA1  RK..SVQRIKARDIVPGDIVEVAVGDKVPADIRILSIKSTTLRVDQSILTGESVSVIKHTEPVPDPR
KdpB    KYGAAADKVPADQLRKGDIVLVEAGDIIPCDGEVIEGGAS...VDESAITGESAPVIRESG......
```

η2   β7   β8   TT   η3   α6   α7

SERCA1

```
200       210       220       230       240       250       260
SERCA1  AVNQDKKNMLFSGTNIAAGKALGIVATTGVSTEIGKIRDQMAATEQDKTPLQQKLDEFGEQLSKVIS
KdpB    ....GDFASVTGGTRILSDWLVIECSVNPGETFLDRMIAMVEGAQRRKTPNEIALTILLIALTIVFL
```

α8   TT   α9   β9

SERCA1

```
270       280       290       300       310       320       330
SERCA1  LICVAVWLINIGHFNDPVHGGSWIRGAIYYFKIAVALAVAAIPEGLPAVITTCLALGTRRMAKKNAI
KdpB    LATATLWPFSA.......WGGNAVS.....VTVLVALLVCLIPTTIGGLLSAIGVAGMSRMLGANVI
```

α10   β10   β11   TT   β12   β13   TT

SERCA1

```
340       350       360       370       380       390
SERCA1  VRSLPSVETLGCTSVICSDKTGTLTNQMSVCKMFIIDKVDGDFCSLNEFSITGSTYAPEGEVLKND
KdpB    ATSGRAVEAAGDVDVLLLDKTGTITLGNRQASEFIPAQGVD................
```

β14   η4   α11   β15   β16   α12   TT   α13

SERCA1

```
400       410       420       430       440       450       460
SERCA1  KPIRSGQFDGLVELATICALCNDSSLDFNETKGVYEKVGEATETALTTLVEKMNVFNTEVRNLSKVE
KdpB    .......EKTLADAAQLASLADET...................PEGRSIVILAKQRFNLRERDVQSLH
```

α14   β17   β18   TT   β19   α15   β20   TT

SERCA1

```
470       480       490       500       510       520       530
SERCA1  RANACNSVIRQLMKKEFTLEFSRDRKSMSVYCSPAKSSRAAVGNKMFVKGAPEGVIDRCNYVRVGTT
KdpB    AT..............FVPFTAQSRMSGINIDNRMIRKGSVDAIRR.....HVEAN
```

β21   α16   β22   η5   η6   α17   β23

SERCA1

```
540       550       560       570       580       590       600
SERCA1  RVPMTGPVKEKILSVIKEWGTGRDTLRCLALATRDTPPKREEMVLDDSSRFMEYETDLTFVGVVGML
KdpB    GGHFPTDVDQKVDQVARQGAT...............PLVVVEGS........RVLGVIALK
```

α18   β24   α19   β25   α20   α21

SERCA1

```
610       620       630       640       650       660
SERCA1  DPPRKEVMGSIQLCRDAGIRVIMITGDNKGTAIAICRRIGIFGENEEVADRAYTGREFDDLPLAEQR
KdpB    DIVKGGIKERFAQLRKMGIKTVMITGDNRLTAAAIAAEAGVDD................
```

β26   α22   β27   α23   β28   TT   α24   β29

SERCA1

```
670       680       690       700       710       720       730
SERCA1  EACRRACCFARVEPSHKSKIVEYLQSYDEITAMTGDGVNDAPALKKAEIGIAMGSGTAVAKTASEMV
KdpB    .......FLAEATPEAKLALIRQYQAEGRLVAMTGDGTNDAPALAQADVAVAMNSGTQAAKEAGNMV
```

Figure 63: Sequence comparison of the sarcoplasmic reticulum Ca²⁺-ATPase and *E. coli* KdpB. The alignment was performed using CLUSTALW (Thompson *et al.*, 1994). The resulting .aln file was introduced to ESPript (http://prodes.toulouse.inra.fr/ESPript/cgi-bin/nph-ESPript_exe.cgi) and compared to the secondary structure of the Ca²⁺-ATP in the E1 state (Toyoshima *et al.*, 2000). The structural data 1EUL were retrieved from the Brookhaven protein database. The ESPript alignment was performed using default parameters. The secondary structure elements are shown above the sequences. Identical amino acid residues are boxed in red, similar residues are written in red, gaps are indicated by dots.

This unexpected result led to a new inspection of the KdpB sequence and its proposed topology. In fact, the conserved motifs, common for all P-type ATPases, suggested that the cytoplasmic loop and hence the phosphorylation domain might end directly after the Rossman fold around amino acid 570 (this is the case in all family members). Furthermore, hydrophobicity plots predict a very hydrophobic region in the C-terminal half of the protein, making it fairly difficult to judge whether there exist two or three TM domains. Thus, a new construct was designed, ranging from methinonie 282 to glutamine 567. Since this new construct, called H4H5 (see 3.4.1.), was soluble it seemed to be obvious that the old model predicted a cytoplasmic loop, which was extended in its C-terminal part and accordingly containing a component of the membrane integral part. Thus, it is most likely that KdpB contains seven instead of six transmembrane helices. A breakthrough in the structural analysis of P-type ATPases came with the 2.6 Å resolution structure of the sarcoplasmic reticulum Ca²⁺-ATPase (Toyoshima *et al.*, 2000). With this structure at hand, modeling of any P-type ATPase was possible, using the key motifs as landmarks. Modeling of KdpB based on the structural data of the SERCA pump in the E1 state (Toyoshima *et al.*, 2000) and the E2 state (Xu *et al.*, 2002, 1KJU) was performed. The models of KdpB in the E1 and E2 conformation also provided a first hint about the domain movements and interactions occurring during the E1/E2 transition (figure 64).

The model of the KdpB subunit confirms the topological predictions derived from the cloning experiments and the hydrophobicity plots. Furthermore, the new KdpB model reveals similarities as

well as differences between KdpB and the Ca^{2+}-ATPase. The P-domain of KdpB ends after residue 555 and is therefore in good agreement with the alignment of this domain (figure 63). Interestingly, the extension of the large cytoplasmic domain is exactly as predicted for the subcloning of the H4H5 domain (section 3.4.1.). The seven TM domains are arranged as follows: TM1 (26-51), TM2 (68-99), TM3 (216-238), TM4 (251-280), TM5 (555-592), TM6 (605-623), and TM7 (647-671). TM5 includes the stalk domain, since it starts in the P-domain and ends up at the periplasmic side without being kinked. The idea that the KdpB polypeptide may have seven TM's seems to be commonly accepted, since this model was also introduced into the P-type ATPase database (http://biobase.dk/~axe/Patbase.html). The fact that KdpB might have seven instead of six TM's separates the KdpB subunit drastically from the related heavy metal-transporting P-type ATPases. The hypothesis that the KdpFABC complex displays an ancestor of later-evolved P-type ATPases might therefore not be true. Rather, the KdpB subunit might have lost the TM domains 8-10, which are found in the larger eukaryotic P-type ATPases, when it acquired the channel-like subunit KdpA.

Modeling of KdpB was not possible in the region of the proposed nucleotide-binding domain. This part of KdpB is roughly 100 amino acids smaller compared to the Ca^{2+}-ATPase. The extension of the nucleotide-binding domain is similar as found for the heavy metal-transporting ATPases and the plasma membrane H^+-ATPase, which led to the grouping of KdpB into the type I class of P-type ATPases (type Ia: Kdp-ATPases; type Ib: heavy metal-transporting ATPaes) (Axelsen and Palmgren, 1998). The validity of the KdpB model is strongly dependent on the sequence alignment with the SERCA pump. The alignment, however, is only flunky within the region of the N-domain. The transmembrane parts of the KdpB polypeptide and the Ca^{2+}-ATPase align quite well and without larger gaps, providing evidence for the quality of the model within these domains. Sequence alignment studies with KdpB polypeptides from different organisms revealed that the TM5 region is highly conserved. Interestingly, two charged residues Asp583 and Lys586 are located directly in the middle of TM5 according to the new topology model (compare figure 9). Both residues are highly conserved among all KdpB sequences known so far.

4.2. Mutational analysis of KdpB leads to a new transport model

As already mentioned above, the KdpB subunit contains two charged amino acids within TM5 (figure 9), Asp583 and Lys586. These amino acids are highly conserved throughout the KdpB polypeptides, but have no counterpart in other P-type ATPases. Therefore, these residues were subjected to site-directed mutagenesis. The Asp583 residue was changed to alanine, serine, asparagines, lysine, and glutamate (named D583A, D583S, D583N, D583K, and D583E). The residue Lys586 was changed to alanine, arginine, threonine, and aspartate (K586A, K586R, K586T, and K586D). The substitutions D583A, D583S, D583N, and D583K showed no growth below 15 mM KCl on solid agar plates. However, the conservative exchange D583E behaved like the wild-type. The K586 mutant complexes

allowed growth at potassium concentrations above 0.3 mM. The K586R derivative, where the positive charge is restored, is again similar to the wild-type. The fact that the K586 and D583 complexes exhibit different phenotypes with respect to growth on potassium limited media, rule out the possibility that D583 and K586 might form a salt bridge. Another argument against the formation of a salt bridge is the insertion of all mutant proteins into the cytoplasmic membrane (compare figure 10). Examples of salt bridges within P-type ATPases demonstrate the importance of such bonds for a correct membrane insertion and routing of the enzymes. The yeast plasma membrane H^+-ATPase contains a salt bridge between transmembrane segments 5 and 6 (Gupta *et al.*, 1998). Site-directed mutagenesis at the residues R695 and D730 was performed where positively and negatively charged residues were swapped or eliminated (R695D:D730R and R695A:D730A). The results revealed that the double mutants retain their correct membrane insertion and pumping activity (Gupta *et al.*, 1998). In case of the charged residues within the putative TM5 of KdpB, a double mutant (D583A:K586A) was constructed. This double mutant exhibited the same phenotype as observed for those D583 mutant complexes, where the negative charge was removed. This result indicates that the D583 residue has a dominant effect and plays a major role in the function of KdpB.

In order to characterize the altered KdpFABC complexes biochemically, TKW3205 cells carrying the corresponding pSMC10His derivatives were grown in minimal medium supplemented with 0.5 (for K586 mutant complexes) or 5 mM KCl (for D583 mutant complexes). The overall ATPase activity was similar between mutant enzymes and wild-type enzyme complexes, however, the ATPase activity of the D583A complex was not stimulated by potassium. Furthermore, the sensitivity against *ortho*-vanadate was drastically reduced (figure 12). Two plausible explanations are possible: i) The mutated enzyme complex is disturbed in the intra subunit communication of KdpB. It is commonly accepted that P-type ATPases undergo domain movements during the reaction cycle. Movements of the cytoplasmic parts, e.g. the phosphorylation domain and nucleotide-binding domain, induce movements in the transmembrane segments. A mutation at D583 could disturb or eliminate this interaction. ii.) The function of KdpB is not affected, but the hydrolysis of ATP is no longer coupled to ion transport. Additional experiments are necessary to distinguish between these two possibilities. Reduced vanadate sensitivity can be explained for both cases. If the conformational changes between the E1~P state and the E2-P state are disturbed, accumulation of E1~P would occur. Since vanadate is supposed to bind to the E2 state it is obvious, why the inhibitory effect is lowered. On the other hand, it is well accepted that ion binding and transport is necessary for a proper reaction cycle of P-type ATPases. A typical example is the Na^+-ATPase activity and the K^+-pNPPase activity of the Na^+, K^+-ATPase. In case of a direct interaction of the D583 residue in KdpB on this transport activity, accumulation of an E1 state could also be possible. To provide evidence that the D583A and D583E complexes were able to transport ions or not, reconstitution experiments were carried out. Reconstitution of the altered complexes into proteoliposomes revealed that the D583A mutant has lost the ability to transport potassium ions, although the ATPase activity was not affected (figures 15 and

16). In contrast, the D583E complex was still able to facilitate ion translocation, although the transport activity was less compared to the wild-type KdpFABC complex. Assuming that the D583 residue is involved in ion translocation, the question remains, whether this interaction is direct or indirect. Electrophysiological measurements with KdpFABC complexes, adsorbed to black lipid membranes (BLM), suggested that a protein-bound negative charge might move relative to the membrane during the reaction cycle (Fendler *et al.*, 1996; 1999). Localization of this charge has hitherto not been possible. However, it is likely that this charge is located within KdpB and not in KdpA, since the channel-like KdpA structure seems to be more rigid than KdpB. Major vertical movements are not observed in potassium channels. The D583 residue in KdpB might be a good candidate for that, since this residue is membrane embedded and conserved throughout the KdpB polypeptides of different organisms (in contrast to D614, located in TM6, which is not conserved). First BLM experiments with the D583A mutant indicated that D583 might be a candidate for the protein-bound charge (data not shown), which moves during the reaction cycle. However, further experiments have to be carried out to substantiate this hypothesis.
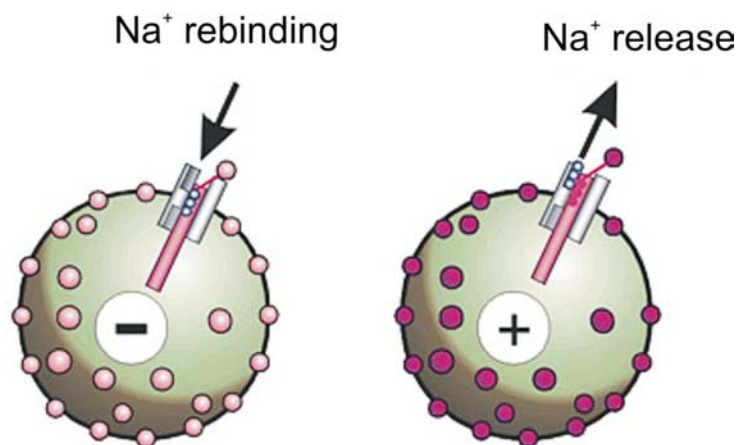
Figure 64: Model of TM domain movement in the Na$^+$, K$^+$-ATPase, as detected by fluorescence labeling.
Upon injection of cRNA Na$^+$, K$^+$-ATPase constructs carrying single cysteine mutations within the TM5-TM6 loop are functionally expressed in *Xenopus laevis* oocytes. Prior to measurements, oocytes are placed in a solution containing tetramethylrhodamine-maleimide to label extracellularly exposed cysteines, giving rise to strong fluorescence. Charge movements and fluorescence changes were observed simultaneously by two-electrode voltage-clamps mounted on the stage of a fluorescence microscope. The Na$^+$ transport steps are the electrogenic events of the reaction cycle and kinetically coupled to the E$_1$P–E$_2$P transition. Therefore, changes in membrane potential shift the distribution of E$_1$P–E$_2$P conformational states. Negative potentials favor the formation of E$_1$P, whereas E$_2$P is formed at positive potentials. After a voltage pulse relaxation into the new equilibrium occurs, which is accompanied by charge movement leading to a transient current. Charge movement and fluorescence change were kinetically equivalent. The change in fluorescence indicates the movement of TM5 in case of the Na$^+$, K$^+$-ATPase. (Taken from T. Friedrich, http://www.biophys.mpg.de)

The results obtained for the D583 and K586 mutants led to a complete new ion transport model for the Kdp-ATPase. The key question is: How does ATP hydrolysis and domain movement in KdpB trigger ion translocation through a channel-like KdpA subunit, which might be located adjacent to

90

KdpB? Ion transport through P-type ATPases is not understood in detail, although several amino acids contributing to the ion translocation have been pinpointed down in other P-type ATPases. With the exception of the Kdp-ATPase all other enzymes of the P-type family couple ATP hydrolysis and domain movement directly to ion transport. These enzymes share an ion binding pocket within the membrane and exhibit an occluded state as a logical consequence. The example of the well-studied sarcoplasmic reticulum Ca^{2+}-ATPase shows that the ion binding pocked is formed by TM4-TM6 and TM8. The helices TM4 and TM6 are unwound at the level of the calcium binding sites (McIntosh, 2000). Site-directed mutagenesis has identified most of the contributing residues (Clarke *et al.*, 1989). However, not all coordinating residues were discovered by site-directed mutagenesis, since backbone oxygen atoms contribute to ion coordination. Toyoshima and co-workers postulated a water filled access channel from the cytoplasm to the occlusion site and from there to the luminal site (Toyoshima *et al.*, 2000). In fact, sequence alignments seem to substantiate the idea that all P-type ATPase of the type II-V classes share an overall topology, including an access channel for ions (Sweadner and Donnet, 2001). The Kdp-ATPase, however, must have a different ion translocation mechanism. A substantial body of experimental evidence exists in favor of KdpA being the ion-translocating subunit. Sequence alignments exhibit homologies between KdpA and potassium channels, like HKT1, KtrAB, and Trk (Durell *et al.*, 2000; Jan and Jan, 1994). Furthermore, random mutagenesis (Buurman *et al.*, 1995) identified mutations affecting the affinity for potassium in the proposed P-loop regions predicted by Jan and Jan (1994). In addition, site-directed mutagenesis at the proposed selectivity filter regions G232, G233, G233 (van der Laan *et al.*, 2002), and G345 (J. Bertrand, M. Bramkamp and K. Altendorf, unpublished results) support the hypothesis that KdpA has indeed a channel-like function. The physiological properties of channels are the transport of ions along a chemical gradient. Active accumulation against a gradient is not possible. The Kdp-ATPase has solved this problem by acquiring the high affinity KdpA subunit and the ATP-hydrolyzing KdpB subunit, thereby forming an active ion pump. The interplay between KdpB and KdpA can either be explained by an ion channel, which is build up of residues from both subunits or an inductive transport, mediated by charge movement only within KdpB. This inductive transport hypothesis is based on the mast-like TM5 structure in KdpB, which starts directly under the phosphorylation site and which is spanning the stalk and the membrane parts. The two charged residues discussed above, D583 and K586, located in the middle of the membrane part are probably forming a strong dipole. Movement of such a dipole will have effects on potassium ions sitting in the selectivity filter of KdpA (see below). A general principle of potassium channels is the removal of the hydration shell of the ion. The water molecules are stripped of when the ion moves through the selectivity filter, where it is almost occluded in a bottleneck. Most likely, the filter contains two ions at a time, separated by two water molecules. The two ions move in a concerted fashion between the two configurations, K^+-H_2O-K^+-H_2O (1, 3 configuration) and H_2O-K^+-H_2O-K^+ (2, 4 configuration), until a third ion enters, displacing the ion on the opposite side of the queue (Morais-Cabral *et al.*, 2001, Sansom *et al.*, 2000, Luzhkov and Åqvist, 2001). The difference between a pump

and a channel is the generation of a chemical gradient by the pump. Therefore, the Kdp-ATPase needs to "push" the ion through the bottleneck of the selectivity filter into a putative, water filled cavity of KdpA where the potassium ion is rapidly re-hydrated and released into the cytosol. In addition, a gating mechanism must exist in KdpA, which permits backflow of the ions when the enzyme is undergoing the E2-E1 transition. Movements of transmembrane domains, which might close the central cavity within KdpA from the cytosolic side, probably mediate the gating. The energy to push the ion through the bottleneck could come as electrical energy in form of a moving dipole within KdpB. The residues D583, K586 could represent such a dipole. In view of the fact that the membrane compartment has a comparatively low dielectric constant, the de-hydrated ion in the selectivity filter would be quite sensitive to such electrical forces. The new transport model is presented in figure 65. Recently, E. Bamberg and T. Friedrich presented experimental evidence in favor of the vectorial movement of TM5 in the Na^+, K^+-ATPase (figure 64). Cysteine residues were introduced into the extracellular loop between TM5 and TM6 for site-specific fluorescence labeling. Using the fluorescent dye tetramethylrhodamine-maleimide to label the extracellularly exposed cysteines, they were able to show that TM5 moves vectorially upon ion binding / ion release (http://www.biophys.mpg.de).
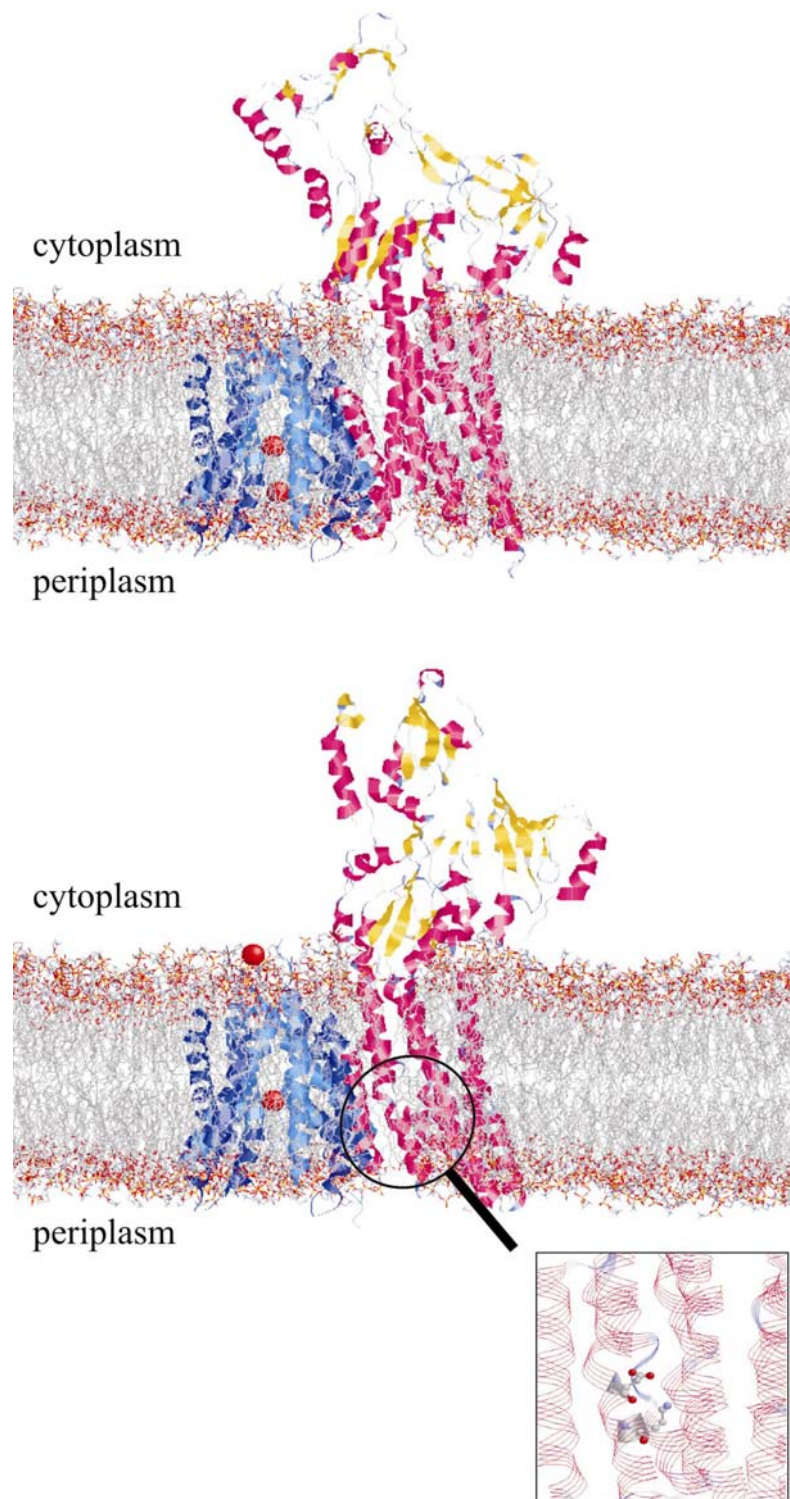
Figure 65: New transport model for the Kdp-ATPase. Illustrated are models of the E1 and E2 state of the enzyme. The KdpB subunit was modelled according to structural data of the SERCA pump in E1 (Toyoshima *et al.*, 2000) and E2 (Xu *et al.*, 2002). The structure of the prokaryotic potassium channel KcsA (Doyle *et al.*, 1998) served as model for the KdpA subunit (blue). Potassium ions (red) are bound to the selectivity filter in the 1, 3 conformation in the E1 state. The ATP driven conformational transition to the E2 state induces large domain movements in KdpB. Subsequently, the charged amino acids in TM5 (Asp583 and Lys586) are moved and consequently their dipole moment changes. The electric influence on the potassium ion may trigger the release of the occluded K^+ from the adjacent KdpA subunit into the cytosol. The charged residues are highlighted in the magnification box.

93

4.3. Biochemical features of the KdpFABC complex

FITC modification at a lysine residue in the KGAPE motif of the Ca^{2+}-ATPase (SERCA) (Pick and Bassilian, 1981), the Na^+, K^+-ATPase (Farley *et al.*, 1984), the plasma membrane Ca^{2+}-ATPase (Fioleto *et al.*, 1997) and H^+-ATPase (Pardo and Slayman, 1988) abolishes the hydrolysis of ATP, but pNPP hydrolysis is maintained (Linnertz *et al.*, 1995; Donnet *et al.*, 1998). Sequence comparison with these enzymes revealed that KdpB has a similar motif, 395-KGSV-398, which might be the site of FITC modification. Siebers *et al.* (1988) already reported that FITC is a potent inhibitor of the Kdp-ATPase. However, unspecific labeling of all three subunits (KdpF cannot be seen in 12-14 % SDS PAGE) was observed (compare figure 17). In contrast, at high ionic strength exclusive labeling of KdpB was achieved. In order to identify the FITC modified residue in KdpB the protein was cleaved with CNBr. Two of the digestion products, which still exhibited FITC fluorescence were sequenced. Although, there are five other lysine residues in the C-terminal end of both peptides, for analogy reasons it is most likely that the 395-KGSV motif is the FITC binding site. Furthermore, convincing evidence that Lys395 is indeed the binding site of FITC comes from the observation that the KdpB polypeptide of *Enterococcus faecalis* (former: *Streptococcus faecalis*) does not contain the KGSV motif, and is therefore not inhibited by FITC (Solioz *et al.*, 1987). In addition, the labeled fragments are part of in the nucleotide binding region of the KdpB subunit, indicating that FITC binds in the same region as found for other P-type ATPases (Møller *et al.*, 1996; Serrano, 1988).

Since Steve Karlish introduced FITC as a tool for probing the high affinity ATP binding site (E1ATP) of the Na^+, K^+-ATPase (Karlish, 1980), a large body of experimental data are available in which FITC or related fluorescence dyes were used for studying the catalytic properties of P-type ATPases. Based on the observation that FITC binds specifically to the KdpBN-domain, a number of experiments could be designed to characterize the catalytic properties of the KdpFABC complex and to study soluble subdomains of KdpB.

The influence of nucleotides on the FITC modification was described for a variety of P-type ATPases (Pick and Bassilian, 1981; Farley *et al.*, 1984; Fioleto *et al.*, 1997; Pardo and Slayman, 1988; Linnertz *et al.*, 1995; Donnet *et al.*, 1998). The most extensive work, however, was done with the Na^+, K^+-ATPase (Karlish, 1980; Rephaeli *et al.*, 1986; Ward and Cavieres, 1996; 1998; Scheiner-Bobis *et al.*, 1993; Linnertz *et al.*, 1995; 1998). In case of the sodium pump FITC is an inhibitor of the high affinity ATP binding site (Linnertz *et al.*, 1999). This fluorescent dye monitors the E1-E2 transition (Karlish, 1980; Rephaeli *et al.*, 1986), inhibits the partial reactions of the E1 site, e.g. the Na^+-ATPase activity, but lets the partial reactions of the proposed low affinity E2 site, e.g. K^+-stimulated pNPPase and backdoor phosphorylation *via* P_i untouched (Linnertz *et al.*, 1995). In addition to FITC, a variety of ATP analogs have been used to study either the E1 or the E2 site. Erythromycin (ErITC) was shown to modify the E1 and the E2 site (Linnertz *et al.*, 1998), $Cr(H_2O)_4ATP$ is a

phosphorylating agent acting on the E1 site (Linnertz *et al.*, 1995), Cr(H$_2$O)4-Ado*PP*[CH2]*P^1* is a non-phosphorylating analog binding to the E1 site (Linnertz *et al.*, 1995), Co(NH$_3$)$_4$ATP and DANS-ATP[2] derivatives bind specifically to the low affinity E2 site (Buxbaum and Schoner, 1980; Thoenges and Schoner, 1997). Furthermore, H$_2$DIDS[3] (Gatto *et al.*, 1997) and azido-ATP analogs (Tran *et al.*, 1994; Ward and Cavieres, 1998) were used for studying reactive residues within the ATP binding site of the sodium pump. Despite this intensive studies, there is still a long-standing discussion, where these ATP sites are located (McIntosch, 2000). In the early days of P-type ATPase research, the ATP dependent catalytic mechanism was described by the so-called Alberts-Post mechanism (Albers, 1967; Post *et al.*, 1972). This simplified mechanism, however, cannot explain the diphasic kinetic behavior of P-type ATPases. Therefore, Fortes and co-workers proposed a single ATP binding site, that alternates between a high and a low affinity state (single site model) (Moczydlowski and Fortes, 1981). A second model, based on suggestions by Repke and co-workers, includes two catalytic α-subunits, which cooperate with eachother. Each of the catalytic subunits in the proposed (αβ)$_2$ diprotomer undergoes the same conformational transitions as proposed in the Alberts-Post mechanism, but the individual subunits are 180° out-of-phase with respect to each other (Repke and Schön, 1973, Stein *et al.*, 1983) (Repke-Schön-Stein model). Plesner suggested that the cooperativity of α-subunits occurs only in the presence of Na$^+$ and K$^+$, while otherwise the protomeric enzyme catalyzes only partial reactions (Plesner, 1987). Evidence in support for all theses models has been published. In addition Ward and Cavieres and others proposed a catalytic and a regulatory ATP binding site in the same molecule (Ward and Cavieres, 1996; 1998a; Gatto *et al.*, 1997), while others assume that the ATP binding sites are located on different subunits of an (αβ)$_2$ diprotomer (Linnertz *et al.*, 1995; 1998) or tetramer (Tsuda *et al.*, 1998; Taniguchi, *et al.*, 2001). Furthermore, Stokes and Green proposed two possible cavities for ATP binding in the large cytoplasmic loop for the Ca^{2+}-ATPase by analyzing the 8 Å density map (Stokes and Green, 2000). Even the atomaric structures of the SERCA pump in the E1 state (Toyoshima *et al.*, 2000) and the E2 state (Toyoshima and Nomura, 2002; Xu *et al.*, 2002) did not clarify this point, since none of the crystals was grown in the presence of nucleotides.

Although, it was reported that pNPP is not a substrate for the Kdp-ATPase (Siebers, 1988), here it could be shown that the KdpFABC complex hydrolyzes pNPP in an Mg^{2+}-dependent way. Interestingly, the V$_{max}$ (~ 11µmol mg^{-1} min^{-1}) is 50-60 times higher compared to the Ca^{2+}-ATPase (0.2 µmol mg^{-1} min^{-1}). Since the hydrolysis of pNPP is associated with the E2 conformation in case of other P-type ATPases (Post *et al.*, 1972), the hydrolysis of pNPP by the Kdp-ATPase lends support to the notion that the Kdp-ATPases has at least two catalytic states.

It was previously shown that nucleotides like ATP and ADP have a protective effect on FITC modification (Pick and Karlish, 1980; Gatto *et al.*, 1998) of the Na$^+$, K$^+$-ATPase. For the Kdp-ATPase

---

[1] β,γ-bidentate complex of chromium(III)-tetraaqua-adenylyl [β,γ-methylene]diphosphonate
[2] 2'-O-(6-dimethylaminonaphthalenesulfonyl)adenosine 5'-triphosphate
[3] dihydro-4,4'-diisothiocyanostilbene-2,2'-disulfonate

a similar protective effect of ATP and ADP was observed. Interestingly, the best protective effect was mediated by AMP, which had no protective effect in case of the sodium pump. This result support the idea that the FITC binding site is located in the N-domain of KdpB, as suggested by the CNBr cleavage studies. However, it reveals that differences exist in the FITC binding site between the sodium pump and the Kdp-ATPase. This could be explained in two ways, (i) the N-domain of the sodium pump could bind both, AMP and FITC and the N-domain of KdpB, which is ~ 100 residues smaller, cannot; (ii) FITC could bind to the E1ATP and E2ATP site in case of the Kdp-ATPase. Although it was shown that the catalytically active sodium pump could bind both, TNP-ADP (or TNP-AMP) and FITC (Scheiner-Bobis *et al.*, 1993), it is unlikely that FITC and a nucleotide molecule bind exactly at the same side, since the adenosine ring occupies the same site as the fluorescein moiety of FITC (Carilli *et al.*, 1982). Therefore, it could be possible that FITC binds to the E1ATP and E2ATP site in the KdpB polypeptide. Evidence in support of this idea comes from the fact that FITC modification does not only abolish the ATPase activity but also the pNPP hydrolysis in case of the Kdp-ATPase (figure 27). Furthermore, it was not possible to detect any E1-E2 transition using FITC modified KdpFABC complex (data not shown). If FITC binds to the proposed E1 and E2 site, fluorescence changes would quench themselves.

The fact that the Kdp-ATPase, as probably all other P-type ATPases, undergoes a reaction cycle, which is not compatible with the simplified Albers-Post scheme, became apparent during this thesis. Although, Siebers *et al.* (1988) presented a reaction cycle in accordance with the Albers-Post scheme (Siebers *et al.*, 1988) data do exist, which are in not in accord with a single ATP site. The ATPase activity of the Kdp-ATPase exhibits a complex, non-Michaelian dependence on ATP concentration. Results obtained within this thesis are in good accord with data obtained by quenched flow measurements, which describe the ATP dependence of E-P formation (J. Froehlich, S. Dröse and K. Altendorf, personal communication). Like other P-type ATPases, the KdpFABC complex exhibits diphasic kinetics towards ATP. The cycle includes E1, E2 and E1~P, E2-P intermediate states that undergo interconversion during ATP hydrolysis. K^+ is not required for phosphorylation, but rather activates E2-P hydrolysis. The apparent affinity of the E1 form of the enzyme for ATP is about 1 μM or lower, while the affinity of the overall ATPase reaction is about 0.1 mM (J. Froehlich, personal communication). This implies that ATP binds with low affinity to an intermediate state and accelerates the turnover of E2 (or E2-P) and the release of K^+ into the cytoplasm. It is noteworthy, that the reaction cycle of the Kdp-ATPase shares similarities with the reaction cycle of the Na^+, K^+-ATPase. However, also differences exist between both systems. The Kdp-ATPase and the sodium pump share the E1-E2 interconversion, the binding of potassium ions to the E2 form of the enzyme and the different affinities for ATP (in case of the sodium pump (Thoenges *et al.*, 1999; Glynn, 1985) there are K_d(ATP) values around 0.3 μM for the E1 form and 120 μM for the E2 form). The ADP sensitive phosphorylated intermediate (E1~P) and K^+ binding to the E2-P form of the enzyme are other similarities between the Kdp-ATPase and the sodium pump. However, also differences exist between

Na^+, K^+-ATPase and the Kdp-ATPase. Phosphorylation of the Kdp-ATPase does not require ions; hence, significant ATP hydrolysis by E1ATP breakdown to E2, ADP, and P_i in the Kdp-ATPase (uncoupled ATP hydrolysis) occurs. Furthermore, K^+ is transported during E2-E1 transition of the Na^+, K^+-ATPase (Apell and Karlish, 2001), while there is convincing evidence that K^+ is transported during the E1~P-E2-P transition in case of the Kdp-ATPase (J. Froehlich, personal communication). The translocation of K^+ during the E1~P / E2-P transition in the Kdp-ATPase resembles that of the Na^+-translocation in case of the sodium pump. This effect seems to be quite logic, since both steps require most of the free energy (note that E1~P and E2-P are high and low energy intermediate states, respectively).

The existence of at least two, distinct ATP binding sites is also indicated by the influence of *ortho*-vanadate on ATP and pNPP hydrolysis. The ATPase activity of the KdpFABC complex is inhibited in a complex manner by *ortho*-vanadate. At ATP concentrations below 200 μM ATP (it should be noted that the K_M (ATP) is 80-120 μM) a double reciprocal plot shows true uncompetitive inhibition kinetics. *Ortho*-vanadate is obviously able to bind to the enzyme and to the enzyme substrate complex with almost the same affinity. However, at higher ATP concentrations the ATPase activity is inhibited non-competitively by vanadate. These effects indicate that vanadate and ATP are not competing for the same binding site. A non-competitive inhibition of the ATPase activity is described for the *Saccharomyces cervisiae* plasma membrane H^+-ATPases (PMA1 and PMA2) (Supply *et al.*, 1993). Since *ortho*-vanadate is supposed to bind to the E2 conformation of P-type ATPases (Fedosova *et al.*, 1998) and assuming that the Kdp-ATPase, as other P-type ATPases, exhibits at least two ATP binding sites, the diphasic behavior of the both, ATP hydrolysis and *ortho*-vanadate inhibition of the ATPase activity can be explained. Vanadate, when it binds to E2, will form an E2-vanadate complex, which will not bind ATP. The fact that non-competitive inhibition of ATPase activity by *ortho*-vanadate is observed, suggests that a simple model does not exist, i.e. that vanadate and ATP interact with different E2 intermediate states, possibly in an oligomer. As indicated by quenched flow analysis (discussed above), the KdpFABC complex has a high affinity ATP binding site, which is accessible in the E1 state, and a low affinity ATP binding site which is exposed in the E2 state. This would provide different environments for the inhibitor *ortho*-vanadate. At low ATP concentrations ATP binds predominantly to the high affinity sites. The enzyme becomes phosphorylated by ATP hydrolysis. After dephosphorylation, E2 is blocked by the binding of vanadate. This cycle appears as an uncompetitive inhibition, since the substrate ATP has first to be bound and hydrolyzed. At low ATP concentrations the uncompetitive inhibition dominates with respect to the substrate ATP. At higher concentrations of ATP the high and low affinity binding sites are saturated and the enzyme is in an accelerated steady state. ATP is now competing non-competitively with vanadate since both, the low affinity ATP binding site, and the binding of vanadate may occur in the E2 state. The non-competitive inhibition occurs since *ortho*-vanadate binds not within the nucleotide-binding domain. There is evidence that *ortho*-vanadate binds to a similar site

than phosphate does (Fedosova *et al.*, 1998), forming an E2-V intermediate, in analogy to the E2-P form. Evidence in support for this fact in KdpB is the competitive inhibition of *ortho*-vanadate with respect to pNPP hydrolysis (figure 25), which occurs exclusively at the E2 site and hence competes directly with *ortho*-vanadate.

Convincing evidence for the existence of two catalytically active sites in the active KdpFABC unit can be taken from pNPP hydrolysis. For other P-type ATPases it has been reported that ATP or analogs have a stimulating effect on the pNPP hydrolysis (Rega *et al.*, 1973; Pitts and Askari, 1971a; 1971b; Scheiner-Bobis *et al.*, 1993; Donnet *et al.*, 1998). Experiments with the plasma membrane Ca^{2+}-ATPase (PMCA) of erythrocyte membranes revealed that this ATPase exhibits an ATP dependent and a calmodulin dependent pNPPase activity (Donnet *et al.*, 1998). Using FITC labeled enzyme it was shown that the catalytic sites (e.g. E1 or E2 ATP site) play no role in the calmodulin dependent pNPPase activity. However, it was demonstrated that both FITC and eosin-Y could bind to the enzyme, indicating that there are two different binding sites, which do not overlap (Donnet *et al.*, 1998). A conclusion drawn from the results of Donnet and co-workers (1998) is that blocking ATP from the high affinity E1 site inhibits pNPP hydrolysis. Thus, binding of micromolar concentrations of ATP or analogs thereof (at least in the case of the sarcoplasmic reticulum Ca^{2+}-ATPase eosin stimulates pNPP hydrolysis (Micnaco *et al.*, 1996)) can increase the basal level of pNPP hydrolysis. The similar stimulatory effect of ATP towards the pNPP hydrolysis mediated by the KdpFABC complex was observed (figure 26) and thus provides evidence for an analogy to other P-type ATPases. The stimulatory effect, however, could only be observed by addition of ATP (and in millimolar concentrations with GTP) and not with non-hydrolysable analogs like AMP-PNP. The necessity of a nucleotide-triphosphate for pNPPase stimulation indicates that not only binding, but also hydrolysis has to occur in order to exert the stimulatory effect. Yet, the stimulation of pNPP hydrolysis by ATP indicates a second catalytic site present in the KdpFABC complex. Farley and colleagues could show that the stimulating effect of ATP towards pNPPase activity was absent in the FITC modified Na^+, K^+-ATPase, indicating that ATP must bind to the E1-ATP site to facilitate pNPP hydrolysis (Scheiner-Bobis *et al.*, 1993). Higher concentrations of ATP (millimolar range), however, inhibited the pNPP hydrolysis of the sodium pump (Scheiner-Bobis *et al.*, 1993). The K^+ stimulated phosphatase activity of the Na^+, K^+-ATPase was inhibited by ATP (K_i 1.67 mM) and P_i (1.9 mM). The inhibitory effect of AMP, however, was weak (K_i 10.5 mM) (Scheiner-Bobis *et al.*, 1993). In contrast, the pNPPase activity of the KdpFABC complex was inhibited effectively by AMP (K_i 0.51 mM) and less effectively by ATP (K_i 2.61) and ADP (K_i 4.5 mM). Surprisingly, the K_i of inorganic phosphate was 25.6 mM, although P_i is a reasonable good inhibitor of this reaction in other P-type ATPases. The fact that P_i does not inhibit the pNPP hydrolysis of the Kdp-ATPase in an efficient way, reflect that the KdpFABC complex might be not phosphorylated by P_i. In fact backdoor phosphorylation *via* P_i and Mg^{2+} was not detected for the Kdp-ATPase. It remains a subject of discussion why AMP is a more potent inhibitor of the pNPP hydrolysis of the Kdp-ATPase, than ATP or ADP. One plausible

explanation might be that AMP binds with high affinity to the E2-P site in KdpB, where pNPP hydrolysis most obviously occurs.

Taken together, the results demonstrate that the Kdp-ATPase must contain at least two catalytic centers, one with high affinity for ATP (E1ATP site) and one with low affinity (E2ATP site). FITC binds specifically to Lys395 in the N-domain of KdpB. In contrast to other P-type ATPases, FITC might bind to the E1 and E2 site, and hence blocks pNPP and ATP hydrolysis. However, another explanation for this effect could be, that the N-domain of KdpB is more compact in size compared to other P-type ATPases, and therefore the bulky fluorescein moiety does not allow excess of small substrates like pNPP in to their site. The results presented here are in good accord with quenched flow analysis (J. Froehlich, S. Dröse and K. Altendorf, personal communication) of solubilized KdpFABC complex and with genetic data provided by Epstein and Davis (1970):

1) Complementation of two different mutations in the *kdpA* gene, each of which resulted in inactive protein when expressed alone, led to growth on low potassium concentrations (Epstein and Davis, 1970).

2) Quenched flow analysis using solubilized KdpFABC complex provided evidence for an E1, E1~P, E2-P, E2 interconversion and for the effect of a second ATP site causing a diphasic effect with respect to ATP (J. Froehlich, personal communication).

3) ATP binding has a stimulating effect on pNPP hydrolysis.

4) *Ortho*-vanadate inhibited the ATPase activity of the Kdp-ATPase with diphasic kinetics, while inhibition of pNPP hydrolysis follows competitive kinetics.

Therefore, it is proposed that the Kdp-ATPase forms a dimer, in which the two units interact with each oher (figure 66).
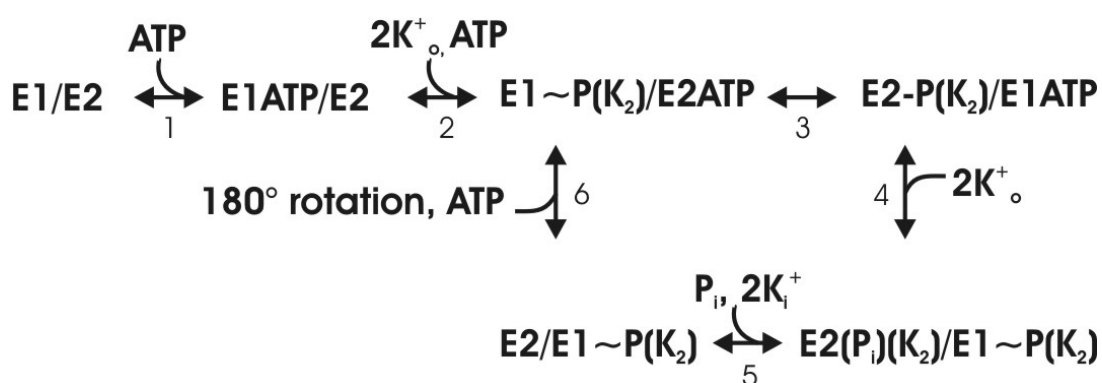
Figure 66: Dimeric model of the Kdp-ATPase. Dimeric model of the Kdp-ATPase with two subunits following each ATP hydrolysis according to the Albers-Post mechanism with 180° out-of-phase with respect to each other. The high affinity E1 ATP site is occupied even at low ATP concentrations (1). The resulting transition into E1~P is accompanied by potassium binding (K^+_o). The transition into the phospho-enzyme form is accelerated by ATP binding with low affinity to the E2 state enzyme of the dimer (3). Transition into E2-P facilitates the transition into the E1 state of the second subunit, which is now able to hydrolyze ATP and bind potassium ions (K^+_o) (4). The release of ions into the cytosol (K^+_i) goes along with dephosphorylation (5). (Based on suggestions made by J. Froehlich)

A look at other ATP-hydrolyzing membrane proteins reveals that cooperativity between ATP sites seems to be the rule rather than the exception. F_1F_0-ATPases have three ATP binding sites, which work in sequential order (reviewed by Boyer, 1997). Furthermore, cooperativity has been observed for members of the ABC transporter family, like the *E. coli* maltose transporter (Davidson *et al.*, 1996), the periplasmic histidine permease (Liu *et al.*, 1997) and the multi-drug resistance transporter Mdr1 (P-gylcoprotein, gp70) (Buxbaum, 1999a).

4.4. Soluble domains of KdpB

The fact that the modular design of P-type ATPases is well-conserved, and the existence of proteins, which are homologous to single modules of the cytoplasmic parts of P-type ATPases (e.g. the Rossman-fold in the P-domain) (Aravind *et al.*, 1998; Ridder and Dijkstra, 1999), led to the idea that cloning of the corresponding gene fragments should result in the synthesis of autonomously folded proteins, which retain their native structure (Moutin *et al.*, 1998). For more than a decade now, gene fragments coding for the catalytic loops of different P-type ATPases were expressed separately within *E. coli* and the resulting proteins were characterized with respect to their ability to bind and hydrolyze ATP and pseudo-substrates like pNPP (Wang *et al.*, 1991; Moutin *et al.*, 1994; Capieaux *et al.*, 1993; Tran & Farley, 1999; Gatto *et al.*, 1998; Obsil *et al.*, 1998; Tsivkovskii *et al.*, 2001). However, with the exception of the SERCA pump, structural information is rather scarce for P-type ATPases. The soluble domains (P-, N- and A-domains) of KdpB are much smaller in size compared to the SERCA pump, probably representing a kind of minimal scheme for a functional catalytic domain of a P-type ATPase. The knowledge of this structure and a detailed view on the dynamic processes during substrate binding and hydrolysis will have strong implications on other P-type ATPases, in particular the heavy metal-transporting ATPases such as Menkes and Wilson's disease proteins, important for copper homeostasis in humans (Harris, 2000), and the plasma membrane H^+-ATPase (Kühlbrandt *et al.*, 2002).

Although the cloning and production of the so called A-domain of KdpB, called H2H3 loop here, ranging from amino acids Glu83 to Glu218, was described in 3.4.1., it is not discussed in detail here, since this module does not exhibit any enzymatic activity. The H2H3 loop might play an interesting role in the interaction with the N-domain, which has clearly been shown for the E1-E2 transition of the SERCA pump (Toyoshima and Nomura, 2002; compare the animation given in the supporting material at www.nature.com).

The construct named H4H5 loop ranging from Met282 to Gln567 contained the amino acids representing the P- and N-domain of KdpB. The N-domain was synthesized also separately, resulting in a protein ranging from amino acid Asn316 to Gly451, subsequently called KdpBN.

Routinely, 20-40 mg of purified protein per liter cell culture were obtained in rich media and almost half of this amount using minimal media. However, upscale experiments from 50 ml cultures to

1 liter or 5 liter fermenter cultures always resulted in a massive degradation of the desired H4H5 protein. This degradation must occur already within the cells prior lysis, since addition of a variety of protease inhibitors did not prevent this process. Even in 50 ml cultures at 37°C degradation and formation of inclusion bodies could be observed. Lowering the temperature to 30°C prior induction minimized the formation of inclusion bodies. Formation of inclusion bodies was reported for the synthesis of several catalytic loops of P-type ATPases, such as the H4H5 loop of the SERCA pump (Moutin et $al.$, 1994) and the synthesis of the corresponding fragment of the yeast plasma membrane proton pump (Capieaux et $al.$, 1993). The fragment representing the H4H5 loop of the Na^+, K^+-ATPase, however, was reported to be soluble (Tran and Farley, 1999; Gatto et $al.$, 1998). Furthermore, concentration of the H4H5 protein also turned out to be difficult. Concentration experiments with the dialyzed H4H5 loop were only successful up to 2 mg ml^{-1}, which is sufficient for biochemical characterization, but not for further structural analysis such as NMR or crystallography. Interestingly, similar results were reported for other catalytic loops of P-type ATPases, such as the fragment of the Wilson's disease protein (S. Lutsenko, personal communication). Solubility of the H4H5 loops could be increased by addition of high salt. This seems to be quite logical, since the cytoplasmic exposed domains are highly charged. In contrast, the KdpBN domain was much more resistant against degradation. The use of a fermenter enabled the production of large amounts of recombinant KdpBN, which could be concentrated above 1 mM (17 mg ml^{-1}).

Biochemical and structural characterizations were carried out to elucidate, whether the KdpBN domain and the H4H5 loop of KdpB were folded and hence useful for further investigation.

Spectroscopic methods are powerful tools for the structural analysis of proteins. Circular dichroism (CD) spectroscopy provides rapid determination of protein secondary structure. Furthermore, it is a way to rapidly assess conformational changes of proteins upon addition of ligands (Pelton and McLean, 2000; Siligardi and Hussain, 1998). Therefore, CD-spectroscopic analysis of the purified H4H5 loop and the KdpBN domain was performed to test whether these recombinant proteins are folded and hence suitable for further characterization. The spectrum of H4H5 exhibited minima at 207 nm and 221 nm, which were shifted to lower wavelength upon ATP binding (205 nm and 218 nm). The spectrum of the KdpBN domain exhibited a strong minimum at 208 nm and a minimum around 219 nm, although the latter one is not as distinct as the first one. Both spectra suggest a mainly α-helical structure. The calculated values were 38 % α-helix and 13 % β-sheet for the H4H5 loop and 40 % α-helix and 10 % β-sheet for the KdpBN domain. Although this method does not allow a detailed structural analysis, it provided evidence that the H4H5 loop and the KdpBN domain have retained an ordered structure. A similar CD spectrum is reported for the catalytic loop of the Na^+, K^+-ATPase (Gatto et $al.$, 1998), with minima at 206 nm and 221 nm. The calculated secondary structure values were 23 % α-helix and 27 % antiparallel β-sheet. CD-spectroscopic analysis of the large cytoplasmic loop of the SERCA pump revealed an α-helical content of 23 % and a β-strand content of 21 % (Carvalho-Alves et $al.$, 2000). The differences in the α-helical and the β-sheet content between

the sodium pump loop and the SERCA pump loop on the one hand, and the KdpB domains on the other hand, are probably reflecting the differences within the N-domain, which is smaller in case of the KdpB polypeptide and may contain less β-sheet parts in comparison to type II P-type ATPases.

As discussed in section 4.3., P-type ATPases containing the FITC binding motif (KGAPE, or KGSV for KdpB) are often examined using FITC binding. It was shown here that FITC binds in the ATP binding site located within the N-domain of KdpB in the native KdpFABC complex. Interestingly, the covalent modification of P-type ATPases by FITC was only achieved with intact proteins. Denatured proteins have lost the ability to bind FITC. Therefore, FITC binding to H4H5 and KdpBN was tested. Both proteins were able to bind FITC, although only the H4H5 loop exhibited the same protective effect of nucleotides towards FITC modification (figure 36) as the native full length KdpB protein within the KdpFABC complex. In contrast to the Na$^+$, K$^+$-ATPase (Gatto *et al.*, 1998), both the Kdp-ATPase and the H4H5 loop were able to bind AMP with high affinity as judged by the protective effect of AMP towards FITC. Moreover, nucleotides, which do not bind with high affinity to the Kdp-ATPase, like GTP and ITP, were not able to compete with FITC. These results clearly show that the recombinant H4H5 loop is not only able to bind nucleotides, thus forming a proper binding pocket, but also shows selectivity, like the native loop in the full-length enzyme. Furthermore, the substrate specificity of KdpB shows clear differences to other P-type ATPases of the type II class, like the sodium pump. Furthermore, the protection experiments revealed that the FITC-binding site is indeed within the N domain of KdpB, a finding that supports the CNBr cleavage (section 3.3.1) results. The KdpBN domain could also be labeled with FITC, but in contrast to the H4H5 loop nucleotides had no protective effect. The fact that denatured KdpBN was unable to bind FITC revealed that FITC modification is due to proper folding of the protein. At first glance this behavior might suggest that adenosine nucleotides do not bind to the FITC site, or that amino acid residues of the P-domain might be necessary to form a complete nucleotide-binding pocket. In order to test whether the KdpBN domain was able to bind nucleotides, a second approach using TNP-nucleotides was employed. The determination of nucleotide-binding affinities using TNP-nucleotides to full length P-type ATPases (Moczydlowski and Fortes, 1981a,b; Watanabe and Inesi, 1982; Faller, 1989) and separately synthesized modules was achieved in several cases (Capieaux *et al.*, 1993; Moutin *et al.*, 1994; Gatto *et al.*, 1998; Tsivkovskii *et al.*, 2001). TNP-nucleotides bind with high affinity to the Kdp-ATPase H4H5 loop and KdpBN domain. The calculated affinity constants for TNP-ATP were 18.5 µM for the H4H5 loop and 12.2 for the KdpBN domain. These values are lower compared to the affinities determined for other P-type ATPase loops. The TNP-ATP K_d value for the Na$^+$, K$^+$-ATPase loop was 3.2 µM (Gatto *et al.*, 1998), for the Ca^{2+}-ATPase loop 1.9 µM (Moutin *et al.*, 1994), for the H$^+$-ATPase loop 6.5 µM (Capieaux *et al.*, 1993), and 1.89 µM in the case of the Wilson's disease protein loop (Tsivkovskii *et al.*, 2001). Interestingly, TNP-ATP bound with higher affinity to the KdpBN domain than to the H4H5 loop, suggesting that the binding pocket might be more accessible for the nucleotide in case of KdpBN. Beside TNP-ATP, the K_d values for TNP-ADP and TNP-AMP

were determined for the H4H5 loop and the KdpBN domain. The affinities decreased from TNP-ATP>TNP-ADP>TNP-AMP for both KdpBN domain and H4H5 loop, indicating the specificity of the binding site for ATP. An even more convincing evidence for the binding of adenosine nucleotides is the observation that ATP is able to displace competitively TNP-ATP from its binding site. ATP induced a competitive chase of TNP-ATP and a binding constant of 0.68 mM was determined for free ATP for the H4H5 loop and 0.76 mM for KdpBN. At first glance, the affinity for ATP towards H4H5 and KdpBN seems to be quite low. A comparison with other P-type ATPases relativizes this notion. The affinity for ATP is almost seven fold lower for the H4H5 loop compared to the E2 site ATP affinity of 0.1 mM. A similar increase is observed for the sarcoplasmic reticulum Ca^{2+}-ATPase (E2 site affinity of 30 µM and 250 µM to the isolated loop) (Moutin et $al.$, 1994) and for the Na^+, K^+-ATPase with 0.1 mM in E2 and 0.3-0.4 mM for the recombinant loop (Gatto et $al.$, 1998). These results suggest that the ATP binding site within the isolated loops of P-type ATPases is most probably within an E2 like conformation. Differences in the ATP affinity found with different P-type ATPases and their corresponding loops seem to reflect differences in the structure of the nucleotide binding site. The plasma membrane H^+-ATPase exhibits lower affinities for both TNP-ATP and ATP compared to the sodium pump and SERCA pump, while the affinities determined for the Kdp-ATPase are even lower. Interestingly, the size of the nucleotide binding domain is smaller in the H^+-ATPase and Kdp-ATPase, compared to the type II class ATPases, which may be responsible for the different substrate affinities. However, the values for K_M will always be larger than the dissociation constant, since K_d is lower compared to K_M by virtue of the rate constant leading to hydrolysis. The rate constant for the breakdown of substrates into the products is enzyme specific, making it fairly easy to understand differences between P-type ATPases. Beside the effect of nucleotide binding, another important calculation can be carried out using the TNP-nucleotide binding to the isolated KdpB domains. According to an equation described by Gutfreund (1972), which was applied by Carvalho-Alves et $al.$ (2000), it was possible to determine the molar ratio of bound TNP-nucleotides to the H4H5 loop and the KdpBN domain. An average of 1.23 mol nucleotide binding sites per mol H4H5 was calculated from the TNP-ATP, TNP-ADP, and TNP-AMP binding to the H4H5 loop. The average value determined for the KdpBN domain was 1.096 mol nucleotide binding sites per mol KdpBN. These results clearly support the one binding site hypothesis for P-type ATPases. Modeling of the three dimensional structure of the Na^+, K^+-ATPase H4H5 loop deduced by restraint–based comparative modeling revealed that only one ATP binding site exist (Ettrich et $al.$, 2001). Using the soluble domains of KdpB, it is clear that only one nucleotide binding site exists per catalytic loop. The idea that two ATP binding sites are located within one catalytic loop (Ward and Cavieres, 1996; 1998) are contradictory to these findings. The main evidences for the two-site model are that solubilized, monomeric Na^+, K^+-ATPase retains the diphasic ATPase kinetics (Ward and Cavieres, 1996). However, the one site model suggested by Fortes and colleagues (Moczydlowski and Fortes, 1981) cannot be ruled out by the results presented here. Finally, only the structure of the catalytic domains in

the presence of nucleotide will tell us the number of nucleotide binding sites within the catalytic domains of P-type ATPases.

8-azido[α-^{32}P]ATP labeling of the H4H5 loop also revealed that this loop is able to bind ATP. However, it should be noticed that 8-azido-ATP is only a weak substrate for the Kdp-ATPase (S. Dröse, personal communication), probably due to the cis-conformation of the adenine moiety. Therefore, more convincing evidence for ATP binding could be provided by labeling with 2-azido-ATP, in which the adenine moiety is in the proper anti-conformation.

The TNP-nucleotide binding to the KdpBN domain and the chase experiments with adenosine nucleotides reflect that the isolated N-domain of KdpB is able to bind nucleotides with high affinity (K_d (TNP-ATP) 12.23 µM; K_d (ATP) 0.76 mM). The values are in the same order of magnitude as found for the H4H5 loop and clearly indicate that a complete nucleotide binding pocked is formed by the N-domain itself. The fact that nucleotide binding to KdpBN does not prevent FITC modification (as mentioned above) indicates that FITC is not directly placed within the nucleotide binding site, but might block the access of adenosine nucleotides to the binding site in case of the Kdp-ATPase. The ATP site within the isolated N-domain might be accessible from the site, which is normally attached to the P-domain. As a consequence, FITC modification is not preventing nucleotides from reaching the binding pocket in case of KdpBN. Evidence for this hypothesis could be obtained from simultaneous binding of FITC and TNP-ATP to KdpBN. Since the fluorescence of FITC and TNP-ATP interfere with each other, it was impossible to carry out this experiment.

Since hydrolytic activity was reported for the H4H5 loop of the Na$^+$, K$^+$-ATPase (Obsil *et al.*, 1998; Tran and Farley, 1999) and the Wilson's disease protein (Tsivkovskii *et al.*, 2001), the recombinant H4H5 loop of KdpB was tested for catalytic activity. Using the sensitive EnzChek$^®$ phosphate determination assay from Molecular Probes (Eugene, Oregon, USA) it was possible to measure ATP hydrolyzing activity mediated by the H4H5 loop. The specific activity (20 nmol mg^{-1} min^{-1}) was in a range also found for the ATP binding loop of the Wilson's disease protein (67,6 nmol mg^{-1} min^{-1}) (Tsivkowskii 2001). In addition, the hydrolysis of pNPP, discussed for the KdpFABC complex in section 4.3., was measured. The specific activity of pNPP hydrolysis was much higher compared to the ATP hydrolysis and exhibited a maximal velocity of 1.4 µmol mg^{-1} min^{-1}. The calculated K_M was 24 mM. Compared to the pNPP hydrolysis catalyzed by the H4H5 loop of the Na$^+$, K$^+$-ATPase (2-3 nmol mg^{-1} h^{-1}) (Tran and Farley, 1999), the activity of the H4H5 loop of KdpB was quite high. However, the pNPP hydrolyzing activity of the KdpFABC complex was determined to be 11 µmol mg^{-1} min^{-1}, while that of the Na$^+$, K$^+$-ATPase was around 0.75 µmol mg^{-1} min^{-1} (Linnertz *et al.*, 1998). The high pNPP hydrolysis rate in comparison to the low ATPase activity provides support to the notion that the H4H5 loop is in the E2 like state. Furthermore, the hydrolytic activity of the H4H5 loop provides convincing evidence that a proper folded subdomain of KdpB is formed.

4.5. NMR analysis of KdpBN

In order to determine the structure of a polypeptide by NMR analysis, a variety of prerequisites have to be fulfilled. The main points are high concentration of the protein (at least 1 mM), high stability at elevated temperatures (300 K) and slightly acid pH (pH 6.0) (Wider and Wüthrich, 1999). Preliminary experiments revealed that only the KdpBN domain fulfilled these criteria and was therefore chosen for further analysis.

In order to determine the optimal conditions for NMR analysis, several ^{15}N, ^{1}H-HSQC spectra (Heteronuclear Single Quantum Coherence) at different temperatures from 280 K to 300 K in steps of 5 K were recorded (M. Haupt, personal communication). It turned out that the best signals were obtained at 300 K and that the sample is stable under these conditions for almost 10 days, before extensive degradation occurs.

For sequential assignment a number of heteronuclear edited NMR experiments were carried out. From the ^{15}N-labelled sample HNHA and HNHB experiments were performed (nomenclature according to Sattler *et al*., 1999). The data indicate the affiliation of the amide protons and nitrogen atoms to their sequential Hα's or Hβ's, respectively. Using ^{15}N, ^{1}H-HSQC a complete fingerprint of the KdpBN domain was obtained. The HSQC spectra revealed that KdpBN has a highly ordered structure and that the signals of all amino acids were visible. Furthermore, the ^{15}N, ^{1}H-HSQC spectra confirmed the high purification grade of the sample (figure 46). The signals obtained were well distributed and allowed further analysis of the KdpBN domain using NMR spectroscopy. For that a ^{13}C, ^{15}N-labelled sample of KdpBN was prepared. The double labelling with ^{15}N and ^{13}C is absolutely essential to gain enough distance data for the 17 kDa KdpBN polypeptide. The first approach was carried out using the commercially available Silantes OD4 CN medium. The Silantes CN media series are rich media (similar to LB medium) optimised for expression using the Bl21(DE) system for obtaining ^{13}C, ^{15}N labelled proteins used in NMR analysis. Pre-experiments using unlabeled Silantes medium revealed that a similar expression level was reached compared to LB medium and hence giving a better protein yield than minimal medium. Purification from Silantes medium also resulted in a soluble protein and, therefore, a Silantes CN medium for ^{13}C and ^{15}N labelling was used. However, the HSQC spectra recorded from the resulting protein revealed that most of the purified KdpBN was unfolded (compare figure 49). In order to check, whether the reason for that unfolding was due to the use of rich medium, samples were prepared from LB medium, minimal medium, and Silantes medium. Purified KdpBN samples from each medium were subjected to ^{1}H-NMR analysis. The 1D NMR experiments confirmed that the KdpBN domain was only unfolded when expression was carried out in Silantes medium. The sample from conventional LB rich medium was folded, identical to the protein obtained from minimal medium. So far, no explanation for this problem exists. A possible explanation might be that the high concentration of trace elements in the Silantes medium may influence the folding of the N-domain of KdpB. For this reason, the synthesis of ^{13}C, ^{15}N-KdpBN had to be carried out in minimal medium,

although the expression level and hence the protein yield is lower compared to rich media. For all further experiments a ^{13}C, ^{15}N-labeled sample of KdpBN was prepared from cells grown in minimal medium (0.2 % ^{13}C$_{1-6}$-glucose). The ^{15}N, ^{1}H-HSQC spectrum of the double-labelled samples was in accord with the spectra obtained from the ^{15}N-labelled samples of KdpBN. From the ^{13}C, ^{15}N-KdpBN samples it has been possible to acquire heteronuclear edited three-dimensional NMR spectra that were necessary for backbone assignment. Among those were the HNCO, CBCA(CO)NH, HBHA(CO)NH, HNCA, HNCACB and HN(CA)HA experiments (nomenclature according to Sattler *et al.*, 1999). The HNCO (figure 51) showed the direct linkage of ^{1}H-^{15}N to the carbonyl group in (i-1) position. The CBCA(CO)NH showed the Cα's and Cβ's in (i-1)-position, so did the HBHA(CO)NH for the Hα's and Hβ's. In contrast, the HNCA, HNCACB and HN(CA)HA experiments displayed the correlations of Cα, (Cα & Cβ) and Hα in (i)- and (i-1)-position to the ^{1}H-^{15}N resonances (M. Haupt, personal communication). A complete backbone assignment was achieved with the ^{13}C, ^{15}N labelled KdpBN. Chemical shift index (CSI) and analysis of the angle ϕ via the H^{N}, H$^{\alpha}$ coupling constants are in accord with respect to the secondary structure of KdpBN.

Recently, a model of the plasma membrane H^{+}-ATPase was published (Kühlbrandt *et al.*, 2002). The model was based on the structure of the Ca^{2+}-ATPase and fitted to an 8 Å map of the *Neurospora crassa* proton pump determined by cryo-electron microscopy (Auer *et al.*, 1998). The structural model was deposited in the Protein Data Bank (1MHS). Intriguingly, the N-domain of the H^{+}-ATPase has a similar size compared to the KdpBN domain. The two N-domains align quite well without larger gaps (figure 67).

```
        1        10        20        30        40        50        60
        .         .         .         .         .         .         .
KdpBN   NRQASEFIPAQGVD.EKTLADAAQLASLADETPEGRSIVILAKQRFNLRERDVQSLHAT..FVPFTA
1MHS_N  ...HDPYTVA.GVDPEDLMLTACLAASRKKKGIDAIDKAFLKSLKYYPRAKSVLSKYKVLQFHPFDP
consensus>50  ......%..A.GVD.E..$..A...AS......#......L....%..R...V.S......F.PF..
```

```
       70        80        90        100       110
        .         .         .         .         .
KdpBN   QSR.MSGI..NIDNRMIR..KGSVDAIRRHVEANGGH.FPTDVDQ....KVDQVARQGATPLVVV..
1MHS_N  VSKKVVAVVESPQGERITCVKGAPLFVLKTVEED..HPIPEEVDQAYKNKVAEFATRGFRSLGVARK
consensus>50  .S.....!....#...I...KG....!...VE.#..H..P.#VDQ....KV.#.A..G...L.V...
```

```
       120       130
        .         .
KdpBN   ..EGS.RVLGVIALKDIVKG
1MHS_N  RGEGSWEILGIMPCM.....
consensus>50  ..EGS..!LG!.........
```

Figure 67: Sequence comparison of the N-domains of the KdpB polypeptide and the *Neurospora crassa* plasma membrane proton pump. The sequences were retrieved from SWISSPROT and aligned using the Multialign 5.4.1. interface (Corpet, 1988) with a gap opening penalty of 2 and default settings. Identical amino acid residues are boxed in red, similar residues are written in red.
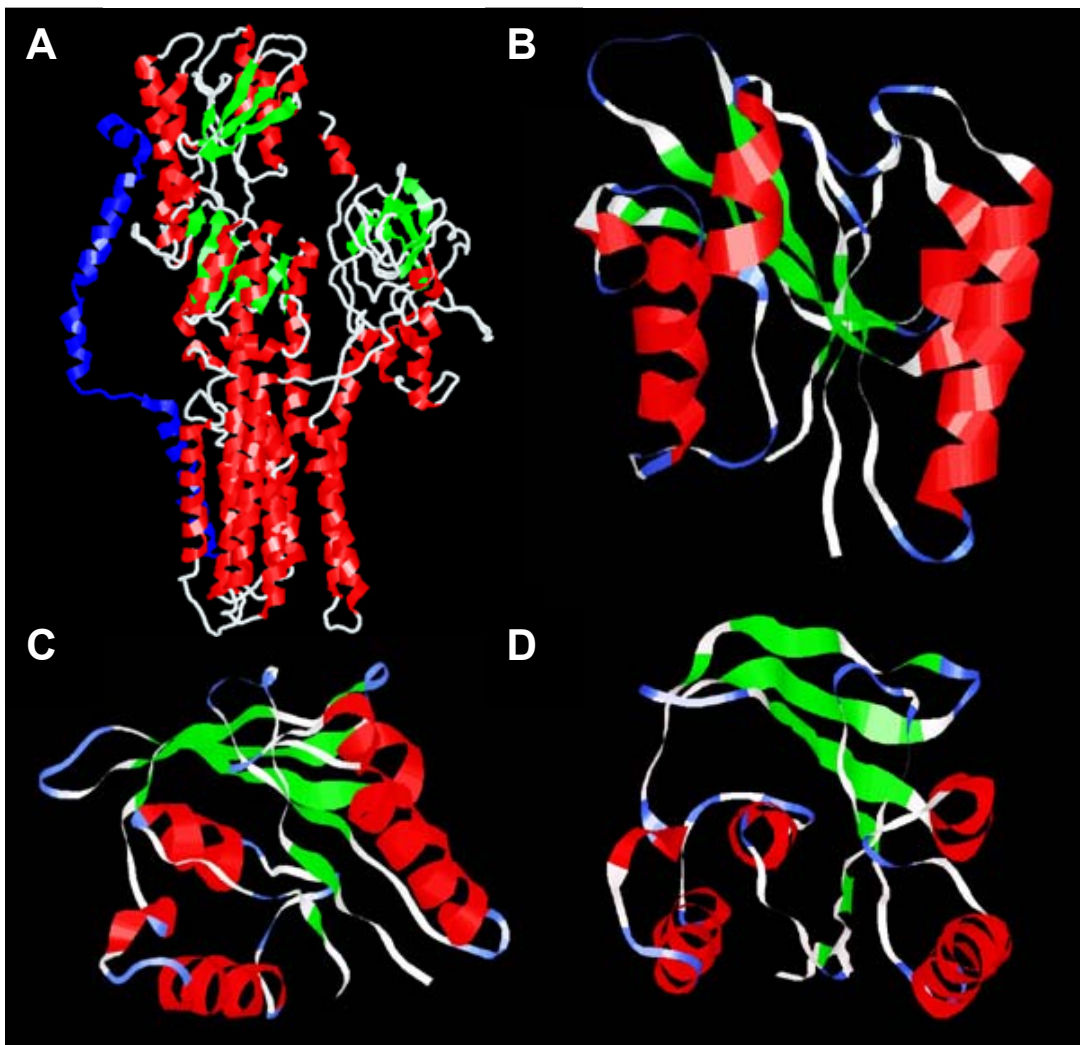
Figure 68: Structural model of the *Neurospora crassa* plasma membrane H⁺-ATPase (Kühlbrandt *et al.*, 2002). Helices were colored in red, β-sheet were colored in green. The C-terminal extension of the H⁺-ATPase is colored in blue (note that the C-terminus is in contact with the N-domain). A, shown is the full length H⁺-ATPase according to the structural data 1MHS. B, C, and D show the N-domain of the H⁺-ATPase from different angles. A, side view; B, 90° angle; C, top view.
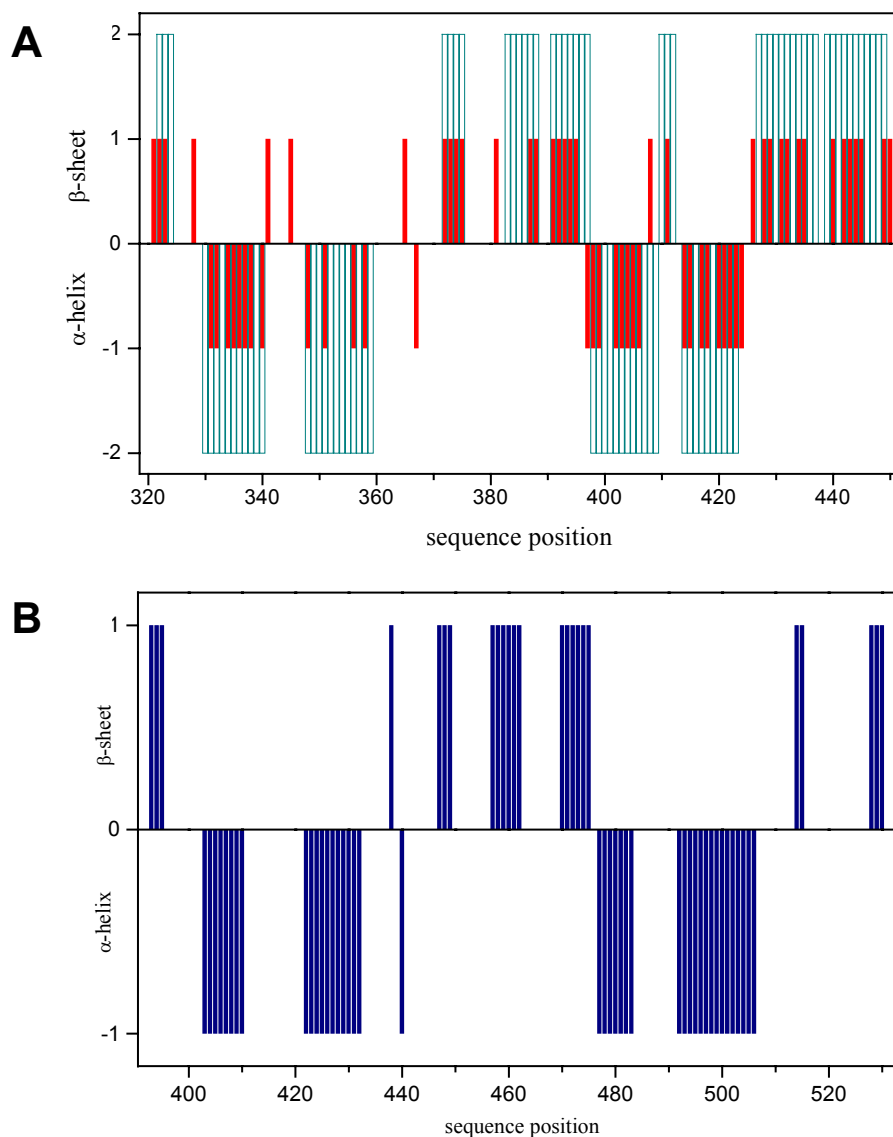
Figure 69: Structure prediction *via* the homonuclear $^3J(H^NH\alpha)$ coupling constants for the KdpBN (A) and the H$^+$-ATPase N-domain (B). A, the calculated consensus plot of the chemical shift index, CSI (green) and the structure prediction *via* the homonuclear $^3J(H^NH\alpha)$ coupling constants (red) are shown. B, the predicted homonuclear $^3J(H^NH\alpha)$ coupling constants for the H$^+$-ATPase N-domain based on the structural model data 1MHS (Kühlbrandt *et al.*, 2002). Note the similarity between the $^3J(H^NH\alpha)$ coupling constants of KdpBN (red, panel A) and the H$^+$-ATPase N-domain (panel B) (Melina Haupt, personal communication).

Hypothetical structure prediction *via* the homonuclear $^3J(H^NH\alpha)$ coupling constants of the H$^+$-ATPase N-domain is almost identical to the CSI index obtained for the KdpBN domain, reflecting the close similarity between these domains (figure 69). Interestingly, both CSI indices indicate a putative 3_{10} helix (around residue 370 in case of KdpBN and around residue 440 in case of the H$^+$-ATPase N-domain) (figure 68). Figure 68 shows a model of the full-length plasma membrane H$^+$-ATPase (1MHS) and the N-domain of the H$^+$-ATPase. The N-domain of the proton pump is composed of six

central β-sheets flanked by two helices on each side (one side has the additional short 3_{10} helix). In comparison to the N-domain of the Ca^{2+}-ATPase (1EUL) (Toyoshima *et al.*, 2000), the N-domain of the H^+-ATPase is almost half in size. Nevertheless, the overall architecture with a central β-strand domain flanked by α-helices, is similar in the SERCA and the proton pump. This "sandwich" of helix flanked β-sheets is a common structural motif, found in a variety of enzymes, such as the arsenite translocating ATPase (1IHU), the haloacid dehalogenase (1JUD) and the phosphoserine phosphatase (1L7M), to quote just a few of them (structural data derived from the Protein Data Base, Brookhaven, USA).

The results obtained so far are encouraging that the structure of KdpBN will be solved by NMR analyis. The availability of a solution structure bears the possibility to examine dynamic properties of the protein with respect to substrate binding. For example, the solution dimerization interface of p53 bound to the consensus DNA was observed using NMR, (Klein *et al.*, 2001). Solution structure, dimerization, and dynamics of a lipophilic alpha/3(10)-helical, C alpha-methylated peptide, and hence implications for folding of membrane proteins, were obtained, applying NMR techniques (Dehner *et al.*, 2001).

This studies will also shed light on the number of ATP binding sites and the amino acids, which are participating in forming the ATP binding pocket in P-type ATPases. Using the isolated, recombinant catalytic loop of the SERCA pump, nucleotide binding was already examined with multidimensional NMR (Abu-Abed *et al.*, 2002). Chemical shifts of amino acids involved in AMP-PNP binding were described. In contrast to the SERCA pump loop, the structure determination of KdpBN has important implications on the N-domains of all type I class P-type ATPases, since they are all similar in size. Among the type I ATPases are the important heavy metal-transporting ATPases such as Menkes and Wilson's disease proteins.

4.6. The Mj0968 protein of *M. jannaschii*

The idea that the archaeon *M. jannaschii* harbours a soluble P-type ATPase was supported by sequence alignments (Aravind *et al.*, 1998) and biochemical data (Ogawa *et al.*, 2000). Since the existence of such an enzyme would have a profound effect on the discussion about the evolution of P-type ATPases, the Mj0968 protein was investigated in more detail. First, with the help of polyclonal antibodies it could be demonstrated that the Mj0968 protein exists *in vivo* in *M. jannaschii*. This result demonstrates that the corresponding gene is expressed and that the protein itself will certainly fulfil a function *in vivo*. Pre-experiments revealed that Mj0968 is not influenced in its catalytic activity when the protein was heated up to 80°C during the purification procedure in order to achieve an enrichment of the Mj0968 protein. Mj0968 protein obtained from purification procedures including the 80°C step had the same ATPase and pNPPase activity as Mj0968 protein obtained from purification procedures without the 80°C enrichment step. The Mj0968 protein exhibits phosphatase activity as measured by

the hydrolysis of pNPP (K_M ~2.9 mM, V_{max} ~10.8 µmol mg^{-1} min^{-1}). Compared to the previously reported ATPase activity (Ogawa *et al.*, 2000) the phosphatase activity is about 80 times higher. The enzymatic activity increased with temperature up to 85°C, which is in accord with the growth optimum of *M. jannaschii*. A similar temperature dependency was recently shown for a P-type ATPase of *M. jannaschii* (Morsomme *et al.*, 2002). The purified Mj1226 P-type ATPase was inactive at 40°C, but exhibited high specific activity, up to 180 µmol mg^{-1} min^{-1} Pi production from ATP at 95°C (Morsomme *et al.*, 2002).

Furthermore, using the sensitive EnzCheck$^{®}$ phosphate determination assay it was possible to measure ATP hydrolysis with Mj0968. The V_{max} was determined to be around 4 nmol mg^{-1} min^{-1}, which is almost 40 times less compared to the data of Ogawa et al. (2000). However, the Mj0968-D7A, in which the aspartate residue (phosphorylation site in other P-type ATPases) was replaced by an alanine residue, still exhibited the same ATPase activity.

In contrast, the Mj0968-D7A mutant protein, exhibits residual phosphatase activity with a similar V_{max} of 9.5 µmol mg^{-1} min^{-1}, but a drastically increased K_M of 96.5 mM (figure 58). If Mj0968 were indeed a P-type ATPase, deletion of the aspartate residue in the phosphorylation site would result in a complete lack of activity. Therefore, it is presumed that the native function of Mj0968 is not that of an ATPase, but rather that of a phosphatase or another hydrolytic activity. Since Aravind *et al.* (1998) clearly pointed out that all HAD family members exhibit a similar hydrolytic mechanism (compare figure 7), it is not surprising that ATP is to some extent cleaved by Mj0968. We were also able to demonstrate that the Mj0968 protein binds adenosine nucleotides with high affinity by using the fluorescent derivatives TNP-ATP, TNP-ADP, and TNP-AMP. It has been reported for similar proteins like the soluble ATP binding domain of the Na$^+$, K$^+$-ATPase that TNP-ATP binds with an apparent K_d value of 3.2 µM (Moczydlowski and Fortes, 1981), while the binding of TNP-ATP to Mj0968 had an apparent K_d of 0.4 µM. It was possible to chase the TNP-ATP competitively with ATP. The determined K_d value for ATP was 0.26 mM. TNP-ATP was furthermore competitively chased by ADP (K_d 0.76 mM) and AMP (K_d 17.1 mM). Furthermore, the Mj0968 is not necessarily forming a phosphointermediate. The experiments using the Mj0968-D7A mutant protein and the use of [α-^{32}P]ATP made it clear that the labeling experiments might detect ATP binding rather than phosphointermediate formation. However, it is still possible that adenylation of Mj0968 may take place, similar to the adenylation of DhbE (the nonribosomal peptide synthase for the synthesis of the catecholic siderophore bacillibactin, encoded by the *dhb* operon) (May *et al.*, 2002). All these results argue against the notion that Mj0968 represents a soluble P-type ATPase or being part of a kind of composite ATPase.

5. Literature

Abu-Abed, M., Mal, T. K., Kainosho, M., MacLennan, D. H. and Ikura, M. (2002). Characterization of the ATP-binding domain of the sarco(endo)plasmic reticulum Ca(2+)-ATPase: probing nucleotide binding by multidimensional NMR. *Biochemistry*. **41**, 1156-1164.

Alahari, A., Ballal, A. and Apte, S. K. (2001). Regulation of potassium-dependent Kdp-ATPase expression in the nitrogen-fixing cyanobacterium Anabaena torulosa. *J. Bacteriol*. **183**, 5778-5781.

Albers, R. W. (1967). Biochemical aspects of active transport. *Annu. Rev. Biochem*. **36**, 727-756.

Altendorf, K. and Epstein, W. (1996). The Kdp-ATPase of *Escherichia coli*. In: *Biomembranes (ATPases)* Vol. 5 (Lee, A.G., ed.), pp. 403-420, JAI Press Inc., Greenwich, London.

Altendorf, K., Gaßel, M., Puppe, W., Möllenkamp, T., Zeeck, A., Boddien, C., Fendler, K., Bamberg, E. and Dröse, S. (1998). Structure and function of the Kdp-ATPase of *Escherichia coli*. *Acta Physiol. Scand.* **163**, 137-146.

Altendorf, K., Voelkner, P. and Puppe, W. (1994). The sensor kinase KdpD and the response regulator KdpE control expression of the *kdpFABC* operon in *Escherichia coli*. *Res. Microbiol.* **145**, 374-381.

Andersen, J. P. and Vilsen, B. (1993). Functional consequences of substitution of the seven-residue segment LysIleArgAspGlnMetAla240 located in the stalk helix S3 of the Ca(2+)-ATPase of sarcoplasmic reticulum. *Biochemistry*. **32,** 10015-10020.

Antelmann, H., Bernhardt, J., Schmid, R. and Hecker, M. (1995). A gene at 333 degrees on the Bacillus subtilis chromosome encodes the newly identified sigma B-dependent general stress protein GspA. *J. Bacteriol*. **177,** 3540-3545.

Apell, H. J. and Karlish, S. J. (2001). Functional properties of Na,K-ATPase, and their structural implications, as detected with biophysical techniques. *J. Membr. Biol*. **180**, 1-9..

Aravind, L., Galperin, M.Y. & Koonin, E.V. (1998). The HD domain defines a new superfamily of metal-dependent phosphohydrolases. *Trends Biochem. Sci*. **23**, 469-472.

Arnold, A., Wolf, H.V., Ackermann, B.P. and Baader, H. (1976). An automated continuous assay of membrane-bound and soluble ATPases and related enzymes. *Anal. Biochem.* **71**, 209-213.

Arystarkhova, E., Wetzel, R. K., Asinovski, N. K. and Sweadner, K. J. (1999). The gamma subunit modulates Na(+) and K(+) affinity of the renal Na, K-ATPase. *J. Biol. Chem*. **274,** 33183-33185.

Asha, H. and Gowrishankar, J. (1993). Regulation of *kdp* operon expression in *Escherichia coli*: evidence against turgor as signal for transcriptional control. *J. Bacteriol.* **175**, 4528-4537.

Auer, M., Scarborough, G.A. and Kühlbrand, W. (1998). Three-dimensional map of the plasma membrane H$^+$-ATPase in the open conformation. *Nature* **392**, 840-843.

Axelsen, K.B. and Palmgreen, M.G. (1998). Evolution of substrate specificities in the P-type ATPase superfamily. *J. Mol. Evol.* **46**, 84-101.

Bakker, E.P. (1993a). Cell K$^+$ and K$^+$ transport systems in prokaryotes. In: *Alkali cation transport systems in prokaryotes* (Bakker, E.P., ed.), pp. 205-224, CRC Press, Boca Raton, Florida.

Bakker, E.P. (1993b). Low-affinity K$^+$ uptake systems. In: *Alkali cation transport systems in prokaryotes* (Bakker, E.P., ed.), pp. 253-276, CRC Press, Boca Raton, Florida.

Ballal, A., Heermann, R., Jung, K., Gaßel, M., Apte, S. K. and Altendorf, K. (2002). A chimeric *Anabaena / Escherichia coli* KdpD protein (Anacoli KdpD) functionally interacts with *E. coli* KdpE and activates kdp expression in *E. coli*. *Arch. Microbiol.* **178,** 141-148.

Berrebi-Bertran, I., Robert, P., Camelin, J. C., Bril, A. and Souchet, M. (2001). The gamma-subunit of (Na+,K+)-ATPase: a representative example of human single transmembrane protein with a key regulatory role. *Cell. Mol. Biol.* (Noisy-le-grand). **47**, 285-296.

Berrier, C., Besnard, M., Ajouz, B., Coulombe, A. and Ghazi, A. (1996). Multiple mechanosensitive ion channels from *Escherichia coli*, activated at different threshold of applied pressure. *J. Membr. Biol.* **151**, 175-187.

Blum, H., Beier, H. and Gross, H.J. (1987). Improved silver staining of plant proteins, RNA and DNA in polyacrylamide gels. *Electrophoresis* **8**, 93-99.

Bodley, A. L. and Jencks, W. P. (1987). Acetyl phosphate as a substrate for the calcium ATPase of sarcoplasmic reticulum. *J. Biol. Chem.* 262, 13997-14004.

Booth, I.R. (1985). Regulation of cytoplasmic pH in bacteria. *Microbiol. Rev.* **49**, 359-378.

Booth, I.R., Jones, M.A., McLaggan, D., Nikolaev, Y., Ness, L.S., Wood, C.M., Miller, S., Tötemeyer, S. and Ferguson, G.P. (1996). Bacterial ion channels. In: *Handbook of Biological Physics* Vol. 2 (Konings, W.N., Kaback, H.R. and Lolkema, J.S., eds.), pp. 693-729, Elsevier Science, Amsterdam.

Bossemeyer, D., Schlösser, A. and Bakker, E.P. (1989). Specific caesium transport via the *Escherichia coli* Kup (TrkD) K^+ uptake system. *J. Bacteriol.* **171**, 2219-2221.

Boyer, P. D. (1997). The ATP synthase – a splendid molecular machine. *Annu. Rev. Biochem.* **66**, 717-749.

Burkovski, A., Deckers-Hebestreit, G. and Altendorf, K. (1994). Hybrid Fo complexes of the ATP synthases of spinach chloroplasts and *Escherichia coli*. Immunoprecipitation and mutant analysis. *Eur. J. Biochem.* **225,** 1221-1228.

Buurman, E.T., Kim, K.-T. and Epstein, W. (1995). Genetic evidence of two sequentially occupied K^+ binding sites in the Kdp transport ATPase. *J. Biol. Chem.* **270,** 6678-6685.

Buxbaum, E. and Schoner, W. (1991). Phosphate binding and ATP-binding sites coexist in Na+/K(+)-transporting ATPase, as demonstrated by the inactivating $MgPO_4$ complex analogue $Co(NH_3)_4PO_4$. *Eur. J. Biochem.* 30;**195**, 407-419.

Buxbaum, E. (1999a). Co-operating ATP sites in the multiple drug resistance transporter Mdr1. *Eur. J. Biochem.* **265**, 54-63.

Buxbaum, E. (1999b). Co-operative binding sites for transported substrates in the multiple drug resistance transporter Mdr1.. *Eur. J. Biochem.* **265**, 64-70

Capieaux, E., Rapin, C., Thines, D., Dupont, Y. and Goffeau, A. (1993). Overexpression in Escherichia coli and purification of an ATP-binding peptide from the yeast plasma membrane H(+)-ATPase. *J. Biol. Chem.* **268,** 21895-21900.

Carafoli, E. (1994). Biogenesis: plasma membrane calcium ATPase: 15 years of work on the purified enzyme. *FASEB J.* **8**, 993-1002.

Carilli, C. T., Farley, R. A., Perlman, D. M. and Cantley, L. C. (1982). The active site structure of Na^+- and K^+-stimulated ATPase. Location of a specific fluorescein isothiocyanate reactive site. *J. Biol. Chem*. **257**, 5601-5606.

Carvalho-Alves, P. C., Hering, V. R., Oliveira, J. M., Salinas, R. K. and Verjovski-Almeida, S. (2000). Requirement of the hinge domain for dimerization of Ca^{2+}-ATPase large cytoplasmic portion expressed in bacteria. *Biochim. Biophys. Acta*. **1467**, 73-84.

Chang, G., Spencer, R.H., Lee, A.T., Barclay, M.T. and Rees, D.C. (1998). Structure of the MscL homolog from *Mycobacterium tuberculosis*: A gated mechanosensitive ion channel. *Science* **282**, 2220-2226.

Christian, J. H. B. and Waltho, J. A. (1962). Solute concentrations within cells of halophilic and non-halophilic bacteria. *Biochim. Biophys. Acta*.. **65**, 506

Christian, J. H. B. and Waltho, J. A. (1966). Water relations of *Salmonella oranienburg*; stimulation of respiration by amino acids. *J. Gen. Microbiol.* **43,** 345-355.

Clarke, D. M., Loo, T. W. and MacLennan, D. H. (1990). Functional consequences of mutations of conserved amino acids in the beta-strand domain of the Ca^{2+}-ATPase of sarcoplasmic reticulum. *J. Biol. Chem.* 265, 14088-14092.

Clarke, D. M., Loo, T. W., Inesi, G. and MacLennan, D. H. (1989). Location of high affinity Ca^{2+}-binding sites within the predicted transmembrane domain of the sarcoplasmic reticulum Ca^{2+}-ATPase. *Nature*. **339**, 476-478.

Corpet, F. (1988). Multiple sequence alignment with hierarchical clustering. *Nucl. Acid. Res*. **16**, 10881-10890

Davidson, A. L., Laghaeian, S. S. and Mannering, D. E. (1996). The maltose transport system of *Escherichia coli* displays positive cooperativity in ATP hydrolysis. *J. Biol. Chem*. **271**, 4858-4863.

Dehner, A., Planker, E., Gemmecker, G., Broxterman, Q. B., Bisson, W., Formaggio, F., Crisma, M., Toniolo, C. and Kessler, H. (2001). Solution structure, dimerization, and dynamics of a lipophilic alpha/3(10)-helical, C alpha-methylated peptide. Implications for folding of membrane proteins. *J. Am. Chem. Soc.* **123**, 6678-6686.

Dinnbier, U., Limpinsel, E., Schmid, R. and Bakker, E.P. (1988). Transient accumulation of potassium glutamate and its replacement by trehalose during adaptation of growing cells of *Escherichia coli* K-12 to elevated sodium chloride concentration. *Arch. Microbiol.* **150**, 348-357.

Donnet, C., Caride, A. J., Talgham, S. and Rossi, J. P. (1998). Chemical modification reveals involvement of different sites for nucleotide analogues in the phosphatase activity of the red cell calcium pump. *J. Membr. Biol.* **163,** 217-224.

Dorus, S., Mimura, H. and Epstein, W. (2001). Substrate-binding clusters of the K^+-transporting Kdp ATPase of *Escherichia coli* investigated by amber suppression scanning mutagenesis. *J. Biol. Chem.* **276**, 9590-9598.

Doyle, D.A., Cabral, J.M., Pfuetzner, R.A., Kuo, A., Gulbis, J.M., Cohen, S.L., Chait, B.T. and MacKinnon, R. (1998). The structure of the potassium channel: molecular basis of K^+ conduction and selectivity. *Science* **280**, 69-77.

Dröse, S. (1992). Biochemische Charkterisierung funktioneller Bereiche der Kdp-ATPase von *Escherichia coli*. Diplomarbeit, Universität Osnabrück.

Dröse, S. (1997). Biochemische Charakterisierung, Rekonstitution und Transportmodus der Kdp-ATPase von *Escherichia coli* sowie Untersuchungen zur Wirkung von Plekomakroliden als Inhibitoren von P- und V-ATPasen. Dissertation, Universität Osnabrück.

Dupont, Y., Chapron, Y. and Pougeois, R. (1982). Titration of the nucleotide binding sites of sarcoplasmic reticulum Ca^{2+}-ATPase with 2',3'-O-(2,4,6-trinitrophenyl) adenosine 5'-triphosphate and 5'-diphosphate. *Biochem. Biophys. Res. Commun.* **106,** 1272-1279.

Dupont, Y., Pougeois, R., Ronjat, M. and Verjovsky-Almeida, S. (1985). Two distinct classes of nucleotide binding sites in sarcoplasmic reticulum Ca-ATPase revealed by 2',3'-O-(2,4,6-trinitrocyclohexadienylidene)-ATP. *J. Biol. Chem.* **260**, 7241-7249.

Durell, S. R., Bakker, E. P. and Guy, H. R. (2000). Does the KdpA subunit from the high affinity K(+)-translocating P-type KDP-ATPase have a structure similar to that of K(+) channels? *Biophys J.* **78**, 188-199.

East, J. M. (2000). Sarco(endo)plasmic reticulum calcium pumps: recent advances in our understanding of structure/function and biology. *Mol. Membr. Biol.* **17**, 189-200..

Ebashi, S. and Lipmann, F. J. (1962). Adenosine triphosphate-linked concentration of calcium ions in a particulate fraction of rabbit muscle. *J. Cell. Biol.* **14**, 389-400

Epstein, W. (1985). The Kdp system: a bacterial K^+ transport ATPase. *Curr. Top. Membr. Transp.* **23**, 153-175.

Epstein, W. and Davies, M. (1970). Potassium-dependent mutants of *Escherichia coli* K-12. *J. Bacteriol.* **101**, 836-843.

Epstein, W. and Kim B.S. (1971). Potassium transport loci in Escherichia coli K-12. *J. Bacteriol.* **108**, 639-644.

Epstein, W. Walderhaug, M. O., Polarek, J. W., Hesse, J. E., Borus, E. and Daniel, J. M. (1990). The bacterial Kdp K^+-ATPase and ist relation to other transport ATPases, such as the Na^+,K^+- and Ca^{2+}-ATPases in higher organisms. *Philos. Trans. R. Soc. Lond. B. Biol. Sci.* **326**, 479-486.

Ettrich, R., Melichercik, M., Teisinger, J., Etterichova, O., Krumscheid, R., Hofbauerova, K., Kvasnicka, P., Schoner, W. and Amler, E. (2001). Three-dimensional structure of the large cytoplasmic H4-H5 loop of Na+/K+-ATPase deduced by restraint-based comparative modelling shows only one ATP binding site. *J. Mol. Model.* **7**, 184-192.

Faller, L. D. (1989). Competitive binding of ATP and the fluorescent substrate analogue 2',3'-O-(2,4,6-trinitrophenylcyclohexadienylidine) adenosine 5'-triphosphate to the gastric H^+,K^+-ATPase: evidence for two classes of nucleotide sites. *Biochemistry.* **28**, 6771-6778.

Farley, R. A., Tran, C. M., Carilli, C. T., Hawke, D. and Shively J. E. (1984). The amino acid sequence of a fluorescein-labeled peptide from the active site of (Na,K)-ATPase. *J. Biol. Chem.* **259,** 9532-9535

Fedosova, N. U., Cornelius, F. and Klodos, I. (1998). E2P phosphoforms of Na, K-ATPase. I. Comparison of phosphointermediates formed from ATP and Pi by their reactivity towards hydroxylamine and vanadate. *Biochemistry.* 37, 1313634-13642.

Fendler, K., Dröse, S., Altendorf, K. and Bamberg, E. (1996). Electrogenic K^+ transport by the Kdp-ATPase of *Escherichia coli. Biochemistry* **35**, 8009-8017.

Fendler, K., Dröse, S., Epstein, W., Altendorf, K. and Bamberg, E. (1999). The Kdp-ATPase of *Escherichia coli* mediates an ATP-dependent, K^+-independent electrogenic partial reaction. *Biochemistry* **38**, 1850-1856.

Ferguson, G.P., McLaggan, D. and Booth, I.R. (1995). Potassium channel activation by glutathione-S-conjugates in *Escherichia coli*: protection against methylglyoxal is mediated by cytoplasmic acidification. *Mol Microbiol* **17**,1025-1033.

Ferguson, G.P., Nikolaev, Y., McLaggan, D., Maclean, M. and Booth, I.R. (1997). Survival during exposure to the electrophilic reagent N-ethylmaleimide in *Escherichia coli*: role of KefB and KefC potassium channels. *J Bacteriol.* **179**, 1007-1012.

Ferreira-Pereira, A., Alves-Ferreira, M. de Carvalho-Alves, P. C. (1994). p-nitrophenyl-phosphatase activity of plasma membrane H(+)-ATPase from yeast. Implications for the regulation of the catalytic cycle by H^+. *J. Biol. Chem.* **269**, 12074-12079.

Fioleto, A. G., Elwess, N. L., Enyedi, A., Caride, A., Aung, H. H. and Penniston, J. T. (1997). Plasma membrane Ca^{2+} pump in rat brain. Patterns of alternative splices seen by isoform-specific antibodies. *J. Biol. Chem.***272**, 23741-23747.

Galinski E. A., Pfeiffer, H. P. and Truper, H. G. (1985). 1,4,5,6-Tetrahydro-2-methyl-4-pyrimidinecarboxylic acid. A novel cyclic amino acid from halophilic phototrophic bacteria of the genus *Ectothiorhodospira*. *Eur. J. Biochem.* **149**, 135-139.

Gaßel, M. (1999). Charakterisierung, Reinigung und Rekonstitution des Kdp-Komplexes aus *Escherichia coli* unter besonderer Berücksichtigung der Untereinheiten KdpC und KdpF sowie Untersuchungen zur Identifikation der Plekomakrolidbindestelle von P- und V-ATPasen. Dissertation, Universität Osnabrück.

Gaßel, M. (1999). Charakterisierung, Reinigung und Rekonstitution des Kdp-Komplexes aus *Escherichia coli* unter besonderer Berücksichtigung der Untereinheiten KdpC und KdpF sowie Untersuchungen zur Identifikation der Plekomakrolidbindestelle von P- und V-ATPasen. Dissertation, Universität Osnabrück.

Gaßel, M. and Altendorf, K. (2001). Analysis of KdpC of the K(+)-transporting KdpFABC complex of Escherichia coli. *Eur J Biochem.* **268**, 1772-1781.

Gaßel, M., Möllenkamp, T., Puppe, W. and Altendorf, K. (1999). The KdpF subunit is part of the K^+-translocating Kdp complex of *Escherichia coli* and is responsible for the stabilization of the complex *in vitro. J. Biol. Chem.* **274**, 37901-37907.

Gatto, C., Lutsenko, S. and Kaplan, J. H. (1997). Chemical modification with dihydro-4,4'-diisothiocyanostilbene-2,2'-disulfonate reveals the distance between K480 and K501 in the ATP-binding domain of the Na,K-ATPase. *Arch. Biochem. Biophys.* **340**, 90-100.

Gatto, C., Wang, A. X. and Kaplan, J. H. (1998). The M4M5 cytoplasmic loop of the Na,K-ATPase, overexpressed in *Escherichia coli*, binds nucleoside triphosphates with the same selectivity as the intact native protein. *J. Biol. Chem.* **273,** 10578-10585.

Glynn, I. M. (1982). Occluded-ion forms of the Na,K-ATPase. *Ann. N. Y. Acad. Sci.* **402**, 287-288.

Goldshleger, R., Patchornik, G., Shimon, M. B., Tal, D. M., Post, R. L. and Karlish, S. J. (2001). Structural organization and energy transduction mechanism of Na^+, K^+-ATPase studied with transition metal-catalyzed oxidative cleavage. *J. Bioenerg. Biomembr* **33,** 387-399.

Green, N. M. and Stokes, D. L. (1992). Structural modelling of P-type ion pumps. *Acta. Physiol. Scand. Suppl.* 607, 59-68.

Greie, J. C., Deckers-Hebestreit, G. and Altendorf, K. (2000). Secondary structure composition of reconstituted subunit b of the *Escherichia coli* ATP synthase. *Eur. J. Biochem*. **267**, 3040-3048.

Gupta, S. S., DeWitt, N. D., Allen, K., E. and Slayman, C. W. (1998). Evidence for a salt bridge between transmembrane segments 5 and 6 of the yeast plasma-membrane H^+-ATPase. *J. Biol. Chem.* **273**, 34328-34334.

Gutfreund, H. (1972), in: Enzymes, physical principles, Wiley-Inter-Science, London**,** 71

Guzman, L.M., Belin, D., Carson, M.J. and Beckwith, J. (1995). Tight regulation, modulation, and high-level expression by vectors containing the arabinose pBAD promoter. *J. Bacteriol.* **177**, 4121-4130.

Hanahan, D. (1983). Studies on transformation of *Escherichia coli* with plasmids. *J. Mol. Biol.* **166**, 557-580.

Harms, C., Domoto, Y., Celik, C., Rahe, E. Stumpe, S., Schmid, R., Nakamura, T. and Bakker, E. P. (2001). Identification of the ABC protein SapD as the subunit that confers ATP dependence to the K^+-uptake systems Trk(H) and Trk(G) from *Escherichia coli* K-12. *Microbiology*.**147**, 2991-3003.

Harold, F.M. and Altendorf, K. (1974). Cation transport in bacteria: K^+, Na^+ and H^+. *Curr. Top. Membr. Transp.* **5**, 1-50.

Harris, E. D. (2000). Cellular copper transport and metabolism. *Annu. Rev. Nutr.* **20**, 291-310.

Hartree, E.F. (1972). Determination of protein: A modification of the Lowry method that gives a linear photometric response. *Anal. Biochem.* **48**, 422-427.

Hasselbach, W. and Makinose, M. (1961). Die Calciumpumpe der "Erschlaffungsgrana" des Muskels und ihre Abhängigkeit von der ATP-spaltung. *Biochem. Zeitschrift.* **333**, 518-528

Heermann, R., Altendorf, K. and Jung, K. (1998). The turgor sensor KdpD of *Escherichia coli* is a homodimer. *Biochem. Biophys. Acta* **1415**, 114-124.

Heermann, R., Altendorf, K. and Jung, K. (2000). The hydrophilic N-terminal domain complements the membrane-anchored C-terminal domain of the sensor kinase KdpD of *Escherichia coli*. *J. Biol. Chem*. **275**, 17080-17085.

Heermann, R., Fohrmann, A., Altendorf, K. and Jung, K. (2003). The transmembrane domains of the sensor kinase KdpD of *Escherichia coli* are not essential for sensing K^+ limitation. *Mol Microbiol.* in press.

Heginbotham, L., Abramson, T. and MacKinnon, R. (1992). A functional connection between pores of distantly related ion channels as revealed by mutant K^+ channels. *Science* **258**, 1152-1155.

Heginbotham, L., Abramson, T. and MacKinnon, R. (1994). Mutations in the K^+ channel signature sequence. *Biophys, J.* **66**, 1061-1067.

Helmer, G.L., Laimins, L.A. and Epstein, W. (1982). Mechanism of potassium transport in bacteria. In: *Membranes and transport* Vol. 2 (Martonosi, A.N., ed.), pp. 123-128, Plenum Publishing Corp., New York.

Henkel, R.D., Van De Berg, J.L. and Walsh, R.A. (1988). A microassay for ATPase. *Anal. Biochem.* **169,** 312-318.

Hesse, J.E., Wieczorek, L., Altendorf, K., Reicin, A.S., Dorus, E. and Epstein, W. (1984). Sequence homology between two membrane ATPases, the Kdp-ATPase of *Escherichia coli* and the Ca^{2+}-ATPase of sarcoplasmic reticulum. *Proc. Natl. Acad. Sci. USA* **81**, 4746-4750.

Hirata, H., Altendorf, K. and Harold, F. M. (1974). Energy coupling in membrane vesicles of *Escherichia coli*. I. Accumulation of metabolites in response to an electrical potential. *J. Biol. Chem.* **249**, 2939-2945.

Hisano, T, Hata, Y., Fujii, T, Liu, J. Q., Kurihara T., Esaki, N. and Soda, K. (1996). Crystal structure of L-2-haloacid dehalogenase from *Pseudomonas* sp. YL. An alpha/beta hydrolase structure that is different from the alpha/beta hydrolase fold. *J. Biol. Chem.* **271,** 20322-20330.

Hoang, T. T., Ma, Y., Stern, R. J., McNeil, M. R. and Schweizer, H. P. (1999). Construction and use of low-copy number T7 expression vectors for purification of problem proteins: purification of *Mycobacterium tuberculosis* RmlD and *Pseudomonas aeruginosa* LasI and RhlI proteins, and functional analysis of purified RhlI. *Gene.* **237**, 361-371.

Holloway, P.W. (1973). A simple procedure for removal of Triton X-100 from protein samples. *Anal. Biochem.* **53**, 304-308.

Imhoff, J. F. (1988). Halophilic phototrophic bacteria, in *Halophilic Bacteria, Vol. I*, Rodriguez-Valera, F. Ed. , CRC Press, Boca Raton, FL, 85

Inesi, G. (1971). p-nitrophenyl phosphate hydrolysis and calcium ion transport in fragmented sarcoplasmic reticulum. *Science.* 171, 901-903.

Iwane, A.H., Ikeda, I., Kimura, Y., Fujiyoshi, Y., Altendorf, K. and Epstein, W. (1996). Two-dimensional crystals of the Kdp-ATPase of *Escherichia coli. FEBS Lett.* **396**, 172-176.

Jan, L.Y. and Jan, Y.N. (1994). Potassium channels and their evolving gates. *Nature* **371**, 119-122.

Jan, L.Y. and Jan, Y.N. (1997). Cloned potassium channels from eukaryotes and prokaryotes. *Annu. Rev. Neurosci.* **20**, 91-123.

Johnson, W. C. Jr. (1988). Secondary structure of proteins through circular dichroism spectroscopy. *Annu. Rev. Biophys. Biophys. Chem.***17**, 145-166.

Jones T. A. and Kjeldgaard M. (1998). Essential 'O', software manual, Uppsala, Sweden, pp. 178

Jørgensen, P. L. (1975). Purification and characterization of (Na+, K+)-ATPase. V. Conformational changes in the enzyme Transitions between the Na-form and the K-form studied with tryptic digestion as a tool. *Biochim. Biophys. Acta.* **401,** 399-415.

Jung, K. and Altendorf K. (1998a). Truncation of Amino Acids 12-128 causes deregulation of the phosphatase activity of the sensor kinase KdpD of *Escherichia coli. J. Biol. Chem.* **273**, 17406-17410.

Jung, K. and Altendorf, K. (1998b). Individual substitutions of clustered arginine residues of the sensor kinase KdpD of *Escherichia coli* modulate the ratio of the kinase to phosphatase activity. *J. Biol. Chem.* **273**, 26415-26420.

Jung, K., Heermann, R., Meyer, M. and Altendorf, K. (1998). Effect of cysteine replacements on the properties of the turgor sensor KdpD of *Escherichia coli. Biochim. Biophys. Acta* **1372**, 311-322.

Jung, K., Tjaden, B. and Altendorf, K. (1997). Purification, reconstitution, and characterization of KdpD, the turgor sensor of *Escherichia coli. J. Biol. Chem*. 272, 10847-10852.

Kaneko, T., Sato, S., Kotani, H., Tanaka, A., Asamizu, E., Nakamura, Y., Miyajima, N., Hirosawa, M., Sugiura, M., Sasamoto, S., Kimura, T., Hosouchi, T., Matsuno, A., Muraki, A., Nakazaki, N., Naruo, K., Okumura, S., Shimpo, S., Takeuchi, C., Wada, T., Watanabe, A., Yamada, M., Yasuda, M. and Tabata, S. (1996). Sequence analysis of the genome of the unicellular cyanobacterium *Synechocystis sp.* strain PCC6803. II. Sequence determination of the entire genome and assignment of potential protein-coding regions (supplement). *DNA Res.* **3**, 185-209

Karlish, S. J. (1980). Characterization of conformational changes in (Na,K) ATPase labeled with fluorescein at the active site. *J. Bioenerg. Biomembr.* **12**, 111-36.

Kimura, Y. and Inui, M. (2002). Reconstitution of the cytoplasmic interaction between phospholamban and Ca(2+)-ATPase of cardiac sarcoplasmic reticulum. *Mol. Pharmacol.* **61**, 667-673.

Klein, C., Planker, E., Diercks, T., Kessler, H., Kunkele, K. P., Lang, K., Hansen, S. and Schwaiger, M. (2001). NMR spectroscopy reveals the solution dimerization interface of p53 core domains bound to their consensus DNA. *J. Biol. Chem.* **276**, 49020-49027.

Kühlbrandt, W., Zeelen, J. and Dietrich, J. (2002). Structure, mechanism and regulation of the *Neurospora* plasma membrane H$^+$-ATPase. *Science.* **297**, 1692-1696

Kushner, D. J. and Kamekura, M. (1988). Physiology of halophilic bacteria, in *Halophilic Bacteria, Vol. I*, Rodriguez-Valera, F. Ed. , CRC Press, Boca Raton, FL, 109

Laemmli, U.K. (1970). Cleavage of structural proteins during the assembly of the head of bacteriophage T4. *Nature* **227**, 680-685.

Laimins, L.A., Rhoads, D.B. and Epstein, W. (1981). Osmotic control of *kdp* expression in *Escherichia coli*. *Proc. Natl. Acad. Sci. USA* **78**, 464-468.

Laimins, L.A., Rhoads, D.B., Altendorf, K. and Epstein, W. (1978). Identification of the structural proteins of an ATP-driven potassium transport system in *Escherichia coli*. *Proc. Natl. Acad. Sci. USA* **75**, 3216-3219.

Larsen, P. I., Sydnes, L. K., Landfald, B. and Strom, A. R. (1987). Osmoregulation in *Escherichia coli* by accumulation of organic osmolytes: betaines, glutamic acid, and trehalose. *Arch. Microbiol.* **147**, 1-7.

Lee, A. G. (2002). Ca^{2+}-ATPase structure in the E1 and E2 conformations: mechanism, helix–helix and helix–lipid interactions. *Biochim. Biphys Acta* **1565**, 246-266

Linnertz, H., Lanz, E., Gregor, M., Antolovic, R., Krumscheid, R., Obsil, T., Slavik, J., Kovarik, Z., Schoner, W. and Amler, E. (1999). Microenvironment of the high affinity ATP-binding site of Na$^+$/K$^+$-ATPase is slightly acidic. *Biochem. Biophys. Res. Commun.* **254**, 215-221.

Linnertz, H., Thoenges, D. and Schoner, W. (1995). Na+/K(+)-ATPase with a blocked E1ATP site still allows backdoor phosphorylation of the E2ATP site. *Eur. J. Biochem.* **232**, 420-424.

Linnertz, H., Urbanova, P., Obsil, T., Herman, P., Amler, E. and Schoner, W. (1998). Molecular distance measurements reveal an (alpha beta)2 dimeric structure of Na$^+$/K$^+$-ATPase. High affinity ATP binding site and K$^+$-activated phosphatase reside on different alpha-subunits. *J. Biol. Chem.* **273,** 28813-28821.

Liu, C. E., Liu, P. Q. and Ames, G. F. L. (1997). Characterization of the adenosine triphosphatase activity of the periplasmic histidine permease, a traffic ATPase (ABC transporter). *J. Biol. Chem.* **272**, 21883-21891.

Lucassen, M. (1998). Regulation des Kdp-Systems aus *Escherichia coli*: Biochemische Charakterisierung des Antwortregulators KdpE und Nachweis von Konformationsänderungen im Zuge der Aktivierung. Dissertation, Universität Osnabrück.

Lutsenko, S. and Kaplan, J.H. (1995). Organization of P-Type ATPases: Significance of structural diversity. *Biochemistry* **34**, 15607-15613.

Luzhkov, V. B. and Åqvist, J. (2001). K(+)/Na(+) selectivity of the KcsA potassium channel from microscopic free energy perturbation calculations. *Biochim. Biophys. Acta.* **1548**, 194-202.

Mac Lennan, D. H., Rice, W. J. and Odermatt, A. (1997). Structure/function analysis of the Ca^{2+} binding and translocation domain of SERCA1 and the role in Brody disease of the ATP2A1 gene encoding SERCA1. *Ann. N. Y. Acad. Sci.* **834**, 175-85.

Malli, R. and Epstein, W. (1998). Expression of the Kdp ATPase is consistent with regulation by turgor pressure. *J. Bacteriol.* **180**, 5102-5108.

Manavalan, P. and Johnson, W. C. Jr. (1987). Variable selection method improves the prediction of protein secondary structure from circular dichroism spectra. *Anal. Biochem.* **167,** 76-85.

Martiniac, B., Buechner, M., Delcour, A.H., Adler, J. and Kung, C. (1987). Pressure-sensitive ion channel in *Escherichia coli. Proc. Natl. Acad. Sci. USA* 84, 2297-2301.

May, J. J., Kessler, J., Marahiel, M. A. and Stubbs, M. T. (2002). Crystal structure of DhbE, an archetype for aryl acid activating domains of modular nonribosomal peptide synthetases. Proc. *Natl. Acad. Sci. USA*. **99**, 12120-12125.

McIntosh, D. B. (1992). Glutaraldehyde cross-links Lys-492 and Arg-678 at the active site of sarcoplasmic reticulum Ca(2+)-ATPase. *J. Biol. Chem.* **267,** 22328-22335.

McIntosh, D. B. (2000). Portrait of a P-type pump. *Nat. Struct. Biol.* 7, 532-535.

McLaggan, D., Naprstek, J., Buurman, E.T. and Epstein, W. (1994). Interdependence of K^+ and glutamate accumulation during osmotic adaption of *Escherichia coli. J. Biol. Chem.* **269**, 1911-1917.

Measures, J. C. (1975). Role of amino acids in osmoregulation of nonhalophilic bacteria. *Nature.* **257**, 389

Mignaco, J. A., Barrabin, H. and Scofano, H. M. (1996). Effects of photo-oxidizing analogs of fluorescein on the sarcoplasmic reticulum Ca^{2+}-ATPase. Functional consequences for substrate hydrolysis and effects on the partial reactions of the hydrolytic cycle. *J. Biol. Chem.* **271**, 18423-18430.

Milkman, R. (1994). An *Escherichia coli* homologue of eukaryotic potassium channel proteins. *Proc. Natl. Acad. Sci. USA* **91**, 3510-3514.

Moczydlowski, E. G. and Fortes, P. A. (1981a). Characterization of 2',3'-O-(2,4,6-trinitrocyclohexadienylidine)adenosine 5'-triphosphate as a fluorescent probe of the ATP site of sodium and potassium transport adenosine triphosphatase. Determination of nucleotide binding stoichiometry and ion-induced changes in affinity for ATP. *J. Biol. Chem.* **256,** 2346-2356.

Moczydlowski, E. G. and Fortes, P. A. (1981b). Inhibition of sodium and potassium adenosine triphosphatase by 2',3'-O-(2,4,6-trinitrocyclohexadienylidene) adenine nucleotides. Implications for the structure and mechanism of the Na:K pump. *J. Biol. Chem.* **256,** 2357-2366.

Møller, J.V., Juul, B. and le Maire, M. (1996). Structural organization, ion transport, and energy trans-duction of P-type ATPases. *Biochim. Biophys. Acta* **1286**, 1-51.

Morais-Cabral, J. H., Zhou, Y. and MacKinnon, R. (2001). Energetic optimization of ion conduction rate by the K$^+$ selectivity filter. *Nature*. **414**, 37-42.

Morsomme, P., Chami, M., Marco, S., Nader, J., Ketchum, K. A., Goffeau, A., Rigaud, J. L. (2002). Characterization of a hyperthermophilic P-type ATPase from *Methanococcus jannaschii* expressed in yeast. *J. Biol. Chem*. **277,** 29608-29616.

Morsomme, P., Slayman, C. W. and Goffeau, A. (2000). Mutagenic study of the structure, function and biogenesis of the yeast plasma membrane H(+)-ATPase. *Biochim. Biophys. Acta.* 1469, 133-157.

Moutin, M. J., Cuillel, M., Rapin, C., Miras, R., Anger, M., Lompre, A. M. and Dupont, Y. (1994). Measurements of ATP binding on the large cytoplasmic loop of the sarcoplasmic reticulum Ca(2+)-ATPase overexpressed in *Escherichia coli*. *J. Biol. Chem*. **269,** 11147-11154.

Moutin, M. J., Rapin, C., Miras, R., Vincon, M., Dupont, Y. and McIntosh, D. B. (1998). Autonomous folding of the recombinant large cytoplasmic loop of sarcoplasmic reticulum Ca^{2+}-ATPase probed by affinity labeling and trypsin digestion. *Eur. J. Biochem*. **251**, 682-690.

Nakamura, J.M., Anderson, J.A. and Gaber, R.F. (1997). Determination of key structural requirements for a K$^+$ channel pore. *J. Biol. Chem.* **272**, 1011-1018.

Nakamura, T., Yuda, R., Unemoto, T. and Bakker, E.P. (1998). KtrAB, a new type of bacterial K$^+$-uptake system from *Vibrio alginolyticus*. *J. Bacteriol.* **180**, 3491-3494.

Nakamura, Y. and Tonomura, Y. (1978). Reaction mechanism of p-nitrophenylphosphatase of sarcoplasmic reticulum. Evidence for two kinds of phosphorylated intermediate with and without bound p-nitrophenol. *J. Biochem*. (Tokyo). **83**, 571-583.

Nakashima, K., Sugiura, A., Kanamaru, K. and Mizuno, T. (1993). Signal transduction between the two regulatory components involved in the regulation of the *kdpABC* operon in *Escherichia coli*: phosphorylation-dependent functioning of the positive regulator, KdpE. *Mol. Microbiol.* **7**, 109-116.

Nakashima, K., Sugiura, A., Momoi, H. and Mizuno, T. (1992). Phosphotransfer signal transduction between two regulatory factors involved in the osmoregulated *kdp* operon of *Escherichia coli. Mol. Microbiol.* **6**, 1777-1784.

Ness, L.S. and Booth, I.R. (1999). Different loci for the regulation of the activity of the KefB and KefC glutathione-gated K$^+$ efflux systems. *J. Biol. Chem.* **274**, 9524-9530.

Obsil, T., Merola, F., Lewit, B. A. and Amler, E. (1998). The isolated H4-H5 cytoplasmic loop of Na,K-ATPase overexpressed in *Escherichia coli* retains its ability to bind ATP. *Gen. Physiol. Biophys*. **17** Suppl 1, 52-55.

Ogawa, H., Haga, T. and Toyoshima, C. (2000). Soluble P-type ATPase from an archaeon, *Methanococcus jannaschii*. *FEBS Lett*. **471**, 99-102.

Pardo, J. P. and Slayman, C. W. (1988). The fluorescein isothiocyanate-binding site of the plasma-membrane H$^+$-ATPase of *Neurospora crassa*. *J. Biol. Chem.* **263**, 18664-18668.

Pedersen, P.L. and Carafoli, E. (1987). Ion motive ATPases. I. Ubiquity, properties, and significance to cell function. *Trends Biochem. Sci.* **12**, 146-150.

Pelton, J. T. and McLean, L. R. (2000). Spectroscopic methods for analysis of protein secondary structure. *Anal. Biochem*. **277,** 167-176..

Pick U. and Bassilian S. (1981). Modification of the ATP binding site of the Ca^{2+}-ATPase from sarcoplasmic reticulum by fluorescein isothiocyanate. *FEBS Lett*. **123,** 127-130

Pick, U. (1981). Interaction of fluorescein isothiocyanate with nucleotide-binding sites of the Ca-ATPase from sarcoplasmic reticulum. *Eur. J. Biochem*. **121,** 187-195.

Pick, U. and Karlish, S. J. (1980). Indications for an oligomeric structure and for conformational changes in sarcoplasmic reticulum Ca^{2+}-ATPase labelled selectively with fluorescein. *Biochim. Biophys. Acta.***626**, 255-261.

Pick. U. (1982). The interaction of vanadate ions with the Ca-ATPase from sarcoplasmic reticulum. *J. Biol. Chem*. **257,** 6111-6119.

Pitts, B. J., Askari, A. (1971a). Stimulation of the phosphatase activity of (Na^+, K^+)-ATPase preparations by ouabain. *Biochim. Biophys. Acta*. **225**, 388-391.

Pitts, B. J., Askari, A. (1971b). A fluorimetric assay method for the K plus-phosphatase associated with the (Na+ + K+)-activated ATPase. *Biochim. Biophys. Acta*. **227**, 453-459.

Plesner, I. W. (1987). Oligomycin inhibition of Na,K,ATPase. Analysis of half-of-sites moderator interaction with a dimeric enzyme. *Cell. Biophys*. **11**, 279-307.

Polarek, J.W., Williams, G. and Epstein, W. (1992). The products of the *kdpDE* operon are required for expression of the Kdp ATPase of *Escherichia coli. J. Bacteriol.* **174**, 2145-2151.

Post, R. L., Hegyvary, C. and Kume, S. (1972). Activation by adenosine triphosphate in the phosphorylation kinetics of sodium and potassium ion transport adenosine triphosphatase. *J. Biol. Chem.* **247,** 6530-6540.

Pucell, A. and Martonosi, A. (1971). Sarcoplasmic reticulum. XIV. Acetylphosphate and carbamylphosphate as energy sources for Ca++ transport. *J. Biol. Chem*. **246**, 3389-3397

Puppe, W. (1991). Kalium-Transport bei *Escherichia coli*: Molekulargenetische und biochemische Untersuchungen zu funktionellen Domänen der Kdp-ATPase. Dissertation, Universität Osnabrück.

Puppe, W., Siebers, A. and Altendorf, K. (1992). The phosphorylation site of the Kdp-ATPase of *Escherichia coli*: site-directed mutagenesis of the aspartic acid residues 300 and 307 of the KdpB subunit. *Mol. Microbiol.* **6**, 3511-3520.

Puppe, W., Zimmann, P., Jung, K., Lucassen, M. and Altendorf, K. (1996). Characterization of truncated forms of the KdpD protein, the sensor kinase of the K^+-translocating Kdp system of *Escherichia coli*. *J. Biol. Chem*. **271**, 25027-25034.

Rega, A. F., Richards, D. E. and Garrahan, P. J. (1973). Calcium ion-dependent p-nitrophenyl phosphate phosphatase activity and calcium ion-dependent adenosine triphosphatase activity from human erythrocyte membranes. *Biochem. J*. **136**, 185-194. 1

Rephaeli, A., Richards, D. and Karlish, S. J. (1986). Conformational transitions in fluorescein-labeled (Na, K)ATPase reconstituted into phospholipid vesicles. *J. Biol. Chem.* **261**, 6248-6254.

Repke, K. R., Schön, R. (1973). Flip-flop model of (NaK)-ATPase function. *Acta. Biol. Med. Ger*. **31** Suppl, 19-30.

Rhoads, D.B. and Epstein, W. (1977). Energy coupling to net K^+ transport in *Escherichia coli*. *J. Biol. Chem*. **252**, 1394-1401.

Rhoads, D.B. and Epstein, W. (1978). Cation transport in *Escherichia coli*. IX. Regulation of K^+ transport. *J. Gen. Physiol.* **72**, 283-295.

Rhoads, D.B., Waters, F.B. and Epstein, W. (1976). Cation transport in *Escherichia coli*. VIII. Potassium transport mutants. *J. Gen. Physiol.* **67**, 325-341.

Ridder, I. S. and Dijkstra, B. W. (1999). Identification of the Mg^{2+}-binding site in the P-type ATPase and phosphatase members of the HAD (haloacid dehalogenase) superfamily by structural similarity to the response regulator protein CheY. *Biochem. J.* **339**, 223-226.

Robinson, J. D., Levine, G. M. and Robinson, L. J. (1983). A model for the reaction pathways of the K^+-dependent phosphatase activity of the $(Na^+ + K^+)$-dependent ATPase. *Biochim. Biophys. Acta*. **731**, 406-414.

Rossi, B., de Assis Leone, F., Gache, C. and Lazdunski, M. (1979). Pseudosubstrates of the sarcoplasmic Ca^{2+}-ATPase as tools to study the coupling between substrate hydrolysis and Ca^{2+} transport. *J. Biol. Chem.* **254**, 2302-2307.

Saccomani, G. and Mukidjam, E. (1987). Papain fragmentation of the gastric $(H^+ + K^+)$-ATPase. *Biochim. Biophys. Acta.* **912,** 63-73.

Sambrook, J., Fritsch, E. F. and Maniatis, T. (1989). *Molecular Cloning. A Labotory Manual*. Cold Spring Habor Laboratory Press, Cold Spring Harbor, New York.

Sansom, M. S., Shrivastava, I. H., Ranatunga, K. M. and Simth, G. R. (2000). Simulations of ion channels-watching ions and water move. *Trends Biochem. Sci.* **25,** 368-374.

Sattler, M., Schleucher, J. and Griesinger, C. (1999). Heteronuclear multidimensional NMR experiments for the structure determination of proteins in solution employing pulsed field gradients. *Prog. NMR Spectr.* **34**, 93-158.

Schaffner, W. and Weissmann, C. (1973). A rapid, sensitive, and specific method for the determination of protein in dilute solution. *Anal. Biochem.* **56**, 502-514.

Scheiner-Bobis, G., Antonipillai, J. and Farley, R. A. (1993). Simultaneous binding of phosphate and TNP-ADP to FITC-modified Na+,K(+)-ATPase. *Biochemistry* **32**, 9592-9599.

Schleyer, M., Schmid, R. and Bakker, E.P. (1993). Transient, specific and extremly rapid release of osmolytes from growing cells of *Escherichia coli* K-12 exposed to hypoosmotic shock. *Arch. Microbiol.* **160**, 424-431.

Schlösser, A., Hamann, A., Bossemeyer, D., Schneider, E. and Bakker, E.P. (1993). NAD^+ binding to the *Escherichia coli* K^+-uptake protein TrkA and sequence similarities between TrkA and domains of a family of dehydrogenases suggest a role for NAD^+ in bacterial transport. *Mol. Microbiol.* **9**, 533-543.

Schlösser, A., Meldorf, M., Stumpe, S., Bakker, E. P. and Epstein, W. (1995). TrkH and its homolog, TrkG, determine the specificity and kinetics of cation transport by the Trk system of *Escherichia coli. J. Bacteriol.***177**, 1908-1910.

Schrader, M., Fendler, K., Bamberg, E., Gassel, M., Epstein, W., Altendorf, K. and Dröse, S. (2000). Replacement of glycine 232 by aspartic acid in the KdpA subunit broadens the ionspecificity of the K^+-translocating KdpFABC complex. *Biophys. J.* **79,** 602-613.

Schrempf, H., Schmidt, O., Kummerlen, R., Hinnah, S., Muller, D., Betzler, M., Steinkamp, T. and Wagner, R. (1995). A prokaryotic potassium ion channel with two predicted transmembrane segments from *Streptomyces lividans*. *EMBO J.***14,** 5170-5178.

Schuldiner, S. and Padan, E. (1993). Na^+/H^+ antiporters in *Escherichia coli.* In: *Alkali cation transport systems in prokaryotes* (Bakker, E.P., ed.), pp. 25-51, CRC Press, Boca Raton, Florida

Serrano, R. (1988). Structure and function of proton translocating ATPase in plasma membranes of plants and fungi. *Biochim. Biophys. Acta* **947**, 1-28.

Siebers, A. (1988). Kalium-Transport bei *Escherichia coli*. Funktionelle, immunologische und topographische Untersuchungen der Kdp-ATPase. Dissertation, Universität Osnabrück.

Siebers, A. and Altendorf, K. (1988). The K$^+$-translocating Kdp-ATPase from *Escherichia coli*. Purification, enzymatic properties and production of complex- and subunit-specific antisera. *Eur. J. Biochem*. **178**, 131-140.

Siebers, A. and Altendorf, K. (1989). Characterization of the phosphorylated intermediate of the K$^+$-translocating Kdp-ATPase from *Escherichia coli*. *J. Biol. Chem*. **264**, 5831-5838.

Siebers, A. and Altendorf, K. (1993). K$^+$-translocating Kdp-ATPases and other bacterial P-type ATPases. In: *Alkali cation transport systems in prokaryotes* (Bakker, E.P., ed.), pp. 225-252, CRC Press, Boca Raton, Florida.

Siebers, A., Kollmann, R., Dirkes, G. and Altendorf, K. (1992). Rapid, high-yield purification and characterization of the K$^+$-translocating Kdp-ATPase from *Escherichia coli*. *J. Biol. Chem.* **267**, 12717-12721.

Siebers, A., Wieczorek, L. and Altendorf, K. (1988). K$^+$-ATPase from *Escherichia coli*: isolation and characterization. *Methods Enzymol*. 157, 668-680.

Siligardi, G. and Hussain, R. (1998). Biomolecules interactions and competitions by non-immobilised ligand interaction assay by circular dichroism. *Enantiomer*. **3**, 77-87.

Slesinger, P.A., Patil, N., Liao, Y.J., Jan, Y.N., Jan, L.Y. and Cox, D.R. (1996). Functional effects of the mouse *weaver* mutation G protein-gated inwardly rectifying K$^+$ channels. *Neuron* **16**, 321-331.

Solioz, M., Mathews, S. and Furst, P. (1987). Cloning of the K$^+$-ATPase of *Streptococcus faecalis*. Structural and evolutionary implications of its homology to the KdpB-protein of *Escherichia coli*. *J. Biol. Chem.* **262**, 7358-7362.

Soteropoulos, P., Valiakhmethov, A., Kashiwazaki, R. and Perlin, D. S. (2001). Helical stalk segments S4 and S5 of the plasma membrane H$^+$-ATPase from *Saccharomyces cerevisiae* are optimized to impact catalytic site environment. *J. Biol. Chem*. **276**, 16265-16270.

Sreerama, N. and Woody, R. W. (1993). A self-consistent method for the analysis of protein secondary structure from circular dichroism. *Anal. Biochem*. **209**, 32-44.

Sreerama, N. and Woody, R. W. (1994). Protein secondary structure from circular dichroism spectroscopy. Combining variable selection principle and cluster analysis with neural network, ridge regression and self-consistent methods. *J. Mol. Biol*. **242,** 497-507.

Stallkamp, I., Dowhan, W., Altendorf, K. and Jung, K. (1999). Negatively charged phospholipids influence the activity of the sensor kinase KdpD of *Escherichia coli*. *Arch. Microbiol*. **172**, 295-302.

Stein, W. D., Lieb, W. R. Karlish, S. J. and Eilam, Y. (1973). A model for active transport of sodium and potassium ions as mediated by a tetrameric enzyme. *Proc. Natl. Acad. Sci. U S A*. **70,** 275-278.

Stewart, L.M.D., Bakker, E.P. and Booth, I.R. (1985). Energy coupling to K$^+$ uptake via the Trk system in *Escherichia coli*: the role of ATP. *J. Gen. Microbiol*. **131**, 77-85.

Stokes, D. L. and Green, N. M. (2000). Modeling a dehalogenase fold into the 8-Å density map for Ca(2+)-ATPase defines a new domain structure. *Biophys. J*. **78**, 1765-1776.

Stumpe, S., Schlösser, A., Schleyer, M. and Bakker, E.P. (1996). K^+ circulation across the prokaryotic cell membrane: K^+ uptake systems. In: *Handbook of Biological Physics* Vol. 2 (Konings, W.N., Kaback, H.R. and Lolkema, J.S., eds.), pp. 473-499, Elsevier Science, Amsterdam.

Suelter, C.H. (1970). Enzymes activated by monovalent cations. Patterns and predictions for these enzyme catalysed reactions are explored. *Science* **168**, 789-795.

Sugiura, A., Hirokawa, K., Nakashima, K. and Mizuno, T. (1994). Signal-sensing mechanisms of the putative osmosensor KdpD in *Escherichia coli. Mol. Microbiol.* **14**, 929-938.

Sugiura, A., Nakashima, K., Tanaka, K. and Mizuno, T. (1992). Clarification of the structural and functional features of the osmoregulated *kdp* operon of *Escherichia coli. Mol. Microbiol.* **6,** 1769-1776.

Sukharev S., Betanzos, M., Chiang, C. S. and Guy, H. R. (2001). The gating mechanism of the large mechanosensitive channel MscL. *Nature.* **409**, 720-724.

Sukharev, S.I., Martinac, B., Arshavsky, V.Y. and Kung, C. (1993). Two types of mechanosensitive channels in the *Escherichia coli* cell envelope: solubilization and functional reconstitution. *Biophys. J.* **65**, 177-183.

Supply, P., Wach, A. and Goffeau, A. (1993). Enzymatic properties of the PMA2 plasma membrane-bound H^+-ATPase of *Saccharomyces cervisiae. J. Biol. Chem.* **268**, 19753-19759.

Sutherland, L., Cairney, J., Elmore, M.J., Booth, I.R. and Higgins, C.F. (1986). Osmotic regulation of transcription: induction of the proU betaine transport gene is dependent on accumulation of intracellular potassium. *J. Bacteriol.* **168**, 805-814.

Sweadner, K. J. and Donnet, C. (2001). Structural similarities of Na, K-ATPase and SERCA, the Ca^{2+}-ATPase of sarcoplasmic reticulum. *Biochem. J.* **356**, 685-704.

Szabo, I. and Zoratti, M. (1991). The giant channel of the inner mitochondrial membrane is inhibited by cyclosporin A. *J. Biol. Chem.* **266**, 3376-3379.

Taniguchi, K., Kaya, S., Abe, K. and Mardh, S. (2001). The oligomeric nature of Na/K-transport ATPase. *J. Biochem.* (Tokyo) **129**, 335-342.

Therien, A.G., Karlish, S.J.D. and Blostein, R. (1999). Expression and functional role of the γ subunit of the Na, K-ATPase in mammalian cells. *J. Biol. Chem.* **274**,12252-12256.

Thoenges D. and Schoner, W. (1997). 2'-O-Dansyl analogs of ATP bind with high affinity to the low affinity ATP site of Na^+/K^+-ATPase and reveal the interaction of two ATP sites during catalysis. *J. Biol. Chem.* 272, 16315-16321.

Thoenges, D. and Schoner, W. (1997). 2'-O-Dansyl analogs of ATP bind with high affinity to the low affinity ATP site of Na^+/K^+-ATPase and reveal the interaction of two ATP sites during catalysis. *J. Biol. Chem.* **272**, 16315-16321.

Thoenges, D., Amler, E., Eckert, T. and Schoner, W. (1999). Tight binding of bulky fluorescent derivatives of adenosine to the low affinity E2ATP site leads to inhibition of Na^+/K^+-ATPase. Analysis of structural requirements of fluorescent ATP derivatives with a Koshland-Nemethy-Filmer model of two interacting ATP sites. *J. Biol. Chem.***274**, 1971-1978.

Tholema, N., Bakker, E.P., Zuzuki, A. and Nakamura, T. (1999). Change to alanine of one of four selectivity filter glycines in KtrB causes a two orders of magnitude decrease in the affinities for both K^+ and Na^+ of the Na^+ dependent K^+ uptake system KtrAB. *FEBS Lett.* **450**, 217-220.

Thompson, J. D., Higgins, D. G. and Gibson, T. J. (1994). CLUSTALW: improving the sensitivity of progressive multiple sequence alignment through sequence weighting, positive-specific gap penalties and weight matrix choice. *Nucleic Acids Res*. **22**, 4673-4680.

Toyoshima C. and Nomura, H. (2002). Structural changes in the calcium pump accompanying the dissociation of calcium. *Nature* **418**, 605-611.

Toyoshima, C., Nakasako, M., Nomura, H. Ogawa, H. (2000). Crystal structure of the calcium pump of sarcoplasmic reticulum at 2.6 Å resolution. *Nature* **405**, 647-655.

Tran, C. M. and Farley, R. A. (1986). Inhibition of ion pump ATPase activity by 3'-O-(4-benzoyl)benzoyl-ATP (BzATP): assessment of BzATP as an active site-directed probe. *Biochim. Biophys. Acta.* **860,** 9-14

Tran, C. M. and Farley, R. A. (1999). Catalytic activity of an isolated domain of Na, K-ATPase expressed in *Escherichia coli*. *Biophys. J.* **77,** 258-266.

Tran, C. M., Huston, E. E., and Farley, R. A. (1994). Photochemical labeling and inhibition of Na, K-ATPase by 2-Azido-ATP. Identification of an amino acid located within the ATP binding site. *J. Biol. Chem.* **269**, 6558-6565.

Tran, C. M., Scheiner-Bobis,, G., Schoner, W. and Farley, R. A. (1994). Identification of an amino acid in the ATP binding site of Na+/K(+)-ATPase after photochemical labeling with 8-azido-ATP. *Biochemistry*. **33,** 4140-4147.

Tsivkovskii, R., MacArthur, B. C. & Lutsenko, S. (2001). The Lys1010-Lys1325 fragment of the Wilson's disease protein binds nucleotides and interacts with the N-terminal domain of this protein in a copper-dependent manner. *J. Biol. Chem.* **276**, 2234-2242.

Tsuda, T., Kaya, S., Yokoyama, T., Hayashi, Y. and Taniguchi, K. (1998). Half-site modification of Lys-480 of the Na^+, K^+-ATPase alpha-chain with pyridoxal 5'-diphospho-5'-adenosine reduces ATP-dependent phosphorylation stoichiometry from half to a quarter. *J. Biol. Chem*. **273**, 24334-24338.

Van der Laan, M. (1999). Construction and characterization of mutants in KdpA, the potassium-binding and –translocating subunit of the KdpFABC complex from *Escherichia coli*. Diplomarbeit, Universität Osnabrück.

Van der Laan, M., Gaßel, M. and Altendorf, K. (2002). Characterization of Amino Acid Substitutions in KdpA, the K(+)-Binding and -Translocating Subunit of the KdpFABC Complex of *Escherichia coli*. *J. Bacteriol*. **184**, 5491-5494.

Verkhovskaya, M.L., Verkhovsky, M.L. and Wikström, M. (1995). A novel antiporter activity cataly-zing sodium and potassium transport from right-side-out vesicles of *E. coli*. *FEBS Lett.* **363**, 46-48.

Voelkner, P., Puppe, W. and Altendorf, K. (1993). Characterization of the KdpD protein, the sensor kinase of the K^+-translocating Kdp system of *Escherichia coli*. *Eur. J. Biochem.* **217**, 1019-1026.

Voges, D. and Jap, B.K. (1998). Recombinant expression, purification and characterization of Kch, a putative *Escherichia coli* potassium channel protein. *FEBS Lett.* **429,** 104-108.

Völker, U., Engelmann, S., Maul, B., Riethdorf, S., Völker, A., Schmid, R., Mach, H. and Hecker, M. (1994). Analysis of the induction of general stress proteins of *Bacillus subtilis*. *Microbiology*.**140**, 741-752.

Vriend, G. (1990). WHAT IF: A molecular modeling and drug design program. *J. Mol. Graph.* **8**, 52-56

Walderhaug, M.O., Polarek, J.W., Voelkner, P., Daniel, J.M., Hesse, J.E., Altendorf, K. and Epstein, W. (1992). Kdp D and KdpE, proteins that control expression of the *kdpABC* operon, are members of the two-component sensor-effector class of regulators. *J. Bacteriol.* **174**, 2152-2159.

Wang, K, Huston, E.E. & Farley, R. A. (1991). In: The Sodium Pump: Recent Developments. (Kaplan, J.H. & DeWeer, P., eds.) pp. 61-64, The Rockerfeller University Press, New York, USA.

Ward D. G. and Cavieres, J. D. (1998a). Photoinactivation of fluorescein isothiocyanate-modified Na, K-ATPase by 2'(3')-O-(2,4,6-trinitrophenyl)8-azidoadenosine 5'-diphosphate. Abolition of E1 and E2 partial reactions by sequential block of high and low affinity nucleotide sites. *J. Biol. Chem*. **273**, 14277-14284.

Ward D. G. and Cavieres, J. D. (1998b). Photoinactivation of fluorescein isothiocyanate-modified Na, K-ATPase by 2'(3')-O-(2,4,6-trinitrophenyl)8-azidoadenosine 5'-diphosphate. Abolition of E1 and E2 partial reactions by sequential block of high and low affinity nucleotide sites. *J. Biol. Chem*. **273,** 14277-14284.

Ward, D. G. and Cavieres, J. D. (1996). Binding of 2'(3')-O-(2,4-6-trinitrophenyl) ADP to soluble alpha beta protomers of Na, K-ATPase modified with fluorescein isothiocyanate. Evidence for two distinct nucleotide sites. *J. Biol. Chem*. **271,** 12317-12321.

Watanabe, T. and Inesi, G. (1982). The use of 2',3'-O-(2,4,6-trinitrophenyl) adenosine 5'-triphosphate for studies of nucleotide interaction with sarcoplasmic reticulum vesicles. *J. Biol. Chem*. 257, 11510-11516.

Weber, K. and Osborn, M. (1969). The reliability of molecular weight determinations by dodecyl sulfate-polyacrylamid gel electrophoresis. *J. Biol. Chem.* **244**, 4406-4412.

Wider, G. and Wüthrich, K. (1999). NMR spectroscopy of large molecules and multimolecular assemblies in solution. *Curr. Opin. Struct. Biol*. **9**, 594-601.

Williams, K. A. (2000). Three-dimensional structure of the ion-coupled transport protein NhaA. *Nature* **403**, 112-115

Wood, J. M., Bremer, E., Csonka, L. N., Krämer, R., Poolman, B., van der Heide, T. and Smith, L. T. (2001). Osmosensing and osmoregulatory compatible solute accumulation by bacteria. *Comp. Biochem. Physiol. A. Mo.l Integr. Physiol.* **130,** 437-460.

Xu, C. Rice, W. J., He, W. and Stokes, D. L. (2002). A structural model for the catalytic cycle of Ca(2+)-ATPase. *J. Mol. Biol*. **316**, 201-211.

Zhang, P., Toyoshima, C. Yonekura, K., Green, N.M. and Stokes, D. (1998). Structure of the calcium pump from sarcoplasmic reticulum at 8-Å resolution. *Nature* **392**, 835-839.

Zimmann, P., Puppe, W. and Altendorf, K. (1995). Membrane topology of the sensor kinase KdpD of *Escherichia coli*. *J. Biol. Chem.* **270**, 28282-28288.

Contributions to international meetings

- FEBS Advanced Lecture Course on P-type ATPases (2000). Structural analysis of functional domains of the *Escherichia coli* KdpFABC complex (short lecture and poster) Mauloff, Germany

- FASEB Summer Research Conference: Meeting on Transport ATPases: From Genomics to Mechanism (2001). Functional domains of KdpB, the catalytic subunit of the *Escherichia coli* KdpFABC complex (poster and oral poster presentation). Snowmass, Colorado, USA

- 10th Int. Conference on Na, K-ATPase and Related Cation Pumps (2002). The Kdp-ATPase: A unique P-type ATPase of prokaryotes (short lecture and poster), Elsignore, Denmark

Publications

- Bramkamp, M., Gaßel, M., Herkenhoff-Hesselmann, B., Bertrand, J. and Altendorf, K. (2003). The *Methanococcus jannaschii* protein Mj0968 is not a P-type ATPase. *FEBS Lett.*, in preparation.

- Bramkamp, M. and Altendorf, K. (2003). Mutational analysis of charged residues in the putative KdpB-TM5 domain of the Kdp-ATPase of *Escherichia coli*. Proceedings, 10th Int. Conference on Na, K-ATPase and Related Cation Pumps (2002), *Ann. N. Y. Acad. Sci.*, in press.

- Bramkamp, M., Gaßel, M. and Altendorf, K. (2003). New biochemical characteristics of the Kdp-ATPase of *Escherichia coli*: Identification of the FITC binding site and *p*-nitrophenyl phosphatase activity. *Biochemistry*, in preparation.

- Bramkamp, M. and Altendorf, K. (2003). Overexpression and biochemical characterization of soluble domains of the KdpB subunit of the KdpFABC complex of *Escherichia coli*. *J. Biol. Chem.*, in preparation.

- Bramkamp, M, Gaßel, M and Altendorf, K. (2003). Substitution of charged residues in the putative KdpB-TM5 domain of the Kdp-ATPase of *Escherichia coli* uncouples ATP hydrolysis and ions translocation. in preparation.

Affirmation

Hereby I declare to have prepared the present dissertation autonomously without illegitimate assistance. No other supplemental material or references have been used than those, which are annotated.

Osnabrück, January 2003

(Marc Bramkamp)

Curriculum Vitae

Personal data

Name	Marc Bramkamp
Date/Place of Birth	05.07.1974, Georgsmarienhütte, Germany
Family Status	unmarried

Education	08/1980	Grundschule Icker
	08/1984-08/1986	Orientierungsstufe, Thomas Morus Schule, Osnabrück
	08/1986-05/1993	Gymnasium, Angela Schule, Osnabrück
	05/1993	Abitur
	10/1993	Study of Biology, University Osnabrück
	08/1995	Prediploma
	12/1997-09/1998	Diploma thesis, prepared at the National Research Center for Biotechnology, GBF, Dept. of Microbiology, Braunschweig,
	09/1998	Diploma
	since 12/1998	Doctoral thesis, Dept. of Microbiology, University Osnabrück, Schoolarship of the Fonds der Chemischen Industrie